UAB
Universitat Autònoma de Barcelona

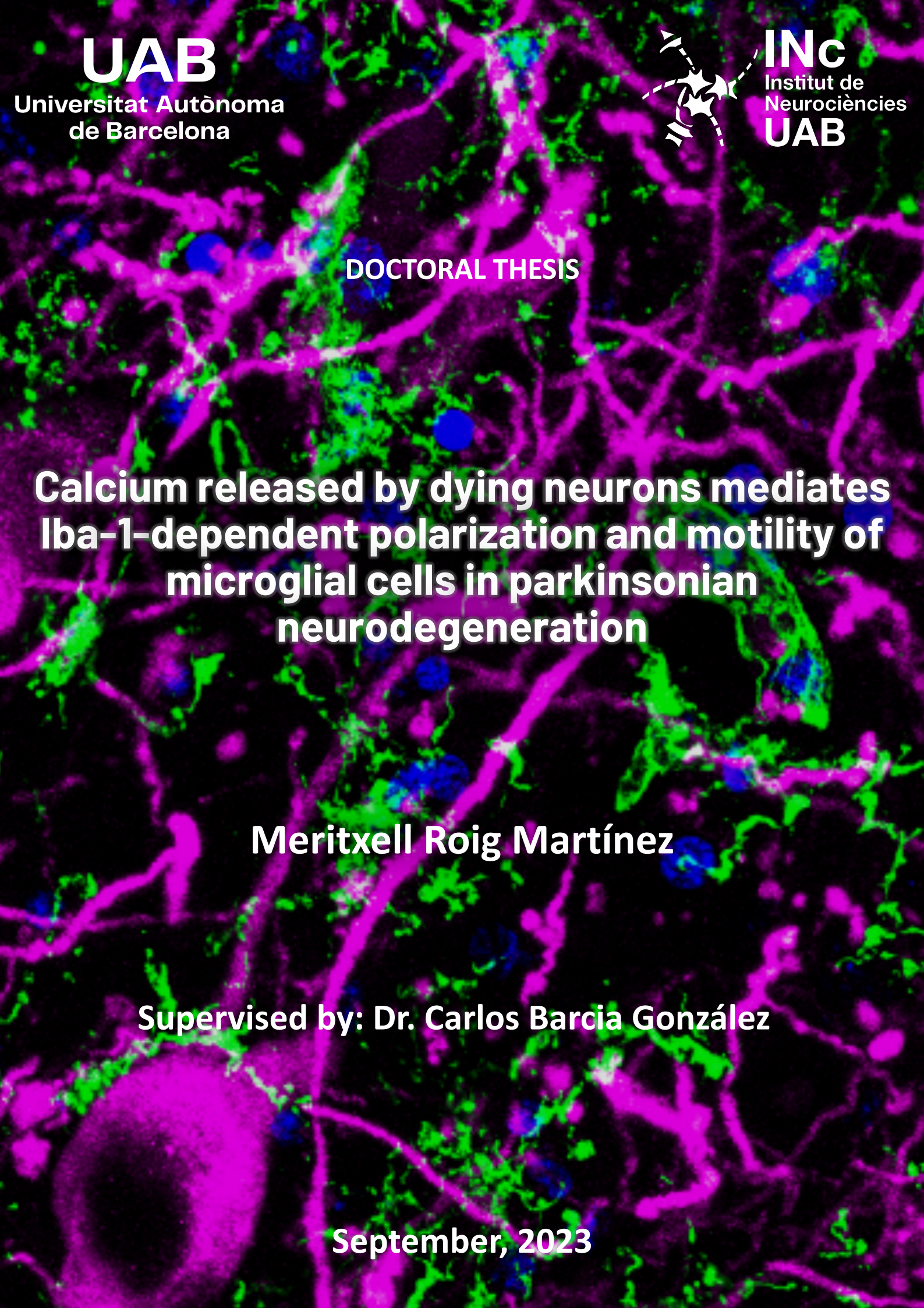
Calcium released by dying neurons mediates Iba-1-dependent polarization and motility of microglial cells in parkinsonian neurodegeneration

Meritxell Roig Martínez

ADVERTIMENT. L'accés als continguts d'aquesta tesi queda condicionat a l'acceptació de les condicions d'ús establertes per la següent llicència Creative Commons: https://creativecommons.org/licenses/?lang=ca

ADVERTENCIA. El acceso a los contenidos de esta tesis queda condicionado a la aceptación de las condiciones de uso establecidas por la siguiente licencia Creative Commons: https://creativecommons.org/licenses/?lang=es

WARNING. The access to the contents of this doctoral thesis it is limited to the acceptance of the use conditions set by the following Creative Commons license: https://creativecommons.org/licenses/?lang=en



UAB
Universitat Autònoma de Barcelona

INc
Institut de Neurociències
UAB

DOCTORAL THESIS

Calcium released by dying neurons mediates Iba-1-dependent polarization and motility of microglial cells in parkinsonian neurodegeneration

Meritxell Roig Martínez

Supervised by: Dr. Carlos Barcia González

September, 2023

UNIVERSITAT AUTÒNOMA DE BARCELONA

INSTITUT DE NEUROCIÈNCIES UAB

Biochemistry and Molecular Biology Dept.

Calcium released by dying neurons mediates Iba-1-dependent polarization and motility of microglial cells in parkinsonian neurodegeneration

Meritxell Roig Martínez

PhD. Director: Dr. Carlos Barcia González

PhD. Academic Tutor: Dr. José Aguilera Ávila

PhD in Neuroscience

Cerdanyola del Vallès, Barcelona

September 2023

This thesis has been done in the Biochemistry and Molecular Biology Department (*Departament de Bioquímica y Biologia Molecular*) and in the *Institut de Neurociències* of the *Universitat Autònoma de Barcelona*, directed by

Dr. Carlos Barcia González

Meritxell Roig Martínez

Director: Dr. Carlos Barcia González

Tutor: Dr. José Aguilera Ávila

Cerdanyola del Vallès, September 2023

Epigraph

“What I love about science is that as you learn, you don't really get answers.

You just get better questions.”

John Green

INDEX

Epigraph _____ **9**

INDEX _____ **13**

LIST OF ABBREVIATIONS _____ **19**

LIST OF FIGURES _____ **31**

LIST OF TABLES _____ **35**

SUMMARY _____ **39**

RESUMEN _____ **41**

INTRODUCTION _____ **41**

1. Exploring the knowledge of Parkinson's Disease _____ **43**

1.1. Pathophysiology of Parkinson's disease _____ **44**

1.2. The lack of dopamine provoking PD symptoms _____ **48**

1.3. A drug called MPTP promoting parkinsonism _____ **48**

1.4. Related genes in PD pathology _____ **50**

1.5. Other implicated factors _____ **52**

1.6. Current treatments for PD _____ **52**

2. Neuroinflammation and its implication in PD pathogenesis _____ **54**

3. Microglial cells and their role in neuroinflammation and PD progression _____ **61**

3.1. Origin of microglial cells _____ **61**

3.2. Microglial morphology and phenotypes _____ **63**

3.3. Microglial function _____ **64**

3.4. Neuroinflammation mediated by microglia in PD _____ **70**

3.5. Modulation of microglia during a neuroinflammatory process _____ **72**

3.6. Implicated molecules during microglial sensitization, migration, and phagocytosis _____76

4. Calcium ions as signals for microglia _____85

5. Iba-1 as the responsible protein for the microglial sensitization through calcium_ _____90

OBJECTIVES _____95

MATERIALS AND METHODS _____97

1. In vitro experiments_____97

1.1. Cell lines and primary cultures_____97

1.2. Lipopolysaccharide and interferon -induced microglial activation _____100

1.3. GRIESS assay _____101

1.4. Extracellular calcium inputs to BV2 microglial cells _____101

1.5. Cocultures BV2-PC12 _____102

1.6. Immunocytofluorescence for cell lines _____102

1.7. Microfluidic live cells analysis _____103

1.8. Cell tracking in CellASIC™ONIX microfluidic plates_____108

1.9. MPP^+ administration to MSF neurons _____108

1.10. Cocultures primary MSF neurons and microglia _____109

1.11. Immunocytofluorescence in primary cultures_____111

1.12. Epifluorescence and confocal microscopy and quantification _____112

1.13. Colocalization analyses in cell lines and primary microglia _____112

1.14. MTOC location_____113

1.15. Differences in intensity and morphology when administering extracellular $Ca^{2+}$to BV2 cells _____113

1.16. Homogenates and western blot for Iba-1 intensity _____113

1.17. Contacts/phagocytosis BV2-PC12 _____116

1.18. Measurement of calcium released by neurons when exposed to a dopaminergic neurotoxic insult _____116

1.19. Number of neurons in the primary culture and coculture _____117

1.20. Calcium internalization by microglia in live analyses _____117

1.21. Pilot experiments with viral vectors infections to microglia _____118

2. In vivo experiments _____120

2.1. Pilot experiment with Ca^{2+} injections in mice _____120

2.2. Ca^{2+} and Ca^{2+} chelator injections into the striatum _____122

2.3. Analysis of polarization in MPTP-injected mice _____125

2.4. Pilot experiments with viral vectors infections in mice _____127

2.5. Calcium injections in Iba-1-KO mice _____130

2.6. Polarization quantification in Iba-1-KO mice injected with calcium _____132

3. Studies in human samples _____133

3.1. Sectioning of human samples _____133

3.2. Immunohistofluorescence for human samples_____133

3.3. Confocal microscopy in human samples _____135

3.4. Quantification of human samples _____135

4. Statistics _____137

RESULTS_____141

1. Microglia polarizes to contact remaining DA neurons in the SNpc of PD patients_ _____141

2. MPTP-induced parkinsonian mice show microglial polarization towards remaining DA neurons_____148

3. Categorization of microglial interactions during homeostasis and stimulating scenarios _____153

3.1. Understanding the process of microglia-target contacts with cell line co-cultures 153

3.2. Interactions are also produced in a more physiological scenario with primary co-cultures 154

3.3. MTOC is located at the front edge in the microglial kinetic morphology regardless of their activation 157

4. Released calcium from dying DA neurons as an important process for microglial sensitization 160

4.1. DA neurons dying in a Parkinsonian scenario release calcium to the medium 160

4.2. Microglial cells internalize extracellular calcium 164

4.3. Understanding calcium release in an in vitro model of PD 168

4.4. Calcium promotes microglial kinetic shape 175

4.5. Calcium-induced kinetic morphology corresponds with increasing microglial motility 178

4.6. Calcium administration promotes polarization of microglia in vivo 184

5. Iba-1 as a key molecule present in microglial cells to sense Ca^{2+} signals 195

5.1. Extracellular calcium inputs induces an increase of Iba-1 expression 195

5.2. After microglial activation Iba-1 is positioned in essential cytoskeletal elements for motility 200

6. Ca^{2+}-mediated polarization is Iba-1-dependent 204

6.1. Ca^{2+} administration results in migration impairment in Aif-1 knock out mice 204

GENERAL DISCUSSION 209

CONCLUSIONS 219

SCIENTIFIC CONTRIBUTIONS 223

SUPPLEMENTARY MATERIAL 225

ANNEX OF MATERIALS USED_____**235**

BIBLIOGRAPHY_____**239**

LIST OF ABBREVIATIONS

2D	Two dimensional
3D	Three dimensional
α	alfa
AAV	Adeno-associated virus
Aβ	Amyloid β
Ad	Adenovirus
AD	Alzheimer Disease
Aif-1	Allograft Inflammatory factor-1
ALS	Amyotrophic Lateral Sclerosis
ANOVA	Analysis Of Variance
AP	Anteroposterior
APC	Antigen-Presenting Cell
AR	Adenosine Receptor
Ara-C	Cytosine β-D-arabinofuranoside
ATP	Adenosine Triphosphate
AZ	Arizona
β	beta
B cells	Bone-marrow cells
BBB	Blood Brain Barrier
BCA	Bicinconinic Acid

BDNF	Brain-derived neurotrophic factor
BMEC	Brain Microvessel Endothelial Cells
BrdU	Bromodeoxyuridine
BSA	Bovine Serum Albumine
CA	California
Ca^{2+}	Calcium ion
$CaCl_2$	Calcium Chloride
CBD	Corticobasal Degeneration
Cd11b	Cluster of Differentiation 11b
CD14	Cluster of Differentiation 14
CD4	Cluster of Differentiation 4
CD8	Cluster of Differentiation 8
cDNA	complementary DNA
cm	Centimeters
CNS	Central Nervous System
CO_2	Carbon Dioxide
COMT	Catechol-o-methyl transferase
CSF	Cerebrospinal Fluid
CSF1R	Colony-stimulating Factor 1 Receptor
Cu^{1+}	Cupper 1+
Cu^{2+}	Cupper 2+
CX_3CL1-CX_3CR1	Fractalkine ligand-fractalkine receptor

CXCL12	Chemokine ligand 12
DA	Dopamine
DAP12	DNAX Activation Protein of 12 kDa
DAPI	4',6-diamino-2-phenylindole
DAT	Dopamine Transporter
DBS	Deep Brain Stimulation
DCs	Dendritic Cells
DIV	Days *In Vitro*
DLB	Dementia with Lewy Bodies
DMEM	Dulbecco's Modified Eagle Medium
DNA	Deoxyribonucleic Acid
DNase	Deoxyribonuclease
DV	Dorsoventral
E17	Embryos day 17
EAE	Experimental Autoimmune Encephalomyelitis
ECL	Enhanced Chemiluminiscence
EDTA	Ethylenediaminetetraacetic Acid
EGF	Epidermal Growth Factor
EMR1	EGF-like Module-containing mucin-like hormone Receptor-like 1
EPDA	European Parkinson's Disease Association
ER	Endoplasmic Reticulum
ERK	Extracellular signaled-Regulated Kinase

FBS	Fetal Bovine Serum
FcR	Fc Receptor
γ	gamma
gc	Genome Copies
GDNF	Glial cell Derived Neurotrophic Factor
GFAP	Glial Fibrillary Acidic Protein
GFP	Green Fluorescent Protein
Glu	Glutamine
Gly	Glycine
GM130	Golgi Matrix protein 130
GPCR	G Protein-coupled Receptors
GPi	Globus Pallidus internal
H_2O	Water
HAPI	Highly Aggressively Proliferating Immortalized
HD	Huntington Disease
HLA	Human Leukocyte Antigen
HOCl	Hypochlorous Acid
HS	Horse Serum
HSCs	Hematopoietic Stem Cells
Hz	Hertz
Iba-1	Ionized Calcium-Binding Adapter molecule 1
ICF	Immunocytofluorescence

IFNγ	Interferon γ
IFNγR	Interferon γ Receptor
Ig	Immunoglobuline
IGF-1	Insulin-like Growth Factor 1
IHF	Immunohistofluorescence
IL	Interleukin
INc	Institut de Neurociències
iNOS	inducible Nitric Oxide Synthase
IP_3	Inositol Triphosphate
IU	Infection Units
JAK	Janus Activated Kinase
KCl	Potassium Chloride
KD	Knock Down
kDa	kilo Daltons
KO	Knock Out
Kg	Kilograms
KH_2PO_4	Monopotassium Phosphate
LBs	Lewy Bodies
LCMV	Lymphocytic Choriomeningitis Virus
a	L-3,4-dihydroxyphenylanine
LLC	Limited Liability Company
LNs	Lewy Neurites

LPS	Lipopolysaccharide
LRP1	Low-density lipoprotein Receptor-related Protein 1
LRRK2	Leucine-rich repeat serine/threonine protein kinase 2
Ltd	Limited
M	Molar
M1	Classically Activated Macrophages
M2	Alternatively Activated Macrophages
MA	Massachusetts
MAO-B	Monoamine Oxidase type B
MAP-2	Microtubule-associated protein 2
MAPK	Mitogen-activated protein kinase
MD	Maryland
mg	Milligrams
$MgCl_2$	Magnesium Chloride
$MgSO_4$	Magnesium Sulfate
MHC	Major Histocompatibility Complex
MJFF	Michael J Fox Foundation
ML	Mediolateral
mL	Milliliters
mm	Millimeters
mM	Millimolar
MN	Minnesota

MO	Missouri
MPP^+	1-Methyl-4-phenylpyridinium
MPTP	1-Methyl-4-phenyl-1,2,3,6-tetrahydropyridine
MS	Motor Symptoms
MSA	Multiple System Atrophy
MSF	Mesencephalon
MTOC	Microtubule Organizing Center
NA	Noradrenaline
NaCl	Sodium Chloride
NADPH	Nicotinamide Adenine Dinucleotide Phosphate
$NaHCO_3$	Sodium Bicarbonate
NaN_3	Sodium Azide
$NaNO_2$	Sodium Nitrite
NaOH	Sodium Hydroxide
NE	Nebraska
NED	N-(1-naftil) ethildiamide
NF-κB	Nuclear Factor kappa B
ng	Nanogram
NGF	Nerve Growth Factor
NIH	National Institutes of Health
NK	Natural Killers
nm	Nanometer

nM	Nanomolar
NM	Neuromelanin
NMS	Non-Motor Symptoms
NO	Nitric Oxide
NOS2	Nitric Oxide Synthase 2
NSAID	non-steroidal anti-inflammatory drugs
ºC	degree Celsius
O_2^-	Superoxide
P/S	Penicillin/Streptomycin
P0	Post-natal day 0
P2	Post-natal day 2
P2XR	P2X receptor
P2YR	P2Y receptor
PBS	Phosphate-Buffered Saline
PCR	Polymerase Chain Reaction
PD	Parkinson's Disease
PDL	Poly-D-Lysine
PF	Paraformaldehyde
PINK1	PTEN-induced kinase 1
PLL	Poly-L-Lysine
Poly I:C	Polyinosinic-polycytidylic Acid
PSP	Progressive Supranuclear Palsy

Ref.	Reference
rpm	Revolutions per minute
RNA	Ribonucleic Acid
ROS	Reactive Oxygen Species
RPMI	Roswell Park Memorial Institute
RT	Room Temperature
SD	Sprague Dawley
SDS	Sodium Dodecyl Sulfate
SEM	Standard Error of the Mean
siRNA	silencer RNA
SNCA	Synuclein Alpha
SNpc	Substantia Nigra *pars compacta*
SOCS	Suppressor of Cytokine Signaling
STAT3	Signal Transducer and Activator of Transcription 3
STN	Subthalamic Nucleus
T cells	Thymus cells
TBS	Trizma Base Solution
TCR	T Cell Receptor
TGFβ1	Transforming Growth Factor β1
TH	Tyrosine Hydroxylase
TKR B	Tyrosine Kinase Receptor B
TNFα	Tumor Necrosis Factor α

™	Trade Mark
TPM	Two-photon microscopy
TREM2	Triggering Receptor Expressed on Myeloid cells 2
UAB	Universitat Autònoma de Barcelona
UK	United Kingdom
UPV	Unidad de Producción de Vectores
USA	United States of America
V	Volts
vg	Viral Genomes
µ slide	Micro slide
µL	Microliters
µm	Micrometers
µM	micromolar
WB	Western Blot
WT	Wild Type

LIST OF FIGURES

INTRODUCTION

Figure 1. Parkinsonian and control MSF showing the differences in the SNpc.

Figure 2. Nigrostriatal pathway in Control and PD.

Figure 3. Braak's stages in PD neurodegeneration.

Figure 4. Process of MPTP conversion to MPP^+ in the brain.

Figure 5. Cellular elements of neuroinflammatory response.

Figure 6. Microglial origin and development.

Figure 7. Microglial morphology changes.

Figure 8. Diagram showing potential signaling of microglia/macrophages towards pro-inflammatory or anti-inflammatory phenotypes.

Figure 9. Microglial polarization after tissue injury.

Figure 10. Potential Ca^{2+} propagating wave through the brain parenchyma to signal microglia.

MATERIALS AND METHODS

Figure I. Diagram of the gradient plate. View of the plate and detail of the chambers and channels to better understand where all the influx and outlet channels are located (CellASIC™).

Figure II. Diagram of the switching plate. View of the plate and detail to better understand how the inlet and outlet channels work and where are located respecting to the central culture chamber (CellASIC™).

Figure III. Schematic representation of the stereotaxic injection at the striatum and the area of picture frames taken on the microscope, going 1280 µm away from the injection site. In each quadrant, the polarization of microglial branches, labeled with Iba-1, were analized in detail.

RESULTS

Figure 11. PD patients show a significantly loss of DA neurons and an increase of microglial reactivity in the SNpc.

Figure 12. Microglial cells increase their interactions, and its extent, with remaining DA neurons in the SNpc of PD patients.

Figure 13. Area of analysis in the mouse SNpc.

Figure 14. MPTP intoxication induces polarization of microglial branches towards DA neurons.

Figure 15. Primary co-cultures performed with MSF microglia and neurons.

Figure 16. Neurons are susceptible to die when exposed to microglia and the depletion is even higher if microglial cells are activated.

Figure 17. Microglial shape in homeostatic and activated state.

Figure 18. Kinetic microglial cells present their MTOC located in front of the nucleus both in a control and activated state.

Figure 19. MPP^{+}-induced dopaminergic neuronal loss results in extracellular calcium release.

Figure 20. Representative image showing the measurement of Fura-2 fluorescence after Ca^{2+} internalization in primary microglia.

Figure 21. Microglial cells internalize extracellular calcium.

Figure 22. Physiological scenario of parkinsonian neurodegeneration promotes calcium release regardless the stimulus.

Figure 23. Phagocytic events in the co-cultures.

Figure 24. Phagocytic events with $MAP2^{+}$ material inside phagosomes.

Figure 25. Extracellular calcium promotes elongated shape in microglial cells.

Figure 26. Calcium-rich medium promotes microglial movement.

Figure 27. Microglial cells respond to calcium waves being more prominent when near to the calcium source.

Figure 28. Microglial cells are susceptible to extracellular calcium administration *in vivo*.

Figure 29. Calcium injected intrastriatally promotes minor changes in morphometric parameters, equivalent to saline injection.

Figure 30. Activated-like morphology provoked by EDTA doesn't mean activation of microglial cells.

Figure 31. Microglial cells polarize most of their branches towards the extracellular calcium source.

Figure 32. Extracellular calcium input induces higher Iba-1 expression.

Figure 33. Activation of microglial cells induces higher Iba-1 expression and colonization of the F-actin rich structures.

Figure 34. Analysis of the polarization in Aif1$^{-/-}$ mice show an impairment in the polarization capacity compared to C57BL/6j mice.

SUPPLEMENTARY MATERIAL

Supplementary Figure 1. Two hours of coculturing microglia and neurons is the best timing to find more interactions.

Supplementary Figure 2. Primary mesencephalic cultures recapitulate parkinsonian dopaminergic neurodegeneration after MPP^+ treatment showing a tendency of calcium release at early timepoint range.

Supplementary Figure 3. Calcium inputs induces Iba-1 production by microglial cells.

Supplementary Figure 4. Aif-1 deficient mice do not express Iba-1 compared with normal expression of WT.

LIST OF TABLES

Table 1. Viral vectors information with the physical titer or infectious titer for each of the vectors used expressed in their respective units.

Table 2. List of primary antibodies used in immunocytofluorescence, immunohistofluorescence and WB.

Table 3. List of secondary antibodies and fluorescent labeling used in immunocytofluorescence, immunohistofluorescence and WB.

SUMMARY

Parkinson's disease is a neurodegenerative disorder in which the loss of dopaminergic neurons, specifically in the Substantia Nigra, causes characteristic motor symptoms and deterioration. Focusing on studying the specific parkinsonian neurodegeneration, we propose that dying neurons release calcium to the extracellular space that may contribute to the neuroimmune response. Particularly, we hypothesize that this released calcium provokes changes in microglial cells which may signal their polarization and motility.

Our *in vitro* experiments performed with microglial cells, revealed that microglia internalizes and binds extracellular calcium and in consequence modify their shape and increase their movement. *In vivo*, administration of calcium to the striatum, as well as a Ca^{2+} chelator, in C57BL/6j mice allowed us to observe slight changes in the morphology parameters of microglial cells between the Ca^{2+}-injected animals and the controls, but not enough to consider significant cytotoxicity due to the injections. However, when measured the polarization of microglial cells in terms of total number of branches oriented either towards the calcium source or to the opposite side, we found clear differences when compared to saline. Thus, calcium diffusion through the parenchyma induced a clear polarization of microglial branches towards the injection site while the saline seemed to remain unpolarized.

Knowing that Iba-1 is a calcium binding protein specific for microglia and macrophages, we hypothesize that Iba-1 may be a crucial factor leading these polarizing changes occurred when they sense calcium changes. In this context, microglial cells, when exposed to extracellular Ca^{2+} inputs, were analyzed to increase their Iba-1 expression. Furthermore, activated microglial cells increase their expression of Iba-1 coinciding with the well-known cytoskeleton formation protein F-actin, suggesting the implication of Iba-1 in the rearrangement of the cytoskeleton to adapt a kinetic shape for later motility. To finally ascertain the implication of Iba-1 in microglial motility, intracranial injections of calcium were performed in Iba-1 lacking mice. These $Aif1^{-/-}$ mice showed their capacity of branches polarization impaired due to the lack of Iba-1.

These results suggest a novel interplay between dying dopaminergic neurons and neighboring microglial cells in which specific Ca^{2+}-dependent responses may contribute to the specific inflammatory response in areas of parkinsonian neurodegeneration which seemed to be Iba-1-dependent.

RESUMEN

La enfermedad de Parkinson es un trastorno neurodegenerativo caracterizado por la pérdida de neuronas dopaminérgicas, específicamente en la Substantia Nigra, lo cual provoca deterioro y síntomas motores característicos. En un escenario de neurodegeneración parkinsoniana, proponemos que las neuronas degenerándose liberan calcio al espacio extracelular, pudiendo contribuir en la respuesta neuroinmune. En especial, planteamos la hipótesis de que este calcio liberado provoca cambios en la microglia, lo cual puede promover su polarización y motilidad.

Experimentos *in vitro* realizados con células microgliales revelaron que la microglía internaliza y une el calcio extracelular y, en consecuencia, modifica su morfología y aumenta su movimiento. *In vivo*, la administración de calcio en el estriado, así como un quelante de Ca^{2+}, en ratones C57BL/6j nos permitió observar ligeros cambios en la morfología de la microglia entre los animales inyectados con Ca^{2+} y los controles, pero no lo suficiente como para considerar la inyección de calcio de significativa citotoxicidad. Sin embargo, al medir la polarización de la microglia en base a número total de ramas orientadas hacia la fuente de calcio o hacia el lado opuesto, encontramos claras diferencias en comparación con los animales inyectados con salino. Así es, la difusión del calcio a través del parénquima cerebral indujo una clara polarización de las ramas hacia el lugar de la inyección, mientras que esto no ocurría con solución salina.

Sabiendo que Iba-1 es una proteína que une calcio y es específica de microglía y macrófagos, nuestra hipótesis es que Iba-1 podría ser un factor crucial promoviendo estos cambios de polarización cuando se detectan señales de calcio. En este contexto, cuando la microglia se expone a diferencias de Ca^{2+} extracelular, aumenta su expresión de Iba-1. Además, la microglia activa aumenta su expresión de Iba-1 coincidiendo con F-actina, una proteína implicada en la formación del citoesqueleto, lo cual sugiere la implicación de Iba-1 en la reorganización del citoesqueleto para adoptar una morfología cinética y después moverse. Finalmente, para determinar la implicación de Iba-1 en la motilidad microglial, se realizaron inyecciones intracraneales de calcio en ratones carentes de Iba-1. Estos ratones $Aif1^{-/-}$ mostraron una capacidad de polarización de ramas mucho menor debido a la falta de Iba-1.

Estos resultados sugieren una nueva interacción entre las neuronas dopaminérgicas en estado degenerativo y la microglia vecina en la que respuestas específicas dependientes de Ca^{2+} pueden contribuir a la respuesta inflamatoria específica en áreas de neurodegeneración parkinsoniana, la cual parece ser dependiente de Iba-1.

INTRODUCTION

1. Exploring the knowledge of Parkinson's Disease

Parkinson's disease (PD) is the second most frequent neurodegenerative disease – after Alzheimer's disease (AD) – and is the most common movement disorder, affecting 1% of the adults with more than 60 years worldwide (Samii et al., 2004). According to the Parkinson's Foundation and the European Parkinson's Disease Association (EPDA), an estimated to 10 million people globally are living with PD, being 1.2 million people just in Europe.

PD is multiethnic – affecting people of all races – and does not depend on the gender. However, according to the Michael J Fox Foundation (MJFF), men are diagnosed with PD at 1.5 times more than women (Beitz, 2014).

PD was first described by James Parkinson in 1817 in his publication "*An essay on the shaking palsy*" in which he distinguished motor symptoms (MS) and non-motor symptoms (NMS) (Parkinson, 1817) in six different patients analyzed.

Within the MS he established bradykinesia – slowness of movements – or akinesia – absence of movement; resting tremor (Reich & Savitt, 2019), muscle rigidity (Przedborski, 2017), postural instability and saccadic ocular movements (T. Sieger et al., 2013) as differential of the disease.

On the other hand, he later described the NMS, which were found variable in some other patients. Within the NMS we could find interrupted speech, sleep disorders, depression, gastrointestinal complications, pain, fatigue, or difficulties swallowing (Hurwitz, 2017; Kalia & Lang, 2015). In some patients, these NMS could be more troublesome than the MS, and they may even appear years earlier than the MS start to be noticeable (Kalia & Lang, 2015).

This disease is defined as idiopathic, with no clear origin, reason for what, similar diseases could be misdiagnosed as PD, like Dementia with Lewy bodies (DLB), Corticobasal degeneration (CBD), Multiple system atrophy (MSA), and Progressive supranuclear palsy (PSP), among others (Beitz, 2014) – all of them showing Parkinson-like symptoms. However, to diagnose a patient with PD they should present at least 3 of the 4 cardinal symptoms; bradykinesia/akinesia, resting tremor, or rigidity (Przedborski, 2017).

During the first few decades after the discovery of PD, the disease was still poorly understood and no evidence of anatomical alterations were correlated with the symptoms. Not until the end of the nineteenth century when Blocq and Marinescu related the parkinsonian symptoms with problems around the cerebral peduncle [Reviewed in (Przedborski, 2017)]. Because of this observation, then, Brissaud suggested that the Substantia Nigra (SN) could be the nucleus with the most relevant lesion in PD (Brissaud, 1899).

1.1. Pathophysiology of Parkinson's disease

Thank to these and subsequent discoveries, now is well-known that the main pathological hallmark in PD patients is the drastic loss of DA (DA) neurons of the Substantia Nigra *pars compacta* (SNpc), occurring from the early stages of the disease (Figure 1) (McGeer & McGeer, 2008; Moore et al., 2005). However, how this phenomenon occurs physiologically remains mysterious (H. Kim et al., 2012). This lesion was first sawn when analyzing brains from patients diagnosed with PD, who showed a clear depigmentation of the SN (Figure 1A), as a result of the neuronal loss located in this specific region (Greco, 1983).

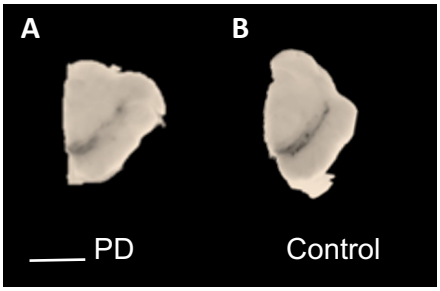


Figure 1. Parkinsonian and control MSF showing the differences in the SNpc. Coronal sections at two different levels of the midbrain from a PD patient on the left **(A)** and a control individual on the right **(B)**. The PD patient show the characteristic neuropathological hallmark in the SNpc with a dramatic loss of neuromelanin pigmented neurons (Scale bar: 1cm).

These SN neurons – specifically the DA neurons, which are more susceptible to die during the course of the disease – are characterized by the amount of containing neuromelanin (NM), characteristic that results in the apparent pigmentation of the SN in the midbrain (Figure 1). Another pathological characteristic of PD brains – although is not always evident – is the appearance of specific protein aggregations in the DA neurons, called Lewy bodies (LBs) (Lewy, 1913). These accumulations were first described by Friedrich Lewy, as protein aggregations in some regions in the cerebral cortex. Years later, Konstantin Nikolaevich Trétiakoff found these Lewy bodies in the SN of some Parkinsonian patients, which were in fact aggregations containing the protein α-synuclein.

Originally, Lewy bodies were reported in the dorsal nucleus of the vagus nerve but not in the SN (Lewy, 1913). This discovery led some scientists to argue that the SN was not the key degenerating brain region in PD. Due to additional observations of striatal degeneration in patients suffering from parkinsonism, the striatum was considered as a more plausible region involved in the disease (Compston, 2009). It was not until the definition of the nigrostriatal pathway (Figure 2) (N. E. Andén et al., 1964; N. -E Andén et al., 1965) – by provoking mechanical unilateral lesions of the ventral midbrain in rats and monkeys and causing the absence of dopamine in the striatum – when the relation between the degeneration of the SN and striatum was established contributing to the understanding of how PD progression was taking part (Goldstein et al., 1967; Poirier & Sourkes, 1965). Since then, although not LBs were yet found specifically in the SN, this region was considered as the critical degenerating area in PD. Later studies revealed that the subregion *pars compacta* of the SN (SNpc) was disproportionately affected (Figure 2) by the disease when compared with other mesencephalic areas (GREENFIELD & BOSANQUET, 1953). As this region was rich in NM-containing neurons (Figure 2A) than other mesencephalic (MSF) areas, when PD brains where studied a noticeable loss of pigmentation was observed (Figure 2B).

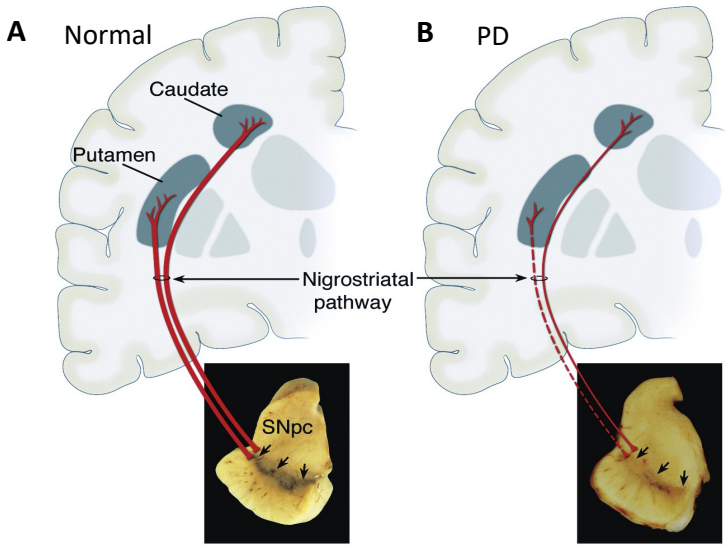


Figure 2. Nigrostriatal pathway in control and PD. A. Diagram showing the connections of the nigrostriatal pathway in a normal brain, from the pigmented neurons of the SNpc (arrows bottom image) to the caudate and putamen in the striatum (upper image). **B.** Diagram showing how the nigrostriatal pathway is reduced (upper image), especially the projections to the putamen, due to the DA neuronal death in the SNpc, which could be seen as less pigmentation in this area (arrows bottom image) (Modified from Dauer & Przedborski, 2003).

During the progression of the disease, the DA neurons, accompanied by LBs formation, degenerate (Dauer & Przedborski, 2003). These neurons project their axons to the striatum –

composed by the caudate and putamen – configuring the nigrostriatal pathway (Figure 2). The loss of these DA neurons of this specific region, and particularly the projections to the putamen, is the main cause of the appearance of the MS in PD patients (Zinger et al., 2011), which it is thought to degenerate years before the onset of the symptoms (Poewe et al., 2017). But this neuronal degeneration not only occurs in the SNpc; the locus coeruleus, nucleus basalis of Meynert, raphe nucleus and dorsal motor nucleus of the vagus are also affected, as well as the olfactory bulbs and the autonomic nervous system (Kalia & Lang, 2015).

As the disease progresses, the PD pathology becomes more severe, increasing the accumulation of misfolded proteins – provoking the LBs formation – accompanied by neuronal processes called Lewy neurites (LNs) potentially contributing to the extension of the synucleinopathy (Mehra et al., 2019). As a result of the DA neurons' degeneration in the SNpc, the nigrostriatal pathway reduces its dopamine signals to the striatum, causing incapacitating alterations of the basal ganglia circuitry (Dauer & Przedborski, 2003).

Within the years with the pathology, other non-DA neurotransmitters may also be affected, such as, cholinergic, glutamatergic, GABAergic, noradrenergic, serotoninergic, and histaminergic. Degeneration in those systems suggest the onset of some non-motor symptoms that do not respond well to DA therapies (Kalia et al., 2013; Kalia & Lang, 2015).

Even though the MS and NMS are well stablished and countless advances have been made to understand the pathophysiology of PD, the origin of the disease remains obscure. Therefore, many hypotheses have been proposed over the years. One of the most successful and controversial was postulated by Braak & Braak in 2003. They proposed that the disorder might be originated by an unidentified agent which could pass through the gastrointestinal mucosal barrier or the olfactory system, triggering abnormal accumulations of α-synuclein. In the firsts steps (Stages 1 and 2) the pathology would enter via the olfactory bulb or the dorsal motor nucleus of the vagus nerve and then extend through the CNS via the enteric neurons present in the vagus nerve that are unmyelinated – colonizing these nerves but also the locus coeruleus (Figure 3B). Once in the CNS, by a retrograde way the pathology could have taken access to the midbrain in which the degeneration starts in the specific regions most affected in PD – substantia nigra – posteriorly this pathogen will invade the neocortex in stages 3 and 4 (Figure 3C) (Braak, Rüb, et al., 2003). Finally, in the last stages – 5 and 6 – the illness could have been spread to the rest of the areas of the brain – the complete neocortex (Figure 3D). This hypothetical spread of the disturbance is thought to happen in a time course within the years of the disease. In addition, the spreading of the synucleinopathy correlates with the clinical symptoms. In the first stages is

when the autonomic system is affected and sleep-related disfunctions are noticeable. Next, the midbrain and basal prosencephalon are affected – where the DA neurons located in the SNpc start dying – ending up in degeneration in the nigrostriatal pathway affecting the striatum neurons, resulting in dramatic motor alterations, and continuedly starts the posterior degeneration in the cortex (Braak, Rüb, et al., 2003).

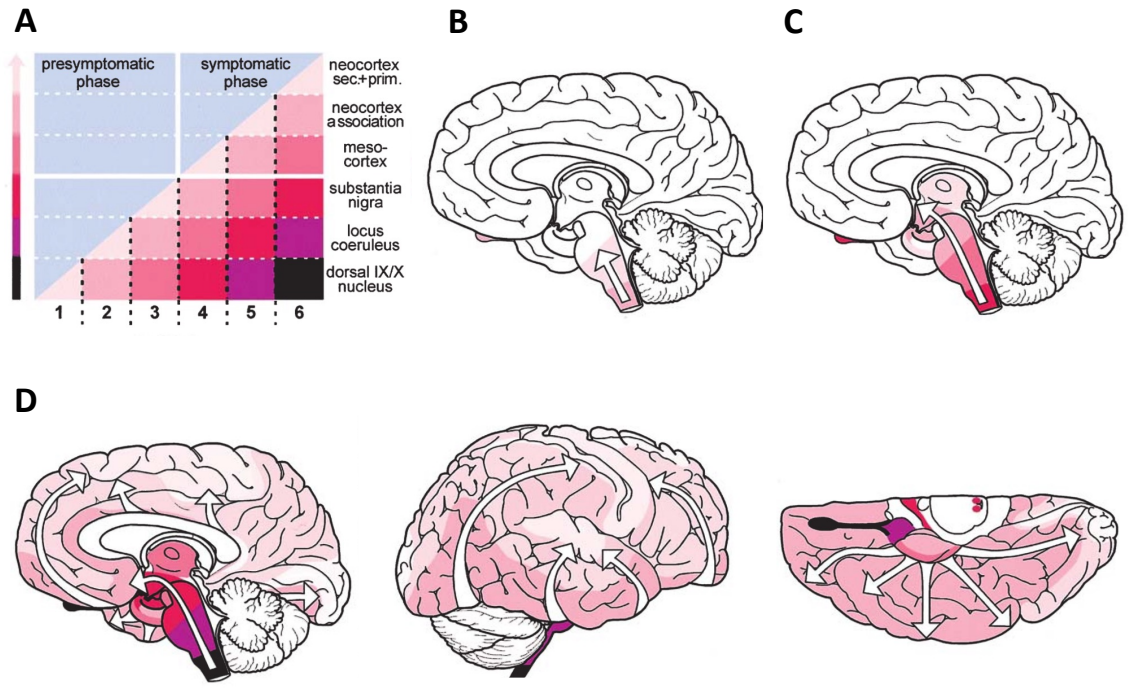


Figure 3. Braak's stages in PD neurodegeneration. A. Graph showing the different stages of the degeneration occurred in PD following the Braak hypothesis. **B.** Diagram showing the regions affected by PD in stages 1 and 2 (locus coeruleus and IX and X nerves). **C.** Diagram showing the regions affected by PD in stages 3 and 4 (substantia nigra, mesocortex plus the regions in stages 1 and 2). **D.** Diagram showing the regions affected by PD in stages 5 and 6 (neocortex plus all the regions previously affected) (Modified from (Braak, Del Tredici, et al., 2003).

However, not all patients suffering from PD presented the same pathological progression and not all the post-mortem cases analyzed had the same distribution of LBs in the specific areas – which should be crucial to support Braak's hypothesis (Surmeier et al., 2017). Besides, some patients do not show LBs (Berg et al., 2014). Then, alternatively, the pathology may also be governed by specific regional factors – which could better reconcile with the variety of patterns of neuronal loss observed in PD. Therefore, it is more reasonable to consider a dual hypothesis that could combine the best assumptions from both premises (Surmeier et al., 2017).

1.2. The lack of dopamine provoking PD symptoms

The first approach uncovering the involvement of dopamine in motor functions came from the studies performed by Carlsson and collaborators. They administered reserpine to animals – to deplete monoamines – which provoked a reduction in dopamine levels and in motor activity. Subsequently, they administered L-3,4-dihydroxyphenylanine (L-DOPA) – a dopamine precursor – and the dopamine levels were restored as the motor activity reversed (Carlsson et al., 1957). These findings indicated the involvement of dopamine signaling in the basal ganglia motor activity.

As PD and other Parkinson-like syndromes were characterized by the absence or reduction of movement, the involvement of dopamine in these diseases was suspected. Different researchers reported a deficit of dopamine in both the striatum and the SN in post-mortem brains from PD patients (Ehringer & Hornykiewicz, 1960; Sano & Murase, 1968). Then, considering these evidences, the lack of dopamine of the patients was tried to reverse by the treatment with L-DOPA (Fahn, 2015).

After the administration, L-DOPA is rapidly converted to dopamine and replace the function of normal dopamine levels in PD patients alleviating the motor difficulties (Fahn, 2015). However, prolonged treatments with L-DOPA provokes tolerance in some patients and they may experience some motor alterations, as dyskinesias, as well as adverse psychiatric effects (Olanow et al., 2006).

1.3. A drug called MPTP promoting parkinsonism

In the early 80s, William Langston, a neurologist working at the Santa Clara Valley Medical Center in California, found a significant case, never reported before, that fitted almost perfectly within the PD symptomatology but with some peculiar features.

Langston and colleagues examined a very young patient, who had “virtually no spontaneous movement and exhibited waxy flexibility”. Langston categorized this person as a patient suffering from the “lead pipe” rigidity with “cog-wheeling” stiffness, typical of PD (Langston, 2017). This person was also tested for rigidity in the upper extremity, finding irregular active resistance when his wrist was flexed passively.

In a first diagnosis attempt, Langston categorized this patient as a typical case of advanced PD, but the difference in age of a typical early onset – which is around 40 years of age – and the fact

that the symptoms appeared in a matter of hours, made Langston change his opinion and categorized it as a "medical mystery" (Langston, 2017).

Months later – by several news outlets and published research – they found six more patients affected by similar symptoms. These patients were not related between each other, lived in different cities and with different ages but all of them young. They had one thing in common, the use of a new synthetic heroin that became very popular in the streets of northern Californian towns. These seven patients, after consuming this drug, experienced the same symptoms characteristic for PD (Ballard et al., 1985). Besides, some of them also experienced NMS such as deficits in cognitive function (Stern et al., 1990). Importantly, these patients were L-DOPA responders, and when treated, their symptoms rapidly reversed.

In subsequent investigations, after examining the synthetic heroine consumed by the patients, it was found to be contaminated with the neurotoxin 1-methyl-4-phenyl-1,2,3,6-tetrahydropyridine (MPTP). Later, another similar case was also reported but not knowing the possible neurotoxic agent (Davis et al., 1979). Langston finally reported all these cases as a chronic parkinsonism provoked by MPTP, suggesting a direct implication in the degeneration of the SNpc – causing the typical DA degeneration as in PD patients (William Langston et al., 1983).

Since then, many scientists have used the molecule MPTP to experimentally induce parkinsonism, contributing to find new insights to understand the disease. Nowadays, MPTP is still used as a common molecule to obtain a reliable animal model for parkinsonism.

1.3.1. Mechanism of action of MPTP

MPTP by itself is not toxic, in fact, to exert its neurotoxic effect it needs to pass through the blood brain barrier (BBB) as a lipophilic compound (Figure 4). Once inside the brain is rapidly converted to 1-methyl-4-phenylpyridinium (MPP^+) – which is the toxic metabolite (Langston et al., 1984; Markey et al., 1984). The transformation of MPTP into the ion MPP^+ is mediated by the enzyme monoamine oxidase B (MAO-B) (Figure 4) (Castagnoli et al., 1985; Chiba et al., 1984), which is thought to occur within astrocytes (Ransom et al., 1987a). Astrocytes uptake the MPTP and by the activity of MAO-B they can rapidly convert it into the MPP^+ molecule and release it (Figure 4). Then, surprisingly, astrocytes are not mainly affected by the neurotoxin but only specifically damaging DA neurons. Then, MPP^+ is selectively internalized into the cells by the dopamine transporter (DAT) – which is specifically expressed in DA neurons (Figure 4) but not in other cell types (Shen et al., 1985).

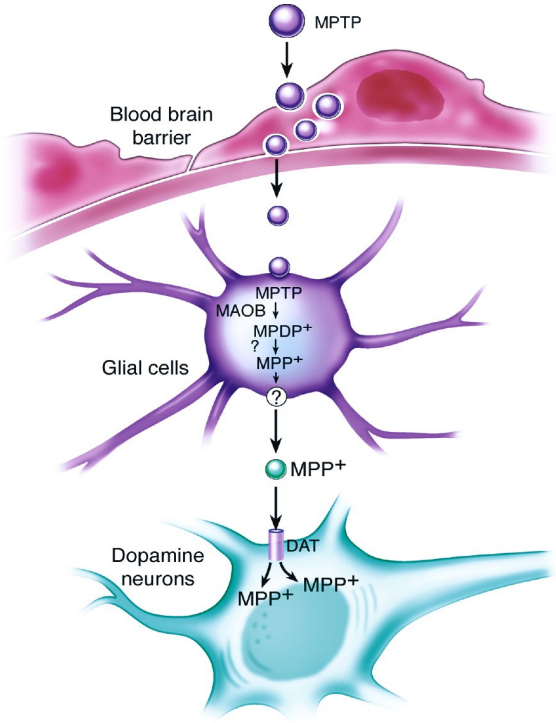


Figure 4. Process of MPTP conversion to MPP^+ in the brain. Diagram showing how the MPTP is crossing the BBB, taken by the glial cells, specifically the astrocytes. Inside the astrocytes is converted to MPP^+ by MAO-B and then externalized, where the ion is selectively taken by the DAT transporter in the DA neurons membrane.

Once internalized, the MPP^+ is accumulated inside the mitochondria inhibiting complex I of the electron transport chain (Ramsay et al., 1986). With mitochondrial dysfunction DA neurons start degenerating and finally die.

1.4. Related genes in PD pathology

Even though PD is generally an idiopathic disorder – meaning that for most of the patients the trigger of the disease is unknown – some of the population suffering from PD – around 10-15% of the patients – have familial forms, indicating a genetic factor.

Some of the genes implicated in the familial PD progression have been widely described. Especially, those involved in the functionality of the mitochondria since mitochondrial dysfunction could be one of the PD triggering factors.

Among the genes implicated, PARK2 – encoding the parkin protein – contains mutations that provoke early onset PD symptoms (Y. Mizuno et al., 2001). Parkin protein participates in the macro-autophagy of defective mitochondria. Moreover, this process is dependent on another protein kinase inside the mitochondria (Geisler et al., 2010; Narendra et al., 2010; Vives-Bauza

et al., 2010) – PINK1 –, mutations of which induce the loss of gene function and have also been described as typical forms of familial PD (Valente et al., 2004).

Another potential link between PD pathology and defective genes was stablished with the SNCA gene – the one encoding the α-synuclein protein. SNCA mutations were originated from missense codes during translation to protein (A30P, E46K, H50Q, G51N and A53T) in the α-synuclein gene (Krüger et al., 1998; Lesage et al., 2013; Polymeropoulos et al., 1997; Proukakis et al., 2013; Zarranz et al., 2004) . With the knowledge of α-synuclein being abundant in LBs, mutations in this gene were said to be the responsible for the appearance of misfolding proteins and in consequence oligomer aggregations of α-synuclein provoking PD (Lashuel et al., 2013; Spillantini et al., 1997). However, in idiopathic PD patients no evidence of mutations in the SNCA gene was found (Muñoz et al., 1997), so, even though, the appearance of α-synuclein aggregations could be enhanced by the presence of these mutations, it could not be the only responsible.

The gene LRRK2 – which encodes a protein kinase – was also described as a related gene implicated in familial PD (Paisán-Ruíz et al., 2004; Zimprich et al., 2004). The function of LRRK2 protein is still not fully understood but it is known that it can bind several 14-3-3 proteins which regulate protein-protein interactions (Dzamko et al., 2010; Nichols et al., 2010); and is probably involved in quite diverse cellular functions, including mitochondrial metabolism, apoptosis, membrane trafficking, and microtubule polymerization that may contribute to PD pathogenicity (Kett & Dauer, 2012). It also interacts with other PD candidate genes so its mutations could lead to additional pathogenesis, increasing the potential of suffering from PD.

Mutations in the glucocerebrosidase gene (GBA) – which encodes a lysosomal protein – and originally identified as the cause of Gaucher's disease, have also been associated with both familial and sporadic PD (Balicki & Beutler, 1995; Lwin et al., 2004). GBA mutations lead to lysosomal dysfunction or interfere in the α-synuclein binding to its receptor (Wong et al., 2004), provoking a reduced α-synuclein degradation and in consequence its aggregation in the cells. When this accumulation occurs in DA neurons it may end in PD.

The UCHL1 gene – also known as PARK5 – have also been suggested as one gene implicated in familial PD. This gene encodes the protein UCHL1 which is a component of the ubiquitin-proteasome system. The UCHL1 protein is highly and specifically expressed in neurons (Doran et al., 1983). This protein removes abnormal or misfolded proteins generating free ubiquitin monomers (Wilkinson et al., 1989). Mutations in that gene could provoke a dysfunctional

protein which cannot eliminate proteins and in consequence they would be accumulated (Schulte & Gasser, 2011).

1.5. Other implicated factors

A number of factors can also contribute to the disease, since not only the underlying pathology or genetic alterations could promote the appearance of PD. Environmental factors could also play a role in the risk of suffering PD. Among them we could find, exposure to some pesticides – like rotenone and paraquat – prior head injuries, and the use of β-blockers.

On the other hand, factors associated with the decreased risk of suffering from PD are the intake of caffeine, nicotine, and the use of non-steroidal anti-inflammatory drugs (NSAID) – like ibuprofen (Jimenez-Ferrer & Swanberg, 2018a; Kalia & Lang, 2015).

1.6. Current treatments for PD

Nowadays, no therapies nor treatments can modify the course of the disease, but they can help to ameliorate the clinical symptoms and lead a fairly normal and healthy life. Currently, the main treatment is the administration of L-DOPA, as mentioned above. L-DOPA is administered orally, when it arrives to the brain is metabolized to restore the striatal dopamine levels and simulate its circuitries. However, prolonged use of L-DOPA can also trigger several side effects, like involuntary movements (dyskinesias), severe on-off motor fluctuations (Lees et al., 2009; Zahoor et al., 2018), and hallucinations (Olanow et al., 2006). New formulations of L-DOPA have been proposed to diminish the side effects, for example, a slow-release formulation or as well novel routes of administration, such as a continuos infusion (Olanow et al., 2006; Smith et al., 2012). Other proposed treatments include focal dopamine delivery systems, intracerebral injections of trophic factors, the use of MAO-B inhibitors and catechol-o-methyl transferase (COMT) inhibitors in combination with the L-DOPA administration (Poewe et al., 2017).

As the administration of L-DOPA to patients is not continued but intermittent, the stimulation of the striatal DA receptors is discontinued, reason for which the motor complications tend to oscillate. Moreover, unfortunately, NMS can also fluctuate in response to dopamine therapies and sometimes these fluctuations can be even more disabling than the motor symptoms themselves (Poewe et al., 2017).

An alternative therapy stablished for treating eligible PD patients, and without apparent secondary adverse effects, is deep brain stimulation (DBS). DBS suppresses the excessive synchronized oscillation in the nuclei of the basal ganglia, and by targeting specially the

subthalamic nucleus (STN) or the internal Globus Pallidus (GPi) may produce symptomatic benefits by alleviating a PD-related pathological synchrony (Hammond et al., 2007). Other targets, rather than the STN and GPi, such as the pedunculopontine nucleus (Smith et al., 2012), have been proposed to produce even better and more personalized control of parkinsonism by DBS. However, patients with low response to L-DOPA treatment are not good candidates for this approach (Poewe et al., 2017) and PD advanced age may also hinder the adequacy. Even with these improvements at the motor level, NMS remain difficult to manage, being poorly reduced with the current treatments (S. Y. Lim & Lang, 2010).

Indeed, since the cause of the DA degeneration is still unknown, several mechanisms implicated in PD pathogenesis could be potential therapeutic targets, such as α-synuclein aggregation, mitochondrial dysfunction, oxidative stress, cytotoxicity, and more important for this thesis, dysregulation of calcium homeostasis and neuroinflammation (Michel et al., 2016).

2. Neuroinflammation and its implication in PD pathogenesis

Since the initial description of PD, the attention was focused on the loss of DA neurons, but very little was reported about the implication of glial cells in the progression of the pathology. Not until 1988 when was first described the presence of reactive microglia in post-mortem samples from PD patients (McGeer et al., 1988). McGeer and colleagues found evidence of neuroinflammation in brain samples, characterized by the activation of microglial cells expressing Human Leukocyte Antigen D-related (HLA-DR) in SNpc. Since then, numerous studies have been performed trying to understand the implication of microglial cells in neurodegenerative disorders, and especially for this thesis in PD neurodegeneration (McGeer & McGeer, 2008).

Nowadays it is well known that in every neuroinflammatory process, microglial cells function as the primary immune response to control anomalous situations. As a general term, neuroinflammation should be considered as a protective and beneficial effect of the immune response. In the initial points, neuroinflammation is triggered by internal or external agents, or malignant components to initiate a healing process (Glezer et al., 2007; Schwartz & Kipnis, 2004; Schwartz & Ziv, 2008), promoting the debris or pathogens clearance, secreting neurotrophic factors, and supporting tissue repair (Tansey & Goldberg, 2010). For example, resident microglia and bone marrow-derived perivascular macrophages have been reported to stimulate myelin repair, remove toxic proteins from the CNS and prevent neurodegeneration in chronic CNS diseases (Glezer et al., 2007; Schwartz & Ziv, 2008; Simard et al., 2006).

Even though neuroinflammation is considered as a positive response, when it becomes chronic could be detrimental and contribute to the pathology progression (Aktas et al., 2005; Gao et al., 2003a; B. Liu & Hong, 2003; Purisai et al., 2007). In this way, an exacerbated reaction can become harmful, due to the excessive prolonged reaction, leading to an increase of some proinflammatory cytokines or reactive oxygen species (ROS), which in some cases could result in a disruption of the BBB (Ransohoff & Perry, 2009).

Neuroinflammation seems to happen as a synergic process, since neurodegeneration potentially provokes the initiation of the neuroinflammatory response and, in consequence, this reaction may lead to additional neurodegeneration in which the exacerbated reaction explained above takes part. In addition, the beneficial effects of neuroinflammation appear to be inadequate or insufficient in neurodegenerative diseases, since the neuroinflammation is triggering a higher

microglial response than in normal situations, worsening the disease progression (Gao & Hong, 2008).

The start of the neuroinflammatory process could promote the disruption of the BBB. The BBB is a multicellular structure composed by brain micro vessel endothelial cells (BMEC), pericytes, astrocytes and perivascular macrophages, forming a physical barrier which separates the CNS from the peripheral tissues (Stewart & Wiley, 1981). This BBB has a specific permeability thanks to the endothelial cells, but when some pathological process occurs this permeability is somehow modified, the secretion of inflammatory cytokines and related inflammatory mediators produced by reactive glia, among others, may enhance this BBB permeability modifications (Y. Zhao et al., 2022). When the BBB permeabilization is compromised, local inflammation in the brain may induce a certain influx of peripheral blood cells into the brain parenchyma, exacerbating the inflammatory response (Brown & Neher, 2010).

Therefore, neuroinflammation is characterized by three main phenomena: neuronal pathology or degeneration (A), which incites the activation of local glial cells (B and C), the release of specific cytokines and chemokines and the potential recruitment and infiltration of peripheral blood cells into the brain parenchyma (D) (Saavedra-López et al., 2016). (Figure 5). Generally, these three aspects are considered as elements of a protective response in order to initiate the healing process and restore homeostasis in most of brain injuries.

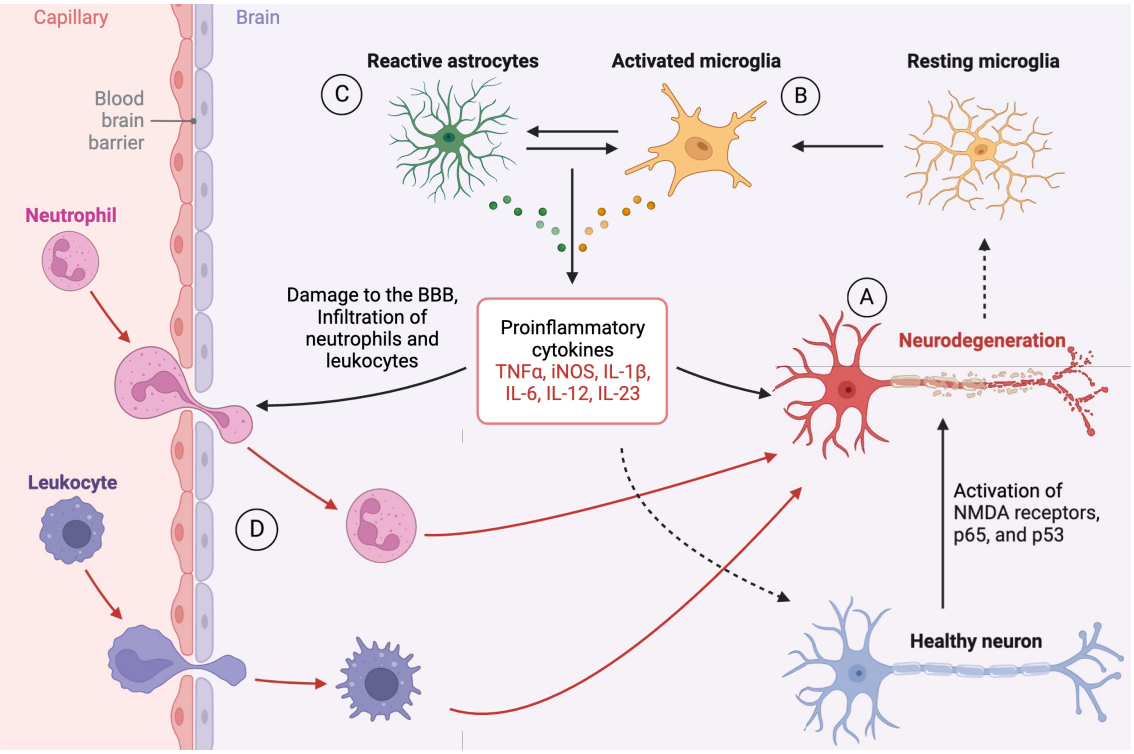


Figure 5. Cellular elements of neuroinflammatory response. After neuronal damage (A) microglial (B) and astroglial (C) cells get activated. The activation causes the release of proinflammatory cytokines and chemokines, which attract monocytes (D) and lymphocytes to the brain parenchyma. (Created by BioRender®)

The implication of these neuroinflammatory phenomena in PD was poorly understood, but a number of discoveries suggested a primordial role of local microglia. One of the tipping points occurred with the postmortem analysis of some of the MPTP-intoxicated patients described by Langston in 1982. Initially, the decreased number of neurons in the SNpc was the main interest of study. However, thanks to the previous research performed by McGeer and colleagues in 1988, finding microglial reactivity in the SNpc of PD patients, Langston and colleagues also decided to examine neuroinflammation in the MPTP patients' samples. Surprisingly, the areas of DA degeneration presented active microglia also expressing HLA-DR, identical to the PD samples described by McGeer (Langston et al., 1999), reinforcing the idea of the implication of microglial-mediated neuroinflammation in the disease progression.

Most importantly, these results demonstrated not only that an active degeneration was occurring many years after the MPTP intoxication, as previously said, but also that was able to initiate a persistent inflammatory response over the years. Once discovered in humans, more studies were conducted in animals performing the same type of intoxication. Monkeys intoxicated with MPTP revealed microglial activation in the SNpc years after the inoculation of the neurotoxin, confirming that neuroinflammatory response persists through the years (Barcia

et al., 2004; McGeer et al., 2003). MPTP-treated mice also expressed microglial activation in the areas of DA neurons' degeneration (Barcia et al., 2012).

In similar research lines, parallel to these studies, injections with inflammatory molecules, such as lipopolysaccharide (LPS), were performed in animals and the results indicated that activates glial cells, being deleterious to DA neurons (Herrera et al., 2000; W. G. Kim et al., 2000). Additionally, the combination of an injection of LPS and MPTP is synergistic and exacerbate both glial activation and neuronal degeneration in specific regions affected (Gao et al., 2003b).

The analyses of the implication of neuroinflammation in PD were not only performed in histological samples, but further biochemical analyses were also accomplished in *in vivo* and postmortem PD samples, revealing increased levels of certain cytokines and chemokines, probably mediated by glial cells in a neuroinflammatory response (Mogi, Harada, Kondo, et al., 1994a; Mogi, Harada, Riederer, et al., 1994). Cytokines and chemokines are small-secreted proteins playing roles in growth, differentiation, and activation functions that regulate and determine the nature of immune responses and control immune cell trafficking and the cellular arrangement of immune organs (Borish & Steinke, 2003). They are also essential proteins released during inflammatory processes; they have been defined as being crucial for the development of the immune response. Depending on which type of cytokines are being released, in response to an immunological insult, determines the type of signaling cascade response, being cytotoxic, humoral, cell-mediated or allergic (Borish & Steinke, 2003). The array of cytokines released in every neurodegenerative disorder is different, being specific for each disorder.

Particularly, pro-inflammatory cytokines such as interferon γ (IFNγ), tumor necrosis factor α (TNFα), interleukins (IL), such as IL1β, IL6 or IL2; chemokine ligand 12 (CXCL12), as well as the anti-inflammatory cytokine transforming growth factor β1 (TGFβ1) were found to be increased in the striatum and SNpc of PD *postmortem* samples (Hunot et al., 1999; Mogi et al., 1996; Mogi, Harada, Kondo, et al., 1994b; Shimoji et al., 2009). Thus, combined with studies performed in blood, plasma and cerebrospinal fluid (CSF) of PD patients, which showed upregulation of proinflammatory (IFNγ, TNFα, IL1β, IL6 and IL2) and anti-inflammatory (TGFβ1, IL4 and IL10) cytokines (Brodacki et al., 2008; Mogi et al., 1996; Mogi, Harada, Kondo, et al., 1994b; Mount et al., 2007a; Nagatsu et al., 2000) reveal that inflammation in PD is not only affecting the brain but also affects other systemic components in the body. Interestingly, the concentration of these markers in peripheral tissues might also depend on PD severity and progression. Higher levels of TNFα in serum have been described as characteristic of PD patients with severe clinical

features and impaired cognition, depression, sleep disturbances and fatigue (Lindqvist et al., 2012; Menza et al., 2010).

Interestingly, parkinsonian models also replicate these cytokines increase. In mice injected with MPTP some cytokines were found in higher levels than normal in the striatum and MSF, among others TNFα, IL 1β or IL6, days after the injection, suggesting its implication in the inflammatory response (Hébert et al., 2003; Luchtman et al., 2009). Moreover, in chronic MPTP-injected primates were also found higher levels of IFNγ and TNFα, both in the sera and CNS (Barcia et al., 2011), suggesting a long-term response after the neurotoxic insult.

On the other hand, ROS and its possible implication in the progression of the disease and the neuroinflammation should be considered. There is reasonable evidence supporting an "oxidative stress hypothesis" for PD, that provokes the initiation of the DA neuronal loss in the SN (Beal, 2005; Jenner & Olanow, 1996; M. T. Lin & Beal, 2006; Owen et al., 1996). Oxidative stress occurs when there is an intracellular accumulation of ROS due to either the overproduction or the reduced capacity to metabolize them inside the cells. The brain is considered highly sensitive to oxidative damage, in part because oxygen consumption by the brain constitutes 20% of the total oxygen consumption in the body (Floyd, 1999). Specifically, the midbrain, and particularly the SN, functions under a pro-oxidative state, relative to other parts of the brain, becoming one of the most vulnerable regions to be affected by ROS dysregulation (J.-K. Lee et al., 2009), fact that could be related to PD progression, suggesting the oxidative stress hypothesis as a potential origin of the disease.

Considering the implication of cytokines and chemokines in PD, their role during the progression of the disease is still poorly understood. Inflammatory processes could be considered as a "double-edged sword" (Wyss-Coray & Mucke, 2002). As explained above, a neuroinflammatory reaction may be beneficial or detrimental for the brain tissue. During the first steps of the response, cytokines and chemokines are released to the brain parenchyma triggering signaling cascades to resolve the potential damage and return to a homeostatic state, ending the immune response. Hypothetically for PD, the potential harm may come when the response appears to be persistent, triggering new release of cytokines and chemokines, which, consequently, will induce further glial activation to be spread to neighboring cells. Then, the exacerbated and destructive immune response is thought to lead to a chronic inflammatory state that may become harmful for DA neurons (Barcia, 2013; Gao & Hong, 2008).

These aspects seen in neuroinflammatory processes along the time have been evidenced in parkinsonian-induced macaques (Barcia et al., 2004, 2011) and mice (Barcia et al., 2012), in which the effect of exacerbated cytokine release concur together with glial activation. In both models the glial activation was mediated by IFNγ signaling, aided by TNFα, suggesting that both cytokines are responsible for enhancing the activation of the surrounding glial cells contributing to neuronal degeneration (Barcia et al., 2011).

Specifically for PD, some genetic polymorphisms have been related with an enhanced inflammatory response. Polymorphisms in the LRRK2 gene are the most common variations with a direct implication in the neuroinflammatory response (Jimenez-Ferrer & Swanberg, 2018; Russo et al., 2014). LRRK2 could be involved in the IFNγ-mediated immune response (Gardet et al., 2010) but also contributes to TNFα production by microglia, which is critical for maintaining glial activation (Nayak et al., 2014). HLA-DR polymorphisms are other common alterations that have been reported to be related with an increase in the risk of suffering idiopathic PD (Hamza et al., 2010; Jimenez-Ferrer & Swanberg, 2018), as the HLA-DR is a receptor expressed in reactive microglia, polymorphisms in this gene may result in a more plausible exacerbated microglia and enhance the neuronal death.

As we have been postulating on this thesis manuscript, in the CNS, the neuroinflammatory response is mainly executed by microglial cells. However, the inflammatory response could also be orchestrated by macrophages, monocytes, and lymphocytes, among other cells. Nevertheless, some authors have described the implication of other glial cells, like astrocytes, besides microglia, as well as other immune cells coming from the bloodstream, such as lymphocytes, to be involved in PD pathogenesis.

Astrocytes are the more abundant glial cells of the CNS. Their function was first described by Ramon y Cajal and del Rio-Hortega as merely supporting cells for the brain parenchyma. However, currently astrocytes are intimately associated with many different and complex functions including synapses formation and plasticity (Gelders et al., 2018; Neal & Richardson, 2018), triggering an inflammatory response, balancing the debris clearance and restricting additional cytotoxic inflammation, among other tasks (Liddelow & Barres, 2017). Astrocytic reactivity is mainly detected by the expression of glial fibrillary acidic protein (GFAP), a component of their cytoskeleton. This protein has been found highly expressed in the areas of degeneration in PD patients (Barcia, 2013; Forno et al., 1992). Moreover, reactive astrocytes with high levels of GFAP expression were also present in the SNpc of macaques and mice after MPTP-exposition (Barcia et al., 2011; Saavedra-López et al., 2016). However, the role of

astrocytes reactivity in the parkinsonian degeneration is still scarcely known. One of the possibilities, as microglial cells, is to generate an overreactive response, where the neuroinflammation is exacerbated, and may become detrimental in pathological conditions such as PD (Gelders et al., 2018; Liddelow & Barres, 2017).

Regarding lymphocytes, they are immune cells orchestrating the adaptive immune response, however, they are not present in the CNS by its own. They mainly travel through the blood stream. Lymphocytes enter the brain through the active penetration of the BBB, then once inside the parenchyma perform specific immune responses. The presence of lymphocytes in the areas of DA degeneration have been described in PD samples as well as in models of PD, indicating a possible involvement in the progression of the pathology (Brochard et al., 2009; Galiano-Landeira et al., 2020). In postmortem samples of PD patients, the presence of Cluster of Differentiation (CD) 4^+ and $CD8^+$ T cells have been reported in the SNpc, but not B cells or NK (Brochard et al., 2009; Galiano-Landeira et al., 2020). The increase in CD8 is compatible with the increased expression of the β_2-microglobulin (which is a part of the major histocompatibility complex (MHC) I) in the striatum of parkinsonian patients (Kurkowska-Jastrzebska et al., 1999). (Vivier et al., 2011). Therefore, the neuroinflammation triggered in PD should be considered as a process that includes all types of immune response in the CNS even though we are still too far to fully understand all the implications (Saavedra-López et al., 2016).

3. Microglial cells and their role in neuroinflammation and PD progression

As already mentioned above, one of the key cells implicated in the parkinsonian neuroinflammatory response, are microglial cells. In the following sections we will describe their origin and functions as well as new insights in their implication in PD, a fundamental aspect of the present thesis.

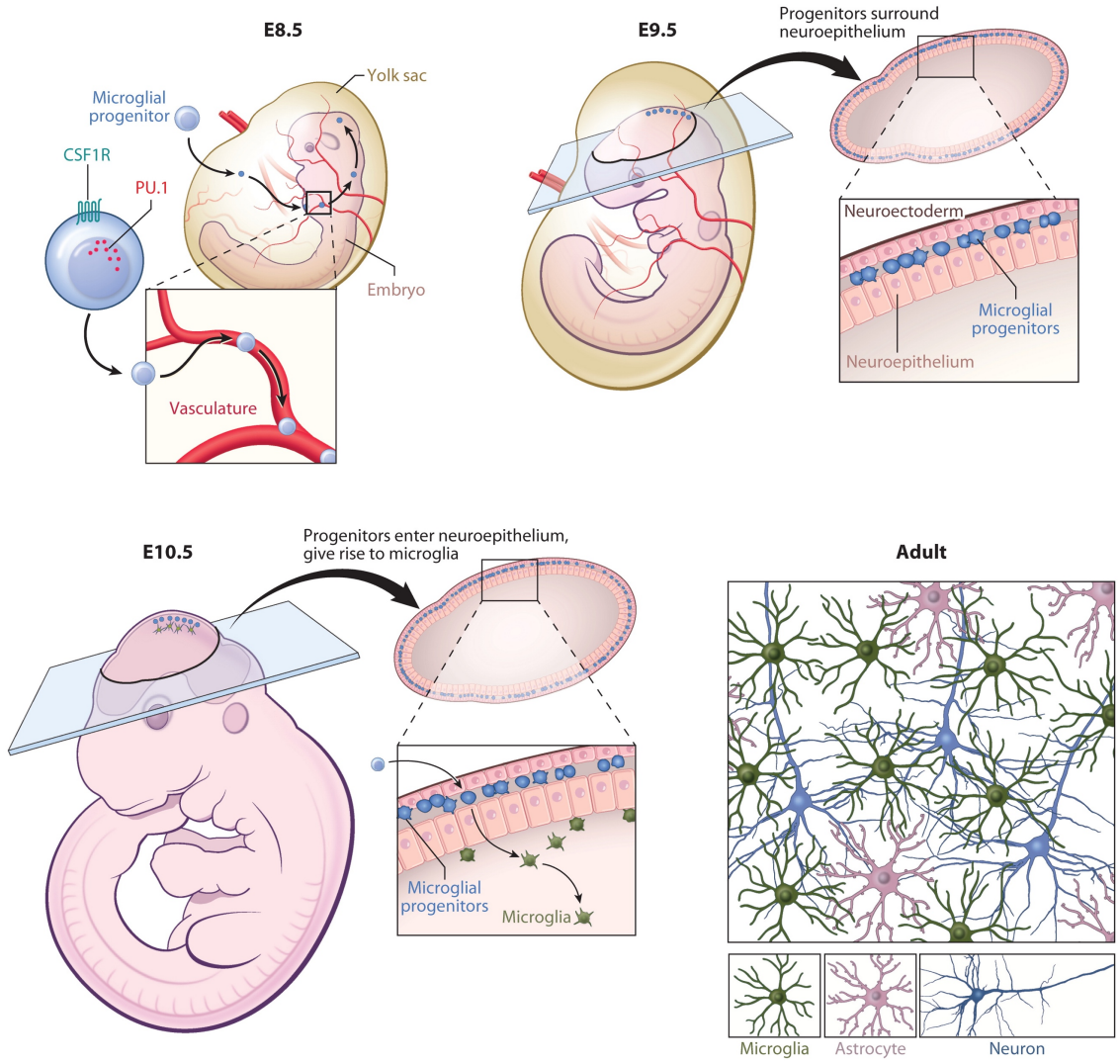
3.1. Origin of microglial cells

Microglial cells are the resident immune cells of the CNS. They were first described as the brain macrophages by del Rio-Hortega (Nayak et al., 2014; Pérez-Cerdá et al., 2015), with similar functions and origin. Del Rio-Hortega first described microglia as immune cells originated from the mesoderm that were then invading the CNS during the embryonic development, when the blood vessels began to form (Río-Hortega P, 1919). During years most of the scientific community assumed microglia of hematopoietic origin, deriving from the blood monocytes due to their similarities in markers and gene expression, morphology and phagocytic capacity (Pérez-Cerdá et al., 2015). Microglia express many macrophage-associated markers, such as CD11b, CD14, EGF-like module-containing mucin-like hormone receptor-like 1 (EMR1) – in mice known as the F4/80 receptor – or the colony-stimulating factor 1 receptor (CSF1R) among others (Saijo & Glass, 2011a). Some bone marrow reconstitution studies first showed that microglia were from myeloid origin and derive from the hematopoietic system (Eglitis & Mezey, 1997; Hickey & Kimura, 1988; Simard & Rivest, 2004).

However, other research lines also hypothesized an alternative origin for microglial cells, supposedly derived from the embryonic yolk sac. In the early 1990s, Cuadros *et al*. generated chick embryos with quail yolk sacs chimeras to identify the microglial origin. They found primitive myeloid cells invading the brain, independently from the blood supply during development (Cuadros et al., 1993). Unfortunately, although they provide a spatiotemporal map of where to find microglial cells during development, they could not specifically assert a different origin of microglia.

It was not until 2010, when the particular origin of microglia, different from macrophages and monocytes, was established. In the study by Ginhoux *et al*, two different transgenic mice strains were crossed. One of the strains had a reported only expressed in the yolk sac by tamoxifen administration, when they administered tamoxifen at different timepoints during the embryonic development they could fate map the yolk sac-derived cells *in vivo*. In the experiment, the injection of tamoxifen before the E7.5, revealed that microglia progenitors came from the

embryonic yolk sac (Figure 6), later entering the brain rudiment in a circulatory system dependent manner (Ginhoux et al., 2010).



Nayak D, et al. 2014.
Annu. Rev. Immunol. 32:367–402

Figure 6. Microglial origin and development. Recent studies have shown that microglia are ontologically distinct from bone marrow-derived monocytes/macrophages found in peripheral tissues. Microglia are derived from the embryonic yolk sac during development and posteriorly enter the brain rudiment via the circulatory system. At this stage microglia are mainly ameboid rather than ramified, while in a postnatal stage it is found completely ramified. (Adapted from Nayak et al., 2014).

During the embryonic development, microglial cells were detected in the mouse brain between embryonic days 8.5 and 10.5 (E8.5 and E10.5). In this states, microglial cells did not display the typical ramified processes while in the adult state, posterior to postnatal day 28, they were

found with a ramified phenotype commonly seen in the adult brain (Ginhoux et al., 2010). Once ramified, microglial cells were spread across the parenchyma (Nayak et al., 2014).

Posterior studies also confirmed the yolk sac derivation of microglia with the findings about the transcription factor Myb, which is required for hematopoiesis and the generation of hematopoietic stem cells (HSCs). The findings revealed that the Myb was not essential for the generation of microglia while it is needed to have normal numbers of monocytes/macrophages (Schulz et al., 2012).

3.2. Microglial morphology and phenotypes

In the adult brain, in a homeostatic state, microglia are described as cells with a small and rounded cell body with long and thin ramifications (Nayak et al., 2014), different from macrophages and dendritic cells (DCs). As part of their homeostatic roles, microglial cell bodies remain static while their processes are continuously exploring and scanning their surroundings (Davalos et al., 2005; Nimmerjahn et al., 2005), somehow communicating with neurons, astrocytes, and blood vessels (Nayak et al., 2014). This state, characterized by this particular morphology of microglia, is usually named “resting” state, however, we propose “scanning” state as a more proper name to be used in this manuscript. During this state, microglial cells palpate their surroundings looking for changes that could be deleterious for the brain parenchyma. This perpetual state of motion allows to rapidly respond to any damage or disturbances by transforming into an activated state and consequently perform repair functions (Nayak et al., 2014).

In this process of recognition and response to foreign or deleterious stimuli, achieving a pro-inflammatory phenotype, microglial cells change their morphology reaching an activated state, frequently referred as ameboid. This phenotype is characterized by shortened and extensively branched processes and hypertrophy of the cell body (Perry et al., 2010). In this context, microglial cells becoming reactive are stronger in terms of cell body and branches, meaning an increase in their shape.

The factors by which microglial cells are activated are broad, in consequence, they could display different phenotypes depending on the type of external input (Perry et al., 2007).

Microglial cells activation has traditionally been classified in two different phenotypes, a “classical” activated phenotype, also named pro-inflammatory, or an “alternative” activated phenotype, also known as anti-inflammatory (Saijo & Glass, 2011a). However, further studies

have described a number of intermediate phenotypes of activation that represents a spectrum between both ends with slightly differences in terms of morphology and gene expression along the spectrum (Martinez & Gordon, 2014; Ransohoff, 2016). Recently, some authors pointed to microglia as be named preferably "homeostatic" or "reactive" microglia depending on the state of action they are (Paolicelli et al., 2022). However, even though this classification is not precise, to oversimplify the reading we will name pro-inflammatory and anti-inflammatory reactive phenotypes.

Agonists for the Toll-like receptors (TLR), especially the TLR4 ligand LPS, and for the IFNγ receptor (IFNγR), the IFNγ, are the two factors to induce the change to a canonical pro-inflammatory phenotype *in vitro* (Figure 8). In contrast, most types of interleukins, such as IL4 and IL13 IL10 are commonly used to induce an anti-inflammatory phenotype, (Figure 8), in a process that supposedly oriented to repair the tissue-damage (Martinez et al., 2009).

However, a plethora of molecules are responsible for promoting an activated state of microglia. Many different pathological states, dysregulated molecules or misfolded proteins, typically found in the disease, could be accountable factors for triggering an activated phenotype; and, in consequence, the type of response. For example, smaller molecules and ions could also be released to the external environment, or cell-surface ligands, expressed by neurons, that may interact with microglial receptors (Perry et al., 2010). In response, microglial cells react in different ways, trying to reverse any disturbance (Neher et al., 2011a; Neumann et al., 2009), perform debris clearance, repair damaged tissue, etc.

In general, pro-inflammatory reactive microglia/macrophages are most commonly related with disease states driven by inflammatory processes (Colton, 2009; B. Liu & Hong, 2003; Odegaard & Chawla, 2011), in which the inflammation could become chronic. By contrast, anti-inflammatory reactive phenotypes are generally associated with protective role of microglia in which classical activation may result pathogenic (Saijo & Glass, 2011a). However, depending on the situation, this anti-inflammatory phenotype can be deleterious, such as in cancer, where it has been described reactive anti-inflammatory microglia in the surrounding regions of the tumour, promoting its survival (Sica et al., 2008).

3.3. Microglial function

Microglial cells, besides being involved in pathological scenarios, play also many other roles keeping the homeostasis of the CNS.

3.3.1. Homeostatic microglia

Microglial cells are essential for normal brain development. Microglia interact with neurons during development and in the adult CNS. During the early stages of brain development, some neurotrophic factors, such as EGF, BDNF, NGF (below described), are involved in promoting survival and differentiation of neuronal lineages and circuit formation (Nayak et al., 2014). At this time, microglia also contributes to the surrounding milieu by releasing specific trophic factors (below described), that promotes the formation and survival of neuronal circuits.

For example, one of the most important neurotrophic factors is insulin-like growth factor 1 (IGF-1), which promotes the survival of layer V cortical neurons during post-natal development (Ueno et al., 2013), is released by microglial cells that accumulate along this layer V early after birth. Specifically, this role for microglia was seen to be mediated by fractalkine (CX3CL1-CX3CR1) signaling, as a deficiency in CX3CR1 resulted in death of layer V cortical neurons (Ueno et al., 2013). Microglial-released IGF-1 not only promotes neuronal survival but also differentiation processes, like in multipotent adult rat hippocampus-derived neural progenitor cells, which differentiate into oligodendrocytes (Hsieh et al., 2004), as well as protects oligodendrocytes from apoptosis mediated by glutamate (Ness & Wood, 2002).

Furthermore, a number of trophic factors, participating in neuronal development, maintenance, and function of neurons, or other linked cells, are released by microglial cells; among others, basic fibroblast factor, hepatocyte growth factor, epidermal growth factor (EGF), nerve growth factor (NGF) or brain-derived neurotrophic factor (BDNF) (Araujo & Cotman, 1992; Nakajima et al., 2001; Trang et al., 2011; Yamagata et al., 1995), suggesting the essential role of microglia in the correct development and survival of the CNS. Also, during the neuronal development, not all immature neurons become mature and survive, approximately half of them die during the process of maturation (Nayak et al., 2014). These neurons are then programmed to die. The process of death is not fully understood but many studies point to microglia as one of the main players during the elimination process (Frade & Barde, 1998). In this scenario, microglial cells could both, contribute to the neuronal death by the secretion of factors, but then, at the same time, clear the resultant cellular corpses (Nayak et al., 2014).

Some precedents of this process have been observed, for example in the retina of the developing chick eye, where the release of NGF by microglia induced apoptosis of retinal nerve cells, as a normal process during the developmental program (Frade & Barde, 1998). Another example has been reported in the developing murine hippocampus, where cells are induced by microglia to undergo programmed cell death (Wakselman et al., 2008). In this region, microglia

releases ROS in a CD11b- and DNAX activation protein of 12 kDa (DAP12)-dependent manner (two important microglial proteins related with microglial reactivity) inducing neuronal death. Thus, microglia are not simply accessory cells that respond to neuronal cell death during development, but rather are active promoters of the process.

Microglia participate in the clearance of previously stimulated dying neurons with a phagocytic process but, importantly, without initiating an inflammatory response (Hristova et al., 2010; Marín-Teva et al., 2004; Takahashi et al., 2005a), that is, preserving a homeostatic state. It has been described this type of non-inflammatory phagocytic response is dependent on the triggering receptor expressed on myeloid cells 2 (TREM2) (Takahashi et al., 2005a). TREM2 promotes phosphorylation of DAP12 protein, which subsequentially induces cytoskeleton reorganization and phagocytosis (Mecca et al., 2018). In this pathway, regulated by TREM2, the typical pro-inflammatory cytokines are not expressed, such as TNFα, IL1β and Nitric oxide synthase 2 (NOS2); in fact, overexpression of TREM2 could actually decrease the proinflammatory potential of microglia (Mecca et al., 2018).

Microglia also participate in the modulation of neuronal synaptogenesis, via eliminating the excessive synaptic proliferation, which leads to a synaptic homeostasis (Paolicelli et al., 2011; Wake et al., 2009). During development, microglia is in contact with developing neurons, participating in the process of neuronal pruning by releasing neurotrophic factors. Some researchers also pointed to DAP12 as a key molecule for synaptic function and plasticity (Roumier et al., 2004), as its deficiency in mice provoked a dramatic reduction in synaptic expression of tyrosine kinase receptor B (TKR B) – receptor for BDNF – leading to impaired synaptic function and plasticity (Roumier et al., 2004). Besides, redundant and excessive neuronal processes, that have the potential to hinder mature neuronal circuit formation, are selectively pruned by microglia. This function of homeostatic microglia is essential for normal brain development (Kettenmann et al., 2013; Paolicelli et al., 2011). Paolicelli *et al*. demonstrated that during synaptic maturation these proteins localize to microglia, showing that microglial cells engulf synaptic structures in the uninjured brain. This synaptic pruning is also mediated by fractalkine signaling, as deficient CX_3CR1 mice had more spines density and less mature synapses when adult than normal mice (Paolicelli et al., 2011).

However, an exaggerated microglial pruning leads to abnormal synaptic development which may aggravate pathological diseases such as AD, schizophrenia, autism, or having detrimental effect in aging (Li & Barres, 2018; Vilalta & Brown, 2018).

All these data indicate that microglia play an important role during neuronal development, differentiation, dendritic spines formation, synaptic development and connectivity, as well as in the clearance of non-mature neurons, being considered as a homeostatic state, with no external or defective signals that may provoke its reactivity. However, microglia have extensively been studied during reactive activation, as they are crucial cells to promote an immune response in the brain.

3.3.2. Reactive (activated) microglia

In disturbances of the CNS, microglial cells have the capacity to sense extracellular inputs, and in consequence change their phenotype to a reactive state initiating a subsequent immune response, within the pro-inflammatory and anti-inflammatory spectrum, depending on the inputs that triggered this activation. Reaching this reactive state, microglia undergo dramatic biochemical and morphological changes, as previously mentioned, characterized, morphologically, by an increase of the cell body and shortened but thicker processes (Figure 7), finally transforming into the so called ameboid morphology (Saavedra-López et al., 2016).

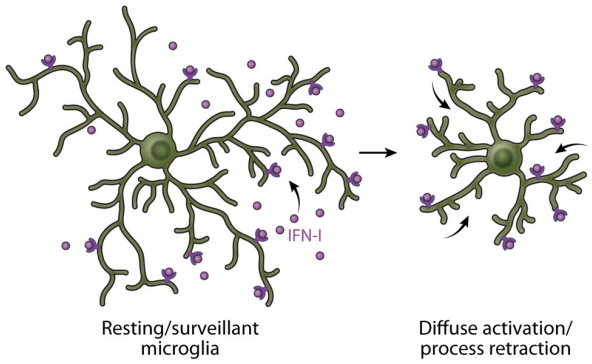


Figure 7. Microglial morphology changes. Diagrams showing the morphology of microglial cells when they are in a scanning or homeostatic state (left), with thin and long ramifications emerging from a small cell body, or when they become activated (right) [i.e. after IFN stimulus], with an increased cell body but also showing shorter and thicker processes (Modified from Nayak et al., 2014).

Reactive microglia rearrange surface molecules to induce cell motility, move to the site of the lesion and release multiple factors with inflammatory effects, which activate neighboring glial cells (Barcia, 2013; Heneka et al., 2014). Among the molecules that sensitize microglia, cytokines are key players, inducing pro-inflammatory and anti-inflammatory responses.

Cytokines such as TGFβ1, IL4, IL10 or IL13 activate microglia inducing anti-inflammatory pathways, promoting tissue repair and restricting the synthesis of pro-inflammatory cytokines

(Hirsch & Hunot, 2009; Tansey & Goldberg, 2010). Anti-inflammatory cytokines TGFβ1, IL4, IL10 may activate subsequent signal cascades in which, among others, the production of the suppressor of cytokine signaling (SOCS) 1 and SOCS 3 are enhanced. SOCS3 inhibits the production of pro-inflammatory cytokines in microglia/macrophages via the signal transducer and activator of transcription 3 (STAT3) (Yoshimura et al., 2007). As STAT3 is a transcription factor involved in the release of pro-inflammatory molecules, inhibiting this signaling pathway impedes microglia to become pro-inflammatory (Guo et al., 2022). Inhibiting STAT3 cascade leads microglia to upregulate the expression of major anti-inflammatory factors, such as IL4 and enhances anti-inflammatory function triggering the polarization towards the anti-inflammatory spectrum phenotype (Zheng et al., 2022). IL13 is another key cytokine with similar recognition by microglial receptors and subsequent anti-inflammatory signaling pathway. IL13 promotes the signaling cascade via the Janus activated kinase (JAK)-STAT6, which also upregulates the expression of anti-inflammatory phenotype (Junttila, 2018). In addition to IL4 and IL10, low-density lipoprotein receptor-related protein-1 (LRP1) also promotes the anti-inflammatory phenotype polarization of microglia (Jiang et al., 2021).

Additionally, peroxisome proliferator-activated receptor γ (PPARγ), a nuclear receptor, also plays an important role in anti-inflammatory responses (Neve et al., 2000). PPARγ agonists were found to reduce the activation of nuclear factor kappa B (NF-κB) (X. Zhao et al., 2006), since this molecule is directly implicated in the transcription of genes which proteins are involved in inflammatory responses, most of them of pro-inflammatory origin. Reducing the activation of NF-κB may result in a decrease of production in the pro-inflammatory microglial factors, such as inducible nitric oxide synthase (iNOS), TNF α, and IL1 (X. Zhao et al., 2007).

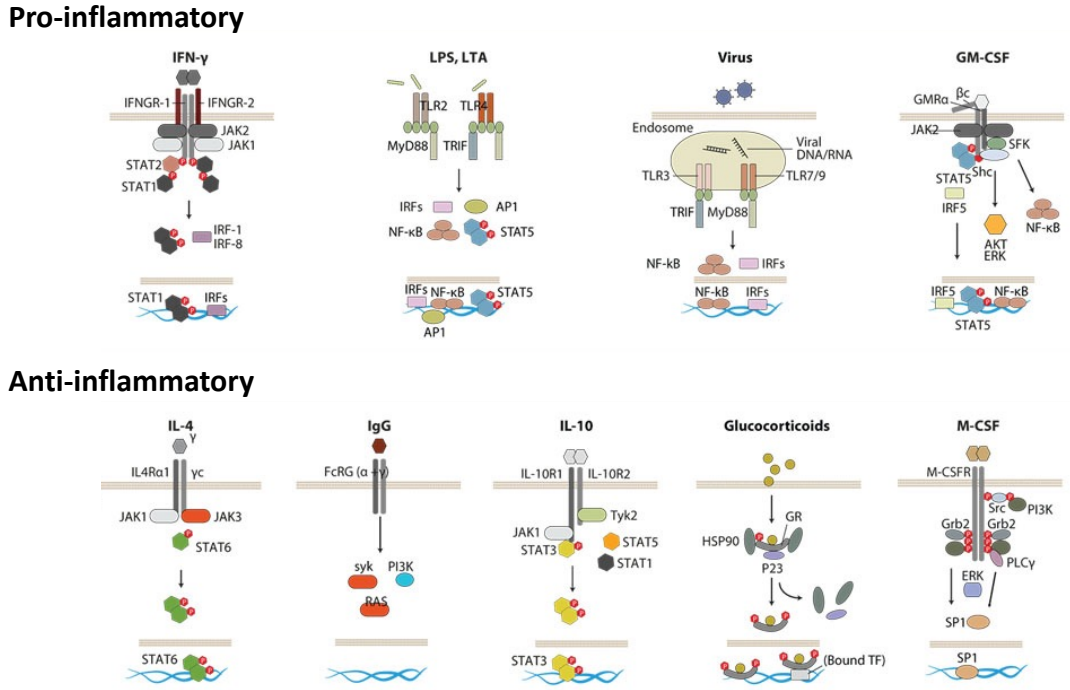


Figure 8. Diagram showing potential signaling of microglia/macrophages towards pro-inflammatory or anti-inflammatory phenotypes. Illustration of the different factors and signaling cascades that intervene in turning the microglia/macrophages to pro- and anti-inflammatory phenotypes. For example, cytokines like IFNγ are capable of activating microglia into a pro-inflammatory phenotype, whereas IL4 and IL10 are turning microglia to an anti-inflammatory phenotype (Modified from Martinez & Gordon, 2014).

On the other hand, pro-inflammatory cytokines, like TNFα, IFNγ, IL1β and IL6 promote the activation of pro-inflammatory pathways. This pro-inflammatory response induces the clearance, removal and phagocytosis of elements that alter the CNS parenchyma, temporarily, with the purpose of neutralizing any harmful substances as well as stopping new release of inflammatory cytokines and chemokines (Gomez-Nicola & Perry, 2015). However, an extended proinflammatory phenotype of microglia, the secretion of pro-inflammatory cytokines, chemokines and other neurotoxic mediators increases (H. Zhao et al., 2015). This provokes a chain reaction in which more reactive microglia results in increasing activation of pro-inflammatory signaling cascades, spreading the reactivity of surrounding microglia. The secretion of pro-inflammatory microglia-specific chemokines may also lead to the infiltration and recruitment of blood leukocytes, which exacerbates the inflammatory response (Yao & Tsirka, 2012). This phenomenon may become a chronic neuroinflammatory process that may have detrimental consequences contributing to neurodegeneration (Barcia, 2013; Gao & Hong, 2008).

As said above, NF-κB regulates the transcription of pro-inflammatory phenotype related genes. NF-κB is canonically activated by the TLR4 signaling pathway, when stimulus, such as LPS, activates the cascade by the TLR4 receptor, the transcription factor NF-κB translocate to the cell nucleus, to induce a pro-inflammatory response (Taetzsch et al., 2015). This response occurs in the CNS, as in human brain tissue, NF-κB p65 was detected to be expressed in the nuclei of glial cells (Z. L. Zhang et al., 2015) and was associated with elevated IL1β and TNFα levels, confirming its role in the secretion of pro-inflammatory cytokines.

Moreover, the IFNγ molecule has been seen increased in some neuroinflammatory processes (Barcia, 2013). IFNγ via the IFNγR contributes to the polarization of microglia to a proinflammatory phenotype leading to a significant increase in the expression of iNOS, which subsequently provokes an increase in the number of pro-inflammatory microglia (P. Chauhan et al., 2017, 2021; Gordon & Taylor, 2005; Villalta et al., 2009).

In experimental models *in vitro*, this type of pro-inflammatory response is induced by the exposure to LPS and IFNγ, which is considered the canonical pro-inflammatory polarization (Martinez & Gordon, 2014). However, in the absence of antigens, as LPS, similar responses, within the pro-inflammatory spectrum, could be also triggered as a result of trauma, ischemia, chemical exposure (G. Y. Chen & Nuñez, 2010; McPherson et al., 2014; Shechter & Schwartz, 2013), degeneration or other alterations of the brain parenchyma. Microglial response in this stimulation produces pro-inflammatory cytokines, as explained above, such as IL1β, IL6 or TNFα; but also chemokines, and other compounds. Among them, redox molecules, such as nicotinamide adenine dinucleotide phosphate (NADPH) oxidase, phagocytic oxidase or iNOS; and co-stimulatory proteins, such as MHC-II (Boche et al., 2013; Colton & Wilcock, 2010; Hanisch & Kettenmann, 2007; Henkel et al., 2009; Ransohoff & Perry, 2009; Varnum & Ikezu, 2012) that contribute to the propagation of the inflammatory response. These transformations of microglial morphology, phenotype, and function are observed during almost all neuropathological conditions (Nayak et al., 2014).

3.4. Neuroinflammation mediated by microglia in PD

As already mentioned, PD is neuropathologically characterized by the loss of DA neurons in the SNpc, the accumulation of particular α-synuclein aggregations (Braak, Del Tredici, et al., 2003; Lashuel et al., 2013; Spillantini et al., 1997) and accompanied by some relevant signs of glial-mediated neuroinflammation. However, since the first relevant analyses performed in post-mortem tissue of parkinsonian patients, finding reactive HLA-expressing microglial cells in the

areas of degeneration (McGeer et al., 1988), their implication in the progression of the disease has been controversial. After decades of research, the precise contribution of microglia to PD is not entirely understood, but their potential participation include the chronic production of proinflammatory molecules as well as the modulation of adaptive immune cells (Nayak et al., 2014).

It is not known whether microglial activation precedes or follows DA neuronal loss. Potentially, the death of DA neurons in PD may induce the activation of neighboring microglial cells, via the purinergic receptors, among others. On the other hand, underlying microglial activation may also be responsible for new DA neurodegeneration. Furthermore, aggregated proteins, such as α-synuclein in LBs, of disease-affected DA neurons are likely to promote a self-propelling cycle of microglial activation. Thus, increasing the production of inflammatory mediators in the SN, providing a multifactorial environment that may spread the PD-associated dysfunction to neighboring neurons (Y. S. Kim & Joh, 2006; Sulzer, 2007; W. Zhang et al., 2005).

Conversely, activation of microglia by external agents, as the bacterial antigen LPS, is sufficient to cause DA loss in the SNpc (Herrera et al., 2000). Some studies revealed that a single dose of LPS performed directly into the SNpc of mice brains induced a drastic microglial inflammatory response, followed by the death of DA neurons (Dutta et al., 2008) intraperitoneally LPS, when injected, induces the activation of the TLR4 signaling pathway, which results in a massive neuroinflammatory response (Heman-Bozadas et al., 2022).These responses largely affect the parenchyma and DA neurons in the SNpc, being eliminated consequently. In contrast with the expected outcome of any neuroinflammatory response, which ultimately should be resolved, chronic death of DA neurons enhanced by microglial reactivity would potentially result in a chronic, and hence pathological form of microglial cell-mediated neuroinflammation (Saijo & Glass, 2011a). However, few studies have linked the PD onset to a viral or bacterial infection; the more plausible explanation would be that the immune responses may be triggered secondary to cellular damage or neuronal loss in the affected regions of the CNS with the same signaling pathway occurring in an LPS-mediated infection (Hirsch et al., 2012).

As part of their neurotoxic potential, activated microglia can induce the production of enzymatic complexes including NADPH and iNOS. These enzymes form superoxide (O_2^-), nitric oxide (NO) and hypochlorous acid (HOCl) (Hunot et al., 1996; D. C. Wu et al., 2003) and could create a toxic oxidative environment damaging enclosed DA neurons (Hunot et al., 1996). Studies performed in post-mortem samples of idiopathic PD human brains revealed a significant iNOS-immunoreactivity in the activated microglia in the surroundings of the SNpc. Moreover, in the

parkinsonian rodent model, treated with MPTP, microglial activation in the SNpc has been linked to the induction of the NAPDH oxidase. In fact, the upregulation of the NADPH oxidase correlates topographically and temporarily with the DA degeneration seen in the MPTP and PD brains (D. C. Wu et al., 2003).

Altogether, the combination of LPS with the previous priming with IFNγ signaling, promotes the activation of a pro-inflammatory phenotype assimilable to a parkinsonian scenario (Casanova et al., *in prep*). Knowing that higher levels of IFNγ were detected in the sera of PD patients (Mount et al., 2007b), and microglia is highly sensitive to IFNγ activation in experimental models of PD (Barcia et al., 2011), point to this signaling pathway as a clear candidate. In addition, knowing the potential toxicity of microglia enhancing the activity of the NADPH and iNOS complexes, which are reported to be increased in parkinsonian samples, both in patients and experimental models (Hunot et al., 1996). And the number of studies performed in parkinsonian scenarios in which they corroborate the presence of high amounts of reactive microglia with the progression of the disease (Barcia, 2013; Barcia et al., 2004, 2009; Hirsch et al., 2012; J.-K. Lee et al., 2009; McGeer et al., 1988; McGeer & McGeer, 2004), give a reasonable body of evidence on the direct implication of microglia in the DA degeneration. To execute the process by which microglia finally eliminate DA damaged neurons, a complete but complex set of steps are needed to be accomplished.

3.5. Modulation of microglia during a neuroinflammatory process

Microglial cells could adapt different morphologies depending on their state of action in which they are and within the morphology differs the movement they do.

As already mentioned, homeostatic microglia are constantly moving, by elongating or retracting their processes scanning their surroundings (Nimmerjahn et al., 2005). However, the type of movement of microglia is different depending on the environment. In the brain cortex, microglial processes and protrusions are directly in contact with astrocytes, neurons, and blood vessels (Nimmerjahn et al., 2005), thus, depending on the stimulus, microglial cells could respond differently. For example, after focal stress, microglial processes are extended towards the injured site to shield the injured area. In this context, it has been established that ATP, released by damaged neurons or astrocytes, is a crucial regulator of microglial process dynamics and the rapid response towards the injury (Davalos et al., 2005). However, If the stimulus is neuroprotective, neurons could send signals to microglia to repress their pro-inflammatory response, remaining homeostatic.

Notwithstanding, it is essential to differentiate between the homeostatic movement of microglia in a surveillant mode, and migration and displacement after activation. The use of two-photon microscopy (TPM) has allowed to see these differences. TPM normally uses animals with fluorescent labels, most commonly by visualizing microglia with green fluorescent protein (GFP) inserted in the specific gene CX_3CR1, which encodes microglial-specific fractalkine. These real-time imaging revealed that microglia are highly dynamic cells in a homeostatic state (Davalos et al., 2005; Nayak et al., 2012; Nimmerjahn et al., 2005), constantly moving their branches, but keeping their cell body in place. In contrast, when microglia become reactive, they first move their branches polarizing them towards the stimulus source to finally move and displace their cell body, towards the target. Before this breakthrough reported *in vivo*, time-lapse video microscopy studies were the first describing that microglia were very dynamic cells when being studied in an *in vitro* model with rat microglial cultures. These microglial cells were recorded continuously extending and retracting their processes (Booth & Thomas, 1991; Thomas, 1990). Later, another observation of microglial dynamics performed in acute cortical brain slices, revealed that fluorescently labeled microglia moved and extended its processes towards the cut surface, which suggested a specific response to the injury (Brockhaus J et al., 1996). Additionally, experiment using cultured brain slices showed how ameboid microglial cells migrate towards the regions of excitotoxicity-induced neuronal degeneration (Heppner FL et al., 1998). These studies anticipated the characteristic motility of microglia, and together with TPM analysis confirmed the difference between movement and migration after reactivity. While microglia is constantly moving the processes, until there is no clear stimulus provoking the activation, the complete transformation from a ramified to an ameboid morphology, in which the processes are being retracted, is not produced. When activation occurs, microglial cells start the cellular migration (Dailey & Waite, 1999; Stence et al., 2001), different from the cellular movement performed when surveillance. Given that, when a stimulus induces reactivity, microglia will first extend their branches towards the stimulus, polarizing most of them (Figure 9) with a clear number of branches polarized towards the stimulus, and then adapt to an ameboid morphology facilitating the displacement through the parenchyma. Depending on the stimulus and the signaling pathway stimulated, the response may be different, whether in the anti- or pro-inflammatory spectrum; but after polarization the migration will end up towards the target.

Following the polarization and migration towards the stimulus, microglia will potentially conduct the repair of the tissue damage or drive the clearance of the injured tissue. Most frequently, after the migration towards the stimulus, microglia will exert their phagocytic capacity in the injured site (Figure 9).

Phagocytosis is an essential process of the innate immune response which represents a primary defense against pathogens during infection and clearance of cellular debris produced during normal brain development and injuries (Brown & Neher, 2014; Fricker et al., 2012). Phagocytosis is defined as the cellular process of sensing and engulfing particles larger than 0.5 μm, which also involves dramatic changes in the morphology and migration of the cell, an essential process to restore the brain parenchyma to homeostasis (Barcia et al., 2012; Janda et al., 2018; Uribe-Querol & Rosales, 2020). The particle is internalized into a phagosome, this phagosome changes structure of the membrane and the composition of its contents in a process known as phagosome maturation, with a final process of digestion of the ingested particle (Uribe-Querol & Rosales, 2020). Microglia are said to become highly phagocytic when reactive. Although other types of cells of the brain are able to accomplish phagocytosis, they are not as efficient as microglia, thus microglial cells are termed as professional phagocytes (Fricker et al., 2012; Uribe-Querol & Rosales, 2020).

The number of stimuli that promote the change between homeostatic motility to the ameboid migration are broad. As mentioned above, TPM showed, that after focal laser injury, microglia projected their processes towards the damaged brain tissue by an ATP-dependent mechanism using purinergic receptors (Davalos et al., 2005; Nimmerjahn et al., 2005) (Figure 9). Microglia has been seen to express several relevant purinergic receptors, among others $P2Y_{12}R$ or $P2X_6R$, which allow the cells to be sensitive to slight ATP concentration changes. The ATP, released during brain injury, generates a gradient that promotes the polarization of the microglial branches towards the specific site where the stimulus comes from (Figure 9); followed by the subsequent migration of the cell and finally reaching the target to perform a specific function (i.e. phagocytosis) (Figure 9) (Davalos et al., 2005; Haynes et al., 2006a; Honda et al., 2001; Koizumi et al., 2007a; Ohsawa et al., 2007, 2010). Because microglial process extension usually precedes cellular movement or phagocytosis, inhibition of any relevant purinergic receptors can negatively impact the overall dynamic response of microglia to focal injury (Nayak et al., 2014).

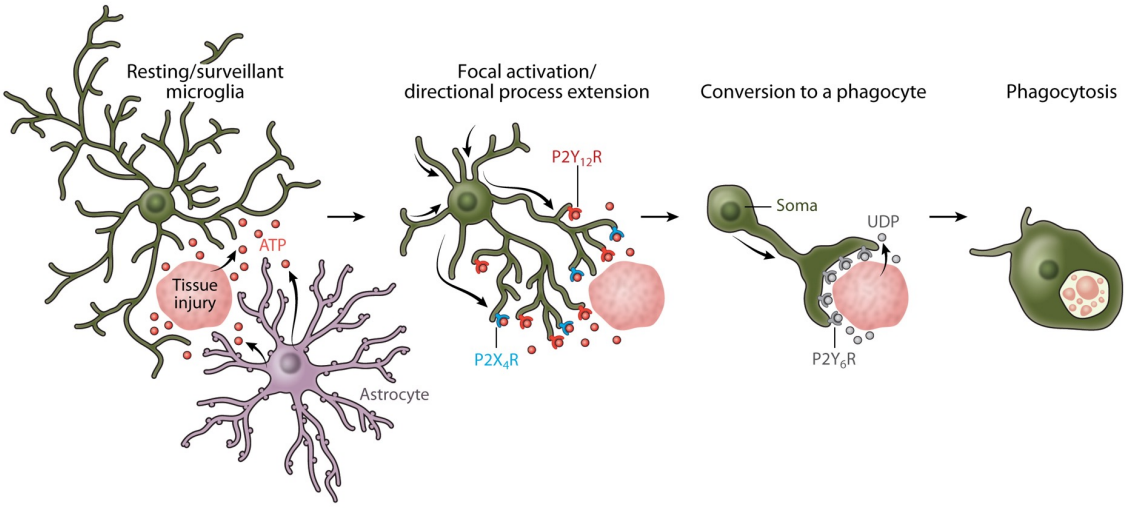


Figure 9. Microglial polarization after tissue injury. Representation of a microglial cell near a brain tissue injury, which secretes ATP to the external milieu. Microglia, via the purinergic receptors ($P2Y_{12}R$ or $P2X_4R$), sense ATP and in consequence most of its branches are polarized towards the injured tissue. Once polarized, microglial cell is converted to a phagocyte also via purinergic receptor (P2Y6R) by UDP and becomes fully activated ending the process of phagocytosis (Modified from Nayak et al., 2014).

In contrast with sterile injury responses, when there is an infection in the CNS, TPM revealed that the response of microglial cells is morphologically different, being diffused rather than focal (Nayak et al., 2013). This results in a broad activation of microglial cells, turning all of them ameboid with the even retraction of their processes. In addition, during this type of infections, the mechanism by which microglia undergo these morphological changes was detected to be IFN-I-signaling dependent. Nayak and colleagues performed an infection with a noncytopathic virus, the lymphocytic choriomeningitis virus (LCMV), and observed that in the absence of IFN-I-signaling, microglial cells seemed to be unresponsive to the infection, remaining in their scanning phenotype (Nayak et al., 2013). These data indicate that IFN-I rather than purinergic receptor signaling could be responsible for microglial dynamics and activation, at least with viral infections (Nayak et al., 2014).

Studies performed with TPM in a murine model of AD revealed that amyloid deposition precedes the activation and migration of microglial cells (Meyer-Luehmann et al., 2008). In this study, microglial cells were actively recruited towards existing plaques, and newly formed plaques, but were not able to eliminate them (Meyer-Luehmann et al., 2008). However, as they were not seen actively phagocytosing the plaques, they were proposed to be participants in preventing the formation of new plaques. Another TPM study, using the same AD mice model, confirmed that microglial cells, associated with plaques, phagocytose some amyloid-β (Aβ) peptides and restrict further plaque growth (Bolmont et al., 2008). During this process of establishing

interactions and phagocytosis of neuronal debris or protein aggregations by microglial cells, some proteins, like fractalkine, play a critical role. Studies performed with fractalkine receptor CX_3CR1 knock out (KO) mice revealed increased neuronal death in a model of AD compared with animals with normal fractalkine levels, suggesting that fractalkine signaling may contribute to neuronal cell protection (Fuhrmann et al., 2010).

Related to PD progression, both *in vivo* and *in vitro* investigations have shown that NM from degenerating DA neurons is a potent trigger of microglial cells activation, stimulating the production of pro-inflammatory mediators and the upregulation of the NF-κB and p38 mitogen-activated protein kinase (MAPK) signaling pathways (Hirsch et al., 2012). This process would, hypothetically, be followed by the dynamic polarization of microglial cell branches and the subsequent migration of the entire cell to those inputs potentially trying to eliminate the NM aggregations.

3.6. Implicated molecules during microglial sensitization, migration, and phagocytosis

Besides the sensitization induced by cytokines and chemokines, many other factors are also involved along the different phases of microglial activation and phagocytic process, triggering a specific action in every step.

First, specific receptors recognize ligands on external particles. Second, these receptors trigger intracellular signals that lead the polymerization and rearrangement of filamentous actin and coordinate the process of particle internalization. Third, membrane trafficking is indispensable to reorganize the loss of surface membrane, due to the internalization, and to create a phagosome (Aderem, 2002). Among the main molecules implicated in the steps of the process are the following.

3.6.1. Purines and purinergic receptors

In the process of activation of microglial cells, the purinergic receptors play an essential role. Based on their endogenous ligands, purinergic receptors are classified into P1 or adenosine receptors (ARs), P2X (P2XR) and P2Y receptors (P2YR) (Abbracchio et al., 2006; Fredholm et al., 2011). There are four different ARs, while within the P2 receptors we differentiate 7 subtypes of P2XR, which are ion channels; and the P2Y subfamily, with 8 different subtypes, that are G protein-coupled receptors (GPCRs) (Zarrinmayeh & Territo, 2020).

The native agonists for these fifteen different receptors are purine nucleosides for the ARs and purine and pyrimidine nucleotides for the P2Rs (Burnstock, 2008). In the CNS, ATP has been

reported to act as an extracellular signaling molecule which controls communication between brain cells (Burnstock, 2006). When the homeostasis of the brain parenchyma in well regulated, ATP is implicated in basal signaling pathways. However, under pathological conditions or insults, such as neuroinflammation or neurodegenerative disorders, high concentrations of ATP are released to the extracellular space as a danger signal, starting a signaling cascade promoting microglial polarization (Roszek & Czarnecka, 2015; Yegutkin, 2008).

Purinergic receptors for ATP, UTP and their metabolites are known to regulate inflammatory responses, including immune cell recruitment and cytokines release (Abbracchio & Ceruti, 2007; Burnstock, 2007; Riteau et al., 2010; Trautmann, 2009; Tsuda et al., 2003). These purines are sensed by microglial cells via the purinergic receptors, which in consequence undergo morphological and phenotypic changes to remove cell debris from the injured or damaged site (Inoue, 2008). When microglial cells are in a homeostatic state, some of these P2R are more expressed than others. When microglial cells become active results in the upregulation of $P2X_4$ and $P2X_7$ (Di Virgilio et al., 2017; Ulmann et al., 2008) receptor subtypes, while the $P2Y_{12}$ receptor expression is downregulated (Haynes et al., 2006a). This balance between the expression of these three receptors dictate the destiny of microglia (Vázquez-Villoldo et al., 2014). Increased levels of $P2X_4$ and $P2X_7$ receptors indicate microglial reactivity, while increased levels of $P2Y_{12}R$ indicate keeping a homeostatic phenotype (Burnstock, 2007). Moreover, $P2Y_1$ and $P2X_7$ receptors have been described to promote the migration of ramified microglia to the damage site with large amounts of ATP, consequently starting the phagocytic process enhanced by the $P2Y_6R$ (Boué-Grabot & Pankratov, 2017; Burnstock, 2008). Moreover, $P2Y_2$ and $P2Y_4$ are reported to be implicated in the regulation of the phagocytic activity and dying cell removal upon leaked UTP and UDP (Hide et al., 2023), while the $P2Y_6R$ seems to be the main receptor executing the phagocytosis of cellular debris (Inoue, 2007; Koizumi et al., 2007b).

Both P1 and P2 receptors are ubiquitously expressed in the CNS. Moreover, the implication of these purinergic receptors in the inflammatory response of some neurodegenerative diseases such as PD, AD, HD, and multiple sclerosis has been widely described (Burnstock, 2008, 2016, 2017; L. Chen & Brosnan, 2006; Pinna, 2014; Woods et al., 2016). Furthermore, it has been reported that not only neurons but microglia and astrocytes are also able to release ATP through a hemichannel when exposed to Aβ, suggesting that glial cells likely contribute to pathogenesis, by providing endogenous agonist or purinergic receptors activation (H. J. Kim et al., 2012; Orellana et al., 2011).

3.6.2. Fcγ receptors and IFN γ signaling

As IFNγ is one of the key cytokines directly implicated with the process of microglial activation and specifically in the PD scenario (Barcia et al., 2011) leading to phagocytosis, the implication of the Fcγ family receptors during the process of activation is plausible and it has been previously proposed (Orr et al., 2005). In addition, recent studies of our group have demonstrated the role of FcγR in the DA degeneration (Casanova et al., *in prep*). Importantly, IFNγ through JAK signaling cascade, which subsequently activates the STAT pathway, increases the expression of FcγR (Ding et al., 2022).

Fc receptors (FcR) are present in some populations of immune cells recognizing different type of immunoglobulins (Ig), including microglia. Depending on the type of the recognizing Ig, they are named differently. Among the Fc receptors, Fcγ receptors (FcγR) form a very important family, which recognize IgG antibodies, the most common opsonizing antibodies in an immune response (Fridman, 1991). Inside the FcγR family, there are three different subtypes: FcγRI, FcγRII and FcγRIII, binding different subtypes of IgGs (Fridman, 1991).

The role of FcγR in response to IgG-induced opsonization have been studied in a murine model of PD. In this study, PD-derived IgG injected in the SNpc increased the numbers of microglia compared with controls. These microglial cells remained in some cases ramified with small cell bodies, that said, in a homeostatic state; but some of them became hypertrophic with round cell bodies and thicker processes (He et al., 2002). However, when used FcγR KO mice, and performing the same PD-derived IgG injection, the number of microglial cells after the inoculation did not change, remaining not only the same amount but with non-reactive phenotype (He et al., 2002). Most importantly, when measuring the number of affected TH neurons, while FcγR positive mice showed a significant decrease after the injection; the FcγR KO mice did not undergo a significant TH cell loss in the SNpc (He et al., 2002). These results suggest a direct implication of the FcγR, in microglial reactivity and subsequently eliminate neurons. Remains, however, unknown whether this phenomenon occurs physiologically in the disease.

On the one hand, IFNγR immunodeficiency is associated with a decrease in the level of macrophage activation (Deckert-Schlüter et al., 1996) and a reduction of iNOS messenger ribonucleic acid (mRNA) levels (Rottenberg et al., 1999), which ends up in an impaired immune response mediated by IFNγ (de Vor et al., 2016; E. Y. Lee et al., 2013). On the other hand, the overexpression of the IFNγR could activate or even enhance the inflammation or specific injury-related signaling to induce human diseases.

IFNγ not only affects microglia and macrophages. Astrocytes also become reactive and potentially neurotoxic in some neurodegenerative diseases (Hashioka et al., 2009), such as ALS, AD, PD and multiple sclerosis, in which IFNγ signaling is upregulated, including the expression of IFNγR. Specially in parkinsonism, the upregulation of the IFNγR within the increase in the IFNγ signaling combined with TNFα promotes and maintains glial cell activation (Barcia et al., 2011). Thus, the IFNγR signaling pathway appears to be essential in initiating and maintaining the glial-mediated immune response.

3.6.3. LPS and Toll-like receptors

As previously mentioned, TLR are the key receptors promoting a pro-inflammatory response. Microglia express various types of TLRs including TLR1-9 (Bsibsi et al., 2002; Olson & Miller, 2004). The expression of these TLRs on microglia is increased by pathogens or other pro-inflammatory stimuli (Olson & Miller, 2004). Thus, the presence of TLRs in the microglial surface plays crucial roles generating neuroinflammation in response to different agents as LPS. When TLRs are induced by the corresponding stimuli provokes a signaling cascade in microglial cells that at the end provokes the release of different type of cytokines. For example, as explained above, TLR4 and TLR2 are involved in sensing the LPS stimulus and in consequence activate the signaling cascade of the transduction of NF-κB to subsequently transduce pro-inflammatory genes of the corresponding cytokines.

Studies performed in an experimental model of AD, Aβ aggregates are able to bind to TLRs to stimulate the innate immune response by inducing a pro-inflammatory response which activates microglia and removing the Aβ in consequence (K. Chen et al., 2006; Landreth & Reed-Geaghan, 2009; Richard et al., 2008). Furthermore, when a mutation is experimentally induced in the TLR4 expression, mice have reduced microglial activation levels, which results in low expression of pro-inflammatory cytokines and, in consequence, increases the deposition of Aβ forming plaques (Song et al., 2011; Tahara et al., 2006). When antagonists for TLR2 and TLR4 are used in experimental models of AD, provokes a reduced production of nitrites, TNFα, and IL6 (Walter et al., 2007). In addition, microglial cells lacking the expression of these two receptors are unable to generate a pro-inflammatory response (Jana et al., 2008; Reed-Geaghan et al., 2009).

On the other hand, other TLRs, like TLR3, are involved in promoting the survival of neurons after cerebral ischemia (Jeong et al., 2016). However, when stimulated with polyinosinic-polycytidylic acid (poly(I:C)), this TLR upregulates the pro-inflammatory pathway followed by the induction of NF-κB transduction (Olson & Miller, 2004). In this study, they demonstrated that activation

of microglia with a variety of TLRs agonists increased the expression not only of the pro-inflammatory cytokines but also up-regulates the expression of co-stimulatory molecules and MHC class II, which could sensitize T cells.

3.6.4. MHC/HLA

HLA are proteins encoded within the genes of the MHC. MHC genes are found to be highly polymorphic, coding for proteins involved in discrimination between self and non-self antigens (Carey et al., 2019). While MHC are the usual nomenclature for most animals, HLA is the homologous nomenclature for humans. They play a significant role in disease and immune defense, either beneficial or detrimental, depending on the stimuli. Two different class of MHC proteins are found, class I and class II.

MHC I and II molecules present protein fragments to $CD8^+$ and $CD4^+$ T cells, respectively, being essential for cell-mediated immunity. Nonetheless, MHC I and MHC II molecules are unique in the proteome due to their high number of polymorphisms, there are more than 10,000 different alleles for each one. The type of polymorphism each individual presents may differ in how the immune response could be triggered (Rock et al., 2016). These MHC molecules interact with the T cell receptor (TCR) and, depending on the polymorphisms, and their specificity for the TCRs, it will be recognized differently. Importantly, when there is a pathogen stimulus which could promote its recognition, one of its antigen epitopes could be recognized, for example, in one individual and then presented to the T cells, triggering the immune response; but not in another individual. This recognition and presentation depend on the MHC polymorphism present (B. V. Schmid et al., 2010). Therefore, MHC polymorphism is good for the survival of the population and not necessarily the individual.

Regarding humans, HLA class I (as MHC I) is found on the surface of all nucleated cells, these antigens are presenting intracellular peptides to the immune system to be recognized as self-peptides, avoiding the assault of the immune system. Then, HLA class II (or MHC II) is present uniquely on specialized antigen-presenting cells (APCs), such as dendritic cells, monocytes, macrophages and, in the brain parenchyma, microglia (Batista & Harwood, 2009). The level of HLA expression on each cell is, however, changeable. Pro-inflammatory cytokines upregulate the expression of HLA class I in all the cells but, but importantly, induce increased levels of class II MHC to enhance the presentation specifically on non-APCs, like T cells (Butler et al., 2017; van den Elsen, 2011; Van Den Elsen et al., 2004).

Within the HLA class I, there are several subtypes playing different roles. HLA-A, B and C, are specialized in detecting and eliminating virus-infected cells. And HLA-E, F and G, play immunoregulatory functions (Braud et al., 1999; Van Den Elsen et al., 2004). Then, regarding the HLA class II family, which are of importance for the microglial function in this thesis; there are also different subtypes: HLA-DR, DQ and DP. These molecules, besides playing a role in the initiation of the immune responses, are also involved in some autoimmune disorders (Van Den Elsen et al., 2004). Importantly, MHC II molecules are induced by some inflammatory cytokines, including IFNγ, which, as indicated, could be related with the progression of degenerative disorders (Boss & Jensen, 2003) as PD.

In fact, patients with senile dementia, related with AD, and in PD human samples show substantial numbers of HLA-DR-positive reactive microglia in different brain areas, including the SNpc (McGeer et al., 1987, 1988). This suggests a relationship between the DR polymorphism or subtype and the reactive microglia/macrophages response, and, consequently, how aggressive the immune response could be. Anti-HLA-DR monoclonal antibodies were reported to abolish the capacity of antigen presentation, promoting the silencing of the immune response to some infectious antigens (Hirayama et al., 1986, 1987; Kikuchi et al., 1986; Nishimura & Sasazuki, 1983; Sone et al., 1985). This reinforce the idea of the implication of HLA-DR polymorphisms in how the immune response is being triggered .

Therefore, HLA-DR is critical for triggering an immune response and it is plausible that depending on the polymorphism present in the deoxyribonucleic acid (DNA) for this HLA class II, microglia or other populations of cells, would become reactive, enhancing the progression of some diseases. In the case of PD, wide genomic studies have detected polymorphisms for HLA-DR, suggesting a potential contributor to the origin of the disease (Hamza et al., 2010).

3.6.5. TREM2-DAP12

TREM2 is a protein included in the cell membrane innate immune response receptors family. There are different receptors encoded by the TREM gene, which are linked to the MHC gene (Colonna, 2003). Among them, TREM1 and TREM2, which activate myeloid cells by signaling through the adaptor protein DAP12. TREM1 is expressed on mature neutrophils, monocytes and macrophages and triggers phagocyte secretion of pro-inflammatory cytokines and chemokines when the inflammatory stimulus is coming from bacteria and fungi. TREM2 is expressed on immature dendritic cells, osteoclasts, and microglia inducing their activation (Colonna, 2003). Interestingly, TREM2 is one of the genes highly transcribed in resting unstimulated microglia,

while the expression is downregulated after canonical pro-inflammatory stimulation with LPS/IFNγ (C. D. Schmid et al., 2002). TREM2 receptor has no cytoplasmic signaling element, in contrast it contains a residue in its transmembrane domain which interacts highly specifically with the adaptor protein DAP12 (Neumann & Takahashi, 2007). The signaling of TREM2 via the DAP12 adaptor stimulates an intracellular cascade, different from the TLRs signaling pathway, since TREM2 does not stimulate NF-κB (Neumann & Takahashi, 2007); indicating why LPS/IFNγ stimulation may not be linked to the TREM2 expression.

However, TREM2-DAP12 signaling regulates the migratory capacity of microglia. Activation of TREM2 by agonists antibodies promotes changes in the actin polymerization process and cytoskeleton reorganization (Takahashi et al., 2005). In addition, stimulation of TREM2 enhances microglial phagocytosis via DAP12 and the extracellular signaled-regulated kinase (ERK). Some studies reported that the knock down (KD) of microglial cells for TREM2 showed a reduced capacity to phagocytose apoptotic neural cell membranes (Takahashi et al., 2005). From different research lines, TREM2-DAP12 signaling pathway *in vitro* has been described to be required in microglial cells for the removal of accidentally apoptotic cells. In addition, a defect on the TREM2-DAP12 complex may result in accumulation of toxic products that may cause brain damage (Neumann & Takahashi, 2007). Also, patients with Nasu-Hakola disease (H. P. Hakola, 1972; Nasu et al., 1973), which is a neurodegenerative disease in which loss of TREM2 or DAP12 function have been widely reported, are characterized by multiple bone cyst-like lesions and progressive encephalopathy leading to severe neurodegeneration (H. P. A. Hakola & Puranen, 1993; Paloneva et al., 2001). At approximately 40 years of age they experience massive neurodegeneration (Bianchin et al., 2004) and finally die during the fifth decade of life.

However, up to date it is not known which neural cell membrane component could stimulate the TREM2 receptor on microglia (Takahashi et al., 2005) but it is known to be crucial for the correct function of microglia during phagocytic events and can be interpreted as a beneficial function of microglia required to keep tissue homeostasis (Neumann & Takahashi, 2007).

3.6.6. Fractalkine (CX_3CL1-CX_3CR1)

CX_3CL1, most named as fractalkine ligand, is a protein member of a subfamily of chemokines which appears to bind exclusively one receptor, CX_3CR1, also known as fractalkine receptor (Rostène et al., 2007). In the CNS, fractalkine ligand is constitutively and abundantly expressed in neurons (Harrison et al., 1998), while in astrocytes its expression could be induced by TNFα and IFNγ (Yoshida et al., 2001). In the brain, the fractalkine receptor expression is exclusive

of microglia. CX_3CL1-CX_3CR1 is a critical signaling pathway for microglia-neuron crosstalk (Lauro et al., 2015; Poniatowski et al., 2017), however, its role during aging, or how it changes during the lifespan, is not fully understood. Some studies have demonstrated that in microglial cells, the activation of the CX_3CL1-CX_3CR1 axis induces a decrease in the IL1β, NO, IL6 and TNFα expression (Lyons et al., 2009; T. Mizuno et al., 2003) and in consequence, lower expression of MHC class II in microglia. CX_3CL1 also inhibits neuronal death via the CX_3CR1 due to a reduced amount of pro-inflammatory microglia and pro-inflammatory factors (T. Mizuno et al., 2003). These results suggest how fractalkine ligand, expressed in neurons, could be implicated in neuronal survival in the adult CNS, as endogenous CX_3CL1 on neurons activates CX_3CR1 on microglia promoting to keep microglia in a quiescent state (Biber et al., 2007; Ransohoff & Perry, 2009). Contrariwise, experiments performed with neuron-microglia cocultures from KO CX_3CR1 mice and $CX_3CR1^{-/-}$ BV2 cells, LPS-induced release of TNFα, NO and O_2^- was reduced compared to controls (Mattison et al., 2013) suggesting the implication of fractalkine ligand in the release of pro-inflammatory molecules by activated microglia.

Besides the implications of the CX_3CL1 and CX_3CR1 in neuronal survival or attachment, when blocking CX_3CR1 in microglial cells, they are unable to respond as well as in normal conditions to CX_3CL1, provoking a decrease in microglial migration (Maciejewski-Lenoir et al., 1999). This supports the hypothesis that the CX_3CL1-CX_3CR1 axis might act as a guide for microglia, promoting the colonization of the CNS (Mecca et al., 2018) but suppressing microglial cells from being activated. In fact, microglial cell activation occurs when levels of fractalkine ligand decrease, as in the hippocampus of aged rats (Lyons et al., 2009).

In pathological states, such as neurodegenerative diseases the CX_3CL1-CX_3CR1 axis have been widely studied. For example, in EAE mice, accumulation of CX_3CR1-expressing microglia has been detected in the brain lesions, while the amount of neuronal CX_3CL1 did not change. Importantly, more astrocytes expressing CX_3CL1 near the areas of inflammation were noticed, which suggests that reactive astrocytes may recruit microglia to these sites of inflammation for a later clearance (Sunnemark et al., 2005). Moreover, studies performed with EAE-affected CX_3CR1 KO mice displayed more severe EAE-related symptoms than WT animals but also overexpression of pro-inflammatory cytokines, such as TNFα. In contrast, the levels of anti-inflammatory cytokines, such as IL10 were significantly higher in symptomatic WT mice compared to the KO animals (Garcia et al., 2013).

Microglia autoregulate their expression of CX_3CR1 as a mechanism to be prepared for overactivation, or to return to a quiescent state. The extent of this autoregulation could push

microglia towards a deleterious or protective phenotype (Mecca et al., 2018). In this manner, as microglia could swift to pro-inflammatory or anti-inflammatory functions, depending on the stimuli. In fact, studies performed on several animal models of neurodegeneration showed that the elimination of the CX_3CR1-CX_3CL1 axis, induces greater neurotoxic activity of microglia and the aggravation of the disease (Cardona et al., 2006). However, whether the signaling impairment of the CX_3CL1-CX_3CR1 axis appears as a consequence or as a cause of increased reactive microglia is still unknown.

4. Calcium ions as signals for microglia

Different molecules or ligands could be acting as a “find-me” or “eat-me” signals to activate microglia. When neurons are stressed or damaged, they release “find-me” signals, as ATP or fractalkine, with the subsequent recruitment and migration of microglia; then, “eat-me” signals, as UDP, promotes the recognition of the target by microglia and in consequence starting the process of phagocytosis (Kettenmann et al., 2013). However, very little is known about other potential signaling molecules that could be used for neurons to promote microglial sensitization to exert an immune response. For example, as we hypothesized in this thesis calcium ions could be one of the key candidates to stimulate microglia during brain damage and degeneration.

Some of the simplest models, suggest that the diffusion of ATP is controlled from the injury site to the microglial location gradually, creating a gradient. But the ATP is a molecule rapidly degraded in the extracellular matrix and it is probably limited in terms of range (Zimmermann, 2000). Later, other hypothesis indicated that ATP sensed by microglial cells could be controlled and enhanced by the cytosolic calcium levels (T. Liu et al., 2011; Pangršič et al., 2007; Striedinger et al., 2007), especially by astrocytes, which could be directly implicated in the process of communication between the dying neurons and microglia. It is known that P2X receptors exhibit high Ca^{2+} permeability upon activation by extracellular ATP (Khakh & North, 2012; North, 2016). In this way, several studies have suggested that P2XRs expression changes when a neuroinflammatory process is in place; moreover, the activation of P2XRs has been associated with various pathological disorders of the CNS, including neuroinflammation and neurodegeneration (Burnstock, 2015, 2017). Concerning the P2YRs, when activated, they induce fast synaptic transmission through the P2XRs in the brain (North, 2016); therefore, P2Y receptors could affect the release of a wide number of neurotransmitters involving the calcium influx (Guzman & Gerevich, 2016).

Regarding neurons, during normal physiological activity, the intracellular Ca^{2+} levels vary with very little differences, and only transiently, which imply the normal activity occurring in neurons and has no adverse effects. However, in pathological states, or in normal aging, neurons become less able to control the Ca^{2+} fluxes and recover to homeostatic state (Mattson, 2007). Oxidative stress, induced by normal aging, or more importantly, by microglia-derived neuroinflammation could be involved in the disruption of neuronal Ca^{2+} homeostasis and neuronal death.

Many studies point to the endoplasmic reticulum (ER) and the mitochondria as the responsible of the calcium changing levels inside the neurons (Duchen, 2000; Mattson et al., 2000). Several

proteins have been identified, located in the ER or mitochondria, that prevent neurons against Ca^{2+}-mediated cell death (Duchen, 2000; Frandsen & Schousboe, 1991; Keller et al., 1998; Mattson et al., 2000).

During aging and aging-related neurodegenerative diseases, supporting data provide evidence of alterations in the Ca^{2+} regulation as a key element in the deteriorating process. For example, neurons in affected brain regions exhibit increased activities of Ca^{2+}-dependent proteases. Besides, studies performed in animal models of neuronal aging have demonstrated that neuronal Ca^{2+} overload inside the neurons could later promote cell death after a stroke (Kristián & Siesjö, 1998; Nellgård & Wieloch, 1992). In addition, neurodegenerative diseases, like AD, have shown alterations in cellular Ca^{2+} homeostasis, which contribute to the neurodegenerative process; for example, amounts of free and protein-bound Ca^{2+}, and the activity of Ca^{2+}-dependent proteases, are increased in neurons containing neurofibrillary tangles as compared with tangle-free neurons in the AD brain samples (Murray et al., 1992; Nixon, 2003). Specially, a different study demonstrated that, apart from the oxidative stress normally seen in neurodegenerative diseases, in AD, the Aβ oligomers can induce and form Ca^{2+}-conducting pores in neuronal surface membranes, promoting the disruption of the Ca^{2+} homeostasis (Kawahara & Kuroda, 2000).

In summary, a high number of studies have pointed to a dysregulation of Ca^{2+} homeostasis in aged or degenerating neurons, including AD and PD (Fairless et al., 2014; GIBBONS et al., 1993; Kawahara & Kuroda, 2000; Nixon, 2003; Smaili et al., 2009; Wojda et al., 2008).

Specially in PD, the neurons that degenerate, DA neurons of the SNpc, have a highly active rate of firing action potentials to promote the signal transduction to drive the movement or absence of movement when required. Many aspects of firing action potential in DA neurons have been described to be Ca^{2+} dependent, and conducted by several types of Ca^{2+} channels expressed in these particular DA neurons (Cardozo & Bean, 1995; Durante et al., 2004; Nedergaard et al., 1993; Wolfart & Roeper, 2002). Calcium ions are important for a wide variety of cellular processes, including the regulation of enzyme activity and gene expression to programmed cell death. There is a complex homeostatic network inside neurons that allows transient increases of Ca^{2+} (Surmeier, 2007). While Ca^{2+} entry to neurons is very rapid, because the different concentration between the cytoplasm and the extracellular space, to be pumped out it is necessary the presence of membrane cation transporters, due to the different membrane potential. These membrane transporters, once the calcium ions have entered the cell, expel the calcium to the extracellular space in a quite fast process. However, in DA neurons of the SNpc,

calcium channels are opened much of the time, allowing the triggering of these action potentials. For this reason, the magnitude of Ca^{2+} in DA cells is much more important, as well as the burden of potential toxicity (Wilson & Callaway, 2000). In addition, recent studies have shown a potential link between the calcium dysregulation and familial PD, being α-synuclein aggregation in damaged neurons one of the responsible for the calcium dysregulation of DA neurons (Angelova et al., 2016; Virdi et al., 2022).

As mentioned above, there is a good number of studies that point to neuronal Ca^{2+} channels as a critical factor affecting degenerating neurons. However, all the supportive studies are based on the effects of the calcium entry inside the cell, the signaling cascade that Ca^{2+} ions induce inside neurons, regulating diverse functions, and how this Ca^{2+} levels are dysregulated in pathological conditions; but little has been studied about the calcium that is potentially released to the external matrix when neuronal death occurs. We hypothesize that in the process of neurodegeneration, Ca^{2+} ions may serve as a "find-me" or "eat-me" signal to surrounding microglia. The release to the external parenchyma could be promoted by the calcium dysregulation inside the cell compartments, or the simple spill to the extracellular space while degeneration is taking place, where, then, could be sensed by surrounding cells, like astrocytes and most importantly microglia. Potentially, the interaction of Ca^{2+} with glial cells could trigger a cascade of events responding to neuronal degeneration.

Previous studies have already pointed the spreading of Ca^{2+} signaling as a way to transmit damage into the brain parenchyma, and specifically to microglial cells (D. Lim et al., 2021; Schipke et al., 2002). In this process, any pathologic impact to the brain is "notified" to microglia by expanding Ca^{2+} waves that trigger the subsequent responses (Figure 10). Schipke *et al*. revealed, in a study performed in green-astrocytes transgenic mice, that when a local electrical stimulation is induced, promotes an activated Ca^{2+} response in both astrocytes and non-astrocytic glial cells, spreading the signal over hundreds of micrometers away (Schipke et al., 2002) (Figure 10). In that way, regenerative ATP release and subsequent activation of metabotropic purinergic receptors caused the propagation of the glial Ca^{2+} wave. Microglial cells were responsive to the calcium wave via the spread of the signal by astrocytes. In addition, it has been shown that bulk exocytosis of ATP-containing vesicles is often dependent on cytosolic Ca^{2+} levels, suggesting another possible link between Ca^{2+} signaling and microglial attraction (T. Liu et al., 2011; Pangršič et al., 2007; Striedinger et al., 2007).

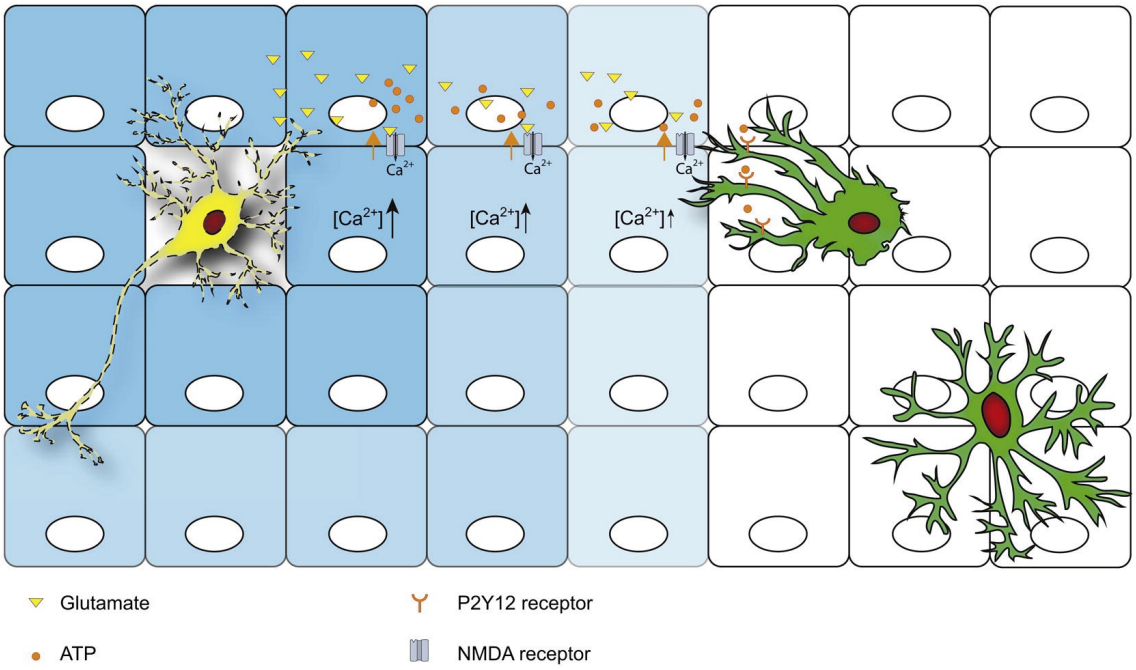


Figure 10. Potential Ca^{2+} propagating wave through the brain parenchyma to signal microglia. Diagram illustrating a damaged neuron (yellow) releasing components to the external parenchyma, and inducing the spreading of Ca^{2+} waves later sensed by microglial cells, who in consequence polarize their branches and migrate towards the damaged neuron (D. Sieger et al., 2012).

In this context, researchers have also discovered, in brain injury models in zebra fish, that microglial cells are sensitized by high Ca^{2+} levels, rapidly polarizing their branches towards the source (D. Sieger et al., 2012). In this study, Sieger and colleagues, performed targeted laser neuronal ablations in transgenic zebrafish brains, revealing rapid calcium waves expansions whose range defined the motility of microglia to the damaged site. Microglial cells were responsive few moments after the calcium spreading around the injury. Importantly, chelating the extracellular calcium was sufficient to suppress microglial targeting to damage sites. Moreover, microglial response to Ca^{2+} was tested by a local induction of Ca^{2+} signaling by photo-uncaging of inositol triphosphate (IP_3), being positive even though there was no neuronal injury (D. Sieger et al., 2012). They also observed that the waves were graded, being the cells closer to the injury with higher Ca^{2+} signaling level than distant cells. The most aggressive the ablation was, the longer range Ca^{2+} waves were created, and, in consequence, a greater number of microglial cells were sensitized to migrate towards the lesion, indicating a strong spatial correlation between these two events. Microglial cells in response to calcium waves polarized their branches within a minute upon the lesion, indicating a strong temporal association between Ca^{2+} signaling and microglial responses (D. Sieger et al., 2012). All these data suggest that calcium, spreading through the brain parenchyma, may serve as a key “find-me” signal to

activate microglia. However, the mechanisms and factors inducing Ca^{2+}-dependent microglial motility and how may affect neurodegenerative disorders as PD, are yet to be explored.

5. Iba-1 as the responsible protein for the microglial sensitization through calcium

Ionized calcium-binding adapter molecule-1 (Iba-1) is a small protein of 17 kilo Daltons (kDa) which has a total of 147 amino acids. It is also known as the allograft inflammatory factor-1 (Aif-1), its gene is encoded within the HLA or MHC class III gene region (Deininger et al., 2002), being in humans in the chromosome 6 and in mice in the chromosome 17, respectively. Iba-1 protein contains two Ca^{2+}-binding EF hand motifs in the central third of the molecule and this portion shows homology with other EF hand proteins, however, no other protein regions have homology with any known proteins (Imai et al., 1996; Ito et al., 1998).

Iba-1 was first described in atherosclerotic lesions in a rat model of chronic cardiac rejection (Utans et al., 1995). Utans *et al*. were examining arterial lesions after transplantation because the arterial lesions typically occurred in the donor vessels but not in the resident. The firsts considerations pointed to the development of atherosclerosis as a localized immune-mediated response. To assess this hypothesis, they used a specific rat strain with cardiac allograft model, and by using differential mRNA display to identify genes whose expression increased in the disease, they found a novel complementary DNA (cDNA) specially expressed, and more interesting for this thesis, which could be upregulated by IFNγ, which they named it Iba-1.

Approximately at the same time, other research lines found the same cDNA expression in IL-2-stimulated brain cells (Imai et al., 1996). Further studies in the same field found that this gene expression was not IL-2 dependent, but time-dependent. When searching for Iba-1 homologous proteins, Imai *et al*. found a high resemblance with the protein calmodulin, which is a calcium-binding protein, containing an EF hand encoding sequence. Then Iba-1 was classified as a new member of the EF hand protein family, considered as a new type of EF hand protein (Imai et al., 1996), due to the unique complete sequence, excepting for the EF hand.

Then, the expression of Iba-1 was tested by Imai and colleagues in different tissues by ribonucleic acid (RNA) blot analysis, being strongly expressed in testis, slightly in spleen and weakly in brain, lung and kidney (Imai et al., 1996). However, when examining brain-derived primary cells, the expression of Iba-1 was restricted to microglia and not being detected in neurons, astrocytes, or fibroblasts. Hence, the expression of Iba-1 in fact was coming from proliferating microglia that co-existed in the primary culture.

Nowadays, it is widely known that Iba-1 protein is expressed by microglia/macrophages. These studies mentioned above also first examined the origin of the protein by using a specific antibody and Iba-1 was clearly shown to be expressed in monocytic cell lines (Imai et al., 1996;

Ito et al., 1998). Iba-1 was also found to be highly specific for microglia in the brain cultures and, knowing the two EF hands present in its encoding sequence, Iba-1 was described as an adapter molecule that mediates calcium signals in the monocytic lineage, including microglia (Ito et al., 1998). In adult rat brain, Iba-1 was shown to be expressed similar to the OX-42 staining, a classical marker for microglia. Moreover, they found Iba-1 expression not only in amoeboid microglia but also in ramified microglia (Ito et al., 1998). Thus, cells with macrophage-like morphology, with rounded nucleus, abundant cytoplasm, and a few short processes in the leptomeninges and choroid plexus were also positive for Iba-1.

To examine the Iba-1 expression in non-activated and activated microglia, researchers performed a facial nerve axotomy in Wistar rats, a well-established experimental model for detecting activated microglia but not infiltrated macrophages. Interestingly, they clearly demonstrated an increase in the Iba-1 expression on the lesioned side compared with the contralateral side, corresponding to reactive/activated microglia compared with non-activated or ramified microglia (Ito et al., 1998).

Since then, Iba-1 has been established as one of the most important and reliable markers for microglia in the brain and macrophages in the rest of the tissues. However, its specific function remains poorly investigated.

Among the most important studies describing the possible function of Iba-1, we highlight those postulating the actin-cross-linking activity (Sasaki et al., 2001), being critically involved in certain aspects of motility-associated rearrangement of the actin cytoskeleton, including the formation of the phagocytic cups (Ohsawa et al., 2000). It is known that organized actin remodeling is critically regulated by the Rho family GTPases, including Rho, Rac and Cdc42 (Hall, 1998). In macrophages, Rho has been described to induce cell contraction (Allen et al., 1997) while Rac and Cdc42 promote the formation of lamellipodia and filopodia (Allen et al., 1997; Kozma et al., 1995; Nobes & Hall, 1995; Ridley et al., 1992). Moreover, Rho GTPases have been related to regulate phagocytosis via the FcRs (Caron & Hall, 1998; Cox et al., 1997; Hackam et al., 1997; Massol et al., 1998). They hypothesized that these events were associated with Iba-1 and not only dependent of the Rho family GTPases (Ohsawa et al., 2000). To ascertain the link between Iba-1 protein and the cytoskeleton formation, researchers double-labelled the cytoskeleton and Iba-1 microglia showing high Iba-1 staining, not only in the cytoplasm, but also in lamellipodia and membrane ruffles (Ohsawa et al., 2000), suggesting the implication of Iba-1 in the actin reorganization. Additionally, Ohsawa and colleagues examined the implication of Iba-1 in the formation of phagocytic cups. For that, using zymosan, a glucan that induce phagocytosis, and

labeling Iba-1 on microglial cells, they observed, by time-lapse imaging that Iba-1 was first diffusely distributed in the cytoplasm, to later being actively participating in the extension of the cytoplasm surrounding the phagocytosed particle, then, Iba-1 was dispersed back into the cytoplasm (Ohsawa et al., 2000).

Little has been published about the function of Iba-1 in other Iba-1 expressing cell types outside the CNS, as for example the spermatids, because most of the research about Iba-1 have been focused on microglia. Iida *et al*. found Iba-1 expressing spermatids in a developmentally regulated stage-dependent manner, suggesting that Iba-1 may also be involved in the reorganization of the actin cytoskeleton during spermatogenesis (Iida et al., 2001), in which, once they mature, the Iba-1 positive reactivity disappears. Besides, a wide number of studies in other tissues pointed to Iba-1 as a protein (or Aif-1) involved in inflammatory processes (Beiter et al., 2005; Schluesener et al., 1998). Some studies demonstrated an increased Aif-1 expression in different scenarios, as kidney and liver after transplant rejection (Grimm et al., 1999; Nagakawa et al., 2004), colitis (Morohashi et al., 2003), arterial lesions (Autieri et al., 2000; Autieri & Chen, 2005), atherosclerosis (Tian et al., 2006), systemic sclerosis (Del Galdo et al., 2006) and rheumatoid arthritis (Kimura et al., 2007). In addition, exogenous or overexpressed Aif-1 has been seen to promote cytokine expression, including IL6, by fibroblasts and mononuclear cells (Kimura et al., 2007), or IL12, by monocyte/macrophages (Watano et al., 2001), promoting the proliferation of cells derived from inflammatory lesions (Kimura et al., 2007). Iba-1 has also been related with the factor NF-κB, which is directly involved in the inflammatory response. AIF-1 gene is closely related to the chromosome mapping of NF-κB gene, and some studies pointed to Iba-1 as a protein related with the transcription levels of NF-κB (S. Liu et al., 2008). *In vitro* studies, using epithelial human breast cancer and mouse adipocyte-like cell lines, have demonstrated that the induction of NF-κB activity is associated with Iba-1 (S. Liu et al., 2008; Ren et al., 2018). Additionally, cells overexpressing Aif-1 showed increased activation of the NF-κB pathway (Sommerville et al., 2012).

Moreover, the largest body of information regarding Aif-1 or Iba-1 function came from studies performed with silenced AIF-1 gene *in vivo* and *in vitro*. In mice lacking the AIF-1 gene, the spleen weight is decreased, and the number of peripheral blood platelets is lower, indicating that the Aif-1 is involved in hematologic development (Casimiro et al., 2013). Although the AIF-1 gene is expressed in T-lymphocytes, monocytes and macrophages, mice lacking the AIF-1 gene revealed no differences in blood monocyte or T-cell numbers compared to WT animals (Egaña-Gorroño

et al., 2019), which is a good feature to consider for posterior studies in which the neuroinflammatory response could be involved somehow.

Regarding proliferation, to assess how Aif-1 deficiency could alter the population of macrophage/microglia, cultured bone marrow-derived macrophages from Aif-1$^{-/-}$ mice resulted in less numbers when compared with the WT. However, by using the bromodeoxyuridine (BrdU) to detect proliferating cells, Aif-1$^{-/-}$ cells were equally proliferative than cells coming from WT animals, suggesting that Aif-1 is not involved in the process of proliferation (Egaña-Gorroño et al., 2019). Interestingly, more apoptotic cells were observed in the Aif-1 KO cell culture compared with the corresponding WT culture, so Aif-1 or Iba-1 deletion may result in a reduced capacity to survive.

Concerning the motility, macrophages from mice lacking Iba-1 display reduced migration and phagocytosis deficit, as well as reduced levels of pro-inflammatory cytokines release compared with WT mice (Egaña-Gorroño et al., 2019). Macrophages in atherosclerotic experimental models, silenced for Aif-1, showed less capacity to migrate than normal macrophages (Tian et al., 2006), supporting previous results related with the Iba-1 function in cell movement (Ohsawa *et al*.). Later analyses, using mice lacking Aif-1 expression, showed impaired microglial function regarding its involvement in the synaptic pruning (Lituma et al., 2021). Interestingly, also in this study, by using TPM, hippocampal CA1 slices of Aif-1$^{-/-}$ mice were imaged to assess whether the lack of Iba-1 was related with impairment in movement. After local ATP application the movement of microglia displayed by Aif-1$^{-/-}$ mice was lower than WT mice, that showed greater dynamics with more motility of the process following ATP exposure compared to KO mice (Lituma et al., 2021).

Altogether, these evidences suggest that Iba-1 is required for microglial motility, including the arrangement of microglial branching complexity and dynamic process of displacement. However, considering that IBA-1 encoding gene sequence has two EF hands motifs, our hypothesis is focused on the effects of Ca^{2+} on Iba-1 function and the subsequent motility related responses exerted by microglia. As it has already been studied in other proteins, Ca^{2+} binding to regulatory EF hand, induces a conformational change that often mediates the induction of different signaling cascades. Given that Iba-1 includes other motifs with capacity to interact with multiprotein complexes as actin fibers (J. Chen et al., 1995; Hung & Sheng, 2002), its function could be directly induced by the calcium binding, triggering specific responses involved in microglial-mediated neuroinflammation.

In the present thesis we want to understand critical features of the microglial response in PD. Particularly, the mechanisms that drive microglial cells to be polarized and moved towards degenerating DA neurons. We attempt to demonstrate the importance of Ca^{2+} release during DA neuronal death and how this Ca^{2+} ions affect microglial polarization and motility. Finally, by using AIF-1 KO mice, we also want to assess whether this Ca^{2+}-dependent motility is mediated by Iba-1 to trigger the proper immune response in the neurodegenerative scenario.

OBJECTIVES

Microglial cells are known to be responsive to neuronal signals. In the context of neurodegeneration, this response may include the elimination of damaged neurons. In this work we wondered how microglial cells respond to a specific neuronal signal, free Ca^{2+}, supposed as a "find-me" signal, potentially released during the process of neuronal death in a parkinsonian scenario. Posteriorly, ascertain in which manner Iba-1 could be implicated in the whole process. For this purpose, the specific objectives are:

- Study PD human samples to corroborate the dopaminergic neuronal death is occurring and quantify the morphological changes and the reactivity of microglia in PD human samples and non-PD patients.
- Quantify the microglial branches' polarization to neurons in MPTP parkinsonian mice.
- Exposing mesencephalic neurons to microglia combined with the administration of a proinflammatory stimulus to determine whether activated microglia promotes more neuronal death.
- Analyze the MTOC location in microglia when exposed to pro-inflammatory stimuli to better define the microglial directionality.
- Quantify the number of neurons in a parkinsonian scenario to observe the lethal capacity of the insult MPP^+ and the susceptibility of dopaminergic neurons. Determine whether these dopaminergic neurons release calcium to the external milieu when dying.
- Observe the microglial capacity to incorporate extracellular Ca^{2+} to the internal component.
- Ascertain the number of neurons and Ca^{2+} being released by dopaminergic neurons when exposed to different MPP^+ concentrations, in the presence of microglial cells or combining different pro-inflammatory scenarios that could occur in PD.
- Determine how aggressive could be the pro-inflammatory environment, provoked by activated microglia, to kill neurons by measuring the neuronal death and the subsequent release of calcium.
- Quantify the morphological changes of BV2 microglial cells when exposed to different Ca^{2+} concentrations.

- Study the movement of microglia when placed in different Ca^{2+}-concentrations media, modeling the potential situation in which microglia are exposed to dying neurons-derived Ca^{2+}.
- Administration of calcium and a Ca^{2+}-chelator to the striatum of C57BL/6j mice to analyze the morphological changes that microglial cells experience.
- Study the sensitization of BV2 microglial cells, by adding different Ca^{2+} concentrations, in changes in the Iba-1 expression.
- Analysis of Iba-1/F-actin colocalization to link the motile capacity of microglia with the cellular location of this molecule.
- Administration of calcium intrastriatally to $Aif1^{-/-}$ mice to analyze whether the polarization of microglial branches to the target is related with Iba-1.

MATERIALS AND METHODS

1. *In vitro* experiments

1.1. Cell lines and primary cultures

BV2 microglial cells

BV2 is an immortalized mouse microglial cell line that exhibits both the phenotypic and functional properties of reactive microglial cells (Park et al., 2017). BV2 cells were grown and maintained in four different media for each experiment on this thesis.

Cells were plated in 75 cm^2 culture flasks (Sarstedt; Nümbrecht, Germany; Ref. 83.3911) and left to grow in Roswell Park Memorial Institute (RPMI) medium (ThermoFisher; Waltham, MA, USA; Ref. 11875093), supplemented with 10% heat-inactivated fetal bovine serum (FBS) and 0.1% penicillin-streptomycin (P/S) and maintained at 37°C and 5% CO_2 for the lipopolysaccharide (LPS)/Interferon (IFN) γ treatment experiments.

For the extracellular Ca^{2+} inputs experiments and chemotactic/microfluidic analyses, the cells were plated in the flasks and were grown and maintained in three different types of Dulbecco's Modified Eagle Medium (DMEM) at 37°C and 5% CO_2: normal DMEM medium (ThermoFisher; Waltham, MA, USA; Ref. 11995065), supplemented with 10% heat-inactivated FBS and 0.1% penicillin-streptomycin; DMEM calcium free (ThermoFisher; Waltham, MA, USA; Ref. 21068028), supplemented with 0.1% P/S; and DMEM modified with different concentrations of Ca^{2+} – conducted according to Dulbecco's protocol adding calcium chloride ($CaCl_2$) (Merck; Darmstadt, Germany; Ref. 102382) – required for the experiments and supplemented with 10% FBS and 0.1% P/S.

PC12 cells

PC12 cells are derived from a transplantable rat adrenal pheochromocytoma (Greene and Tischler, 1976) and closely resembles dopaminergic neurons, as they synthesize and store dopamine (DA), as well as express dopamine transporter (DAT) in their membranes (Westerink & Ewing, 2008).

These cells were also plated in 75 cm^2 culture flasks previously pre-coated with collagen I (Cultek, Madrid, Spain; Ref. 45356236), and left grow in DMEM at 37ºC and 5% CO_2,

supplemented with 7% heat-inactivated FBS, 7% horse serum (HS), 1,14% HEPES 1M pH=6.8 and 0.1% P/S.

Primary microglial cultures

According to the protocol approved by the Ethics Committee on Animal and Human Research of the UAB, newborn Sprague Dawley (SD) rats from the animal house at the UAB, were sacrificed at days 0-2 post-natal to obtain glial cells from the mesencephalon (MSF).

To extract the brain, rat pups were decapitated, and after the skin was removed, we carefully cut and remove the cranial bones. By using a magnifier, the brain extraction was performed, following the dissection of the MSF after separating cortex and cerebellum. Meninges at this level were carefully removed and subsequently the MSF was chopped into small pieces.

Using the MSF, we isolated the microglial cells with a standard protocol (Modified from Tamashiro et al., 2012). For that, five different solutions were previously prepared to perform the culture and all of them were filtered with a 0.2 µm standard filter (Sarstedt; Nümbrecht, Germany; Ref. 83.1826.001); **Solution 1**, containing 50 mL of Krebs-Ringer Buffer 1X (120 mM NaCl, 4.8 mM KCl, 1.2 mM KH_2PO_4, 25 mM $NaHCO_3$, 14.3 mM Glucose) with 0.15 g of Bovine Serum Albumin (BSA) (Sigma-Aldrich; St. Louis, MO, USA; Ref. A7906-100UG) and 0.4 mL $MgSO_4$ 3.8%, **Solution 2**, containing 10 mL of solution 1 with 2.5 mg of trypsin (Sigma-Aldrich; St. Louis, MO, USA; Ref. T9201-500MG), **Solution 3**, containing 10 mL of solution 1 with 0.8 mg DNase (Sigma-Aldrich, St. Louis, MO, USA; Ref. D5025-150KU), 5.2 mg of trypsin inhibitor (ThermoFisher Scientific; Waltham, MA, USA; Ref. 17075-029) and 0.1 mL $MgSO_4$ at 3.8%, **Solution 4** containing 8.4 mL of solution 1 and 1.6 mL of solution 3, and **Solution 5**, containing 5 mL solution 1, 40 µL $MgSO_4$ 3.8% and 6 µl $CaCl_2$ 1.2%.

Once all the solutions were filtered, the chopped MSF were resuspended in 15 mL of Solution 1. After centrifugation of 1500 rpm for 30 seconds, the pellet was resuspended in Solution 2 and incubated at 37 °C for 10 minutes. The enzymatic digestion was stopped by adding Solution 4, followed by a 1-minute 1500 rpm-centrifugation. The pellet was resuspended in 3 mL of Solution 3 and disaggregation was performed by gently pipetting up and down 10 times with a Pasteur pipette through a cell net. The cell suspension was added to Solution 5 and centrifuged for 5 minutes at 1000 rpm, then, the supernatant was discarded, and cells were resuspended in 5 mL of DMEM supplemented with 0,1% P/S and 10% FBS. After resuspension, the cells were plated in 175 cm^2 culture flasks (BD/Fisher; Stanford, CA, USA; Ref. 353112) at a density of 300,000 cells

per milliliter (cells/mL). The cells were grown in supplemented DMEM medium. The cultures were maintained at 37°C and 5% CO_2.

After several weeks maintaining the culture – and changing the medium once a week – since different types of cells grow, the flask was shaken in a horizontal shaker for 3 hours at 300 rpm to obtain the microglia present on the surface of the culture. When the shaken was finished, the supernatant was collected and centrifuged for 5 minutes at 1000 rpm, then the supernatant obtained from the centrifugation was recollected and preserved, and the pellet – containing microglia – was used to plate the microglia in well plates for subsequent experiments. The primary culture was maintained in flasks with 50% fresh DMEM and 50% DMEM preserved from the centrifugation (conditioned medium).

Primary neurons cultures

To obtain primary dopaminergic neurons, a pregnant E17 Sprague Dawley rat from the animal house of the UAB was used. The rat was sacrificed according to the protocol approved by the Ethics Committee on Animal and Human Research of the UAB. The abdomen surface was sterilized with 70 % ethanol and an incision was done through the skin and muscle, then the embryos were removed and placed in a Petri dish with PBS. The embryos were decapitated to extract the brain. Within the brain, with the help of a magnifier, we could differentiate the MSF, specifically the ventral part – where most of the dopaminergic (DA) neurons are located – separated to be used.

All five solutions used in the culture of primary microglia, were previously prepared and filtered and use for the extraction of primary neurons.

Once all the mesencephala were mixed together, were chopped in small pieces. The same protocol to extract primary microglia was followed but with two small differences, as all the pulses were of 2 minutes instead of 30', and the cell net was not used to disaggregate the cells. The cells obtained were plated directly into 24-well plates (Sigma-Aldrich; St. Louis, MO, USA; Ref. 353047) with coverslips pre-coated with poly-D-lysine (PDL) at a density of 300,000 cells/mL for future experiments. Neurons were first cultured with 10 mL of normal DMEM, supplemented with 10% FBS and 0.1% of P/S for 2-4 hours, then the medium was changed to Neurobasal™ (ThermoFisher; Waltham, MA, USA; Ref. 21103049), supplemented with B27 supplement 50X (ThermoFisher; Waltham, MA, USA; Ref. 17504044) at 2%, GlutaMAX™ 100X (ThermoFisher; Waltham, MA, USA; Ref. 35050061) at 1%, P/S at 0.5% and glial cell line-derived neurotrophic

factor (GDNF) (Sigma-Aldrich; St. Louis, MO, USA; Ref. SRP3239-10UG) at a final concentration of 10 nanogram per milliliter (ng/mL).

Technical note: *These cultures need to be maintained by changing the media every 3-4 days until their use, but only with half of the media in the wells, and also adding Ara-C (Cytarabine) to impede other cell types, other than neurons, to grow. At 4-7 days in vitro (DIV) we used the cultured neurons for experiments.*

1.2. Lipopolysaccharide and interferon γ -induced microglial activation

Microglial BV2 or HAPI cells were plated in pre-coated poly-L-lysine (PLL) coverslips in a 24-well culture plate. They were allowed to grow for 24 hours in RPMI or DMEM media – depending on the cell type – with the same conditions as cited above to a concentration of 50,000 cells/mL. At this point, according with the experiment, cells were treated with different stimuli for another 24 hours.

For every experiment we always used a control group, which was a culture with normal medium without stimuli. The other conditions were the experimental groups according to the specific experiment; being the treatments a combination of LPS 100 ng/mL with IFN γ in different concentrations ranging between 0.5 ng/mL and 25 ng/mL.

For primary microglial cells, we took and preserved the supernatant from the shaken culture, as mentioned above, and after centrifugation, microglial cells – present in the pellet – were cultured in 24-well plates with PLL-coated coverslips for the experiments at a density of 100,000 cells/mL. We let them grow for 24 hours in DMEM. At this point cells were treated with different stimuli for another 24 hours. In concordance with the stimuli used for cell lines, we used a concentration of LPS 10 ng/mL in combination with IFN γ ranging from 10 ng/mL to 50 ng/mL.

****Technical note****: *This treatment was optimized taking into account some previous tests activating primary microglial cells. We found these concentrations of LPS and IFN γ as the best option.*

After 24 hours the supernatants were preserved in another well plates to measure the nitrites released by microglia. Then, the cells were fixed with 4% paraformaldehyde (PF) (Electron Microscopy Science; Hatfield, PA, USA; Ref. 15714) for 20 minutes and then were stored for immunostaining. One well for each treatment was used as a secondary-antibody control of the immunostaining.

1.3. GRIESS assay

The Griess assay is a colorimetric analysis to detect the presence of nitrite compounds, in this case, product of the activation of primary microglia or microglial cell lines. The nitrites measured were those released by microglial cells after the corresponding treatments. The Griess reactive (Sigma-Aldrich; St. Louis, MO, USA; Ref. G4410) consists of sulfanilic acid and N-(1-naftil) ethildiamide (NED). Sulfanilic acid reacts with the nitrites in an acidic solution and then becomes a diazotized salt that binds to NED, resulting in a colored compound which can be spectrophotometrically quantified at 540 nm. A standard curve was established using $NaNO_2$ (Sigma-Aldrich; St. Louis, MO, USA; Ref. 237213) in a range between 0.78 µM and 100 µM.

Before doing the spectrophotometric analysis, in a 96-well plate (Sigma-Aldrich; St Louis, MO, USA; Ref. 353072) we put the Griess reagent (100 µL/well) with 100 µL of each of the supernatants recollected from the cultures, leaving four wells for the blank which have Griess reagent with milliQ water. After 15 minutes of incubation at room temperature (RT), absorbance was read at 540 nm and the values were interpolated with the standard curve to obtain the concentration of nitrites released by microglia in the supernatants.

1.4. Extracellular calcium inputs to BV2 microglial cells

Without previous Ca^{2+} deprivation. We used BV2 cells plated in PLL-coated coverslips in a 24-well culture plate. They were first left to grow for 24 hours in RPMI medium with the same conditions as cited above at a concentration of 50,000 cells/mL. From this starting point, cells underwent different changes in Ca^{2+} concentrations. Due to the impossibility of obtaining RPMI without Ca^{2+}, we used Ca^{2+}-free DMEM instead, which is commercially available. For that purpose, we needed to change the cells to DMEM media prior being exposed to increasing calcium concentrations. The experimental conditions were created by adding increasing $CaCl_2$ concentrations: 1.8; 5.4; 9; 12.6 and 20 mM; supplemented with FBS. To be able to stereologically compare the conditions, we used cells cultured in normal DMEM, in Ca^{2+}-free DMEM as well as normal RPMI as a control, with the respective supplementations. After 24 hours of treatment, we fixed the cells with a 4% PF solution for 20 minutes and preserve the cultured cells for immunocytofluorescence.

With previous Ca^{2+} deprivation. This experiment was performed following the same protocol as the non-deprived cells described above but culturing the cells with Ca^{2+}-free DMEM for 24 hours in-between the seeding and the experimental procedure. Control conditions were the same way as we used for the non-deprived microglia.

After 24 hours in Ca^{2+}-free media, cells were submitted to the appropriate conditions. For this, we changed the media with different $CaCl_2$ concentrations as previously indicated: 1.8; 5.4; 9; 12.6 and 20 mM; adding in all of cases 10% of FBS. 24 hours later, microglial cells were fixed with a solution of 4% PF for 20 minutes and then stored for immunocytofluorescence.

1.5. Cocultures BV2-PC12

To determine the optimal timepoint to estimate the highest number of interactions between microglia and dopaminergic cells as well as the phagocytic events a coculture with BV2 and PC12 cells was set up. Both cell lines were incubated at 37°C in culture flasks. BV2 cells were seeded in 24-well plates at a concentration of 50,000 cells/mL and let them grow for 24hours. Then PC12 cells – previously trypsinized – were seeded on top of the BV2 cells layer with fresh DMEM medium at a density of 100,000 cells/mL. The coculture was then fixed with 4% PF after 2, 8 and 24 hours of interaction. Fixed cells were preserved in PBS to later perform multicolor immunocytofluorescence.

1.6. Immunocytofluorescence for cell lines

Immunocytofluorescence was performed on BV2 and PC12 to visualize different events and quantify several cellular aspects depending on the experiment as we describe below. In all cases, we used 24-well plates – as described previously in preceding culture experiments – for the analysis and quantification.

Cells were washed with PBS three times for 5 minutes, then permeabilized with 0.02% saponin/PBS1X at RT, in a volume of 450 microliters per well (µL/well) for 7 minutes. A pre-blockade was done for 15 minutes with 450 µL/well of 0.01% saponin/10mM Gly/PBS1X at RT; and then cells were blocked for 1 hour at RT with 0.01% saponin+10mM Glucose+5% BSA/PBS1X by adding 450µL/well. Cells were next incubated overnight with primary antibodies, using 12 µL/coverslip diluted in 0.01% saponin/1%BSA/PBS1X at RT in a small chamber with a moist cotton bedding.

For the LPS/IFN-γ experiments and Ca^{2+} experiments, the primary antibodies used were: anti-Iba-1 (1:500, polyclonal rabbit immunoglobulin G (IgG); Wako Pure Chemical Industries, Ltd.; Osaka, Japan) which is a common used antibody to stain microglial cells and anti-γ-tubulin (1:500, monoclonal mouse IgG; Sigma-Aldrich; St Louis, MO, USA) to stain the microtubule organizing center (MTOC).

For the coculture of BV2 and PC12 cells the primary antibodies used were: anti-Cd11b (1:100, monoclonal rat IgG) to stain microglial cells and anti-TH (1:500, polyclonal sheep IgG1 Sigma-Aldrich; St Louis, MO, USA) to stain PC12 cells, as they express Tyrosine Hydroxylase (TH).

Note: *the complete references for the antibodies are listed in a table at the end of the methods (Table 2 and 3).*

Secondary fluorescent antibodies diluted 1:1000 in 0.01% saponin/1%BSA/PBS1X, accordingly with the host species of the primary antibodies, were used for the subsequent detection. The secondary antibodies used were: AlexaFluor 488 Goat anti-Rabbit IgG (Life technologies; Carlsbad, CA, USA) for the Ca^{2+} experiment. AlexaFluor 488 Goat anti-Rabbit IgG; and AlexaFluor 555 Goat anti-mouse IgG (Life technologies; Carlsbad, CA, USA) for the LPS/IFN-γ experiments. Then we used a phallotoxin to stain the cytoskeleton f-actin fibers: AlexaFluor Phalloidin 555 (1:40; Life technologies; Carlsbad, CA, USA) for Ca^{2+} experiment and AlexaFluor Phalloidin 647 (1:40; Life technologies; Carlsbad, CA, USA) for the LPS/IFN-γ experiments. And for the coculture we used the AlexaFluor 488 Donkey anti-sheep IgG (Life technologies; Carlsbad, CA, USA) for the PC12 cells and the AlexaFluor 555 Goat anti-rabbit IgG (Life technologies; Carlsbad, CA, USA) to observe the BV2 cells.

Next, 4',6-diamino-2-phenylindole (DAPI) (1:1000; Life technologies; Carlsbad, CA, USA) was added to the wells, 400 µL/well, to stain the nuclei of the cells for 5 minutes. One of the coverslips for each treatment was not incubated with the primary, but with the secondary antibody (secondary-antibody control).

Finally, coverslips were mounted on glass slides using Prolong Gold antifade reagent (Life technologies; Carlsbad, CA, USA; Ref. P36930).

1.7. Microfluidic live cells analysis

We performed a new serial of experiments with live cells using microfluidic platform for gradient plate (CellASIC™, EMD Millipore Corporation; Hayward, CA; USA; Ref. M04G-02-5PK) and switching plate (CellASIC™, EMD Millipore Corporation; Hayward, CA; USA; Ref. M04S-03-5PK).

Microglial cells placed in a constant flowing milieu using gradient plates

The gradient plate contains four independent chambers (A-D), and each chamber has a main channel connected with two lateral channels circulating in parallel – and separated with perfusion barriers (Figure I). In our experiment we used the main channel to administer different

calcium concentrations media constantly flowing to the cells to register the differences in cellular motility.

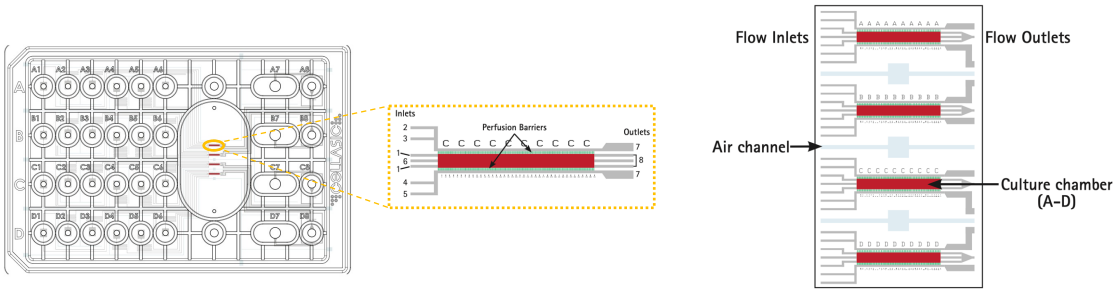


Figure I. Diagram of the gradient plate. View of the plate and detail of the chambers and channels to better understand where all the influx and outlet channels are located (CellASIC™).

The gradient plate has 24 inlet wells (also referred as channels) to channel the different media and 2 output waste wells (7 and 8) per chamber. Channels 1 and 6 are intended to introduce the medium and the cells, respectively. Channels 2 and 3 bring the liquid along one side of the chamber to create a gradient from one side (top channel in Figure I) to the middle of the chamber through the perfusion barrier, whereas channels 4 and 5 run the liquid along the other side of the chamber (bottom channel in Figure I) to promote the migration of the media through the perfusion barrier to the middle of the chamber to also create a gradient (Figure I).

The first step is to cover the culture chambers A-D with PLL for two hours to allow the optimal cell attachment. Then, for these experiments we need to obtain the BV2 cells – by trypsinizing the culture flask and the consecutive centrifugation and resuspension – at a final density of 700,000 cells/mL. Then the cells are seeded inside the chambers. For that procedure, we have an automated protocol, by using the microfluidic system (CellASIC ONIX).

First, waste wells needed to be filled with 50 µL to prevent a massive entry of cells to the chambers. Next, 10 µL of the cell resuspension was added to well 1 for each chamber and immediately after, another 10 µL were added to well 6. Then the gradient plate (CellASIC) was connected to the microfluidic manifold (CellASIC™ONIX, EMD Millipore Corporation; Hayward, CA, USA; Ref. CAX2-MBC20) to seal the plate making the vacuum. And by using the microfluidic system (CellASIC™ONIX, EMD Millipore Corporation; Hayward, CA, USA; Ref. CAX2-S0000) and the computerized user interface software (CellASIC™ONIX FG, EMD Millipore Corporation; Hayward, CA, USA; Ref. CX2-SSW01) we opened an existing protocol “Load cells”. With this protocol, a combination of pressures in wells 1 and 6 is made to push the cells inside the

chambers preventing from going to the waste wells. Then the cells were left for 24 hours in DMEM to grow, at 37ºC and 5% CO_2.

For chambers A and C, we added 9 mM DMEM through 1 and 6 channels (DMEM without calcium modified with $CaCl_2$ to obtain a 9 mM Ca^{2+} concentration) as well as to the side channels (2, 3, 4 and 5) to be sure that the gradient formation was only created with Ca^{2+} 9mM. For chambers B and D, we added DMEM without calcium and without FBS supplementation in the same way we did for chambers A and C.

Then, plates were connected to the system manifold to vacuum the plate and microfluidic system (CellASIC™ONIX). We set the flow of the chambers with the user interface software (CellASIC™ONIX FG) to induce a flow of continuously renewed media in all the chambers. For that, we created a specific protocol of pressures for each channel of the different chambers as preferred.

We performed this experiment for 24 hours and after that we fixed the cells with 4% PF. To fix the cells in these plates the principle is the same as in the 24-well plates, but only adding the fixative solution through wells 1 and 6 and letting them to flow by gravity to the central chambers. To favor the PF entering the chambers it is better to aspirate from the waste wells once added the PF. Then, wait for at least 30 minutes, just to be sure the PF arrived well to the chambers and have passed enough time to fix the cells. Finally, we preserved the plates containing fixed cells for future analysis.

Technical note: *Live cells analyses in this system combine a complex microfluidic plate protocol to create different flows inside the channels but also allows the recording of the experiment by time-lapse at different locations in each chamber continuously for 24 hours. The complete protocol to obtain these time-lapse recordings will be described below with more detail and it is common for all the microfluidic plates experiments on this thesis.*

Creation of Ca^{2+} waves to microglial cells in switching plates

As the gradient plates, the switching plates also contain four chambers (A-D), and each chamber has a circular middle space connected with two smaller channels around it. Each small channel surrounds half of the circular space. In this case we used the middle channel to load the cells in DMEM medium and the lateral channels to administer the different calcium concentrations media to the cells to register the cellular motility.

The switching plate has also 24 inlet wells (also referred as channels) to channel the different media, and 2 output waste wells (7 and 8) per chamber. In this plate type, channel 6 is used to introduce the main medium and load the cells. Channels 2 and 3 are used to place medium to one side of the peripheral channel along the culture chamber, whereas channels 4 and 5 introduce the medium to the peripheral channel along the other side of the culture chamber. Channel 1 can also transports medium along the periphery of the chamber and thrust the media for channels 2-5 to the middle, allowing the diffusion exchange in the chamber (Figure II).

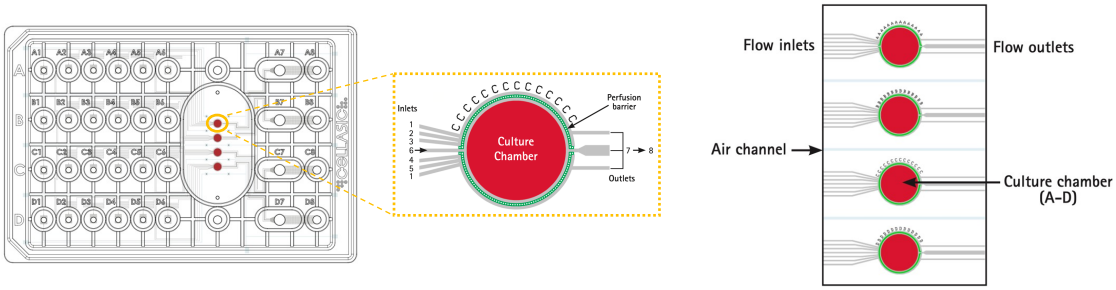


Figure II. Diagram of the switching plate. View of the plate and detail to better understand how the inlet and outlet channels work and where are located respecting to the central culture chamber (CellASIC™).

The usage procedure for the switching plate is the same than described above for the gradient plate, the first step is to cover the chambers A-D with PLL for two hours to allow the cell attachment. Then, BV2 cells are prepared for seeding at a final density of 700,000 cells/mL. Then the cells are cultured inside the chambers. For this, we used the automated seeding protocol as described above. Once microglial cells were inside the plate, we let them grow for 24h in DMEM supplemented with FBS 10% and 0.1% P/S at 37°C and 5% CO_2.

Among the wide range of experiments that can be performed with switching plates, we were interested in generating chemoattractant waves to track microglial cell motility.

In this case we used inlet channels 2, 3, 4 and 5 to generate flow waves, for that we added 9 mM Ca^{2+} DMEM (DMEM without calcium modified with $CaCl_2$ to obtain a 9 mM Ca^{2+} concentration) in each of these inlets for every chamber (A-D).

Then, plates were connected to the system manifold (CellASIC™ONIX) to establish the vacuum in the plate and connect the microfluidic system (CellASIC™ONIX). We then set the flow of the chambers with the user interface software (CellASIC™ONIX FG). With the purpose of generating waves, a specific protocol was created to simulate this phenomenon that may occur physiologically in neurodegeneration (D. Sieger et al., 2012).

In this specific protocol, wells 2 and 5 were pressured together and then 3 and 4 in alternation. With this combination, we assured a switching pulse, simulating a Ca^{2+} waves, in the whole area of the chamber. The pulses were created every 15 minutes and being alternated with another 15 minutes interval with no pulse receiving normal DMEM from inlet 1, following the next scheme: inlet 2+5 for 15 minutes, no Ca^{2+} pulse for 15 minutes, inlet 3+4 for 15 minutes, and no Ca^{2+} pulse for another 15 minutes.

We performed this experiment, repeating the 4 steps mentioned above reiteratively to generate Ca^{2+} pulses throughout 24 hours. Time-lapse video recordings were made to analyze the cell motility in response to these Ca^{2+} waves. After that, we fixed the cells of the plate with 4% PF. To fix these plates we used the same protocol as described for the gradient plate, but in that case only adding the fixative in wells 6 and letting the solution to flow by gravity to the central chambers. Finally, we preserved the plates for additional analyses.

Technical note: *Time-lapse analysis was done by recording different locations of each chamber continuously for 24 hours. The procedure is explained in detail below.*

Time-lapse recording in microfluidic experiments

The time-lapse recording was set up in an inverted microscope (Nikon Eclipse TE-2000E) – which is part of the *Microscopy facility* of the INc-UAB – with a motorized stage. By using an objective of 10x magnification we first located microglial cells at the starting point, after that, we determined the specific positions for capturing images within the culture chamber either in gradient or switching plate. With a specific microscopy software (MetaMorph® Molecular Devices, LLC.; San Jose, CA, USA; version 6.1) connected to the motorized stage, we were able to save a memorized positions list.

For the analysis in the gradient plate, we created 12 different positions, 3 per chamber, whereas for the switching plate, we took 40 different positions, 10 in each chamber, trying to cover the entire chamber's area. We established as an optimal timing to take the pictures every 5 minutes and we created a software journal to execute this command. We first turned on the microfluidic software (CellASIC™ONIX) to start generating the medium flows, whether Ca^{2+} waves or constant flowing milieu, depending on the experiment, and immediately after, the journal was started for the time-lapse recording for 24 hours.

After stopping the recording, cells were fixed. To obtain the final videos, we used a specific software (ImageJ NIH; Bethesda, MD, USA); version 2.0.0) stacking tool, which allows to stack a serial of continuous images into a final movie.

1.8. Cell tracking in CellASIC™ONIX microfluidic plates

With the final time-lapse videos, we analyzed the cell movement in each of the position to obtain a tracking graph. For this quantification, we also used a computer software that includes a plugin for "Manual tracking" (Image J). This plugin sets the parameter of location for each microglial cell within each frame of the time-lapse, according to 5 minutes interval and 0.129 µm as the x/y calibration according to the magnification used on the microscope.

For tracking the cells, by clicking on the center of one cell in the first frame, the track can be traced following every single frame. We then obtained a final track for each cell that can be graphed, and the parameters of velocity and total distance travelled are calculated.

A total of 12 different frame positions were captured for gradient plates and 30 cells per condition regardless of their position inside the chambers. In the switching plate 3 frame positions were recorded close to the inlet channels (left side of the chamber in the diagram [Figure II]) and 3 frames were taken close to the outlet channels (right side in the diagram [Figure II]). A total of 30 cells (CellASIC™ONIX) were analyzed for every position. Changes in motility of microglial cells were then compared and correlated with the specific moment when the calcium wave was generated.

1.9. MPP^+ administration to MSF neurons

To determine the level of toxicity of 1-Methyl-4-phenylpyridinium (MPP^+) iodide on dopaminergic neuronal death, we performed a series of experiments intoxicating primary neurons obtained from MSF of rat embryos.

Primary neurons were first cultured as described above. Then at 4 or 7 DIV, we administered the neurotoxin MPP^+ at different concentrations, 2 µM, 5 µM, 10 µM, 30 µM and finally 100 µM, according to previous procedures (Henze et al., 2005), and define which concentration of MPP^+ could be toxic to lead to a significant dopaminergic neuronal death. A control condition was also established, being only neurons cultured with no MPP^+.

For the administration, a stock solution of MPP^+ iodide (Sigma-Aldrich; St Louis, MO, USA; Ref. D048-100MG) was first prepared in 2 mL of H_2O milliQ, then transferred to a larger tube to add

H_2O to a final volume of 33.65 mL to obtain a final concentration of 10 mM. Immediately after preparing the stock solution, we added to each condition the specific amount of neurotoxin solution to obtain the desired final concentrations. Then, we administered the MPP^+ solution directly to the wells on which we cultured the neurons.

Once the MPP^+ was administered, we left the cells in the incubator at 37°C and 5% CO_2 for either 24 hours or 48 hours. Then, the cultures for each timepoint were fixed with 4% PF for 20 minutes and then preserved in PBS at 4°C for future immunostainings.

1.10. Cocultures primary MSF neurons and microglia

With the purpose of creating a more physiological condition than when using cell lines, we decided to set primary cocultures, proceeding as described in previous experiments, from the mesencephalon of rat embryos.

First, we obtained and cultured primary microglial cells as described in the protocol above. Then, we let the microglial culture from the MSF to grow for approximately three weeks, renewing the media once a week.

At the same time, we performed a culture to obtain MSF neurons and let them grow in 24-well plates for 4-7 DIV at a density of 300,000 cells/mL. After that, we obtained microglia in a density of 100,000 cells/mL to be added to the wells with the neurons.

This procedure was later used to perform different experiments to analyze the effect of microglial activation on dopaminergic neuronal death or vice versa.

MPP^+ intoxication of primary MSF neurons in coculture

As we did with primary neurons, we induced neuronal loss with MPP^+ on microglia-neuron coculture. In this experiment, we created an environment in which the neurons were intoxicated with MPP^+ but with no activation of microglia. For that, we administered the MPP^+ solution in two different concentrations, 10 µM and 100 µM, to cocultures for 24 hours.

Activated primary MSF microglia in coculture

To know whether activated microglial cells could produce dopaminergic neuronal death, we induced the activation of microglia with canonical pro-inflammatory stimuli in the cocultures. We treated the microglia-neuron cocultures with the same procedure that we used for activating microglial cells alone. A combination of LPS and IFN γ was added to the cocultures at

two different concentrations: LPS 10 ng/mL plus IFN γ 25 ng/mL or the combination of LPS 10 ng/mL plus IFN-γ 50 ng/mL. Cocultures underwent this treatment for 24 hours.

Combination of neurotoxic insult to neurons and activation of microglia

To understand if activated microglia could contribute to the MPP^+-induced dopaminergic neuronal death, we added two other conditions of microglia-neuron coculture to combine at the same time the intoxication of dopaminergic neurons with MPP^+ and the activation of microglia to a pro-inflammatory phenotype with the administration of LPS and IFN γ.

Considering how deleterious the exacerbation of activated microglia could be for neurons intoxicated with MPP^+, we decided to use the LPS and IFN γ at the lowest concentration and combined with two different concentrations of MPP^+. To create these conditions, we first administered the MPP^+ solution to the cocultures to a final concentration of MPP^+ 10 µM and 100 µM, respectively. Then, we added a solution of LPS 10 ng/mL plus IFN γ 25 ng/mL to the wells to induce microglial activation. Cocultures were treated with the combination of the neurotoxic insult and the pro-inflammatory stimuli for 24 hours.

Sensitization of neurons by primary microglia supernatant

Because activated microglial cells release pro-inflammatory components to the external milieu, we analyzed in which degree they exacerbate dopaminergic neuronal death. In turn, whether the actual presence of microglial cells or the sole released components after activation may play an important role for dopaminergic neurodegeneration.

For that, we treated neurons with supernatant of previously treated primary microglia cultures. We considered three different conditions: Neurons treated with supernatant from non-activated microglia or treated with the supernatant from microglia activated either with LPS 10 ng/mL plus IFN γ 25 ng/mL or LPS 10 ng/mL plus IFN γ 50 ng/mL. We added 300 µL of supernatant to the neurons, which makes half of the total volume of the well. Cells were under these condition for 24 hours.

For this experiment, we used the following controls: i) Neurons cultured alone but treated with the normal media used for microglia – normal DMEM – to control the differences with the neurons treated with supernatants from microglial cells; ii) Neurons alone with their normal culture media but with the administration of LPS 10 ng/mL + IFN γ 25 ng/mL to check if the pro-inflammatory stimulus by itself could produce some changes in the neurons; or iii) The coculture of neurons and microglia with no treatment either with MPP^+ or LPS – IFN γ.

1.11. Immunocytofluorescence in primary cultures

The protocol followed for the immunostaining in primary cultures was the same described above for cell lines. Cells were incubated overnight with primary antibodies, using 12 µL volume on coverslip, diluted in 0.01% saponin/1%BSA/PBS1X at RT in a small chamber with a moist cotton bedding.

For cultured microglia, the primary antibodies used were, anti-Iba-1 (1:500, polyclonal rabbit IgG) to visualize microglial cells and analyze the distribution of Iba-1 inside the cell and anti-γ-tubulin (1:500, monoclonal mouse IgG) to label the MTOC.

For cultured neurons, the primary antibodies used were, anti-TH (1:500, polyclonal sheep IgG1) to label specifically dopaminergic neurons in the culture and anti-MAP2 (1:500, polyclonal chicken IgY; Abcam; England, UK) to identify all neurons.

For microglia and neurons cocultures, the primary antibodies used were, anti-Iba-1 (1:500, polyclonal rabbit IgG) to identify microglial cells; anti-TH (1:500, polyclonal sheep IgG1) to specifically label dopaminergic neurons and anti-MAP2 (1:500, polyclonal chicken IgY) to mark all neurons.

Note: *the complete references for the antibodies are listed at the end of the methods (Table 2 and 3).*

Secondary fluorescent antibodies diluted 1:1000 in 0.01% saponin/1%BSA/PBS1X, accordingly with the host of the primary antibodies, were used for the subsequent detection. For cultured microglia, the secondary antibodies AlexaFluor 488 Goat anti-Rabbit IgG, and AlexaFluor 555 Goat anti-mouse IgG, were used. Then, as in cell lines, we also used a phallotoxin to stain the cytoskeleton f-actin fibers: AlexaFluor Phalloidin 647 (1:40). For neurons, we label the TH positive neurons with AlexaFluor 488 Donkey anti-sheep IgG, and MAP2 with AlexaFluor 555 Goat anti-chicken IgY (Life technologies; Carlsbad, CA, USA). For the cocultures, we used AlexaFluor 488 Donkey anti-sheep IgG to stain TH positive neurons, AlexaFluor 555 Goat anti-chicken IgY for MAP2 stained neurons, and AlexaFluor 647 Goat anti-Rabbit IgG (Life technologies; Carlsbad, CA, USA) for microglia secondary detection.

Next, DAPI (1:1000) was added to the wells for 5 minutes to stain the nuclei of the cells. In addition, one of the coverslips for each treatment was not incubated with primary antibodies, but only with secondary antibodies (secondary-antibody control).

Finally, coverslips were mounted on glass slides using Prolong Gold antifade reagent.

1.12. Epifluorescence and confocal microscopy and quantification

All these samples were examined with an epifluorescence microscope (Eclipse 90i; Nikon) or a confocal laser-scanning microscope (LSM 700 AXIO Examiner, Carl Zeiss) depending on the purpose of the study.

For the epifluorescence microscope, the Plan-Apochromat 20x/0.75 DIC M/N2 or Plan-Apochromat 40x/0.95 DIC M/N2 objectives were used. Pictures were taken with a digital camera (DXM 1200F) and a specialized software (ACT-1 version 2.70, Nikon) to capture the images.

For the confocal microscope a Plan-Apochromat 20x/0.8 Ph2 M27 and a Plan-Apochromat 40x/1,3 Oil DIC M27 objective lens (Carl Zeiss) were used for examining the samples, and later processed with specific software (Zen 2010 Carl Zeiss). A series range for each section was set by determining an upper and lower threshold using the Z/Y position for spatial image series. Stacks of the images were taken with an optical section interval of 0.8 µm. Three-dimensional reconstructions were generated using an α blending software (ZEN 2010), or image processor (Image J, version 2.0.0; NIH) and visualized with a rendering software (IllucidaFX software version 1.0 (6A); IllucidaLLC; Los Ángeles, CA, USA).

We used a conventional image analysis software (Image J, version 2.0.0; NIH) for the quantifications in 2D epifluorescence images, using macros created specifically for each quantification. Three-dimensional images were quantified with a specialized software for 3D-imaging and rendering (IMARIS software, version 8.3.4; Bitplane AG; Zurich, Switzerland), the analysis with this software allowed to perform a wide range of quantifications in 3D images; as the volumetric colocalization of fluorophores, location of organelles or number of cells.

1.13. Colocalization analyses in cell lines and primary microglia

We wondered if Iba-1 could migrate to different locations within the cell when they are activated, and if this migration could be related with cell movement. For this, we used BV2 cell line, as well as primary microglia, stimulated with pro-inflammatory stimuli previously mentioned. After seeing a clear activation of microglia when exposed to a combination of LPS and IFN-γ, we quantified the location of Iba-1 in relation to F-actin fibers (combining Iba-1 immunocytofluorescence and phalloidin) in all the experimental conditions and different states of activation. For that we used a 3D rendering software (IMARIS software, version 8.3.4) with the *Colocalization tool*, which quantify the total number and percentage of voxels that coincides

for each of the two markers used. In this case, the percentage of Iba-1 staining that coincided with the F-actin cytoskeleton fibers and vice versa.

1.14. MTOC location

As the MTOC is considered a critical organelle controlling cell motility, BV2 and primary microglia cultures, previously treated with pro-inflammatory stimuli, were quantified and classified, regarding the location of the MTOC. For that, the labeling for γ-tubulin combined with phalloidin was utilized. We quantified, by counting manually, the number of MTOC located *in front of*, *besides,* or *behind* the cell nucleus in relation with the classical kinetic morphology evidenced by the cytoskeleton staining.

1.15. Differences in intensity and morphology when administering extracellular Ca^{2+} to BV2 cells

In both experiments, non-calcium deprived cells and previously deprived cells, a total of 30 images per condition were taken, following the same procedure, at 20X magnification, using the epifluorescence microscope already mentioned in previous sections. We measured both intensity and morphology of the cells after different administrations of Ca^{2+} concentrations. For these two quantifications we used a conventional image analysis software (ImageJ).

The morphology of the cells was measured by depicting the contour with the freehand selection tool and following the expression of phalloidin staining. Then, a selection of the whole cell was created following the specific morphology defined by the F-actin staining for every cell in each sample frame.

For measuring Iba-1 intensity, we created a specific macro to obtain the mean intensity between the highest and the lowest value for every cell in the picture, and then, we ran a specific plugin for all the images taken for Iba-1 staining.

1.16. Homogenates and western blot for Iba-1 intensity

To validate the fluorescence results, we also used western blotting as a canonical method to quantify the protein concentrations. We replicated the same culture experiments with BV2 and primary microglia administering different Ca^{2+} concentrations to the cells.

Homogenates

We homogenized the cells from microglia cultures by lysing with a scrapper (Sarstedt; Nümbrecht, Germany; Ref. 83.3950). First, we aspired the supernatant from the wells, then the

cells were washed twice with cold fresh PBS1X. Then 0.5 mL of **NP-40 solution** (150 mM NaCl, 1% Triton X-100, 50 mM Tris pH 8.0; 1x proteases/phosphatases inhibitors) – which is the lysate solution – were added to every sample. After that, we scrapped the cells gently and collected the solution with the scrapped cells to microcentrifuge tubes (Deltalab; Barcelona, Spain; Ref. 200400P) for later protocol. *

**This procedure needs to be carried out on ice*.

Then, we shook the samples in microcentrifuge tubes for 30 minutes in a shaker (300 rpm) at 4°C. Once finished, samples were taken and centrifuged at 16,000G for 20 minutes at 4°C. After the centrifugation, we recollected the supernatant in new microcentrifuge tubes – which would contain the proteins to be analyzed by western blot – and the pellet was discarded.

Protein concentration by BCA assay

The BCA Pierce™ assay (ThermoFisher; Waltham, MA, USA; Ref. 23225) is a well-established method to determine the protein concentration in samples for later quantification. In this assay two different reagents are used. The principle of this method is a reduction of Cu^{2+} to Cu^{1+} by the proteins in an alkaline medium, then a second reaction is produced, in which the bicinconinic acid (BCA) is added and reacts with the copper forming a blue complex which then veers to purple and allows the protein quantification.

In our protocol, 25 µL of the samples were added in a 96-well plate. After that, 200 µL of the BCA solution mix, combining A-B reagents (50:1), was added to every sample well, and the plate was shaken for 30 minutes at RT. Finally, the absorbance was read spectrophotometrically at 560 nm to obtain the protein concentration. This assay requires the interpolation with a standard curve for obtaining the final concentrations. The curve was obtained simultaneously to analyzing the samples with known concentrations of protein, ranging between 15,6 µg/mL and 2000 µg/mL and by adding the same BCA solution.

Western blot protocol

Precast gels (Mini-PROTEAN®, Bio-Rad Laboratories; Hercules, CA, USA; Ref. 4561093), suitable for western blot were used for this protocol, with a gradient of polyacrylamide between 4-20%. Samples were first mixed with loading buffer (Tris pH 6.8, SDS 20%, Glicerol 99%, 2-mercaptoethanol and bromophenol blue) to visualize the migration of the samples within the gel and were loaded according to the original protein concentration diluted to a final concentration of 0.5-1 µg/µL. We also loaded a Full-Range ladder marker

(Amersham™ECL™Rainbow™, Sigma-Aldrich; St. Louis, MO, USA; Ref. GERPN800E) to control the position of the bands and the correlative molecular weights.

Once the precast gels were loaded with the samples, were introduced inside the electrophoresis chamber – which was filled with electrophoresis buffer (Tris Base, SDS, Glycine and H_2O) – and connected to the power supply for 30 minutes at 200 volts (V) to run the electrophoresis. When finished, we performed the transference to a membrane. For that purpose, we removed the gel from the electrophoresis chamber and put them into the transference cassettes. Before closing the cassete holder, we placed a nitrocellulose membrane (Amersham™Protran™, Dd Biolab; Barcelona, Spain; Ref. 10600002) on the top of the gels. These cassettes were then introduced in a transference chamber – previously filled with transference buffer (Glycine, Tris base, H_2O and methanol) – and then we set the power supply for 40 minutes at 100 V to promote the transference of the proteins to the membrane.

When the transference had finished, we used BSA 5% – diluted in TBS-T (NaCl, KCl, Tris, H_2O, and Tween-20) – to block unspecific sites of the proteins, incubating the membrane in a small container. Incubation was done having the membrane completely covered by this solution during 1 hour at RT. Then the membrane was washed 3 times with TBS-T for 5 minutes. After the blocking process, the membranes were incubated with primary antibodies. We used anti-Iba-1 primary antibody (1:1000, polyclonal rabbit IgG; Wako Pure Chemical Industries, Ltd.; Osaka, Japan; Ref. 016-20001) and anti-β Actin primary antibody (1:1000, monoclonal mouse IgG; Novus Biologicals Bio-Techne; Minneapolis, MN, USA; Ref. MAB8929) as a control of the presence of protein in the samples. The incubation with the primary antibodies was performed overnight at 4 ºC.

Then the membranes were washed 3 times for 10 minutes with TBS-T and incubated with the secondary antibodies for 1 hour at 4°C. The secondary antibodies used were, Goat anti-rabbit IgG (1:3000, Invitrogen ThermoFisher; Waltham, MA, USA; Ref. 31460), and Goat anti-mouse (1:5000, Invitrogen ThermoFisher; Waltham, MA, USA; 31430). After finishing the secondary antibodies incubation another set of washes with TBS-T was accomplished.

Finally, we revealed the membranes with the enhanced chemiluminescence (ECL) detection protocol. In this process, we used two different reagents to detect the presence of protein, ECL1 (Tris-HCl 1M pH8.5, luminol 0.5M, ρ-coumaric acid 79.2 mM and H_2O) and ECL2 (Tris-HCl 1M pH8.5, H_2O_2 30% and H_2O). These two reagents were combined in a ratio 1:1, and the solution was added to every membrane, then we waited for up to 1 minute and revealed the membrane

with specific image analysis device (LI-COR® Odyssey Fc Imager) and software (LI-COR® acquisition software, LI-COR® Bioscience; Lincoln, NE, USA).

The images obtained with the acquisition system were then analyzed and quantified with a quantification software (ImageJ) in terms of density and thickness of the bands.

1.17. Contacts/phagocytosis BV2-PC12

Cocultures carried out with BV2 and PC12 cells were used for counting the number of cell-to-cell interactions, as well as phagocytosis found in every timepoint. As we identified different types of approaches or contacts between BV2 cells and PC12, we described four different categories to analyze and determine which timepoint is the optimal to display bona fide cell-cell interactions.

Category 1, BV2 microglia displaying kinetic morphology towards a PC12 dopaminergic cell but without contacting; **category 2,** interaction between a BV2 and a PC12 cell contacting and creating a flat interface; **category 3,** BV2 microglia engulfing a PC12 cell; and finally, **category 4,** BV2 microglia showing a pycnotic nucleus, or nuclei, inside a phagosome.

1.18. Measurement of calcium released by neurons when exposed to a dopaminergic neurotoxic insult

For this analysis, neurons alone or neurons cocultured with microglia treated under different experimental conditions above described (MPP^+ 2-100 μM and combination of MPP^+ with LPS/IFN γ) were used to measure the amount of calcium released to the media. For that, the supernatant from every condition was first taken and preserved up to the analysis. Then, with a calcium colorimetric assay (Sigma-Aldrich; St. Louis, MO, USA; Ref. MAK022-1KT) we determined the calcium ion concentration in the supernatant samples by interpolating the absorbance in each condition.

In this colorimetric assay, a chromogenic complex is formed between the calcium ions, present in the sample, and o-cresolphthalein (chromogenic reagent, Ref. MAK022B). This complex produces a colored solution, which can be spectrophotometrically quantified by absorbance at 575 nm to determine the calcium ion concentration, which is lineally proportional to the absorbance. In this assay a standard curve was established between 0 and 2.0 μg of calcium per well with the Calcium Standard Reagent provided by the commercially available kit (Ref. MAK022C).

According to the manufacturer, to avoid saturation of the measurements, samples should be diluted prior the analysis, because of the high calcium amount that the media may have. In our case, after several trials, we diluted ¼ our samples in water before the measurements. Then, 90 µL of the chromogenic reagent was added to every sample well, as well as the standard curve, followed by an addition of 60 µL of the calcium assay buffer (Ref. MAK022A). The plate was mixed gently, and after 10 minutes of incubation at RT, the absorbance was read with the spectrophotometer.

1.19. Number of neurons in the primary culture and coculture

Since MPP^+ induces dopaminergic neuronal death, we quantified the loss of dopaminergic neurons according with the increase of the MPP^+ concentration, and in combination with microglia to determine the potential contribution to increase this neuronal loss. The number of neurons were analyzed with image analysis software (Image J) counting manually the number of dopaminergic neurons (TH positive staining) and the total number of neurons (MAP2 positive staining) in all the experimental conditions. We also manually counted the number of microglial cells establishing contacts or phagocytosing the neurons.

1.20. Calcium internalization by microglia in live analyses

Since we wondered if microglia were able to internalize calcium, we planned an experiment with primary microglia to measure calcium internalization when they are exposed to an external calcium input. For this we used an inverted microscope (Nikon Eclipse TE2000U) attached to a monochrome camera (Hamamatsu DCAM, 1394 OHCI; Hamamatsu Photonics; Shizuoka, Japan) that allows to focus only on the coverslip with the cells attached. Microinjection of calcium solutions were directly released to the cells without changing the medium and pictures were taken with an interval of ten seconds between the pictures, generating a final short-term time-lapse. The microscope was combined with an OptoScan monochromator (Cairn Research Limited; Kent, United Kingdom) allowing to excite the fluorophores at the specific wavelengths in the visual range.

For this experiment, we used primary microglia obtained from MSF of P0-P2 rats, as previously described for previous experiments. We cultured primary microglia on PDL pre-coated coverslips inside 35mm diameter Petri dishes (Sigma-Aldrich; St. Louis, MO, USA; Ref. 351008) at a density of 300,000 cells/mL and let them grow and attach to the coverslip for 24 hours. Then, we cultured the cells with a buffer solution (Krebs buffer 1X, BSA) containing the fluorophore Fura-2 (ThermoFisher; Waltham, MA, USA; Ref. F1221) for at least 2 hours. This

solution allows the cells to incorporate Fura-2 fluorophore intracellularly. The principle of this technique is that when Fura-2 is not binding any Ca^{2+} molecule emits high fluorescence intensity at 340 nm and low at 380 nm, and when binds Ca^{2+}, the fluorescence remains low at 340 nm but high at 380 nm. Then, the fluorescence intensity is related to the Ca^{2+} molecules internalizing.

Once Fura-2 was internalized by microglia, we placed the coverslip in a specific chamber on the microscope stage – in which we administered calcium at different concentrations. We set all the parameters to capture the images of microglial cells (one picture every 0.15 seconds for 2-5 minutes) generating a time-lapse video. At the initiation of the time-lapse, we administered the calcium solution to visualize the differences. The solutions were added by pipetting directly to the coverslips.

The recording of the time-lapse was performed with a specialized microscopy software (MetaFluor® Microscopy Software, Molecular Devices, LLC.; San Jose, CA, USA; version 8.10) in which we could obtain the taken frames with the 340/380 nm fluorescence ratio for the final video. Then in an image analysis software (Image J) the time-lapse file was built up and analyzed to measure the fluorescence intensity during the experimental span.

1.21. Pilot experiments with viral vectors infections to microglia

With the purpose of silencing Aif-1 gene and observe how the cells behave in contrast with naïve cells. We thought of the use of either Adenovirus (Ad) or Adeno-Associated Virus (AAV) as the only option to transfect microglia, as standard transfecting procedures (i.e., lipofectamine) has usually failed in our hands.

First, we planned a pilot experiment to determine the optimal viral vector type in incorporating Green Fluorescent Protein (GFP) gene. By infecting microglial cells and analyzing GFP expression on the microscope, we were able to choose the best viral vector transfecting microglia. Once determining the optimal viral vector, we design and used an Iba-1 gene silencer.

For this experiment, we used two adenoviruses, Ad5 and Ad5/40 - which have been described as optimal to infect cells in vitro - and four different AAVs; AAV1, AAV6, AAV9 and AAVrh10 - which are described as more efficient infecting mouse cells in vivo. Both, the Ads and the AAVs, were provided by the *Unidad de Producción de Vectores (UPV)* from the *Institut de Neurociències* (INc).

On the one hand, as the adenoviruses titers are counted as Infectious Units (IU), the standard concentration used ranges between 1 and 500 IU/cell. On the other hand, AAVs titers are

estimated as viral genomes (vg), being the standard concentration between 10,000 and 20,000 vg/cell. * Knowing this and the final density of our cells we calculated the final infectious or physical titer to use.

We first cultured microglial cells in 96-well plates as described in previous experiments. However, in this case we did not use coverslips nor pre-coated plates. We left the plate on the incubator for 24 hours to allow the cells to growth. The next day, the viral vectors solutions were prepared, using three different concentrations for each viral vector to determine the most appropriate concentration to use in the following experiments. For the Ad5 and Ad5/40, we used 50, 250 and 500 IU/cell, whereas for the AAVs we used 20,000; 50,000; and 100,000 vg/cell. We diluted the viral vectors stock solution in the cell culture media where these cells normally grow. Once the solutions were prepared, were added directly to the microglial cells, and placed them in the incubator for 72h to promote the transfection. Then, we fixed the cells with PFA 4% for 20 minutes and preserved the plate until analysis.

We directly checked the plate on an inverted microscope to quantify the total number of cells in each well, and how many of them had incorporated the viral vector and, in consequence, expressed the GFP in the green fluorescence channel. To analyze this, 30 pictures for each condition and per viral vector were taken on the inverted microscope (TE2000E) using the Plan Apochromat 10X objective; both in brightfield, to see the total number of microglial cells, and in green fluorescence, to see the total number of transfected microglial cells. For the quantification, we used a grid tool through an image analysis software (Image J) – which allows us to throw 3000 μm^2 quadrants in every picture with the same width – to quantify three quadrants per picture.

Table 1. Viral vectors information with the physical titer or infectious titer for each of the vectors used and expressed in their respective units.

Viral vectors information				
Vector Name	**Type**	**Prep #**	**Physical Titer (vg/mL)**	**Infectious Titer (IU/mL)**
AAV1-CMV-GFP	AAV	UPV-1104a	$1.41 \cdot 10^{13}$	__
AAV6-CMV-GFP	AAV	UPV-1237a	$1.67 \cdot 10^{12}$	__
AAV9-CMV-GFP	AAV	UPV-1243	$1.04 \cdot 10^{13}$	__
AAVrh10-CMV-GFP	AAV	UPV-1305	$4.03 \cdot 10^{12}$	__
Ad5-CMV-GFP	Ad	UPV-776	$1.74 \cdot 10^{12}$	$1.5 \cdot 10^{11}$
Ad5/40-CMV-GFP	Ad	UPV-708 (f3+f8)	$9{,}9 \cdot 10^{11}$	$8{,}9 \cdot 10^{9}$

2. *In vivo* experiments

2.1. Pilot experiment with Ca^{2+} injections in mice

4 weeks old C57BL/6j male mice were used for this experiment. The animals were purchased from a specialized supplier (Janvier Labs) at 3 weeks old and then kept and maintained under standard housing conditions (12h light/dark cycles and fed *ad libitum*) at the UAB Animal House Facility for a week until the experiment was carried out. As this was a pilot experiment, we performed two sets of trials with one animal per condition in each set.

We wondered if calcium, directly injected into the brain parenchyma, was able to induce changes in microglial cells motility or polarity, as we previously observed in cell cultures. For that, to determine the optimal concentration, we proposed 4 different concentrations to be injected in the striatum for later analysis. The Ca^{2+} concentrations used to inject the animals were: 0.25M, 0.5M, 0.75M and 1M to compare the changes between the treatments and consider the inflammation of the injection. In addition, we injected a different set of animals with sodium chloride solution (Saline) as a control condition (Laboratorios ERN, Barcelona, Spain).

First, the solutions were prepared the same day, hours before the injections to ensure they were fresh and ready to be injected. Calcium chloride was diluted in saline solution to the preferred final concentrations (0.25M, 0.5M, 0.75M and 1M). Then, the solutions were filtered with a 0.2 µm filter and preserved on ice until surgery.

The injections were carried out in an appropriate surgical room at the UAB Animal House Facility. Animals were first anesthetized with a mixture of anesthesia and analgesia with ketamine (Imalgene; Merial laboratorios; Barcelona, Spain) at a dose of 100 mg/kg; and medetomidine (Domtor; Orion Corporation; Espoo, Finland), at a dose of 0.5 mg/kg; injected intraperitoneally. After the standard absence of reflex, when pinching the mouse paw, solutions were inoculated stereotaxically into the striatum at the specific coordinates; Anteroposterior (AP): + 0.5 mm; Mediolateral (ML): + 2.1 mm; Dorsoventral (DV): - 3 mm, according to Bregma. For the inoculation, we used a 5 µL 75RN syringe (Hamilton Company; Reno, Nevada, USA; Ref. 87930) with the corresponding needles, 2 µL of the solutions were injected to the animals at a rate of 0.5 µL/minute for 4 minutes. After the injection, we waited up to 1 minute before slowly removing the needle. After the procedure, we stitch back together the skin with surgical suture (R&S; Paris, France; Ref. 3130374). For a faster recovery, animals were administered intraperitoneally with medetomidine reversal atipamezole (Antisedan; Orion Corporation; Espoo, Finland) at a dose of 100 mg/kg and placed on a heated mat to keep an appropriate and stable temperature during the recovery. Once recovered, animals were returned into the cage.

Three days post injection, the animals were euthanized. For this procedure, the same anesthesia was used, with the combination of ketamine at a dose of 100 mg/kg and medetomidine at a dose of 0.5 mg/kg; injected intraperitoneally. Once the standard reflex, when pinching the mouse paw disappeared, we proceeded with the perfusion protocol. The dissection was done by cutting the abdominal cavity and separating the rib cage until exposing the heart. A small incision of the auricle of the right atrium of the heart was done, and a perfusion needle was inserted in the apex of the left ventricle. With the help of a peristaltic pump – which allowed to have a continuous flux of the solutions. – we first placed Tyrode solution (NaCl, KCl, $CaCl_2$, $MgCl_2$, NaH_2PO_4, $NaHCO_3$, D-Glucose and H_2O) to achieve a complete blood perfusion and clearance. Then, a second solution containing 4% PF (PF, NaOH 1M, PBS1X; pH 6.9) was placed in the peristaltic pump and let the solution flow through the needle to the animal vascular system until full fixation of tissues was reached. The brain was then extracted from the perfused mice and post-fixed in 4% PF during 48 h. After post fixation, brains were stored in PBS with sodium azide (NaN_3) (Merck; Darmstadt, Alemania; Ref. 822335), until sectioning.

2.2. Ca^{2+} and Ca^{2+} chelator injections into the striatum

For this experiment the same strain of C57BL/6j male mice were used. The animals were also purchased by the same provider (Janvier Labs) at 3 weeks old and then kept and maintained under standard housing conditions (12h light/dark cycles and fed *ad libitum*) at the Animal House Facility of the UAB for a week until the experiment was carried out. We used 20 animals, distributed in four groups of five mice per cage.

Having the results of the pilot experiment, we established Ca^{2+} 0.5M as the best calcium concentration to induce visible changes in microglia but preserving with the lesser damage of the tissue. As control conditions we used a combination of Ca^{2+}0.5M + Ethylenediaminetetraacetic Acid (EDTA) 0.25M – a calcium chelator – to determine in what extent calcium is the factor inducing these changes, EDTA 0.25M to understand the potential changes produced by EDTA itself, and finally saline as a control of the injection.

The solutions were freshly prepared in advance to follow the administration the same day. Calcium chloride was diluted in saline to a final concentration of 0.5M in two different tubes. Then the EDTA was diluted in one of the tubes containing calcium for the Ca^{2+} + EDTA condition, and in a new one with saline for the EDTA alone condition to a final concentration of 0.25M. Then, the solutions were filtered with a 0.2 µm and preserved on ice until the surgery.

The surgery was performed with the same protocol described above for the pilot experiment. Animals were first anesthetized with a combination of anesthesia (ketamine) and analgesia (medetomidine) injected intraperitoneally. After the absence of reflexes, the animals were placed on the stereotaxic frame for the injections. The different solutions were inoculated stereotaxically into the striatum at the specific coordinates; Anteroposterior (AP): + 0.5 mm; Mediolateral (ML): + 2.1 mm; Dorsoventral (DV): - 3 mm, according to Bregma. For the inoculation we used a Hamilton 5 µL 75RN syringe, injecting 2 µL of the solutions at a rate of 0.5 µL/minute for 4 minutes. After the injection, we waited up to 1 minute before slowly removing the syringe. After stitching the surgical incision, mice received atipamezole intraperitoneally for a faster awakening, and placed on a heated mat to keep an appropriate and stable temperature during the recovery. Once recovered, animals were returned into the cages.

Three days post injection animals were euthanized by perfusion for histological analysis. This procedure was performed with the same protocol as in the pilot experiment.

Sectioning of Ca^{2+} injections experiments

Stored brains were prepared for sectioning as follows; 0.5 cm of the rostral part of each brain was sectioned by using a vibratome (Leica Microsystems; Germany), after removing the olfactory bulbs, to obtain coronal slices of the striatum. Six series of sections of 40 µm were obtained, setting the vibratome at a speed of 0.225 mm/s and a vibrating frequency of 60 Hz. Once sectioned, the brain sections were stored in PBS with NaN_3 until staining.

Immunohistofluorescence in Ca^{2+} injected mice

With the intention of knowing in which extension the calcium may produce changes in microglial cells when injected intrastriatally, either in shape or in number, a free-floating immunohistofluorescence was conducted on serial sections.

The sections were washed with PBS three times during 10 minutes, then antigen retrieval was conducted with a pre-treatment with citrate (10mM, pH 6, 60ºC) for 20 minutes. After washing another three times with TBS-triton 0.5% (Trizma base, NaCl, Triton, H_2O, pH 7.4), blockade for nonspecific binding sites was performed by incubating the sections with 0.5% Triton X- 100 with 10% HS (Sigma-Aldrich; St. Louis, MO, USA) for 1 hour. After blocking, the incubation with primary antibodies was done for 48 hours, diluting the antibodies in TBS-0.5% Triton X-100, 1% HS and 0.1% NaN_3. The primary antibodies used for these experiments were anti-Iba-1 (1:500, polyclonal rabbit IgG) to label all microglial cell phenotypes, and F4/80 (1:50, monoclonal rat IgG; AbDSerotec; Oxford, United Kingdom) to label reactive microglia.

Secondary fluorescent antibodies incubation was then performed for 24 hours diluted 1:1000 in TBS-0.5% Triton X-100, 1% HS and 0.1% NaN_3 according with the host of the primary antibodies. The secondary antibodies used were AlexaFluor 488 Goat anti-Rabbit IgG for Iba-1 detection and with AlexaFluor 555 Goat anti-rat IgG (Life technologies; Carlsbad, CA, USA) for F4/80 detection.

Next day, the sections were washed three times with TBS-T and then incubated with DAPI (1:1000) to stain the nuclei of the cells for at least 30 minutes. Then another set of washes was done with PBS.

Finally, the sections were mounted on glass slides and coverslipped using Prolong Gold antifade reagent.

Note: *the complete references for the antibodies are listed in a table at the end of the methods (Table 2 and 3).*

Confocal microscopy in Ca^{2+} injected mice

Ca^{2+} injected sections were examined with a confocal laser-scanning microscope (LSM 700 AXIO Examiner, Carl Zeiss).

Plan-Apochromat 20x/0.8 Ph2 M27 objective lens (Carl Zeiss) was used to obtain the pictures of the pilot experiment to determine the optimal Ca^{2+} concentration to use in later experiments. Plan-Apochromat 40x/1.3 Oil DIC M27 objective lens (Carl Zeiss) was used for the detailed analysis of microglial polarization labeled with Iba-1, taking pictures at specific regions from the injection. To follow the calcium gradient within the tissue, and to observe the degree of microglial reaction from the injection, pictures were taken at four consecutive quadrants starting from the injection site and going 1280 μm away from the injection (Figure III). Pictures were later processed with confocal software (ZEN 2010 Carl Zeiss). A series range for each section was set by determining an upper and lower threshold using the Z/Y position for spatial image series. Stacks of the images were taken with an optical section interval of 0.8 μm. Three-dimensional reconstructions were generated and visualized using α blending softwares (ZEN 2010) (Image J, version 2.0.0; NIH) (IllucidaFX software (version 1.0 (6A); IllucidaLLC; Los Ángeles, CA, USA).

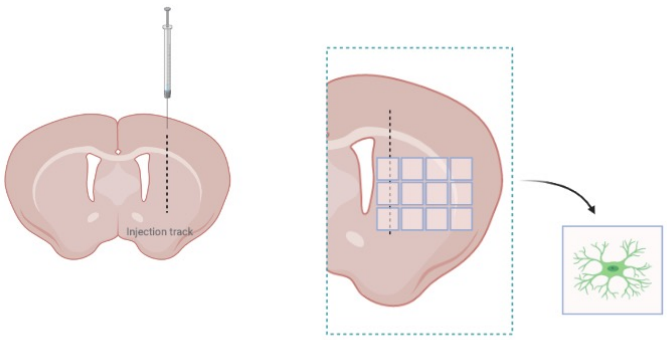


Figure III. Schematic representation of the stereotaxic injection at the striatum and the area of picture frames taken on the microscope, going 1280 μm away from the injection site. In each quadrant, the polarization of microglial branches, labeled with Iba-1, were analized in detail.

3D high resolution confocal images were quantified with a specialized software (IMARIS version 8.3.4; Bitplane AG; Zurich, Switzerland) mentioned above, with the specific *Filament Tracer* module – which allowed to trace the ramifications of single microglial cells emerging from the cell body - for later analyses.

Morphometric analyses

With the rendered images, we traced the ramifications emerging from the cell body of each microglial cell. This tool included in the analysis software (IMARIS), allowed to obtain the total number of cells per picture, the number of branches, the number of branching points, and the total filament length per cell. The data were analyzed to represent the differences of microglial cells shape in all these three parameters comparing the different treatments.

Polarization of microglial cells in Ca^{2+} injected animals

By observing the shape of microglial cells while performing the morphometric analyses, we recognized some differences in the level of arborization towards the calcium source. By using the captured frames, and the Filament Tracer tool (IMARIS), we quantified the total number of branches in each side of the microglial cell, either facing the calcium source or 125opposite to the calcium source. For that purpose, the analysis required to equally divide each microglial cell body in two parts. Once divided, filaments emerging from each side of the cell were counted and later classified depending on the orientation, either towards or opposed to the injection. The numbers were then compared between conditions and frames.

Reactive morphology analysis with F4/80 staining

Since EDTA-injected mice showed iba-1^{+} cells with rounded shape that could be equivalent to reactive microglia in terms of morphology, to rule out whether EDTA by itself or the other experimental conditions could produce a significant activation of microglial cells, we used immunohistofluorescence to label F4/80 in combination with Iba-1.

For this analysis, images were taken as we described in the previous experiment (Figure IV), with four frames starting from the injection site and moving away 1280 µm. In this case, consecutive pictures were taken with a 20% overlap with the purpose of generating a mosaic. Built mosaics were analyzed with relative fluorescence, covering the same area for every picture, and compared between experimental conditions to visualize the variation of the activated-like morphology and F4/80 expression.

2.3. Analysis of polarization in MPTP-injected mice

Note: *for this experiment in this thesis, we used animals from a previous experiment performed in our group.*

MPTP administration

To reproduce a specific dopaminergic neuronal loss to model Parkinson's disease, we used the 1-methyl-4-phenyl-1,2,3,6-tetrahydropyridine (MPTP) toxin. Animals, purchased from specialized supplier (Janvier Labs) were kept and maintained in the UAB *Animal House Facility* as in previous experiments.

In this experiment, we used groups of 5 male mice of the C57BL/6j strain. First group of animals was injected with a single dose of MPTP dissolved in saline solution at a concentration of 20 mg/Kg. The second group, the control, was injected with the same volumetric amount of saline solution. As the injections were conducted intraperitoneally, no method of anesthesia and analgesia was indicated or recommended.

After 72 hours, animals were euthanized by intracardiac perfusion as indicated in previous experiments. Regarding the sectioning, the procedure was the same as in the calcium injected mice. Six series of 40 µm-thick sections were obtained with a vibratome (Leica Microsystems, Germany) after removing the olfactory bulbs and setting the vibratome at a speed of 0.225 mm/s and 60 Hz vibrating frequency. In that case, both the striatum and the MSF were regions of interest. Once sectioned, brain tissue was stored in PBS with NaN_3 until staining.

Immunohistofluorescence

To evaluate changes in the degeneration of dopaminergic neurons and neuroinflammation, floating sections were treated following the protocols of immunohistofluorescence described in previous sections. Antigen retrieval pretreatment with citrate was done at 60°C for 20 minutes. After this, blocking of unspecific binding sites was carried out with 0.5% Triton X-100 with 10% HS for 1 hour. Then, the incubation of primary antibodies was conducted. These antibodies were also diluted in TBS-0.5% Triton X-100, 1% HS and 0.1% NaN_3. The primary antibodies used for this set of experiments were anti-Iba 1 (1:500, polyclonal rabbit IgG) to label microglial cells, and anti-TH (1:500, polyclonal sheep IgG1) to identify dopaminergic neurons. After 48 hours of incubation with the primary antibodies and proper subsequent washes, secondary antibodies diluted in TBS-0.5% Triton X-100, 1% HS and 0.1% NaN_3 (AlexaFluor 555 Goat Anti-rabbit 1:1000 to recognize Iba-1 and AlexaFluor 488 Donkey Anti-sheep 1:1000 to recognize TH) were used accordingly for an overnight incubation of the sections. Finally, DAPI (1:1000) was used to stain the nuclei of the cells. Sections were mounted on glass slides and coverslipped using antifade reagent (Prolong Gold, Thermofisher).

Note: *the complete references for the antibodies are listed in a table at the end of the methods (Table 2 and 3).*

Confocal microscopy

As our study was focused on the loss of dopaminergic neurons and their connection with the reactivity of microglia and the subsequent polarization, we only used the sections of the MSF containing the Substantia Nigra *pars compacta* (SNpc) to be analyzed.

Confocal pictures were taken in the ventrolateral area of the SNpc – which is described to be the area where a higher proportion of dopaminergic neurons undergo degeneration in PD. By using a Plan-Apochromat 40x/1,3 Oil DIC M27 objective lens (Carl Zeiss) we obtained 10 pictures per animal and per experimental condition. To analyze the microglial polarization, sampling frames were taken of microglial cells from adjacent areas to the remaining neurons of the SNpc. We discarded analyzing microglia among dopaminergic neurons since the polarization of branches may not be evident. Then, we took pictures adjacent to the ventrolateral area of the SNpc but visualizing dopaminergic neurons to recognize the location. The pictures were later processed with the specialized software (ZEN 2010 Carl Zeiss). A series range for each section was set by determining an upper and lower threshold using the Z/Y position for spatial image series. Stacks of the images were taken with an optical section interval of 0.8 µm.

Analysis of the polarization in MPTP/saline injected animals

As microglia in Ca^{2+}-injected mice showed differences when analyzing the polarization, we wondered if microglia of animals injected with MPTP could undergo the same phenomenon towards dopaminergic neurons. For that, high-resolution three-dimensional images were quantified with specialized software (IMARIS version 8.3.4; Bitplane AG; Zurich, Switzerland) mentioned above, with the specific *Filament Tracer* module. We conducted the quantification as described for calcium-injected mice, randomly selecting microglial cells in each sampling picture, dividing each microglial cell body, and analyzing the number of emerging branches going towards dopaminergic neurons or to the opposite site. The results were divided by number of branches and their size, opposite or towards the neurons and then compared between experimental conditions.

2.4. Pilot experiments with viral vectors infections in mice

Once we performed the analyses of viral vector transfections in cell cultures and determine which vectors were the optimal to infect microglial cells, we decided to test the same vectors,

only incorporating GFP, in mice. For that purpose, we kept using the same mice strain than in previous experiments (C57BL/6j).

Animals were purchased to the same supplier (Janvier Labs) at 3 weeks of age and then kept and maintained under standard housing conditions (12h light/dark cycles and fed *ad libitum*) at the UAB Animal House Facility for one week until the experiment was carried out. We ordered a total of 27 animals for this pilot experiment, distributed in 3 groups according to the type of viral vector used and, three subgroups depending on the viral concentration. The animals were randomized and distributed evenly, three mice per cage, and every cage was labelled with the experimental vector and concentration (described below).

We decided to use the two adenoviruses (Ad5, Ad5/40) – previously used in vitro, since they had good transfection rate in microglial cell cultures. As AAVs are good viral vectors to infect other brain cells in vivo in mice, although none of them gave us good results in cells, we tested one of the adeno-associated viruses, the AAV1, to check the potential infectivity in vivo. Because we did not have previous results using these viral vectors to transfect microglia, we decided to use three different concentrations according to the titer of each vector. As described in previous studies to inject viral vectors in the striatum (Barcia et al., 2007), we used a potentially optimal concentration of $1{\cdot}10^7$ gc/µL, but also testing a lower and higher concentration of $1{\cdot}10^6$ gc/µL and $1{\cdot}10^8$ gc/µL. According to the titer, the corresponding concentrations were calculated, and the solutions were prepared the same day, hours before the injections. Vectors were diluted in saline to the required final concentration and preserved on ice until their use.

Stereotaxic injections were carried out in an appropriate biosafety surgical room at the UAB Animal House Facility prepared for viral vectors. Animals were first anesthetized with a mixture of anesthesia and analgesia with ketamine at a dose of 100 mg/kg; and medetomidine at a dose of 0.5 mg/kg; injected intraperitoneally, as before. After corroborating the absence of reflex when pinching the mouse paw, the stereotaxic frame was prepared to inoculate the viral vectors into the striatum at the specific coordinates; Anteroposterior (AP): + 0.5 mm; Mediolateral (ML): + 2.1 mm; Dorsoventral (DV): - 3 mm, according to Bregma. For the inoculation, we used three different Hamilton 5 µL 75RN syringe with the corresponding needles for each viral vector, with 0.5 µL volume of the solutions at a rate of 0.25 µL/minute for 2 minutes. After the injection, we waited up to 1 minute before slowly removing the syringe. As in previous experiments, the animals were administered intraperitoneally with atipamezole at a dose of 100 mg/kg and were placed on a heated mat for a faster recovery. Once recovered, animals were returned into their cages.

Seven days post injection – for the adenoviruses – and 21 days after the surgery – for the adeno-associated virus – mice were euthanized by intracardiac perfusion as described in preceding experiments.

Sectioning of injected animals

As we injected in the striatum, we limit the sectioning to this part of the brain. For this, 0.5 cm of the rostral part of the brain was sectioned to obtain coronal sections by vibratome (Leica Microsystems; Germany) after removing the olfactory bulbs. Six series of sections of 40 µm were obtained, setting the vibratome at a speed of 0.225 mm/s and a vibrating frequency of 60 Hz. Once sectioned, brain slices were stored in PBS with NaN_3 until staining.

Immunohistofluorescence in infected mice

To determine which vector was able to transfect microglia, immunohistofluorescences were designed to label all different types of brain cells and quantify the total number GFP^+ cells.

The immunohistofluorescences were carried out as in previous experiments, the sections were washed with PBS three times per 10 minutes, antigen retrieval was conducted with a pre-treatment with citrate for 20 minutes. After three washes with TBS-triton 0.5%, blockade for nonspecific binding sites was performed by incubating the sections with 0.5% Triton X- 100 with 10% HS for 1 hour. After blocking, the incubation with primary antibodies was done for 48 hours, diluting the antibodies in TBS-0.5% Triton X-100, 1% HS and 0.1% NaN_3. The primary antibodies used for these experiments were anti-Iba-1 (1:500, polyclonal rabbit IgG) to label microglia, anti-NeuN (1:100, monoclonal mouse IgG; Merck; Darmstadt, Alemania) for neurons and anti-GFAP (1:500, polyclonal chicken IgG; Abcam; England, UK) to detect astrocytes.

Secondary fluorescent antibodies incubation was then performed for another 24 hours, diluted 1:1000 in TBS-0.5% Triton X-100, 1% HS and 0.1% NaN_3 according with the host of the primary antibodies. The secondary antibodies used were AlexaFluor 647 Goat anti-Rabbit IgG for Iba-1 detection with AlexaFluor 555 Goat anti-mouse IgG for the NeuN or with AlexaFluor 555 Goat anti-chicken IgG for the GFAP detection. The 488 channel was kept available to visualize the GFP expression of the viral vectors in the transfected cells.

Next day, sections were washed three times with TBS-T and then incubated with DAPI (1:1000) for at least 30 minutes to stain the nuclei of the cells. Then another set of washes was performed.

Finally, the sections were mounted on glass slides and coverslipped using antifade reagent (Prolong Gold).

Note: *the complete references for the antibodies are listed in a table at the end of the methods (Table 2 and 3).*

Confocal microscopy in vectors-infected mice

Prior to a detailed analysis, samples were visualized on the epifluorescence microscope With the Plan-Apochromat 20x/0.8 Ph2 M27 objective lens (Carl Zeiss). Then, all the samples were examined with the confocal laser-scanning microscope (LSM 700 AXIO Examiner, Carl Zeiss). Randomly distributed pictures were taken in areas of the striatum containing GFP expression. Unfortunately, none of the vectors was able to transfect microglial cells. Images showed that GFP^+ cells where either neurons or astrocytes. We then discarded the use of vectors in vivo as the way to obtain Iba-1 silenced mice.

2.5. Calcium injections in Iba-1-KO mice

To ascertain involvement of Iba-1 in the characteristics previously analyzed on microglial cells – as the motiliy, polarization of branches and reorganization of the cytoskeleton – Knock Out (KO) mice for Iba-1 were used.

KO mice

Allograft inflammatory factor 1 (Aif-1) KO mice, kindly provided by **Dr. Nicholas Sibinga** from the Albert Einstein College of Medicine, were used for subsequent experiments. Three breeding mice were requested to generate a new colony in the *Animal facility* of the UAB, named IbaPaKO strain.

The colony was set to obtain enough new pups from the progenitors to use the required amount of adult Aif-$1^{-/-}$ mice from both sexes. Newborn mice were distributed in new cages distinguished by sex and delivery date. Animals were kept and maintained under standard housing conditions (12h light/dark cycles and fed *ad libitum*) at the UAB Animal House Facility until the experiment was carried out.

Once the animals were adults they were utilized for the experiments. Both C57BL/6j male and female mice were also used for this experiment. These animals were purchased from commercial supplier (Janvier Labs) at the same age as the KO mice were going to be used and

then kept and maintained under standard housing conditions (12h light/dark cycles and fed *ad libitum*) at the UAB Animal House Facility for a week until the experiment was carried out.

Ca^{2+} injections of KO and WT mice

For this experiment, we used the same Ca^{2+} concentration (Ca^{2+} 0.5M) as used previously with Wild Type (WT) mice. We used the same volume of saline solution as control.

In these experiments, the main interest was to asses potential differences in the morphology of microglial cells between KO and WT mice in response to parenchymal gradient of Ca^{2+}.

All the solutions were prepared the same day immediately before the administration as in previous experiments, by adding calcium chloride to a saline solution to a final concentration of 0.5M. Saline solution was also prepared at the same time. All the solutions were filtered with a 0.2 µm and preserved at 4°C until the surgery.

The surgery was performed following the protocol described above for intra-striatal injections. Animals were first anesthetized and after the absence of reflexes, the animals were placed on the stereotaxic frame for the procedure. The different solutions were inoculated stereotaxically into the striatum at the specific coordinates; Anteroposterior (AP): + 0.5 mm; Mediolateral (ML): + 2.1 mm; Dorsoventral (DV): - 3 mm, according to Bregma. Once recovered, animals were returned into the cages. Three days post injection animals were euthanized by intracardial perfusion and fixation for histological analysis. This procedure was performed with the same protocol as in previous experiments.

Sectioning of injected KO and WT mice

After removing the olfactory bulbs, 0.5 cm of the rostral part of each brain was sectioned by using a vibratome (Leica Microsystems; Germany) to obtain coronal sections of the striatum. Six series of sections of 40 µm thickness were obtained, setting the vibratome at a speed of 0.225 mm/s and a vibrating frequency of 60 Hz. Once sectioned the brain sections were stored in PBS with NaN_3 until staining.

Immunohistofluorescence in Ca^{2+} injected KO and WT mice

The sections were washed with PBS three times during 10 minutes, then antigen retrieval was conducted with a pre-treatment with citrate (10mM, pH 6, 60°C) for 20 minutes. After washing another three times with TBS-triton 0.5% (Trizma base, NaCl, Triton, H_2O, pH 7.4), blockade for nonspecific binding sites was performed by incubating the sections with 0.5% Triton X- 100 with

10% HS (Sigma-Aldrich; St. Louis, MO, USA) for 1 hour. After blocking, the incubation with the primary antibody, anti-P2Y12 (1:500, polyclonal rabbit IgG), was done for 48 hours to label microglial cells, diluting the antibody in TBS-0.5% Triton X-100, 1% HS and 0.1% NaN_3.

Secondary fluorescent antibody incubation was then performed for 24 hours diluted 1:1000 in TBS-0.5% Triton X-100, 1% HS and 0.1% NaN_3 according with the host of the primary antibody. In this case, the secondary antibody used was AlexaFluor 488 Goat anti-Rabbit IgG for P2Y12 detection.

Next day, the sections were washed three times with TBS-T and then incubated with DAPI (1:1000) for at least 30 minutes to stain the nuclei of the cells. Then, another set of washes was done with PBS. Finally, the sections were mounted on glass slides and coverslipped using antifade reagent (Prolong Gold).

Note: *the complete references for the antibodies are listed in a table at the end of the methods (Table 2 and 3).*

Confocal microscopy in Ca^{2+} injected mice

All these samples were examined with a confocal laser-scanning microscope (LSM 700 AXIO Examiner, Carl Zeiss). Confocal images acquisition was performed following the same procedure as the previous analysis of Ca^{2+} injections in WT mice. By using a Plan-Apochromat 40x/1,3 Oil DIC M27 objective lens (Carl Zeiss) pictures were obtained the at specific regions set from the injection site. As in the preceding experiment, pictures were taken at four different quadrants, starting from the injection site, and going 1280 μm away from the injection (Figure III). Pictures were later processed with image analysis software (ZEN 2010, Carl Zeiss). A series range for each section was set by determining an upper and lower threshold using the Z/Y position for spatial image series. Stacks of the images were taken with an optical section interval of 0.8 μm. Three-dimensional reconstructions were generated and visualized using a set of the α blending software (ZEN 2010) (Image J, version 2.0.0; NIH) (IllucidaFX, version 1.0 (6A); IllucidaLLC; Los Ángeles, CA, USA).

2.6. Polarization quantification in Iba-1-KO mice injected with calcium

3D high resolution confocal images were quantified with rendering software (IMARIS version 8.3.4; Bitplane AG; Zurich, Switzerland) mentioned above, with the specific *Filament Tracer* module – which allowed to trace the ramifications of single microglial cells emerging from the cell body for analyses. As the significant differences in the previous experiment with WT animals

were observed in terms of polarized branches towards the injection and, moreover, were evident in the 2nd and 3rd quadrant, only these two quadrants were analyzed in Iba-1 KO animals.

In this analysis, we quantified the total number of branches in each side of the microglial cell, either facing or opposite to the inoculated component. We did this quantification by dividing each microglial cell body in two parts, and then the filaments emerging from each side of the cell were counted and later classified depending on the orientation, either towards or opposed to the injection. The numbers were then compared between conditions.

3. Studies in human samples

We obtained postmortem samples of the MSF of Parkinson's Disease (PD) patients, as well as non-PD control samples of similar anatomical location to compare with. All samples and data from patients included in this thesis were provided by the *Biobank Banco de Tejidos Fundación CIEN (PT17/0015/0014)*, integrated in the Spanish National Biobanks Network and they were processed following standard operating procedures with the appropriate approval of the Ethics and Scientific Committees. Samples were classified according to the pathological diagnosis and labeled with a code provided by the foundation. PD patients' samples were listed as: BCPA 893, BCPA 981T and 981L, BCPA 871, BCPA 835 and BCPA 1030; and control samples were BCPA 972, BCPA 718, BCPA 870, BCPA 732, BCPA 701. Both sets of samples, after extraction, were fixed in the same conditions, with formaldehyde, allowing the preservation of the microstructure.

3.1. Sectioning of human samples

Human MSF samples were first cryo-protected by using a cassette to embed the samples in a cryostat solution. The solution used was a specialized embedding medium (Scigen O.C.T. Compound Cryostat Embedding Medium, Fisher Scientific-ThermoFisher; Waltham, MA, USA; Ref. 23730625) to maintain the samples in freezing conditions. Samples blocks were then sectioned at -20°C in the cryostat (Leica Microsystems, Wetzlar, Germany) in slices of 40 µm thickness into 12 different series. Once sectioned, samples were preserved in anti-freeze solution – which allowed long term storage of the series under the freezing point – until use for free-floating immunohistofluorescence.

3.2. Immunohistofluorescence for human samples

Prior to start the immunolabeling protocol, samples were washed for few minutes with PBS to remove the anti-freeze solution.

Once washed, immunohistofluorescence was carried out following a variation of the protocol previously used for mouse tissue samples. Sections were washed with PBS three times for 10 minutes, then antigen retrieval was applied with a pre-treatment with citrate for 20 minutes at 60°C. Then, three washes with TBS-triton 0.5% were done to eliminate the citrate residues from the samples. Blockade for nonspecific binding sites was performed by incubating the sections with 0.5% Triton X- 100 with 10% HS for 1 hour at RT. After blocking, the incubation with primary antibodies was done for 48 hours, diluting the antibodies in TBS-0.5% Triton X-100, 1% HS and 0.1% NaN_3. The primary antibodies used for these experiments were anti-Iba-1 (1:500, polyclonal rabbit IgG) to visualize microglia, anti-TH (1:250, monoclonal mouse IgG; Bio-Techne; Minneapolis, MN, USA), anti-TH (1:250, sheep polyclonal IgG), anti-TH (1:250, rabbit polyclonal IgG; Merck; Darmstadt, Alemania) and anti-DAT (1:250, rabbit polyclonal IgG; Abcam; England, UK) to visualize the dopaminergic neurons.

Secondary fluorescent antibodies incubation was then performed for another 24 hours diluted in TBS-0.5% Triton X-100, 1% HS and 0.1% NaN_3 according with the host of the primary antibodies. The secondary antibodies used were AlexaFluor 488 Goat anti-Mouse IgG 1:500 (Life technologies; Carlsbad, CA, USA), Alexa Fluor 488 Donkey anti-Sheep IgG 1:500 or Alexa Fluor 488 Goat anti-Rabbit IgG 1:500 for TH or DAT detection – depending on the primary antibody used – whereas AlexaFluor 555 Goat anti-Rabbit IgG 1:1000 was used for Iba-1 detection.

Next day, sections were washed three times with TBS-T and then incubated for at least 30 minutes with DAPI 1:1000 to stain the nuclei of the cells. Then another set of washes was done.

Finally, the slices were mounted on glass slides and coverslipped using antifade reagent (Prolong Gold).

A series of preliminary tests were carried out to find a good combination to better observe TH^+ neurons in combination with microglia. As the most reliable primary antibody to stain DA neurons in human tissue, was obtained in rabbit, as Iba-1, we set up a sequential immunohistofluorescence protocol. In addition, we found that immunofluorescent TH^+ neurons were only visible in the infrared wavelength because of the high content of neuromelanin masked the visible wavelengths. For those reasons, primary antibodies as well as the secondaries were incubated separately. First, the primary antibody to label DA neurons (anti-TH rabbit polyclonal, 1:250) was added to the samples and incubated for 48 hours, then secondary antibody Alexa Fluor 647 Goat anti-Rabbit IgG 1:500 was added to the samples and incubated for 24 hours. Then, an incubation with this same secondary antibody was performed for 1 hour

to block and saturate the available sites and rinsed. Sequentially, the primary antibody to label microglia (anti-Iba-1 rabbit polyclonal, 1:500) was added to the samples and incubated for 24 hours. Secondary antibody, Alexa Fluor 488 Goat anti-Rabbit IgG 1:1000, was added to the samples for 24 hours to detect Iba-1. The rest of the protocol continued as in non-sequential immunohistofluorescence.

Note: *the complete references for the antibodies are listed in a table at the end of the methods (Table 2 and 3).*

3.3. Confocal microscopy in human samples

With the aim of visualizing the reactivity and polarization microglia towards DA neurons, we analyzed control and PD samples with high resolution microscopy.

Confocal microscopy

Sample pictures were taken in the SNpc – the area of higher dopaminergic neuronal loss in PD. The DA neurons were easily found because of the presence of neuromelanin – which appears as dark granules inside these mesencephalic neurons. By using the Plan-Apochromat 20x/0.8 Ph2 M27 objective lens (Carl Zeiss) we obtained 10 3D high resolution images per sample – including PD patients and control individuals – always containing remaining dopaminergic neurons to measure the interactions with microglial cells. The images were later processed with specialized software (ZEN 2010 Carl Zeiss). For 3D analysis, a series range for each section was set by determining an upper and lower threshold using the Z/Y position for spatial image series. Stacks of the images were taken with an optical section interval of 0.8 µm.

3.4. Quantification of human samples

Three-dimensional reconstructions were generated using α blending software (ZEN 2010) (Image J, version 2.0.0; NIH). Then, the images were quantified in a 3D rendering software (IMARIS version 8.3.4; Bitplane AG; Zurich, Switzerland). As microglial filaments, DA neurons cell bodies, and neurites were intermingled and difficult to isolate, differentiate and count, we decided to quantify the amount of DA neurons, as well as microglial cells, by creating isosurfaces (*Surface tool* from IMARIS). This isosurface provides the volumetric surface area and containing volume that, for TH would be reduced in neurodegeneration, and for Iba-1 would be increase correlating with microglial reactivity. Isosurfaces for TH and Iba-1 were generated and quantified. In addition, the interacting points between both cell types were counted in number and area of interaction. For that, a colocalization analysis between both markers was performed

with the *Colocalization Tool* (IMARIS) and subsequently rendered with the *Surface Tool* and quantified.

4. Statistics

All the data were expressed as the mean with the SEM (standard error of the mean). First, in all the experiments, normal distribution of the data was tested with the Shapiro-Wilk and Pearson normality test, being the P value bigger than the α value (α=0.05) to avoid discarding the gaussian distribution of the data.

For *in vitro* experiments an average of 30 pictures (n=30) were taken in every experimental condition for later comparisons and the experiments were repeated at least three times. Normal distribution of the data was tested with the Shapiro-Wilk and Pearson normality test, being the P value bigger than the α value (α=0.05) to avoid discarding the gaussian distribution of the data. Once the normality was tested, for the quantifications of no more than two experimental conditions being compared, the Student's T test was used, and Mann-Whitney U test was used to compare data between groups. For more than two conditions being compared, a one-way ANOVA and multiple comparisons were conducted to compare the mean of every condition with the mean of every other condition. Tukey post-hoc was also performed, being the α=0.05 and P value smaller than the α to accept the significant difference.

Regarding the *in vivo* experiments, as well as in some of the cell cultures experiments, all the data were expressed as the mean with the SEM. The pictures were taken in the confocal microscope as an average between 12 and 15 (n, 12-15) pictures per experimental condition, depending on the analysis. All the *in vivo* experiments were carried out with more than two experimental conditions. For that reason, normal distribution of the data was also tested with the Shapiro-Wilk and Pearson normality test, being the P value bigger than the α value (α=0.05) to avoid discarding the gaussian distribution of the data. Then, one-way ANOVA and multiple comparisons were conducted to compare the mean of every condition with the mean of every other condition. Tukey post-hoc was also performed, being the α=0.05 and P value smaller than the α to accept the significant difference.

In human samples pictures were taken according to the distribution of the dopaminergic neurons and 10 confocal frames were taken in each representative section. Second, we analyzed the samples as two different experimental conditions, Control and PD patients, so both Student's T test and Mann-Whitney U test were used to compare data between these two groups.

In all cases, $P \leq 0.05$ was considered significant (*). Subsequent differences were classified as (**) $P \leq 0.01$, (***) $P \leq 0.001$ and (****) $P \leq 0.0001$. All statistical analyses were performed using Prism 9 software (GraphPad Software; LaJolla, CA, USA).

Table 2. List of primary antibodies used in immunocytofluorescence, immunohistofluorescence and WB.

Primary antibodies				
Antibody	**Host Specie**	**Dilution for ICF/IHF**	**Company**	**Reference**
α-Iba-1 (IF)	rabbit polyclonal	1:500	Wako	019-19741
α-γ-tubulin	mouse monoclonal	1:500	Sigma-Aldrich	T6557
α-TH	sheep polyclonal	1:500	Merck	AB1542
α-MAP2	chicken polyclonal	1:500	Abcam	ab5392
α-TH	rabbit polyclonal	1:250	Merck	AB152
α-NeuN	mouse monoclonal	1:100	Merck	MAB377
α-F4/80	rat monoclonal	1:50	AbD Serotec	MCA497
α-DAT	rabbit monoclonal	1:250	Abcam	ab184451
α-TH	mouse monoclonal	1:250	Bio-Techne	MAB7566-SP
α-CD11b	rat monoclonal	1:100	AbD Serotec	MCA711G
α-GFAP	chicken polyclonal	1:500	Abcam	ab4674
α-P2Y12	rabbit polyclonal	1:500	Anaspec	AS-55043A
α-Iba-1 (WB)	rabbit polyclonal	1:1000	Wako	016-20001
α-β actin	mouse monoclonal	1:1000	Bio-Techne	MAB8929

Table 3. List of secondary antibodies and fluorescent labeling used in immunocytofluorescence, immunohistofluorescence and WB.

Secondary antibodies and other markers					
Antibody	**Host Specie**	**Reactive Specie**	**Dilution for ICF/IHF**	**Company**	**Reference**
Alexa Fluor 488	Goat	Rabbit	1:500 - 1:1000	Life Technologies	A-11034
Alexa Fluor 488	Goat	Mouse	1:500 - 1:1000	Life Technologies	A-11001
Alexa Fluor 488	Donkey	Sheep	1:500 - 1:1000	Life Technologies	A-11015
Alexa Fluor 555	Goat	Mouse	1:1000	Life Technologies	A-21424
Alexa Fluor 555	Goat	Rabbit	1:1000	Life Technologies	A-21429
Alexa Fluor 555	Goat	Chicken	1:1000	Life Technologies	A-21437
Alexa Fluor 555	Goat	Rat	1:1000	Life Technologies	A-21434
Alexa Fluor 555	Phalloidin	__	1:40	Life Technologies	A34055
Alexa Fluor 647	Goat	Mouse	1:1000	Life Technologies	A-21235
Alexa Fluor 647	Goat	Rabbit	1:1000	Life Technologies	A-21244
Alexa Fluor 647	Phalloidin	__	1:40	Life Technologies	A22287
DAPI	__	__	1:1000	Life Technologies	D1306
Secondary antibody HRP	Goat	Rabbit	1:3000	Invitrogen	31460
Secondary antibody HRP	Goat	Mouse	1:5000	Invitrogen	31430

RESULTS

1. Microglia polarizes to contact remaining DA neurons in the SNpc of PD patients

The aim of this neuropathological examination was to determine the dopaminergic (DA) neurodegeneration in PD patient samples, as well as the state of microglia in the areas of degeneration. As explained in the introduction, some proinflammatory cytokines – including IFN γ – are increased in the serum and CSF of PD patients (Imamura et al., 2005; Karpenko et al., 2018; McCoy et al., 2006; Mount et al., 2007b). This, combined with the fact that microglial cells produce some proinflammatory cytokines (Saijo & Glass, 2011b) and release them to the extracellular space, suggest the implication of microglia contributing to the neuroinflammatory environment exacerbating the neurodegeneration of DA neurons (Barcia et al., 2003).

As we obtained human mesencephalon (MSF) postmortem samples provided by the ***Fundación CIEN*** Brain Bank, we planned experiments to better understand the problem of the neuronal death occurring in PD patients, specifically of DA neurons, and how the microglia could take part of it. These samples were from PD patients but also from individuals who died without the illness, taken as controls to compare with. PD samples were coded as: BCPA 893, BCPA 981T and 981L, BCPA 871, BCPA 835 and BCPA 1030 and control samples were coded as: BCPA 972, BCPA 718, BCPA 870, BCPA 732, BCPA 701.

As the initial assessment of the samples, and to corroborate the loss of DA neurons in the Substantia Nigra *pars compacta* (SNpc) of the patients, we wanted to quantitatively examine the DA neuronal loss when comparing with controls. As previously explained, the total number of DA neurons is supposed to be lower specifically in the SNpc of patients suffering from PD than in control samples, as it is the most characteristic neuropathological hallmark of PD. Concomitantly, we also wanted to study the differences in terms of microglial reactivity on these samples and quantitatively compare between controls and PD patients.

Although in this manuscript the reference code for the PD patients and control samples are provided, for the present study and quantification the analysis was done single-blinded to avoid biased assessments.

To quantify the total amount of DA neurons and microglial reactivity the analysis was done based on confocal pictures taken from representative sections of each sample. Since the loss of

DA neurons in PD patients is more drastic in the ventrolateral area of the SNpc, we had technical difficulties to locate quantificable neurons in this area. We took sampling pictures always containing remnant DA cell bodies and neuronal fibers of TH expression regardless of the subregion of the SNpc.

The quantification of the amount of DA neurons was performed by counting the density of TH positive labeling. We observed a clear loss of TH positive rendered material in PD samples compared with the controls. This reduction was clear in terms of volumetric surface area but also holding volume (Figure 111A-B), which could be translated as a significant loss of DA neurons in parkinsonian patients.

With these results we corroborated that the PD patients' samples provided by the brain bank showed indeed a drastic and specific DA neuronal loss in the SNpc (Figure 111B).

Besides, the analysis of microglial cells reactivity was measured in the same way as we did with the DA neurons density. We used the Iba-1 immunolabeling to create a rendering surface of microglial cells and then obtained the values for Iba-1 area and volume in the sampling frames. We obtained clear differences both in the Iba-1 area and volume occupied by microglia when comparing control and parkinsonian samples (Figure 111C-E). These results show an increase in the Iba-1 positive material in the PD patients' samples compared with the controls.

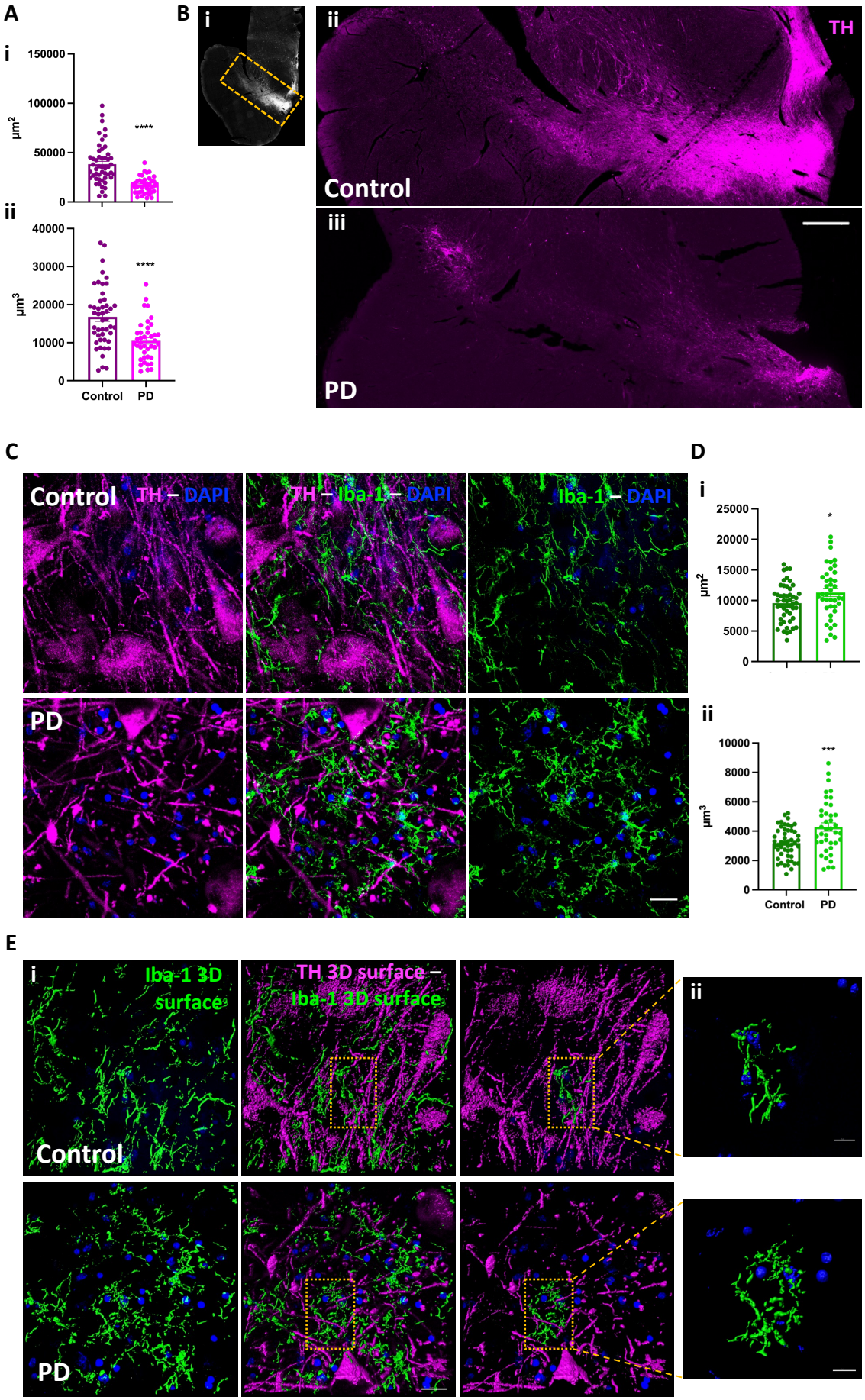

A
i
150000
100000
50000
0
µm²
****
ii
40000
30000
20000
10000
0
µm³
****
Control
PD
B
i
ii
TH
Control
iii
PD
C
Control
TH – DAPI
TH – Iba-1 – DAPI
Iba-1 – DAPI
PD
D
i
25000
20000
15000
10000
5000
0
µm²
*
ii
10000
8000
6000
4000
2000
0
µm³
***
Control
PD
E
i
Iba-1 3D surface
Control
TH 3D surface – Iba-1 3D surface
ii
PD

Figure 111. PD patients show a significantly loss of DA neurons and an increase of microglial reactivity in the SNpc. **A. (i)** Comparison of the quantification of TH volumetric surface area between Control and PD patients. **(ii)** Quantification of the TH holding volume between PD patients and controls. **B. (i)** Mosaic of hemi-section of human mesencephalon to indicate the specific area, including SNpc and VTA, where the mosaic pictures were taken. **(ii** and **iii)** Mosaic reconstruction of a SNpc from a control individual and a PD patient (Scale bar: 1000 µm). **C.** High magnification confocal images of a control and a PD section of the SNpc to see the differences in neuronal density and microglial shape (Scale bar: 20 µm). **D. (i)** Quantification of Iba-1 volumetric surface area between Control and PD patients. **(ii)** Values for Iba-1 holding volume comparing controls and PD samples. **E. (i)** Rendering 3D surface of microglial cells and DA neurons to visualize the differences in terms of Iba-1 shape and volume (Scale bar: 20 µm). **(ii)** Isolation and zoom of one microglial cell for each condition to better see the differences they have. (Scale bar: 10 µm). (* $p<0.05$; ** $p<0.005$, *** $p<0.0005$, **** $p<0.0001$).

Putting all together, we corroborated that the parkinsonian patient samples show a dramatic loss of DA neurons in the SNpc. But importantly, they display changes in microglial reactivity as seen in terms of microglial volumetric surface area and volume – being increased almost 50% in PD patients compared with controls. These suggest a direct implication of microglia in the neurodegenerative process, probably due to a neuroinflammatory environment that may exacerbate the neuronal death of neighboring DA neurons.

Once ascertained that the samples provided showed canonical hallmarks in the SNpc, we focused on how the phenotypical change of microglia may be related with the interaction with remaining neurons in PD.

As previously indicated, microglial cells are always exploring and scanning (Davalos et al., 2005; Nimmerjahn et al., 2005) their surroundings looking for alterations in the parenchyma. During this process microglia polarizes towards the damage to interact with the target (i.e. phagocytosis etc.).

We wondered if microglial cells – due to the process of activation in PD samples – could be increasing their interactions with DA neurons. For that, we quantified the total number of contacts between microglia and remnant DA neurons. This quantification was also performed with 3D rendering software (IMARIS), with the *Colocalization tool*. We classified the contacts as the voxels in the images were both markers – the TH fluorescence and the Iba-1 fluorescence – were colocalizing, meaning establishing a contact between the two cells (Figure 112A). These contacts could be quantified by number but also by the area of colocalization between the cells, a property that may differentiate stochastic contacts from contacts due to the neuroinflammatory process.

For this analysis, we used the high-resolution 3D rendering of both markers, TH and Iba-1, previously generated to measure the volumetric surface areas and holding volumes. With these renderings and the *Colocalization tool*, we could detect the overlapping points of both markers and classify them as a new surface called **Interaction points** (Figure 112A). These interaction points were then quantified as total number for each patient, normalized by the total volumetric surface area of TH positive material, keeping in mind the differences between controls and PD patients. Results of area of contact were also normalized by the total TH surface area to compare controls and PD patients.

High-resolution images of colocalization show clear differences in terms of the number of TH-Iba-1 interactions between control and PD patients (Figure 112B). Normalized quantification showed a significant increase in the number of interactions of Iba-1 cells per square millimeter (mm^2) of TH volumetric surface in patients suffering from PD compared to control individuals (Figure 112C i). The analysis of the total area of Iba-1-TH interactions per sampling 3D stack also showed a big increase in PD patients compared with controls (Figure 112C ii).

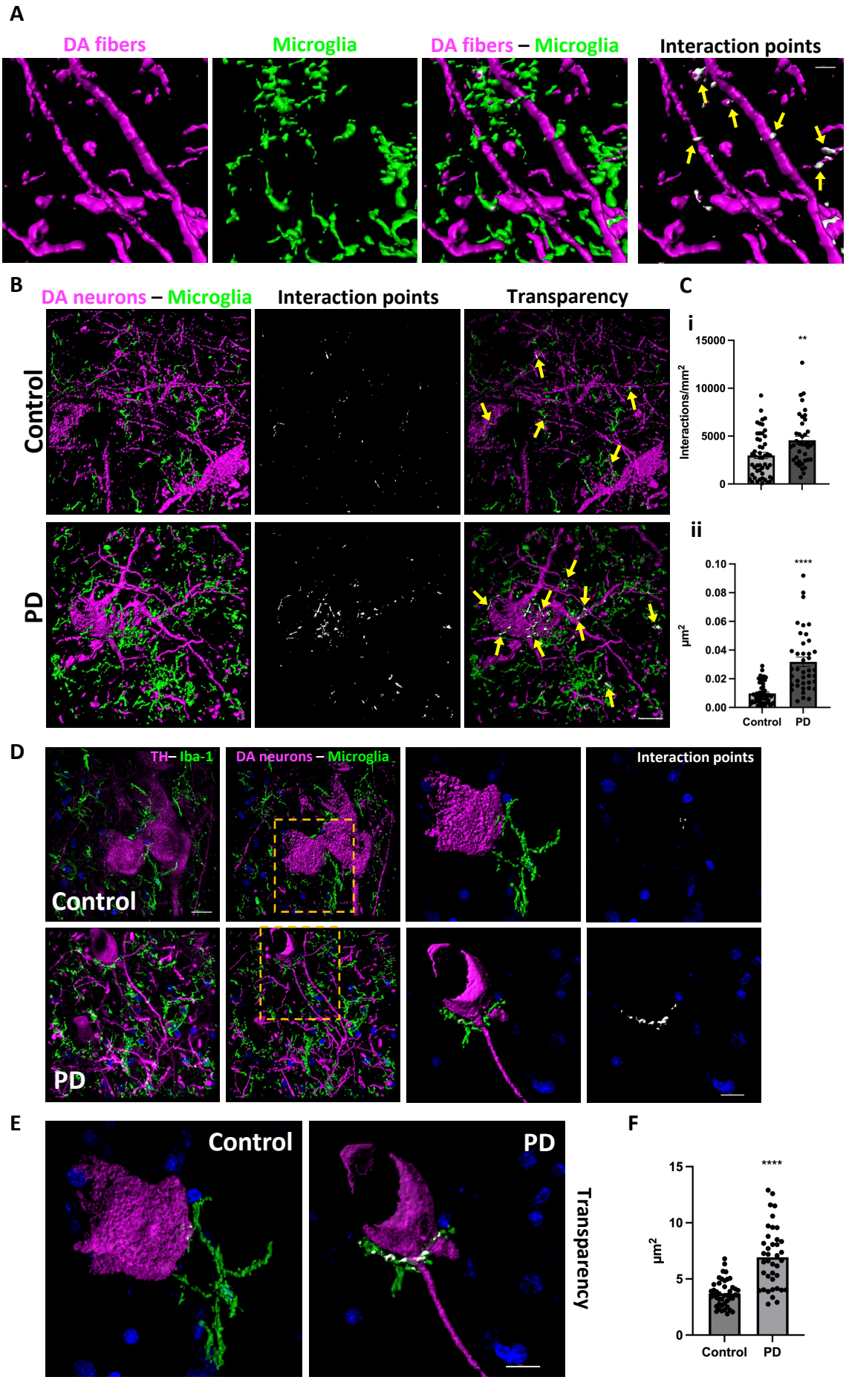

A
DA fibers
Microglia
DA fibers – Microglia
Interaction points
B
DA neurons – Microglia
Interaction points
Transparency
Control
PD
C
i
Interactions/mm²
15000
10000
5000
0
**
ii
µm²
0.10
0.08
0.06
0.04
0.02
0.00
****
Control
PD
D
TH– Iba-1
DA neurons – Microglia
Interaction points
Control
PD
E
Control
PD
Transparency
F
µm²
15
10
5
0
****
Control
PD

Figure 112. Microglial cells increase their interactions, and its extent, with remaining DA neurons in the SNpc of PD patients. A. High-resolution 3D rendering of DA neurons/fibers (magenta) and microglial cells (green) to visualize their contacts in the SNPc of a PD patient. Interaction points between both cell types are seen in white (Scale bar: 10 µm). **B.** 3D rendering of DA neurons and microglia (images on the left), interaction points between them (central images) and the superposition of the three rendering surfaces (transparency) with DA neurons and microglia slightly transparent to better visualize the interaction points (pointed with yellow arrows). Examples of control (top panel) and PD patient (bottom panel) are displayed (Scale bar: 20 µm). **C. (i)** Total number of Iba-1 interactions per mm^2 of TH material, comparing control and PD samples. **(ii)** Total area of Iba-1-TH interaction comparing control and PD samples. **D.** High-resolution confocal stacks and subsequent 3D rendering of the images to visualize a representative interaction in a control individual and a PD patient (Scale bar: 20 µm). Higher magnification of isolated neurons with interacting microglia (from orange broken line inset) are shown. In addition, the interaction points (white) for these microglia-neuron interactions are also shown (Scale bar: 10 µm). **E.** Higher magnification images of the interactions from D, in a control individual and a PD patient. Images are shown with transparency of the DA neuron and microglia rendering surfaces to better see the interaction points (white) (Scale bar: 10 µm). **F.** Quantification of the average of interaction area comparing controls with PD samples (* $p<0.05$; **** $p<0.0001$).

Since PD patients showed an increase of Iba-1-TH interactions both in number and total area, we asked ourselves about the extent of these interactions. Because the total area of interactions was higher in PD patients than in controls, we thought that this could be due to an increase of the interface of interaction of microglial cells with remnant DA neurons.

We then measured the average of the interacting surface area between microglia and DA neurons. This parameter indicates how large are the points of interface between microglia and DA neuron in the samples. For that, we used the interaction points surface described above to quantify the area of interaction. We observed (Figure 112D-F) that the average of interaction area was almost double in parkinsonian patients when compared to control individuals. These results suggest that the type of interaction produced in PD samples are really specific, with not only the branches but the cell body of microglial cells contacting the DA neuron while in controls mostly of them are presented with slightly contacts between the microglial branches and the DA neurons. These stronger interactions found in PD patients made us think that could be occurring more commonly in a neurodegenerative process in which the microglia could be sensing the signals released by the neurons dying and, in consequence, somehow they could become sensitized and posteriorly activated in a way trying to eliminate the problem.

2. MPTP-induced parkinsonian mice show microglial polarization towards remaining DA neurons

Once ascertained that microglial cells were increasing their contacts with DA neurons in the SNpc of PD patients, indicating a phenotype polarization, we wondered if this phenomenon may also occur in parkinsonian mice. For this experiment, mice intoxicated with the neurotoxin 1-Methyl-4-phenyl-1,2,3,6-tetrahydropyridine (MPTP) were used to generate a parkinsonian degeneration with the characteristic DA neuronal loss. These mice show a significant loss of DA neurons in the SNpc after the MPTP treatment as compared with control animals injected with saline.

It is well established that when neurons are dying, they release several components to the extracellular matrix, which are supposed to be crucial for microglial activation and polarization (Haynes et al., 2006b). Moreover, and specifically for DA neurons, it is known that the administration of MPTP induces an early microglial-mediated neuroinflammation that triggers microglial motility with the consequent phagocytosis (Barcia et al., 2012). For those reasons we wanted to analyze in a 3D bases the polarization of microglia towards DA neurons in the SNpc of MPTP-parkinsonian mice.

We set up an experiment with 5 animals injected with MPTP and 5 with saline, euthanatized 72h after the neurotoxin insult. Serial histological sections of the SNpc were obtained by using a vibratome and subsequent immunohistofluorescence was done to labeled DA neurons – with the TH marker – and microglial cells – with the Iba-1 marker (Figure 113).

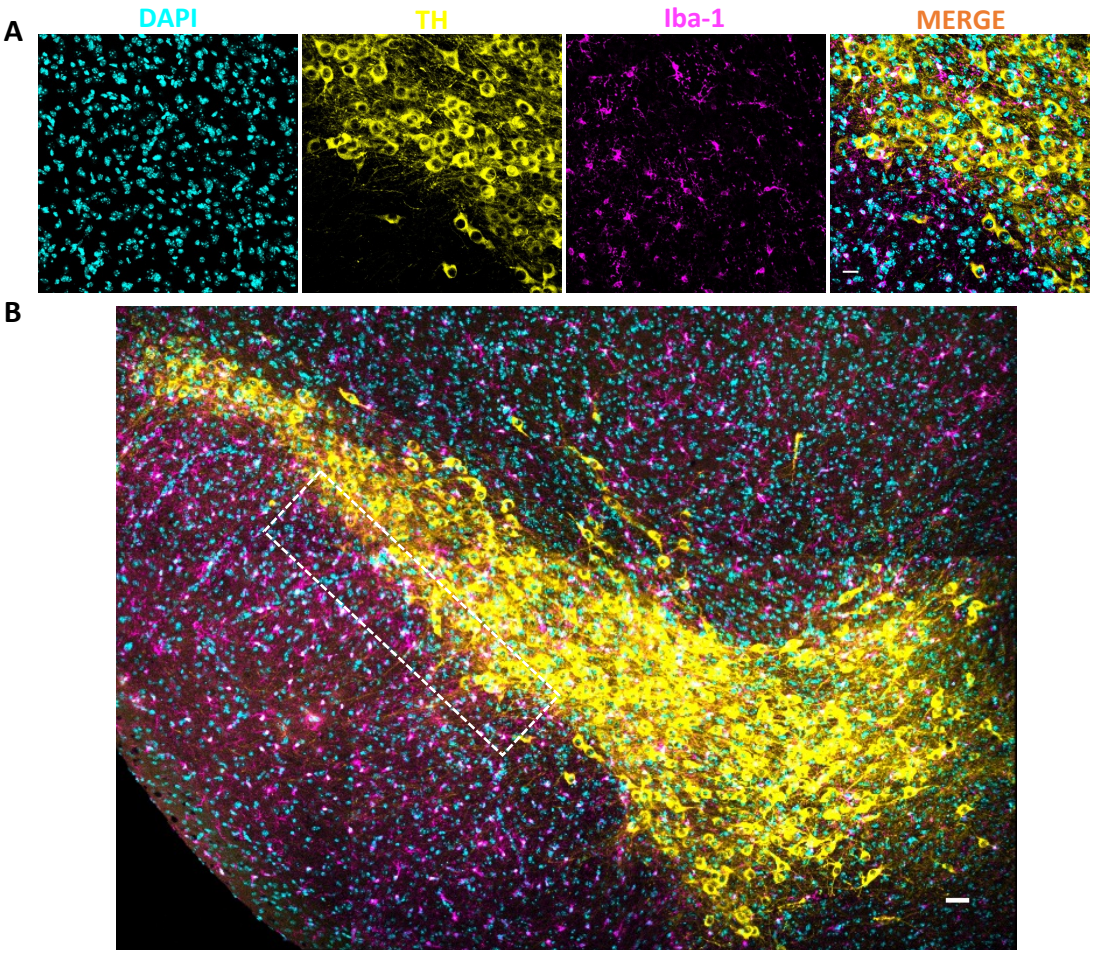


Figure 113. Area of analysis in the mouse SNpc. A. Representative images from the ventrolateral area of the SNpc of a control mouse expressing TH (yellow) and Iba-1 (magenta) (Scale bar: 20 µm). **B.** Mosaic showing the complete SNpc of one hemi-mesencephalon from a control mouse and indicating the ventrolateral area (rectangle with white broken lines), the specific region of analysis in which DA neurons show the highest loss (Scale bar: 60 µm).

In PD, the more susceptible population of DA neurons to degenerate are located in the ventrolateral area of the SNpc (Figure 113B), in which the implication of microglia in the neuroinflammatory process may be critical. In concordance with this, in animals injected with the neurotoxin MPTP, and in an early stage of the neuroinflammation, microglial cells are expected to be polarized, orienting their branches towards dying DA neurons. To analyze this phenomenon, 3D confocal stacks were taken at the region of interest (Figure 113B) with DA neurons at the top of the frame to determine the direction of the microglial branches and the possible contacts with target neurons (Figure 114A).

The resolution of the confocal images did not provide clear visualization of microglial contacts with DA neurons but, in the MPTP intoxicated-mice, microglial cells seemed to be polarized towards DA neurons, presenting an apparent number of branches oriented to the DA neurons.

For the quantification of the number of polarized branches, the rendering of the images was accomplished by using the *Filament Tracer* of the IMARIS software. With this tool we were able to track all the filaments emerging from the cell body of every single microglial cell for quantification (Figure 114B). By counting the total number of microglial branches going towards the DA neurons and the number of branches in the opposite site of the cell body (polarized and non-polarized branches respectively) we observed a clear difference between the conditions. MPTP-injected mice showed a clearly increase of the branches polarized towards the DA neurons, in contrast to the non-polarized branches, while saline-injected animals did not show significant differences between the branches in one side or the other (Figure 114C).

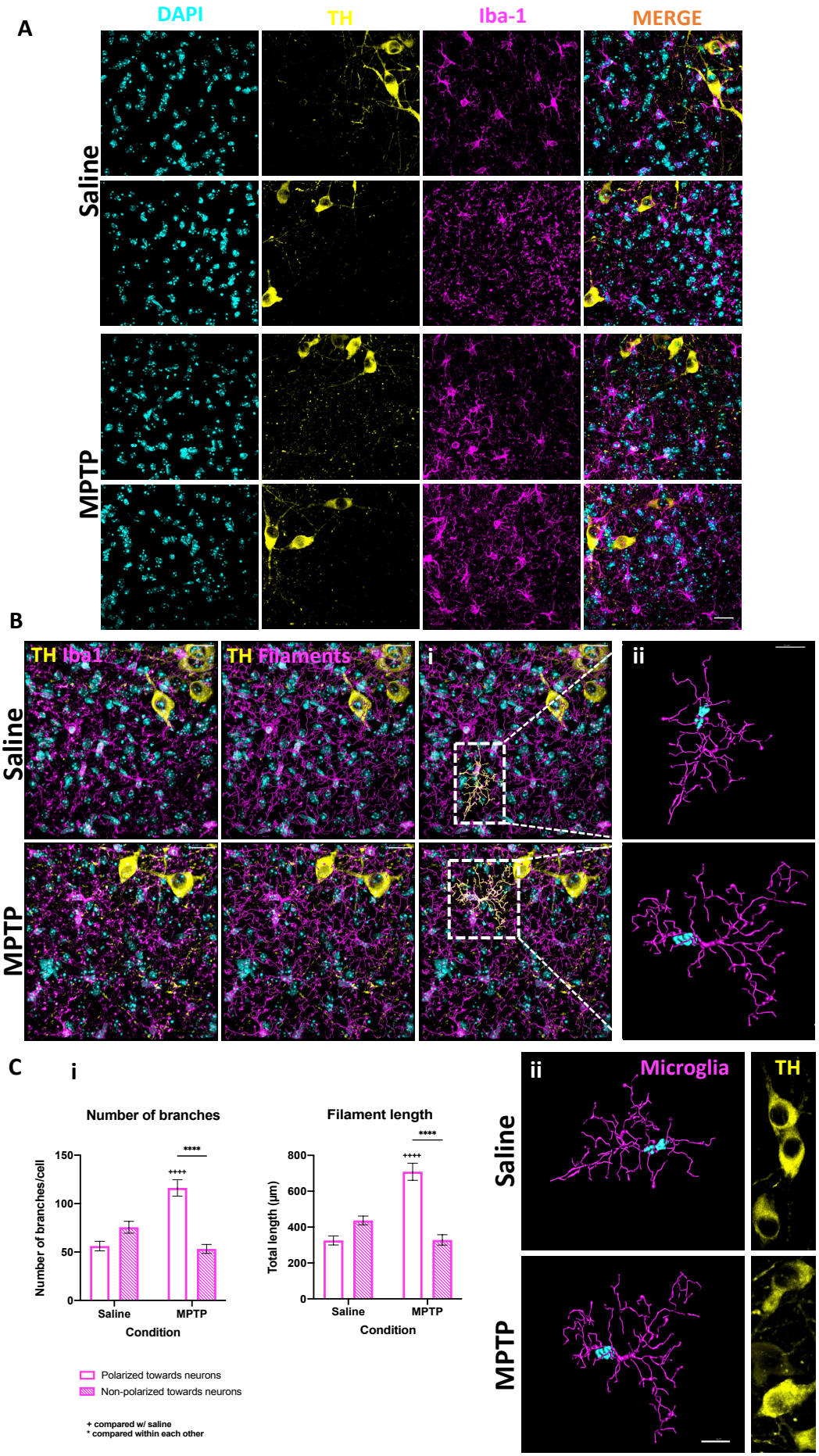

A
DAPI
TH
Iba-1
MERGE
Saline
MPTP
B
TH Iba1
TH Filaments
i
ii
Saline
MPTP
C
i
Number of branches
Number of branches/cell
150
100
50
0
****
++++
Saline
MPTP
Condition
Filament length
Total length (µm)
800
600
400
200
0
****
++++
Saline
MPTP
Condition
Polarized towards neurons
Non-polarized towards neurons
+ compared w/ saline
* compared within each other
ii
Microglia
TH
Saline
MPTP

Figure 114. MPTP intoxication induces polarization of microglial branches towards DA neurons. A. Representative images from the ventrolateral area of the SNpc in control (saline) and parkinsonian mice (MPTP), expressing TH (yellow) and Iba-1 (magenta) (Scale bar: 20 µm). **B.** Confocal images showing the location of microglial cells in relation to the DA neurons in the SNpc (left panels) and the 3D traced filaments (central panels) (Scale bar: 20 µm). **(i).** Selection and identification of a single microglial cell (yellow filament) in control and parkinsonian mice **(ii).** Isolation of a representative microglial cell traced with filaments in high magnification to better visualize the arborization (Scale bar: 10 µm). **C. (i).** Graphs showing the differences in terms of number of microglial branches and filament length polarized or non-polarized towards the DA neurons in both experimental conditions analyzed (**** $p<0.0001$) **(ii).** Representative microglial cells of the ventrolateral area presented towards the DA neurons in an MPTP-injected mouse and a saline injected mouse.

These results suggest, as in human samples, that in a microenvironment of DA neurodegeneration, some components may be released to the external milieu that could be sensed by microglial cells producing their polarization towards the degenerating neurons and inducing subsequent contacts. This polarization is mediated, in a first step, by the orientation of most of the microglial branches towards the DA neurons, then, as a second step, probably approaches its cell body – creating a cell body-cell body contact – and potentially engulf the target neuron.

3. Categorization of microglial interactions during homeostasis and stimulating scenarios

Results obtained – both in PD human samples and parkinsonian mice – indicate the importance microglia-neuron interaction in the process of DA degeneration. Then, we next tried to better establish the process in which microglia approaches and contact dying neurons *in vitro*.

Microglia are motile cells always scanning their surroundings looking for alterations in the parenchyma. In pathological situations – which could be caused by neuronal damage – microglia respond to potentially restore the homeostasis, no matter if the malignant component is a damaged neuron or an external component that could be deleterious for the brain parenchyma.

3.1. Understanding the process of microglia-target contacts with cell line co-cultures

To better understand and describe how microglia-target interactions are accomplished, we performed a first experiment in which we combined the PC12 cell line – DA cells expressing Tyrosine Hydroxylase (TH) – and BV2 cells – microglial cells expressing Iba-1 protein – to simulate the scenario present in the SNpc. BV2 cells were cultured in a 24-well plate for 24 hours and PC12 cells were added later to analyze the interactions of both cell types.

In a first experiment, we characterized the timing in which microglia are approaching and targeting neurons. To observe the different steps during this process, we let the cells interacting in different timepoints.

Prior to capturing microscope images and quantification, four different categories of interactions were defined, depending on the aspect and position of microglial cells regarding the PC12 cells:

- **Category 1.** BV2 microglial cells displaying a protrusion polarized towards a PC12 neuron-like cell, but not contacting.
- **Category 2.** BV2 cells with a kinetic lamellar protrusion contacting with a targeted PC12 cell.
- **Category 3.** Contact body-to-body. BV2 cell body interacting with a PC12 cell body.
- **Category 4.** BV2 microglia phagocytosing a target cell.

The aim of this experiment was to establish the optimal time point to visualize intercellular interactions for each category to be used for subsequent co-culture experiments. While most of the interactions occurred more often after 2 hours of interacting (Supplementary figure 1A), these types of interactions were mostly categorized as type 2 or 3 (Supplementary figure 1A).

Although we expected some category 4 events to appear at late timepoints (4h onwards), we were not able to observe them. Nevertheless, the decrease in PC12 numbers occurred after the establishment of the highest level of interactions (Supplementary figure 1D) suggesting that phagocytic events may occur during these subsequent timepoints.

These results indicate how the timing of the interacting process is taking place. We observed that BV2 cells tend to contact PC12 DA cells relatively fast. At 2 hours we quantified the highest number of contacts, especially for categories 3 and 4. We hypothesized that the contact will be established when a microglial cell is emitting a protrusion towards a PC12 neuron-like cell, then it is contacted with the leading protrusion, and in the next step the microglial cell rearranges to migrate and establish a body-to-body contact (Supplementary figure 1E). Once the contact has took place, a specific modification of both cell morphologies is produced. Microglia and the target are extremely close to each other, and the contact body-to-body creates what it is called a “flat interface” (Supplementary figure 1F). In this structure, the membranes are reorganized in order to have most of their approaching surface strongly touching the other cell, creating a flat structure between them. Finally, we believe that engulfment and phagocytosis may be the consequence of this close encounters.

At 8 hours, we observe the lower number of PC12, in which microglia have probably had enough time to interact and significantly eliminate PC12 cells, potentially by phagocytosis. At 24 hours, PC12 cells, as well as BV2, had enough time to reproduce in number and new contacts are being created between BV2 cells and other PC12 cells.

3.2. Interactions are also produced in a more physiological scenario with primary co-cultures

Once we ascertained the timing of the intercellular contacts in cell line co-cultures, we wondered if these phenomena of microglia-target interactions could also happen in primary co-cultures. For this experiment, we only focused on the optimal timepoints obtained in cell lines, 2h and 24h.

In these co-culture experiments we used neurons obtained from E17 embryos, specifically from the dorsoventral region of the mesencephalon, where most of the DA neurons are located during the late stages of the development, combined with primary microglia, obtained from P0-P2 rats mesencephala. As in previous experiments, microglial cells were labelled with Iba-1. As the neurons obtained from the embryos were not only DA, we had to distinguish between DA and other types of neurons. We then stained all types of neurons with the general marker MAP-2, and specifically the DA neurons with the same TH marker used before (Figure 115).

Another aspect we wanted to assess was if the pro-inflammatory activation of microglia led to a change to an exacerbated response to neurons.

To create a pro-inflammatory microglial phenotype, the canonical procedure is to stimulate the cells with lipopolysaccharide (LPS) – derived from the external membrane of gram negative bacteria – and the interferon γ (IFN γ) cytokine, coincidentally seen in high amounts in PD patients (Mogi et al., 1994; Mount et al., 2007b). The co-culture was performed by seeding the neurons in a 24-well plate, then microglia was added and treated with the combination of LPS and IFN-γ. After 2h or 24h the co-culture was fixed for analysis (Figure 115).

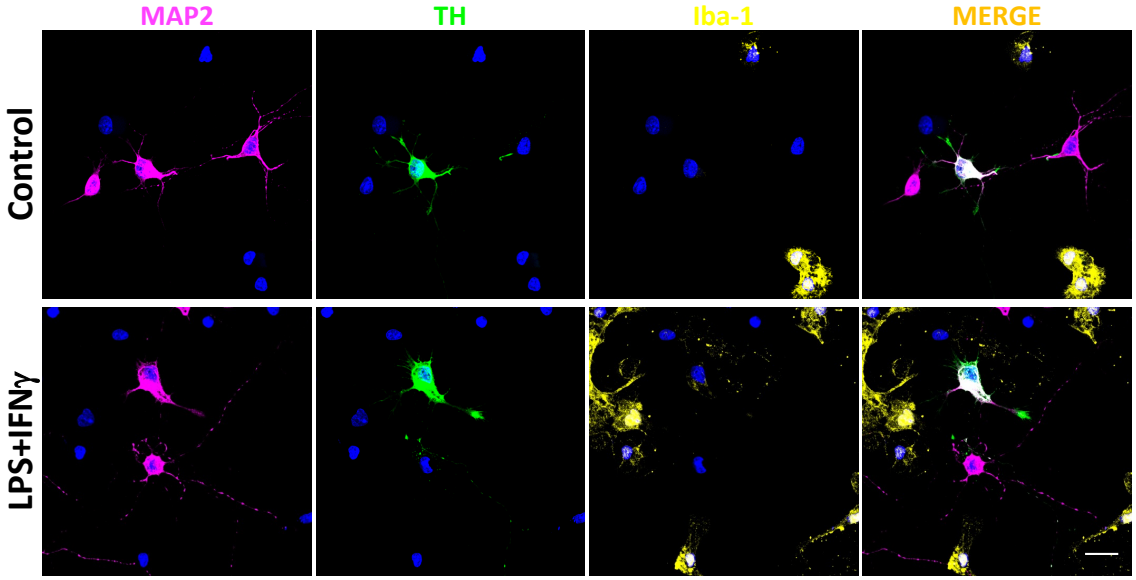


Figure 115. Primary co-cultures performed with MSF microglia and neurons. Confocal images to observe the distribution of neurons, distinguishing between TH positive neurons (green) and other different types of neurons (magenta). Microglial cells could be observed in yellow. Representative images of the control and activated condition, treated with LPS 100ng/mL and IFN-γ 25ng/mL. (Scale bar: 20 μm).

In primary cultures, the microglia-neuron contacts were not as frequent to see as in cell lines, but a significant decrease in the number of neurons, both DA and non-DA neurons, was found when microglial cells were activated (Figure 116A). Independently, when neurons were exposed to microglial cells, either activated or resting, a certain degree of deleterious effect was seen (Figure 116). Moreover, when microglial cells were treated with a pro-inflammatory stimulus, the neuronal loss was increased (Figure 116A and B). It is also important to have in mind the time of interaction. When cells interacted for 24 hours the deleterious capacity of microglial cells to eliminate neurons was more drastic than when they only interact for 2 hours, but especially dramatic for DA neurons (Figure 116A and B).

***Note to Figure 116:** Although the culture was performed with microglial cells, the images were taken with epifluorescence microscope in which the infrared channel could not be visualized, reason why the channel for microglial cells is not shown.*

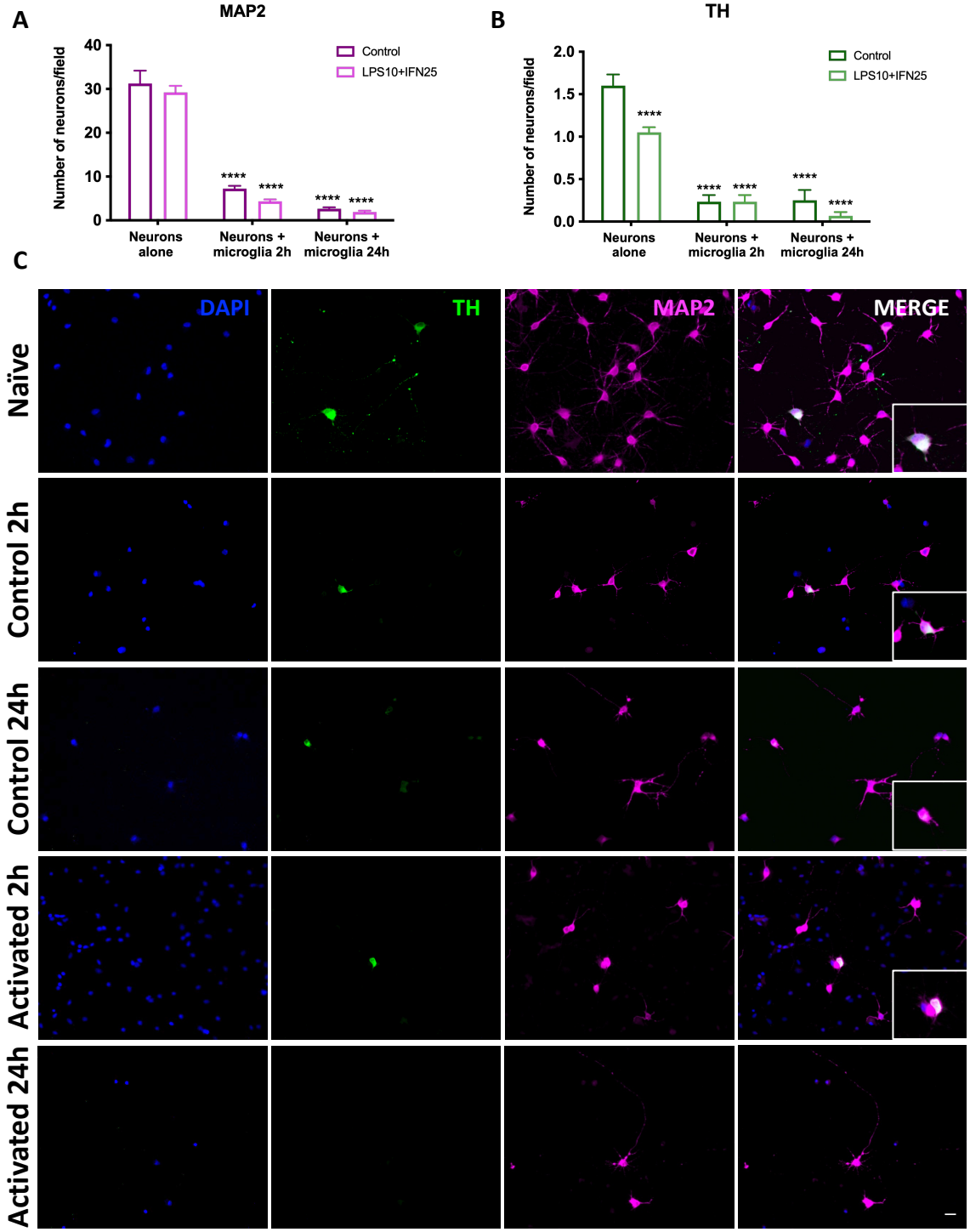


Figure 116. Neurons are susceptible to die when exposed to microglia and the depletion is even higher if microglial cells are activated. A. Comparison of the total number of MAP2 positive neurons in every condition, comparing between neurons alone and co-cultured with microglia, either when they are treated or not. **B.** Comparison of the total number of TH positive DA neurons in every condition, also compared co-cultures with neurons alone and

differentiating by treatment. (* compared to neurons alone) (**** p<0.0001) **C.** Representative images of every condition showing the TH positive neurons and MAP2 positive neurons in the different condition analyzed. (Scale bar: 20 µm) The last image of every condition has a white square right down showing a zoom in of one TH^+ $MAP2^+$ neuron.

These results suggest that primary neurons *in vitro* are extremely vulnerable to the presence of microglial cells because of the homeostatic clearance. However, when microglial cells are stimulated to a pro-inflammatory phenotype, the effect is more severe, resulting in more time-dependent neuronal elimination.

3.3. MTOC is located at the front edge in the microglial kinetic morphology regardless of their activation

Once we analyzed the process by which microglial cells approach and contact the target, another question arises regarding the orientation of the protrusion and their shape to migrate and contact the target.

The microtubule organizing center (MTOC) has an important role in the cytoskeletal reorganization (Wu & Akhmanova, 2017). Knowing the idea of the shape rearrangement of microglial cells to finally contact the target we wondered if the location of the MTOC regarding the nucleus and the protrusion could be crucial for the contact.

In homeostasis, microglial cells are in a scanning mode, with no clear polarized morphology (Figure 117A) and with no defined polarity for its organelles. However, when finding a target, microglia arranges and polarizes in the direction of the chemoattractant. Then, in the process of polarization towards the target, microglia need to reshape their cell body from scanning mode to kinetic morphology – which allows the migration and displacement. This kinetic morphology is characterized by the formation of a typical actin-rich lamellar protrusion in the front of the cell and a trailing end, called uropod, at the back of the cell (Figure 117B).

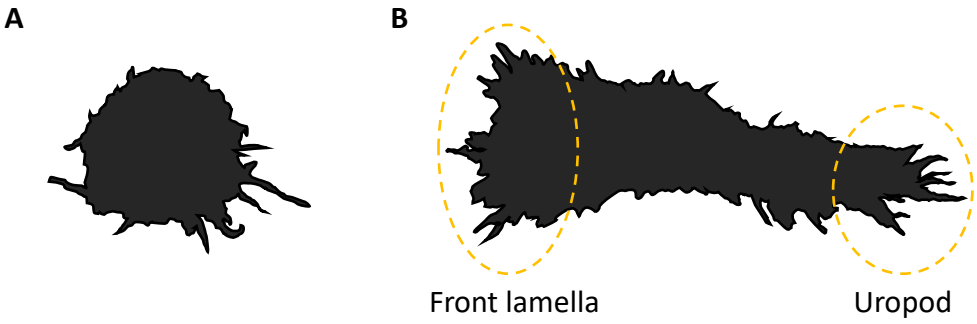


Figure 117. Microglial shape in homeostatic and activated state. A. Camera-lucida representation of a microglial cell in a scanning state, with no polarized protrusions. **B.** Camera-lucida representation of kinetic morphology of a microglial cell, with the characteristic front lamella and the back uropod formation.

In this process of polarization, the MTOC orchestrates the organization of the tubulin cytoskeleton and actin fibers to generate microglial protrusions as front leading lamella and uropod at the rear end (Figure 117). However, the position of the MTOC regarding the direction of microglia has been scarcely studied.

To associate the MTOC position to microglial polarization and directionality, we performed an experiment with microglial cells, both in a control or activated state, but we focused only on cells displaying a clear kinetic morphology. Considering that our hypothesis is based on the signals sent by the target cell – with the concomitant activation of microglia – we wanted to know if this process of reorganization occurs regardless of the state of activation.

For this experiment, microglial cells were activated with the canonical pro-inflammatory stimulus LPS and IFN-γ, and during 24 hours prior to the fixation. Then the cultures were used to label by the MTOC and the F-actin fibers.

We saw no significant differences between non-treated and activated cells in terms of MTOC position regarding the nuclei (Figure 118C and D). In most of the cases microglial cells had the MTOC located between the nucleus and the leading lamella (Figure 118A and B). These results indicates that this positioning of the MTOC to arrange the actin fibers in the kinetic morphology, is achieved either in the presence of or absence of activating stimuli (Roig-Martinez et al., 2019). This location seems to be consistent and not dependent on the pro-inflammatory activation of microglial cells.

We conclude that there is a clear association of the MTOC position with the kinetic morphology that can be used as a way to check the directionality of microglial cells.

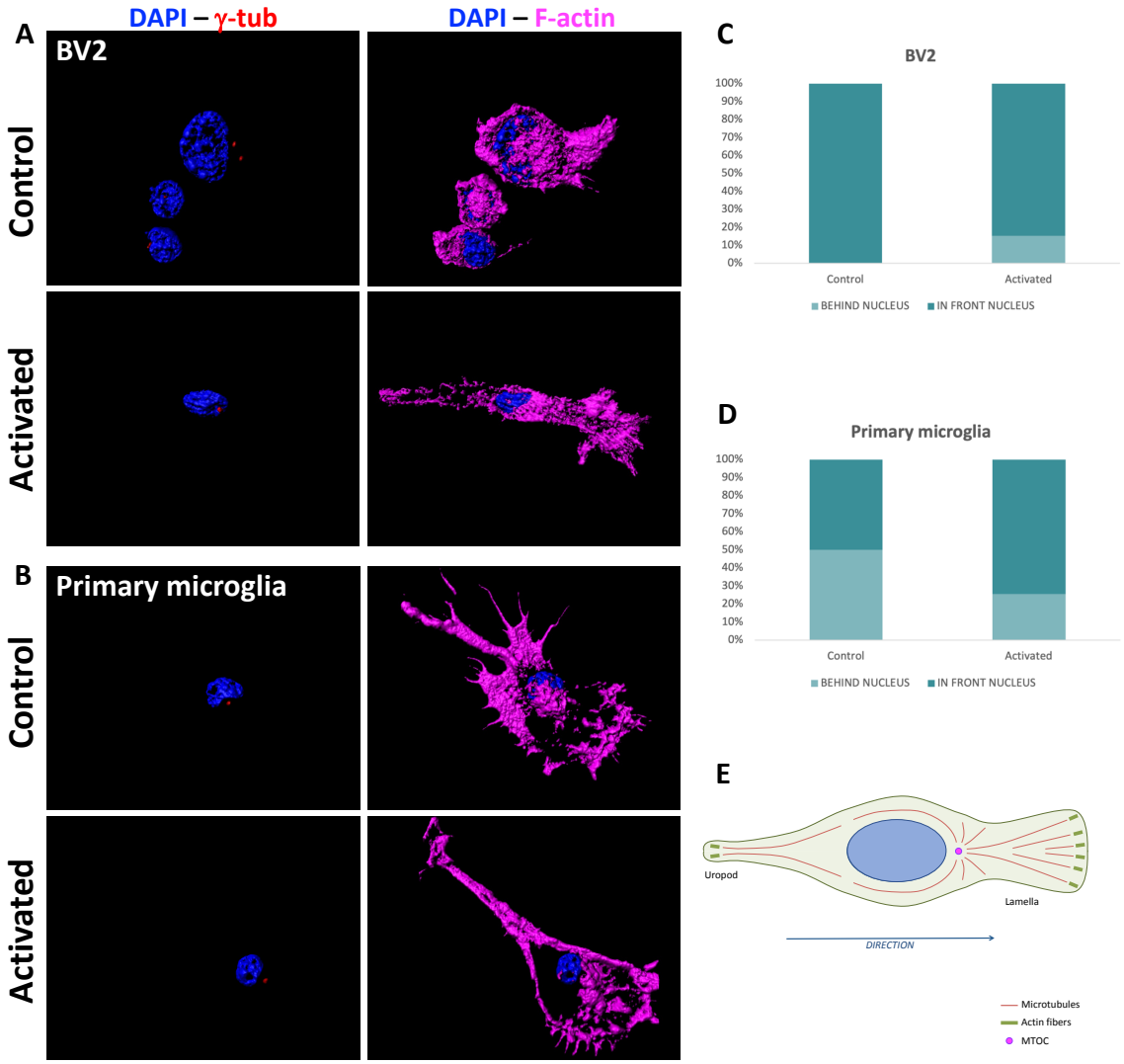


Figure 118. Kinetic microglial cells present their MTOC located in front of the nucleus both in a control and activated state. A. Rendering of BV2 kinetic microglia in both states showing the location of the MTOC (red) regarding the nucleus (blue) and F-actin protruding fibers (magenta). **B.** Iso-surface of primary microglia displaying kinetic morphology in control and activated states depicting the location of the MTOC (red), in relation to the nucleus (blue) and the F-actin protruding arrangements (magenta). **C.** Quantification of the percentage of kinetic BV2 cells positioning their MTOC in front or behind the nucleus in each experimental condition. **D.** Percentage of kinetic primary microglia positioning their MTOC in front or behind the nucleus in control and upon activation. **E.** Schematic representation of a typical kinetic morphology depicting a microglial cell positioning its MTOC in front of the nucleus and organizing the actin fibers and microtubules. (Modified from Roig-Martinez et al., 2019).

4. Released calcium from dying DA neurons as an important process for microglial sensitization

The process of approaching and contact between microglia and dying neurons entails the release of some molecules to the extracellular space. We hypothesize that one of the potential candidates that could be released by neurons in the process of dying is calcium, generating microglial sensitization in the neurodegenerative process.

4.1. DA neurons dying in a Parkinsonian scenario release calcium to the medium

When neurons are under specific physiological conditions or stressful situations, they could start a signaling cascade leading to cell death. This process is called apoptosis and is characterized by cytoplasmic shrinkage (pyknosis), nuclear condensation and fragmentation, and the formation of apoptotic bodies that are released to the external milieu (Kerr et al., 1972; Moujalled et al., 2021), and engulfed and eliminated by neighboring cells (i.e., macrophages/microglia). In other instances, neurons are not committed to die, but under particular external situations, the process of cell death by necrosis takes place. Necrosis – in contrast to apoptosis – is not controlled by the cell, and it is characterized by the loss of ATP, dissipation of ion gradients and cell lysis, releasing the internal components to the embedding environment (Gorman, 2008). Necrosis also causes neuroinflammation in the surrounding region, due to this release of cell contents into the environment.

These released molecules, or cell particles, could be part of the signals by which dying neurons send a message to be potentially eliminated. These “find me” and “eat-me” signals are sensed by microglia and plays an important role removing degenerating neurons (Brown & Neher, 2014; Neher et al., 2011b). Microglia may participate at different stages of the degeneration through phagocytosis, either engulfing the neuronal soma or neuronal particles or fragments. However, in recent years, new research lines have pointed to microglia as able to phagocytose while the target neuron is in the process of dying, or even stressed but alive neurons, a process called phagoptosis (Brown & Neher, 2014). It has been described that in a parkinsonian scenario, both types, apoptosis and necrosis, of degeneration take part (Gorman et al., 2005; Mochizuki et al., 1994).

Regarding the generation of ion gradients, it has been suggested that brain damage can cause calcium waves (D. Sieger et al., 2012) to signal microglia, and importantly, knowing the high internal calcium content in neurons, and particularly important in the highly demanding DA neurons of the SNpc (Zampese et al., 2022), – we hypothesized that calcium being released to

the external milieu, in a process of DA neurodegeneration, may serve as a specific “find-me" signal for microglia. Since MPP^+ provokes specific DA neuronal death, and it is widely accepted as a PD model *in vitro*, we wondered if this neuronal loss induces calcium release to the external milieu.

First, we determined the optimal MPP^+ concentration in which mesencephalic neurons suffer a significant DA neuronal loss. For that, we treated the cultures with the neurotoxin for 24h or 48h to delimit the best time point. Once ascertained the optimal MPP^+ concentration – provoking a significant DA loss – we tested whether calcium release occurs after the DA-specific intoxication.

Mesencephalic neurons were plated and treated after 4-7 DIV. We used increasing concentrations of MPP^+, starting from 2 µM, then 5 µM, 10 µM, 30 µM and finally 100 µM – as the latter was indicated as a lethal concentration for DA neurons in a previous report (Henze et al., 2005). Then, neurons were treated with the neurotoxic insult for 24h and 48h to observe differences. By using immunocytofluorescence to observe and identify the neurons, we performed a stereological quantitation. Similar to previous analyses, as the cultures contained DA and non-DA neurons, we used anti-MAP2 antibody in addition to TH marker.

Then, we measured the calcium release by a commercially available kit. Since, we did not know the calcium dynamics after MPP^+ intoxication, we performed an initial test – prior to the complete experiment – with treated and non-treated neurons with a concentration of 100 µM of MPP^+ – the highest one – to ensure a process of neurodegeneration and considering an early timepoint. For that, we plated and treated the neurons as explained above and after 10h and 24h of intoxication, the supernatants were collected for Ca^{2+} measurements. The calcium released was then quantified by differences in absorbance at 540 nm, being the non-treated neurons the control for this measurement. Early timepoint (10h) for supernatant collection was chosen to delimit how fast calcium dissipation may take place in the process of DA neurodegeneration, before a late timepoint (24h), in which interacting MPP^+ starts to be lethal for neurons.

We observed clear changes in terms of neuronal loss after 24h (Supplementary figure 2A and C) and 48h (Supplementary figure 2B and D) in the presence of MPP^+. Regardless the time exposure, MPP^+ induced a dramatic neuronal death according to the increase of MPP^+ concentration, being the 100 µM dose administration lethal for DA neurons (Supplementary figure 2A and B).

Regarding the calcium measurements in the media, we could observe a slight increase in the concentration after the treatment with MPP^+. We only observe a modest tendency at 10h that became more relevant at 24h (Supplementary figure 2F). This first test suggested that the increase of calcium in the media could be due to the MPP^+-induced neuronal death, but not enough to reach statistically significant results at this early time-point range.

These results show that our model *in vitro*, induced by MPP^+, recapitulates parkinsonian neuronal loss. Low MPP^+ doses – 2 and 5 µM – did not exert a significant decay of neurons, either DA and non-DA neurons, even though DA neurons seemed more susceptible. At higher doses, the deleterious capacity affected both TH-positive and TH-negative MAP2 positive neurons.

We wanted to repeat the analysis of calcium release in later timepoints to control at the same time the DA neuronal death. For that, primary neurons obtained from the ventral part of the mesencephalon of E17 rat embryos were seeded in 24-well plates and treated with different concentrations of MPP^+ as indicated above. After 24h or 48h the supernatant of every condition was taken and preserved for following analyses to observe changes in the calcium release; subsequently, neurons were fixed with 4% PF for 20 minutes for later immunocytofluorescence.

Concomitantly, we labelled the neurons with the markers used above for DA and non-DA neurons; and measured the calcium present in the supernatant for every condition after the treatment with the neurotoxic insult MPP^+.

**Since the total number of DA neurons – counted by the TH^+ staining – was very low compared with the total number of neurons, the graphs were represented with a first Y-axis scale (on the left) for the MAP2 neurons and a second Y-axis scale (on the right) for the TH neurons for better visualization.*

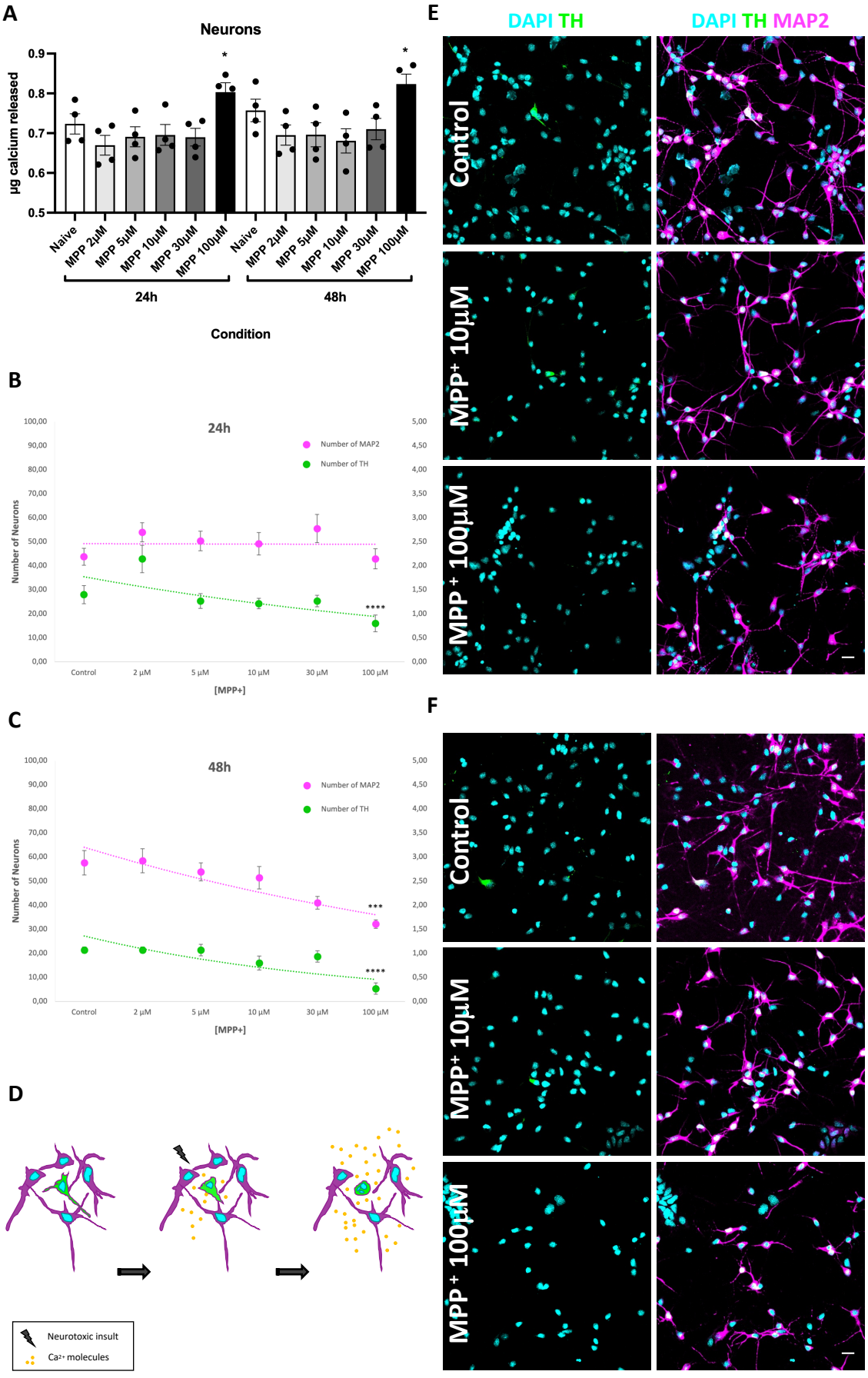

A
Neurons
µg calcium released
0.9
0.8
0.7
0.6
0.5
Naive
MPP 2µM
MPP 5µM
MPP 10µM
MPP 30µM
MPP 100µM
24h
48h
Condition
B
24h
Number of MAP2
Number of TH
Number of Neurons
[MPP+]
Control
2 µM
5 µM
10 µM
30 µM
100 µM
****
C
48h
***
****
D
Neurotoxic insult
Ca²⁺ molecules
E
DAPI TH
DAPI TH MAP2
Control
MPP⁺ 10µM
MPP⁺ 100µM
F
Control
MPP⁺ 10µM
MPP⁺ 100µM

Figure 119. MPP^+-induced DA neuronal loss results in extracellular calcium release. A Graph showing the differences in the amount of calcium measured in the supernatant of non-treated neurons and neurons exposed to the neurotoxic insult MPP^+ in different concentrations ranging between 2 µM and 100 µM, both at 24h and 48h. **B** and **C.** Number of MAP2 (magenta) and TH (green) positive neurons counted at 24h and 48h in every MPP^+ administered concentration as well as in a naïve condition. (* $p<0.05$; ** $p<0.005$, *** $p<0.0005$, **** $p<0.0001$). **D.** Diagram explaining the process of neuronal death and Ca^{2+} release (TH^-/$MAP2^+$ neurons in magenta and TH^+/$MAP2^+$ neurons in green). **E** and **F.** Representative images of TH positive DA neurons (green) and MAP2 positive neurons (magenta) in 3 of the 6 conditions analyzed, comparing the non-treated neurons with an intermediate condition (10 µM) and the highest MPP^+ concentration (100 µM) at 24h and 48h respectively (Scale bar: 20 µm).

When analyzing the number of neurons, we observed changes depending on the time of the MPP^+ treatment. At 24h, TH^+ DA neurons died significantly only when exposed to 100 µM of MPP^+, in contrast with lower doses (Figure 119B and E) that remained more or less stable when compared with non-treated neurons. In terms of MAP2 positive neurons, we observed no differences between the conditions (Figure 119B and E) – including the highest dose – meaning that MPP^+ was affecting specifically the TH^+ DA neurons and no other subpopulations of neurons (Figure 119B).

Similar to 24h treatment, at 48h, the number of TH^+ DA neurons decreased drastically when exposed to the higher dose of MPP^+, and not inducing changes at lower concentrations (Figure 119C and F). However, at this timepoint, we also found a significant decrease in the number of MAP2 positive neurons, meaning that this concentration could be toxic either for non-DA neurons when exposed to MPP^+ during 48h, or to DA neurons non expressing TH, as pointed above (Figure 119C and F).

In terms of calcium release, we only observed a significant increase with the highest concentration of MPP^+ – 100 µM – when compared with the rest of the conditions (Figure 119A). This happens both at 24h and at 48h, concomitant to the significant neuronal loss. This indicates that the DA neuronal loss induced by MPP^+ at 100 µM is provoking the release of calcium to the external environment. Therefore, these results suggest that the MPP^+-dependent DA neuronal loss is directly related with an increase in the release of calcium.

4.2. Microglial cells internalize extracellular calcium

In a neurodegenerative process, the specific signals sent by dying neurons are sensed by microglial cells, which trigger the process of polarization, displacement, and contact with the target, potentially ending in the engulfment and phagocytosis of the damaged neurons. In the

previous section, we showed that dying neurons, in an *in vitro* model of PD, release calcium to the external milieu, which could be considered as one of these signals to attract microglia.

Having in mind this hypothesis and results, we came up with two fundamental questions; i) whether microglial cells may have the ability to sense changes of calcium concentrations in the external milieu, and ii) whether microglial cells have a specific molecule that may be involved in the process of precisely respond to these calcium variations.

Microglial cells, as explained in the introduction, due to their repairing function in the CNS display specific receptors on their surface that could be activated by some of the "find-me" and "eat-me" signals above mentioned. The activation of these receptors initiates a signaling cascade which ends up activating the microglia, either with a pro-inflammatory or anti-inflammatory phenotype. We hypothesize that increasing levels of calcium may play an important role sensitizing microglia and inducing some of the cellular changes promoting its change to a pro-inflammatory phenotype for mounting their repairing function.

Thus, we wondered how microglial cells may respond to the increase of extracellular calcium in vitro, simulating the calcium release induced in the process of DA neurodegeneration.

For that purpose, we cultured primary microglial cells on coverslips, inside 60 millimeters (mm) Petri dishes and let them grow to reach high confluency. Then, microglial cells were cultured in a solution containing the fluorophore Fura-2, which was internalized by microglia, and measured by changes in fluorescence after incorporating extracellular Ca^{2+}.

After the Fura-2 internalization, microglia was set on a specific microscope stage in which we could record a time-lapse video, taking a picture every 0.15 seconds (Figure 20), while adding increasing calcium concentrations to the external medium. This way we could see if the increase of intracellular fluorescence correlates with the increase of calcium in the medium. The increase of calcium internalized by microglia was measured in a plot profile in terms of fluorescence expressed by Fura-2 fluorophore.

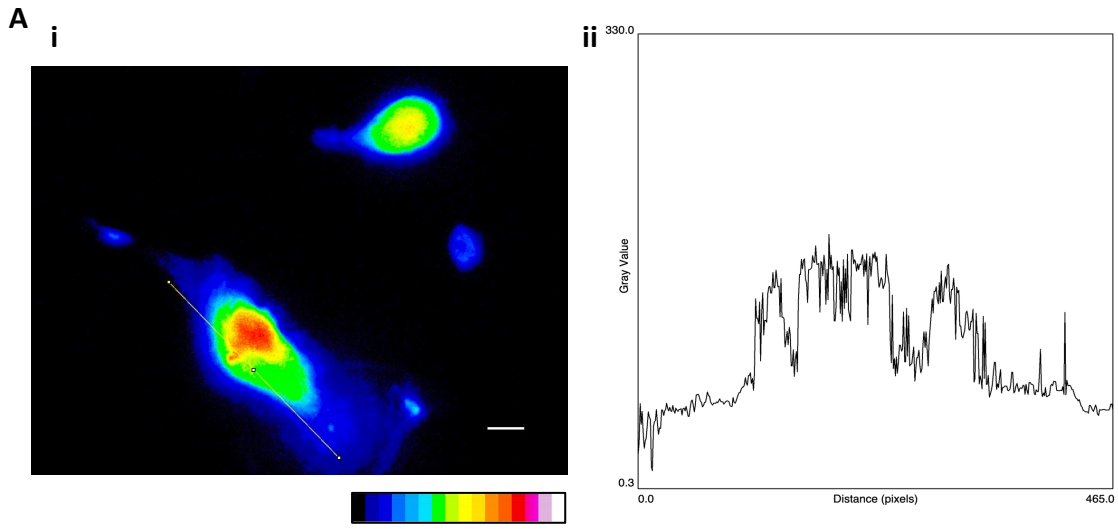


Figure 20. Representative image showing the measurement of Fura-2 fluorescence after Ca^{2+} internalization in primary microglia. A. (i) Microglial cells showing changes of Fura-2 fluorescence due to Ca^{2+} administration. Changes in color indicate correlative changes of fluorescence intensity according to the 16 colors scale (ranging from low intensity, black, to high intensity, white). Measurement of fluorescence intensity at a specific time, was performed on a representative microglial cell along the depicted yellow line crossing its cellular structure (Scale bar: 20 µm). **(ii)** Plot profile showing the intensity of Fura-2 fluorescence from the yellow line drawn.

We observed – in a continuous sequence – how microglial cells internalize calcium along time (Figure 21 A). At the initial point, microglia showed some basal fluorescence (Figure 21 i), and by adding Ca^{2+} to the medium, cells correlatively increased their fluorescence intensity (Figure 21 ii-v). At the end point, in which we had added the maximum calcium concentration, we observed a dramatic increase of fluorescence comparing to the initial point (Figure 21 vi). We measured the differences in fluorescence by a plot profile, as shown above (Figure 20), with a maximum of relative fluorescence set at 255 – as the grey scale was set to 8 bit intensity. We noted how a specific region of the cell increasingly changed its fluorescence intensity, starting at a low fluorescence (around 125) and becoming higher, and even reaching the saturation point (255), but also occupying more area inside the cell. Both phenomena can be seen in the graphs and microscopy images (Figure 21B).

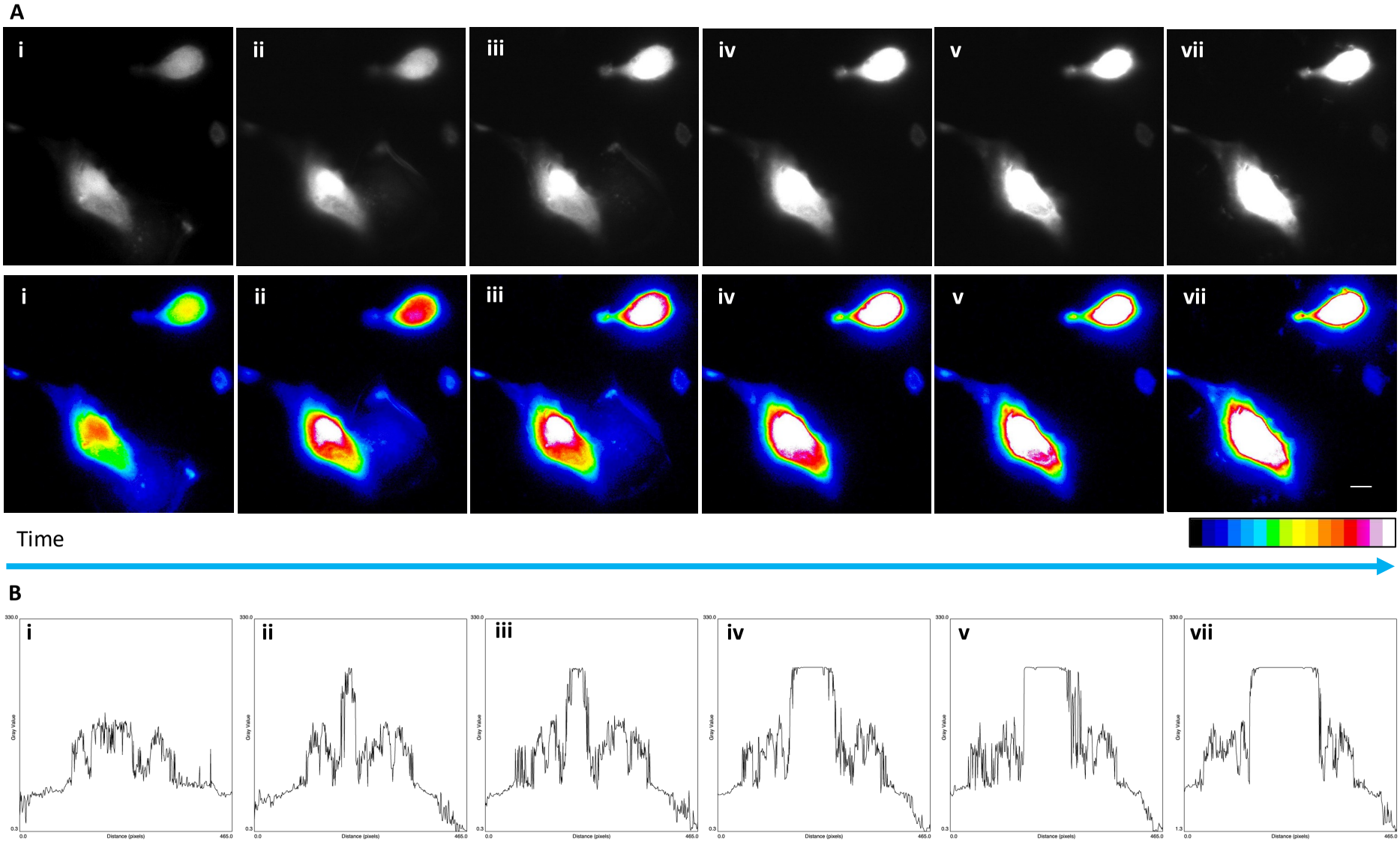

A
i
ii
iii
iv
v
vii
Time
B
Gray Value
Distance (pixels)
330.0
0.3
0.0
465.0

Figure 21. Microglial cells internalize extracellular calcium. A. Continuous image sequence i-vi obtained from a time-lapse video to observe the Fura-2 fluorescence emission changes in microglial cells after calcium administration to the medium. The sequence is shown both in grey scale (upper images) but also in 16 colors intensity (bottom images) to better see the differences in intensity (Scale bar: 20 μm). **B.** Plot profiles of every frame of the time-lapse video i-vi to demonstrate the intensity changes during the time of the experiment (Grey intensity per pixel along the whole cell).

These results suggest that microglial cells are sensitive to the variations of Ca^{2+} concentrations produced in the extracellular environment. This response results in a rapid internalization that appears correlative to the extracellular calcium concentration.

4.3. Understanding calcium release in an in vitro model of PD

To understand how microglia internalize calcium in the presence of DA neurons and to model a physiological scenario similar to PD neurodegeneration, we performed an experiment in which we co-cultured DA primary neurons, obtained from rat embryos and primary microglia – also from the MSF – obtained from P0-P2 rats. To simulate the Parkinsonian scenario, we used the administration of MPP^+, but also in combination with the stimulation of microglial reactivity.

For that, we set up different experimental combinations, including neurons without microglia and treated with the neurotoxic ion MPP^+, neurons in combination with microglia and the neurotoxin, and neurons treated with MPP^+ combined with microglia treated with canonical pro-inflammatory stimuli. All these conditions were generated with their respective controls to assess how much the different stimuli affect the neuronal population.

To perform the experiment, we seeded the neurons in 24-well plates to facilitate the subsequent staining. Neurons were left growing for 4-7 DIV and treated with MPP^+ to induce neuronal degeneration. In the case of the microglia-neurons co-cultures, microglial cells were added to the wells and cultured for another 24h to be attached to the plate. Then, different experimental combinations were performed, either treated only with MPP^+ (10 and 100 μM) or treated only with the canonical proinflammatory stimuli (IFN γ and LPS), or the combination of both the neurotoxic insult and the proinflammatory stimuli. Controls were non-treated neurons and neurons alone treated with LPS. Also neurons were combined with different supernatant of microglia to compare if only the microglial milieu conduces to neurodegeneration. Cells were then immunolabeled to differentiate neurons and microglia.

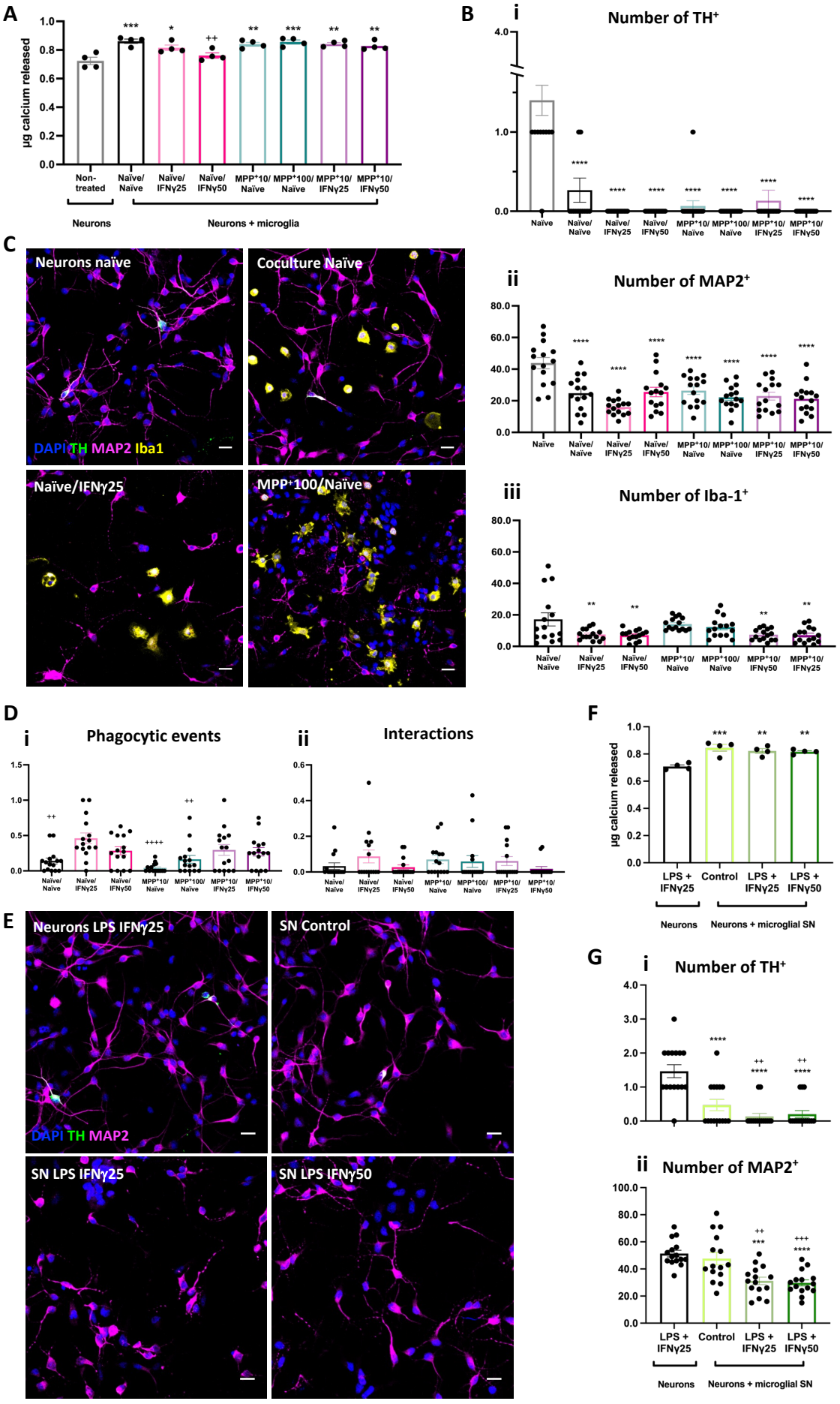

A
µg calcium released
Non-treated
Naïve/ Naïve
Naïve/ IFNγ25
Naïve/ IFNγ50
MPP+10/ Naïve
MPP+100/ Naïve
MPP+10/ IFNγ25
MPP+10/ IFNγ50
Neurons
Neurons + microglia
B
i
Number of TH+
ii
Number of MAP2+
iii
Number of Iba-1+
C
Neurons naïve
Coculture Naïve
DAPI TH MAP2 Iba1
Naïve/IFNγ25
MPP+100/Naïve
D
i
Phagocytic events
ii
Interactions
E
Neurons LPS IFNγ25
SN Control
DAPI TH MAP2
SN LPS IFNγ25
SN LPS IFNγ50
F
µg calcium released
LPS + IFNγ25
Control
LPS + IFNγ25
LPS + IFNγ50
Neurons
Neurons + microglial SN
G
i
Number of TH+
ii
Number of MAP2+

Figure 22. Physiological scenario of parkinsonian neurodegeneration promotes calcium release regardless the stimulus. A. Graph of the amount of calcium released in the different conditions where the neurons were cocultured with microglia and subsequently treated with different stimuli. (* respect non-treated neurons, + respect Naïve/Naïve) **B. (i)** Count of the total number of TH+ neurons in every condition. (* respect non-treated neurons) **(ii)** Total number of neurons counted in the different conditions. (* respect non-treated neurons) **(iii)** Microglial cells' numbers in every condition performed. **(*** respect Naïve/Naïve) **C.** Representative images of four of the eight conditions analyzed to better understand the graphs represented. (Scale bar: 20 µm). **D.** Counts of the number of phagocytic events (+ respect Naïve/IFNγ25) **(i)** and interactions **(ii)** per picture between microglial cells and neurons found in the cocultures. **E.** Representative images of neurons cultured with different microglial supernatants corresponding to the numbers at the right (Scale bar: 20 µm). **F.** Micrograms of calcium released by neurons when exposed to a pro-inflammatory stimulus, LPS and IFN γ 25, (first bar) and when exposed to supernatants of previously treated microglia to become pro-inflammatory (third and fourth bars) or stay homeostatic (second bar). (* respect LPS IFNγ25-treated neurons) **G.** Counts of the total number of TH+ neurons **(i)** and MAP2+ neurons **(ii)** in each of the above-mentioned conditions. (* p<0.05; ** p<0.005, *** p<0.0005, **** p<0.0001). (* respect LPS IFNγ25-treated neurons, + respect Control SN).

Regarding the neurons co-cultured with microglial cells we could see differences in terms of calcium released to the milieu (Figure 22A). Neurons cocultured with microglial cells are releasing more calcium to the external milieu than neurons cultured alone and with any stimulus (Figure 22A). However, when comparing between the different coculture conditions performed in the experiment results in no significative differences. When looking at the number of neurons in each of those conditions, the DA (TH^+) neurons (Figure 22B i) and the total number of neurons ($MAP2^+$) (Figure 22B ii) diminish significantly between neurons cocultured with microglia, regardless of the stimuli used, and neurons cultured alone (Figure 22B and C). But again, no differences were seen comparing the cocultures treated differently (Figure 22B and C).

These results suggest that neurons in a stressful situation, which could be, simply, the presence of microglial cells coming from a different environment (different animals), release calcium in consequence, this could be interpretated as the microglial cells are inducing neuronal death and, in consequence, they release some calcium to the external milieu. When these neurons are treated with the neurotoxic insult MPP^+, in two different concentrations, or even the microglial cells become pro-inflammatory, due to the LPS and IFN γ25 administration, the calcium measured does not seem different from the naïve coculture (Figure 22A). However, we cannot assert these measures are because of less calcium released, or because some other component is eclipsing the real calcium released, in example, microglial cells which could be internalizing the calcium at the same time neurons are releasing it. The different number in terms of neurons (Figure 22B i and ii) and microglia (Figure 22B iii) are other factors which complicate the interpretation and the high variability we could have.

Altogether, the results recommend what we saw in previous experiments (Figure 119A), the neurons release calcium to the extracellular milieu when exposed to a stress situation; but the complex combination of the conditions, being neurons combined with microglia, neurons treated with MPP^+ and microglia, neurons with activated pro-inflammatory microglia or even the cocultures with both stimuli together, difficult the analysis and the comprehension of the results.

Due to specific events found in these cocultures, we also analyzed the number of phagocytic events and interactions microglia-neurons in every condition. Results, again, are difficult to comprehend due to the different number of microglia (Figure 22B iii) and neurons (Figure 22B ii) we had in every condition. Microglia seems to have more phagocytic capacity when are pro-inflammatory-activated than in a homeostatic state (conditions with LPS-IFN γ addition and in combination with MPP^+) (Figure 22D i), while the interactions are more predominant in the conditions in which microglial cells are not stimulated but the neurotoxic insult was added (conditions only with MPP^+) (Figure 22B iii), suggesting a less reactive action of microglia when in a homeostatic phenotype.

On the other hand, within the idea to determine in which range the microglial cells are the responsible indeed for the neuronal death in a pro-inflammatory scenario, or if the pro-inflammatory cytokines released to the external milieu could be involved; we observed clearly that neurons combined with supernatant coming from already-activated microglia released more calcium than neurons cultured with the canonical pro-inflammatory stimuli (as a control of the pro-inflammatory stimuli action to neurons) (Figure 22F). In terms of neurons (Figure 22G i) and especially the DA (Figure 22G ii) both decreased in number when exposed to activated-microglia supernatants more than when neurons were treated with control-microglia supernatant or even with only the pro-inflammatory stimuli. These results show that the pro-inflammatory cytokines released to the external component by activated microglial cells are crucial to promote this neuronal susceptibility to die.

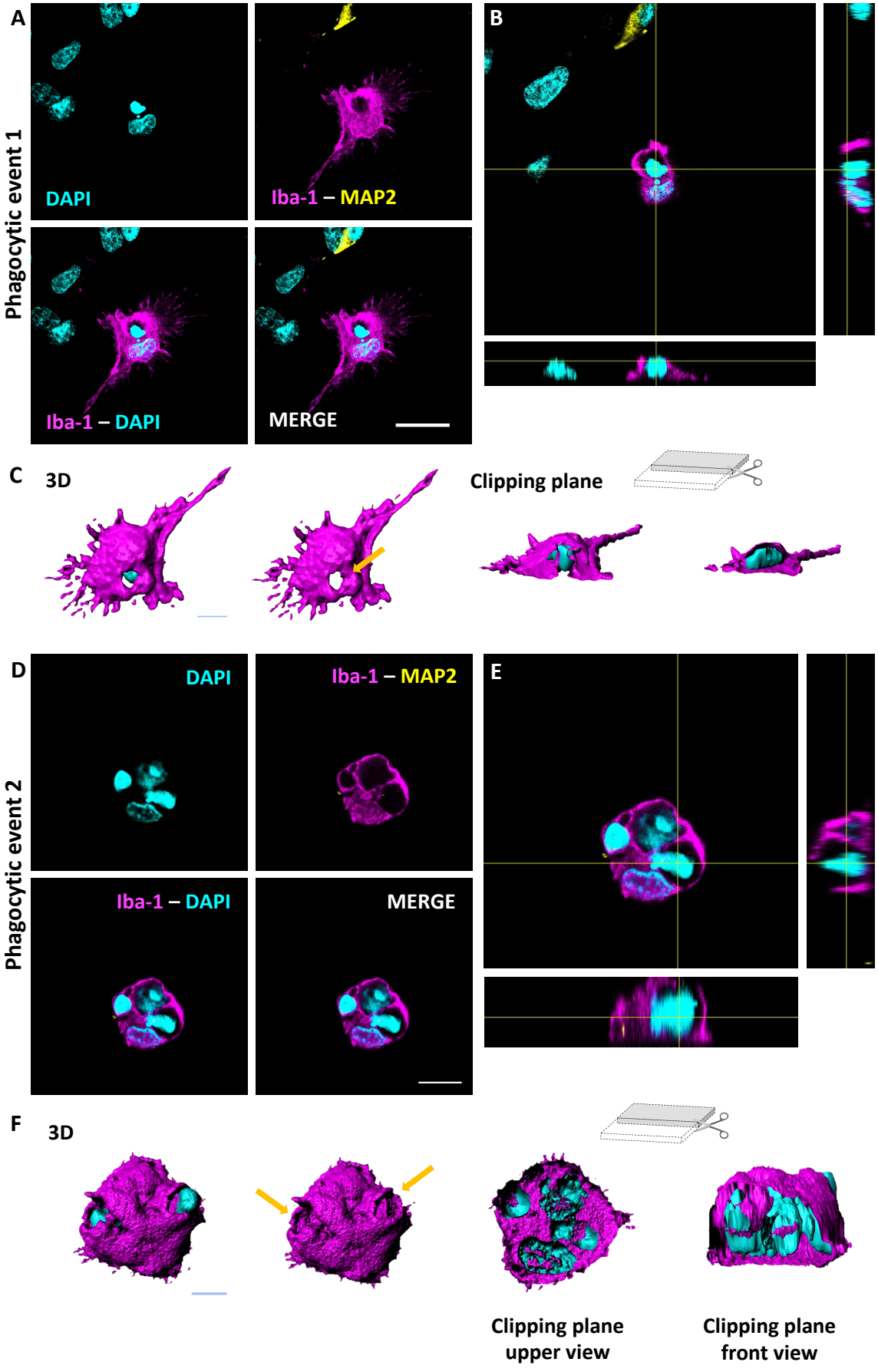

A
Phagocytic event 1
DAPI
Iba-1 – MAP2
Iba-1 – DAPI
MERGE
B
C
3D
Clipping plane
D
Phagocytic event 2
DAPI
Iba-1 – MAP2
Iba-1 – DAPI
MERGE
E
F
3D
Clipping plane
upper view
Clipping plane
front view

Figure 23. Phagocytic events in the co-cultures. A. Image of an optical z-plane showing a phagocytic event of pyknotic nuclei engulfment found in neurons-microglia co-cultures (with MPP^+10/LPS25). Microglia, stained with Iba-1 (magenta) is showing kinetic morphology, combined with MAP-2 (yellow), and DAPI for the nuclei (cyan) (Scale bar: 20 μm). **B.** Orthogonal view of the phagocytic event to visualize the pyknotic nucleus (cyan) inside an Iba-1 negative phagosome outlined by Iba-1 staining (magenta). **C.** 3D rendering of the phagocytic event to see that the pycnotic nucleus is inside a phagosome, indicated with a yellow arrow (second rendering) and a clipping plane in which we could see the pyknotic nucleus inside the microglial cell. Clipping plane diagram is included to better understand the processing. **D.** Optical z-plane of another phagocytic event found in the microglia-neurons co-culture (with MPP^+10 and LPS25) of a microglial cell containing three Iba-1 negative phagosomes outlined by Iba-1 (magenta) and holding pyknotic nuclei inside with high DAPI intensity (cyan) (Scale bar: 10 μm). **E.** Orthogonal view of the microglial phagocytosis in which we visualize three phagosomes inside the cell containing the three pycnotic nuclei (cyan) surrounded by the Iba-1^+ cytoplasmic content (magenta). **F.** 3D rendering of the phagocytic event to better see the 3 pycnotic nuclei inside the three phagosomes or phagocytic cups, indicated two of them with yellow arrows (second rendering) and two different clipping plane-views in which we could see the pyknotic nuclei engulfed by the microglial cell. The clipping plane is also in a diagram to follow the rendering explanation.

Surprisingly, in this same conditions previously analyzed, we found microglial phagocytic events characterized by the presence of phagosomes containing particles inside (Figure 23 and Figure 24). These particles were more often pycnotic nuclei (Figure 23), or pycnotic nuclei fragments, and in some other instances, MAP-2 positive material (Figure 24), indicating phagocytosis of neuronal corpses.

These events were mainly seen in the conditions of co-cultures treated with MPP^+ – having neurons dying because of the neurotoxin – but also combined with the proinflammatory stimulus LPS and IFN γ. The fact that these events repeatedly appeared when co-cultures were treated with the combination of MPP^+ and LPS/IFN γ reinforces our hypothesis of microglia as one of the key components contributing to neuronal death in a PD-related neuroinflammatory scenario. At the same time, although activated microglia may perform their normal function by phagocytosing, it remains to be demonstrated whether exacerbated phagocytosis plays a role in PD.

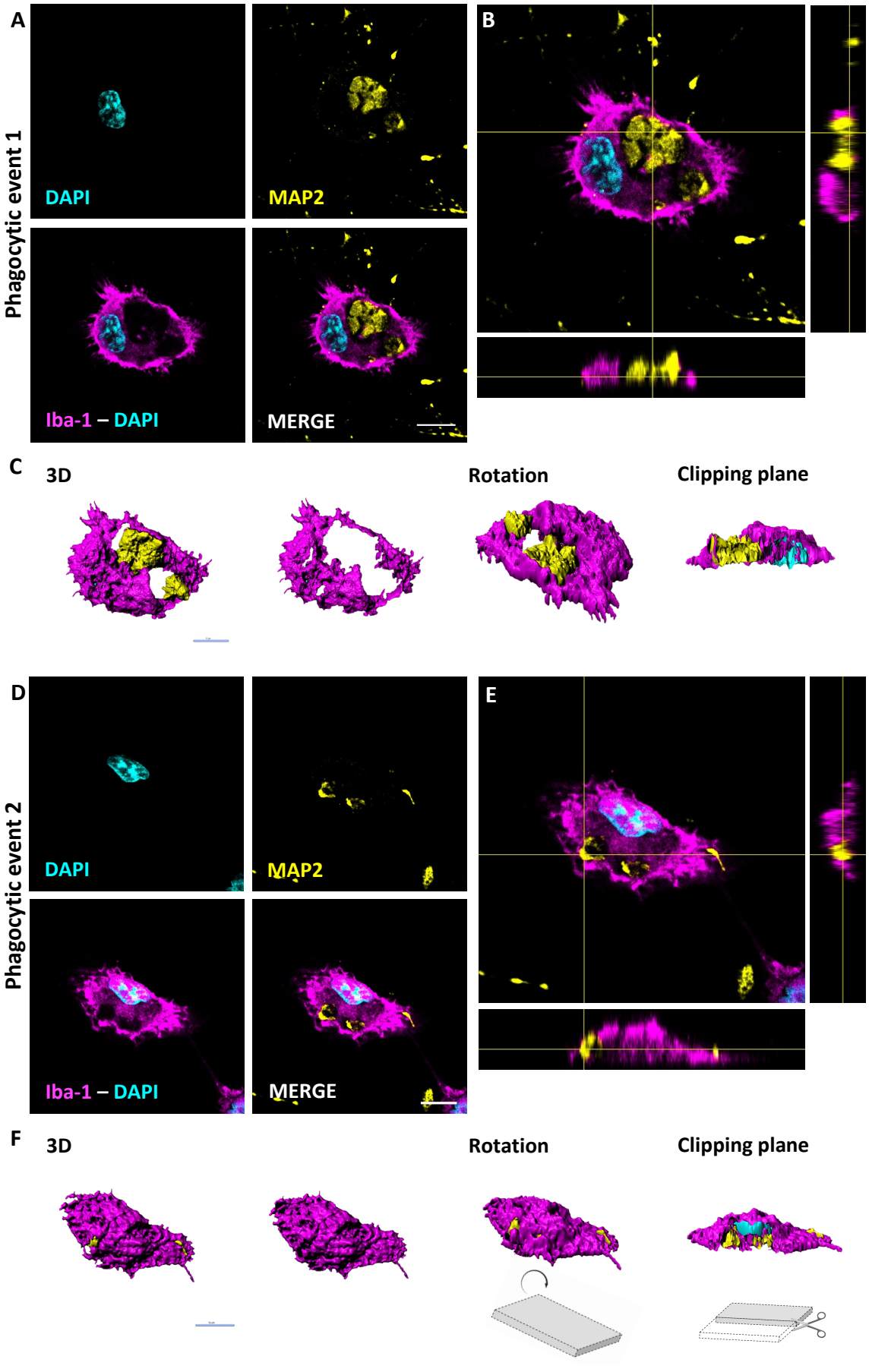

A
Phagocytic event 1
DAPI
MAP2
Iba-1 – DAPI
MERGE
B
C
3D
Rotation
Clipping plane
D
Phagocytic event 2
DAPI
MAP2
Iba-1 – DAPI
MERGE
E
F
3D
Rotation
Clipping plane

Figure 24. Phagocytic events with MAP2$^+$ material inside phagosomes. A. Optical z-plane of a phagocytic event (Phagocytic event 1) in microglia-neurons co-culture, treated with MPP$^+$10 and LPS50, showing a microglial cell, labelled with Iba-1 (magenta), combined with MAP2 for neurons (yellow), and nuclei (DAPI). MAP2$^+$ fragments can be seen inside microglial phagosomes (Scale bar: 10 µm). **B.** Orthogonal view of the phagocytic event to see the MAP2$^+$ particles (yellow) inside Iba-1 negative phagosome surrounded by Iba-1 staining (magenta). **C.** 3D rendering of the phagocytic event to visualize the MAP2 neuronal fragments (yellow) inside the phagosomes, a rotation to better see the phenomenon and a clipping plane to see the MAP2$^+$ material inside the microglial cell. **D.** Optical 1-z plane of another phagocytic event (Phagocytic event 2), in which cells were treated with MPP$^+$10 and LPS25, of a microglial cell (magenta) with two phagosomes containing MAP2$^+$ material inside (yellow) (Scale bar: 10 µm). **E.** Orthogonal view of the phagocytosis showing Iba-1 negative phagosomes with MAP2 positive debris inside. **F.** 3D rendering of the second phagocytic event to see that the MAP2$^+$ particles (yellow) inside the phagosomes, a slight rotation tilting to visualize the phenomenon and a clipping plane in which we could see the MAP2 positive particles inside or being engulfed by the microglial cell. Rotation and clipping plane diagrams are shown to understand the rendered images.

4.4. Calcium promotes microglial kinetic shape

At that point, we were wondering which other changes in microglial cells could have been produced due to calcium. We are trying to build how the whole process is and in which of the steps the calcium is involved.

Knowing that DA neuronal death induces the release of calcium to the external environment, and then, microglial cells are able to sense and internalize this calcium from the extracellular medium, we wondered about its function.

As we demonstrated in section 3, cultured microglial cells adopt different shapes depending on their motility and polarization. When moving towards a target, microglial cells need to rearrange and polarize through the direction of the target, adapting the characteristic elongated kinetic morphology (Figure 117). Then, we hypothesize that, considering calcium as a potential “find-me” signal, it may be involved in promoting the motility of microglia, which can be reflected in displaying kinetic morphology, which facilitates the approaching to the target.

To verify this hypothesis, we cultured BV2 microglial cell line in 24-well plates for a later morphometric analysis with immunofluorescence, then, cells were treated with different calcium concentrations. To ensure that the morphological changes were induced by the added calcium ions, we first eliminated the calcium present in the culture media. For that, we performed two sets of experiments. We added increasing calcium concentrations to the cells for a better understanding of the process. We used calcium free DMEM as the culture medium for these experiments. This medium was mixed with different proportions of a solution with 1M

Ca^{2+} to make different concentrations of calcium, ranging from 1.8mM Ca^{2+} to 20mM Ca^{2+}. We used several controls to compare the differences between the experimental conditions, for example, knowing that normal DMEM medium typically contains 1.8mM Ca^{2+} concentration, we used this condition as a normo-calcemic control for the external administration, other controls entailed standard DMEM medium, normally used in other experiments, and calcium free medium.

The first set of experiments were performed by adding increasing concentrations of Ca^{2+} to a starting solution of standard DMEM, therefore, with no previous deprivation of calcium to the cultured microglia. However, the second set of experiments was performed with a previous deprivation of calcium to the cultured microglia.

The aim of performing these two experiments was to see if the microglial response to extracellular calcium depends on the concentration or it is sensitive to a differential-rate. In addition, from a chemotactic perspective, Ca^{2+} saturation may also hinder the response.

After 24 hours of calcium administration, cells were fixed and preserved until being stained. The staining was performed to visualize F-actin fibers – a key element of the cytoskeleton involved in the arrangement of cellular shape and morphology.

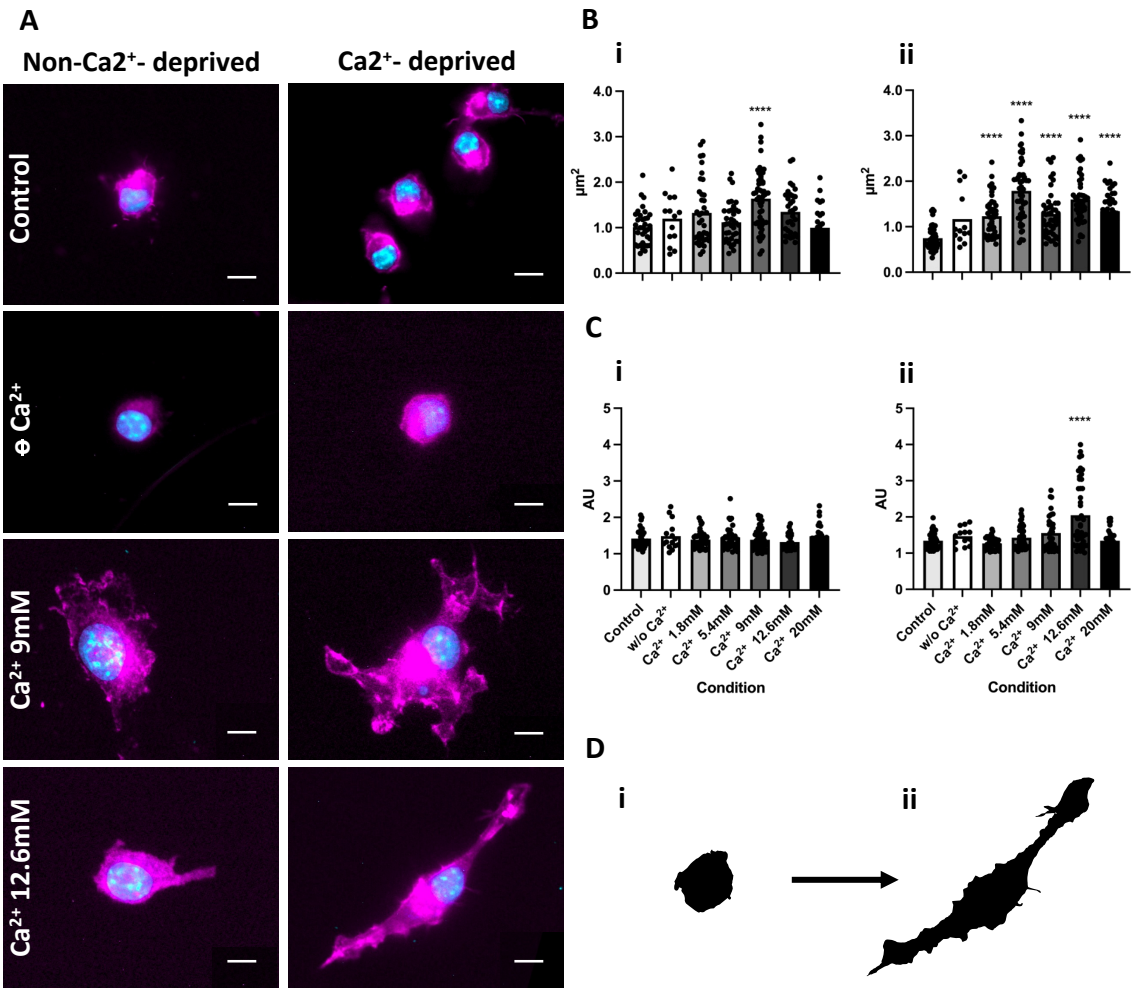


Figure 25. Extracellular calcium promotes elongated shape in microglial cells. A. Microscope pictures to observe the differences in area and elongation microglia after Ca^{2+} treatment. Phalloidin staining was used to visualize F-actin fibers and outline the complete morphology of the cells (magenta) (Scale bar: 10 μm). **B.** Graphs showing the differences in total area occupied by microglial cell, quantified cell by cell, either with non-calcium deprived medium **(i)** and with previous Ca^{2+} deprivation **(ii). C.** Quantification of the aspect ratio of microglia, relative to the level of elongation of the cells. With non-calcium deprivation prior to the experiment **(i)**, and with Ca^{2+} deprivation **(ii)** (**** $p<0.0001$). **D.** Diagrams of a control microglial cell **(i)** changing to an elongated shape after the addition of calcium **(ii).**

The analysis showed clear differences between cells cultured with normo-calcemic medium and cells that received the addition of calcium. Importantly, previous Ca^{2+} deprivation was critical to promote some of these changes. As seen in our images, microglial cells showed a small and characteristic rounded shape when cultured with normo-calcemic medium, consistent with a homeostatic situation (Figure 25A-C). When microglial cells were cultured in a calcium-free environment they showed a similar morphology when compared with the controls (Figure 25B and C), but – as we observed in the images – appeared to show less expression of F-actin staining (Figure 25A), suggesting a potentially stressful state.

In contrast, when adding calcium to the medium to cultured microglia, we observed a significant increase of occupied area (Figure 25B), meaning that cells became bigger after the treatment (Figure 25A). We saw similar differences either when microglial cells where previously deprived from calcium or not (Figure 25). Even though, microglia showed more dramatic changes when previously deprived from Ca^{2+} in the area (Figure 25B), and most especially regarding the elongation (Figure 25C). These analyses indicate that microglial cells became bigger and adopt a kinetic morphology with increasing concentration of calcium, with more patent changes when calcium was previously withdrawn.

These results suggest that after an increase of extracellular calcium into the microenvironment, microglia become sensitive, internalize calcium ions – as we observed in prior experiments – and in consequence, they respond with dramatic cellular arrangements, turning bigger and displaying an elongated and kinetic shape (Figure 25D), which may reflect the initiation of polarization and motility of microglia.

4.5. Calcium-induced kinetic morphology corresponds with increasing microglial motility

As the kinetic morphology is the cellular arrangement that promotes the motility of the cell, we wanted to test if the increase of calcium ions could be directly implicated in the microglial movement. Then, microglial cells should be sensitive to changes of calcium in the external environment modifying parameters of cell movement.

To test this hypothesis, we used microfluidic plates, in which we could seed and subject the cells to different extracellular inputs while recording the live cells on the microscope.

Microglial cells were cultured in normal medium, placed on the microfluidic plates, and left being attached to the bottom of the chamber. Then, microfluidic channels were used to pass through either calcium-free medium or calcium-rich medium through the microglial culture. These media were continuously renewed because of the flowing system of these microfluidic plates. Then we recorded the microglial cells for 24 hours by setting a time-lapse video, capturing frames every 5 minutes.

Time-lapse frames were analyzed to test whether microglial cells present calcium-dependent motility.

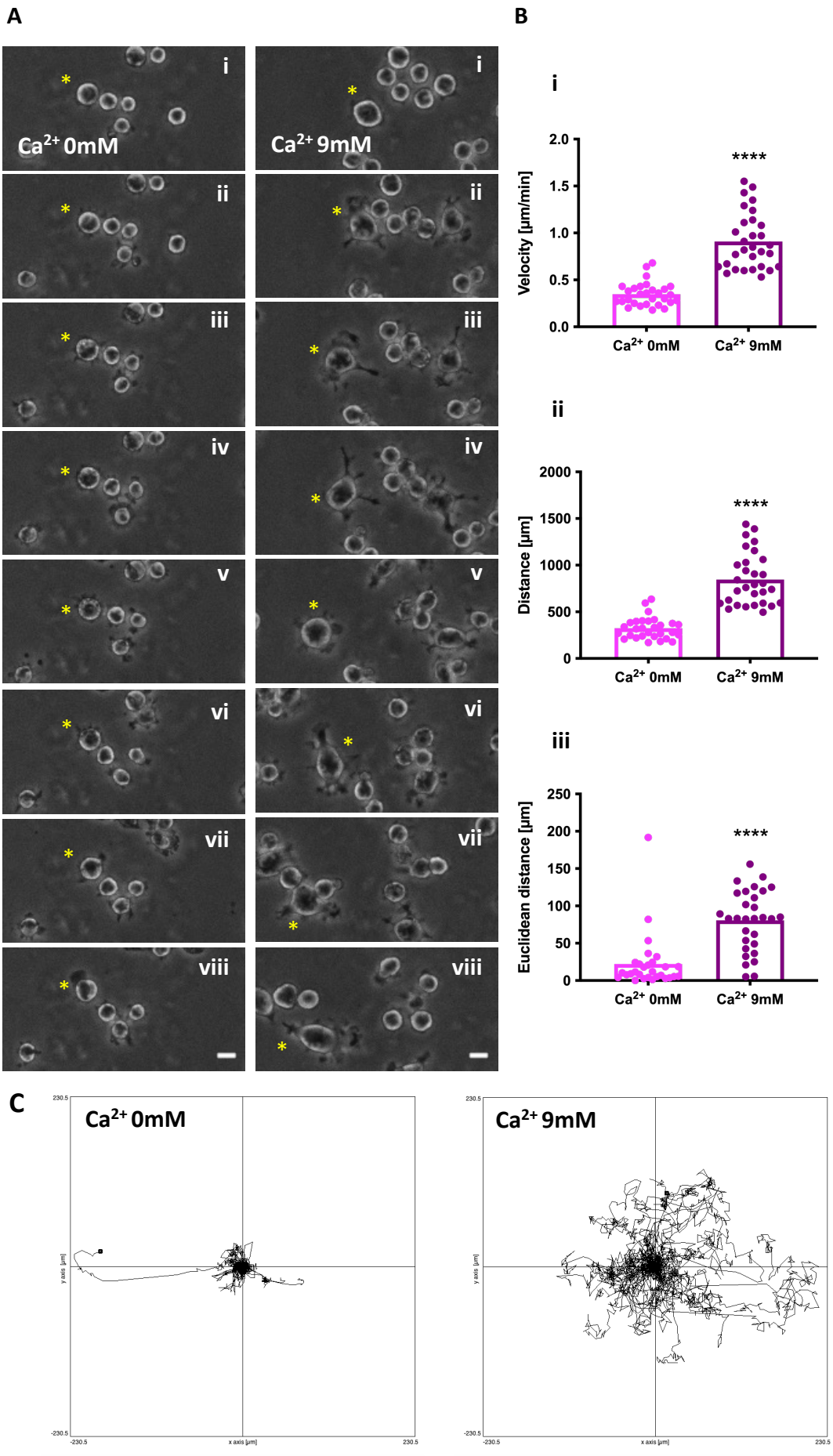

A
B
C
Ca2+ 0mM
Ca2+ 9mM
i
ii
iii
iv
v
vi
vii
viii
Velocity [µm/min]
Distance [µm]
Euclidean distance [µm]
****
2.0
1.5
1.0
0.5
0.0
2000
1500
1000
500
0
250
200
150
100
50
x axis [µm]
y axis [µm]
230.5
-230.5

Figure 26. Calcium-rich medium promotes microglial movement. A. Representative frames of the 24h time-lapse for calcium-free and calcium-rich media, in which we can see differences on microglial cell motility during the time recorded (Scale bar: 20 μm). The yellow asterisk points to one specific microglial cell. Note no apparent movement on calcium-free medium in contrast with motility on calcium-rich medium. **B.** Charts showing statistical differences in velocity **(i)**, total travelled distance **(ii),** and the Euclidean distance in their total path **(iii),** between microglia placed in a calcium-free and a calcium-enriched medium (**** $p<0.0001$) **C.** Tracking plots following the path of 30 cells for each condition during the acquired time-lapse. Plots are represented by distance in the x and y axis.

The results revealed that different parameters of microglial cells motility are dependent on the presence of Ca^{2+} in the medium. When microglial cells were placed in a calcium-free medium, they barely moved during the time recorded, as we could see in the images of representative cells (Figure 26A), the parameters of motility (Figure 26B), and in the cell tracking plot (Figure 26C). In contrast, when microglial cells were placed in a calcium-enriched environment, they display high motility during the time recorded. We could see this feature in the representative images of microglia moving and changing its position during the time-lapse (Figure 26A) as well as the cell tracks analyzed (Figure 26C).

In terms of velocity, when microglial cells were placed in a calcium-rich medium they moved faster when compared with calcium-free environment (Figure 26B i). Regarding the distance, we measured two different parameters, accumulated distance and Euclidean distance. The accumulated distance refers to the total amount of distance that microglia could travel. In this case, microglial cells travelled more distance when calcium was present in the medium when compared with calcium-free medium (Figure 26B ii and C). The Euclidean distance allude to the distance travelled in a straight manner between the starting and final point, meaning that the increase in Euclidean distance allows microglia to travel further. We observed that calcium-enriched medium promoted a dramatic increase of Euclidean distance, more than triple than microglia with no external calcium input (Figure 26B iii), as we could visualize in the cell track plots (Figure 26C).

These results indicate that extracellular calcium inputs are critical in inducing changes in microglial dynamics, facilitating the motility of the cells, which is consistent with the arrangement of a kinetic morphology.

Moreover, as we showed that microglia is sensitive to calcium variations, it is coherent with the hypothesis that this calcium input may come from neighboring degenerating DA neurons – which, as we also showed, release calcium to the extracellular media after a DA neurotoxic

insult. However, the extracellular calcium dynamics in the brain parenchyma is still unclear, as how the communication and Ca^{2+} transfer between neurons and microglia may take place.

One of the hypotheses is that calcium variations travel as long-range waves to signal brain damage to microglia (D. Sieger et al., 2012). Then, we wondered if microglial cells may respond differently when they receive a continuous flow of calcium-rich medium, or when they receive calcium inputs as waves. For this, we performed another set of experiments with microfluidic plates to generate alternating flows directed to the cell culture chamber. In that case, we first plated microglial cells with normo-calcemic medium and let them to be attached to the plate, then by setting the alternating flows we could generate waves of high Ca^{2+}-concentration entering the chambers and passing through the microglial culture. These oscillations generate high Ca^{2+}-concentration waves every 15 minutes. Cells were then recorded by time-lapsing the plate every 5 minutes for 24 hours.

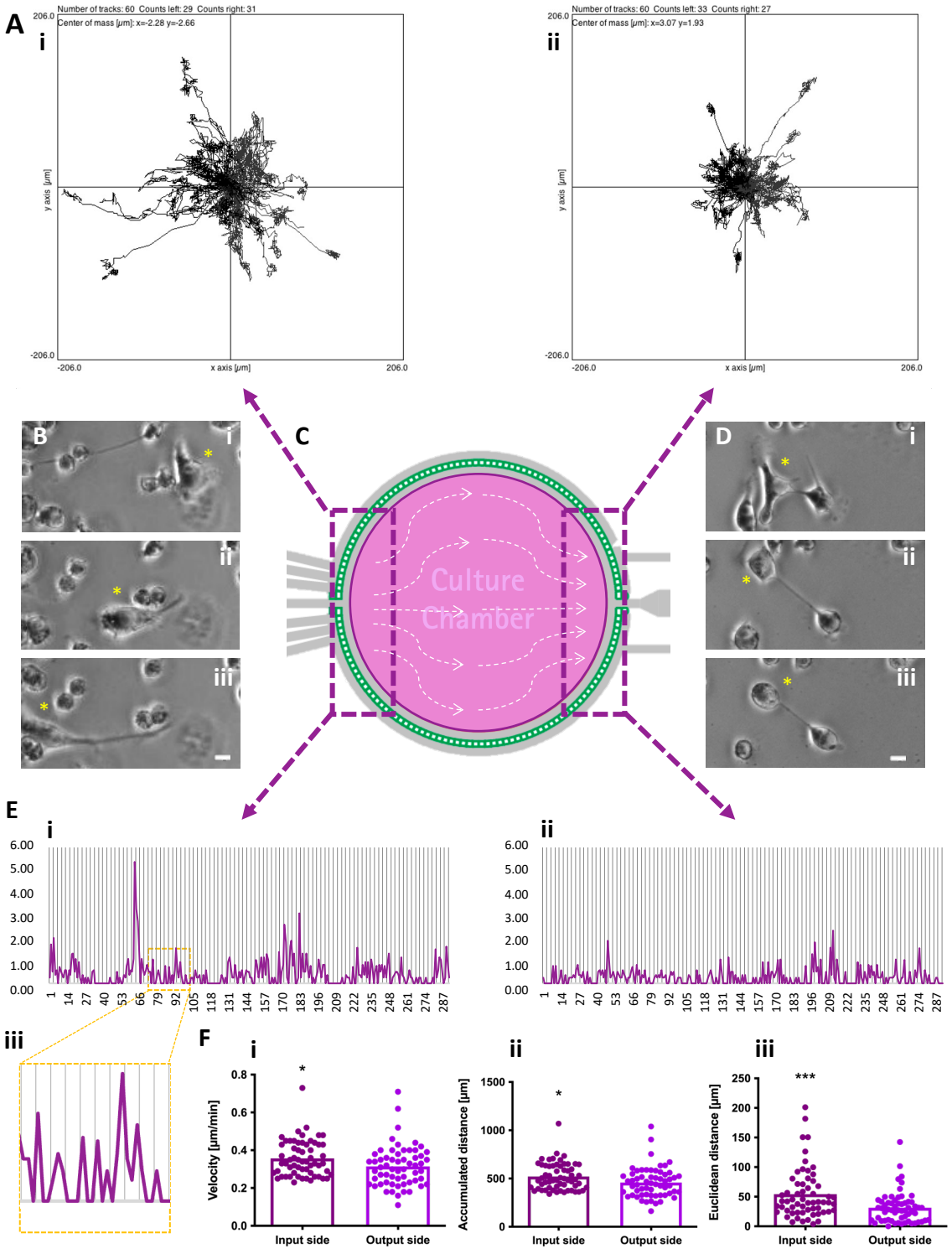


Figure 27. Microglial cells respond to calcium waves being more prominent when near to the calcium source. A. Cell tracking plots of a total of 60 microglial cells analyzed in each side of the plate during the recorded time-lapse. Distance is represented in the x and y axis. **B.** Time-lapse video frames of a microglial cell, indicated with a yellow asterisk, as a representative example of the increasing motility during 24h of the recording at the input side of the chamber (nearest side to the calcium source) (Scale bar: 20 µm). **C.** Diagram of one of the chambers of the microfluidic plate. Purple broken line rectangles indicate the fields where the time-lapse recordings were taken for each side of the chamber. White broken line arrows are representing the direction of the flow for better understating. **D.** Time-

lapse frame of a microglial cell, marked with a yellow asterisk, as an example of the movement during the 24h recorded at the output side of the plate (farthest side to the calcium source) (Scale bar: 20 µm). **E. (i).** Representative example of the variations in velocity of a microglial cell at the input side along the time of the time-lapse acquisition. High velocity peaks coincide with the inputs of calcium waves. **(ii).** Example of one microglial cell at the output side, showing the oscillations of velocity along the experiment. Although the pattern is similar, the velocity peaks of the output side are not as high as at the input side. **(iii).** Zoom-in from the graph in (i) to better see the high velocity peaks coinciding with calcium waves inputs (vertical grey lines behind). **F.** Charts showing statistical differences in velocity **(i)**, total accumulated distance **(ii),** and Euclidean distance travelled by microglial cells **(iii)** when placed in the input side vs output side of the plate. In all instances, Ca^{2+} mediated changes in motility are more prominent in the input side (near to the calcium source) (* $p<0.05$; ** $p<0.005$, *** $p<0.0005$, **** $p<0.0001$).

In this experiment, we initially wondered if microglial cells would polarize towards the calcium source, however, we could not observe a clear directional migration of microglial cells. One plausible explanation was the absence of a real chemotactic gradient. As the calcium solution entered the chamber, tended to be evenly distributed in the whole space during the calcium wave span.

Interestingly, when analyzing the cell tracking of microglia we could see differences between the movement of microglia placed near the calcium source and microglial cells located far away from the calcium entry (Figure 27C). Even though microglial cells were incessantly moving in both cases, cells located near the calcium source were moving faster, traveling longer and straighter distances, and frequently adapting a kinetic morphology (Figure 27B), while microglia found far from the calcium entry were slower (Figure 27D), resulting in travelling shorter distances but also with less straight movements (Figure 27A). Moreover, by analyzing some cell tracks in detail, and graphing the velocity of the cells with time, we could observe that microglial cells placed near the calcium source showed increases of velocity as abrupt peaks coinciding with the precise moment of the calcium wave input (Figure 27E i and iii). While these peaks were less prominent in microglial cells placed far from the calcium entry (Figure 27E ii). Considering these results – and combined with some of the results obtained in previous sections – we could conclude that microglial cell motility depends on the calcium variations of the extracellular milieu. Importantly, the exposure to an abrupt increase of calcium concentration, as generated with calcium waves, microglia potentiate their motile characteristics. Although the microfluidic plates could not generate a gradient and, in consequence, we could not observe a polarization of microglial cells towards the source, we saw clear differences regarding the distance to the calcium input. These differences could be due to the combination of two phenomena, the availability of extracellular calcium and its internalization by microglia. As microglial cells are near the calcium source, they respond to the increasing calcium concentration, internalizing it,

and promoting motile features. However, when the wave arrives to the microglial cells on the opposite side – away from the calcium source – the calcium availability in the medium is lower, as it has been previously internalized by numerous microglial cells near the input, and in consequence, having motility changes in a lesser extent (Figure 27F). These results highlight how important the changes in extracellular calcium are for microglial movement.

4.6. Calcium administration promotes polarization of microglia in vivo

Once we examined how microglial cells behave and respond to changes of extracellular calcium concentration *in vitro*, we wanted to test this phenomenon *in vivo*. We wondered how microglial cells motility may change with the administration of calcium in the brain tissue.

The aim of this experiment was to simulate a more physiological condition and examine calcium-dependent changes of microglia in mice. For that, we administered intracranially, solutions of high concentrations of calcium directly to the striatum to examine the polarization of microglial cells in the cerebral parenchyma. We used the C57BL/6j mice strain to inject the solutions.

First, we injected different calcium concentrations to determine the optimal to induce visible changes in microglia but without damaging the brain parenchyma. For this pilot experiment, four different concentrations of calcium were used: Ca^{2+} 0.25M, Ca^{2+} 0.5M and Ca^{2+} 0.75M. The solutions were administered in the striatum by using a stereotaxic frame with the corresponding stereotaxic coordinates [Anteroposterior (AP): + 0.5 mm; Mediolateral (ML): + 2.1 mm; Dorsoventral (DV): - 3 mm, according to Bregma]. At third day post-injection, we obtained the brains by intracardial perfusion to be processed for immunohistofluorescence and analyzed by confocal microscopy. Brain sections were immunostained with Iba-1 antibody and combined with DAPI as a counterstaining. In this analysis, the morphology of microglial cells and the extension of the inflammatory response were examined (Figure 28A).

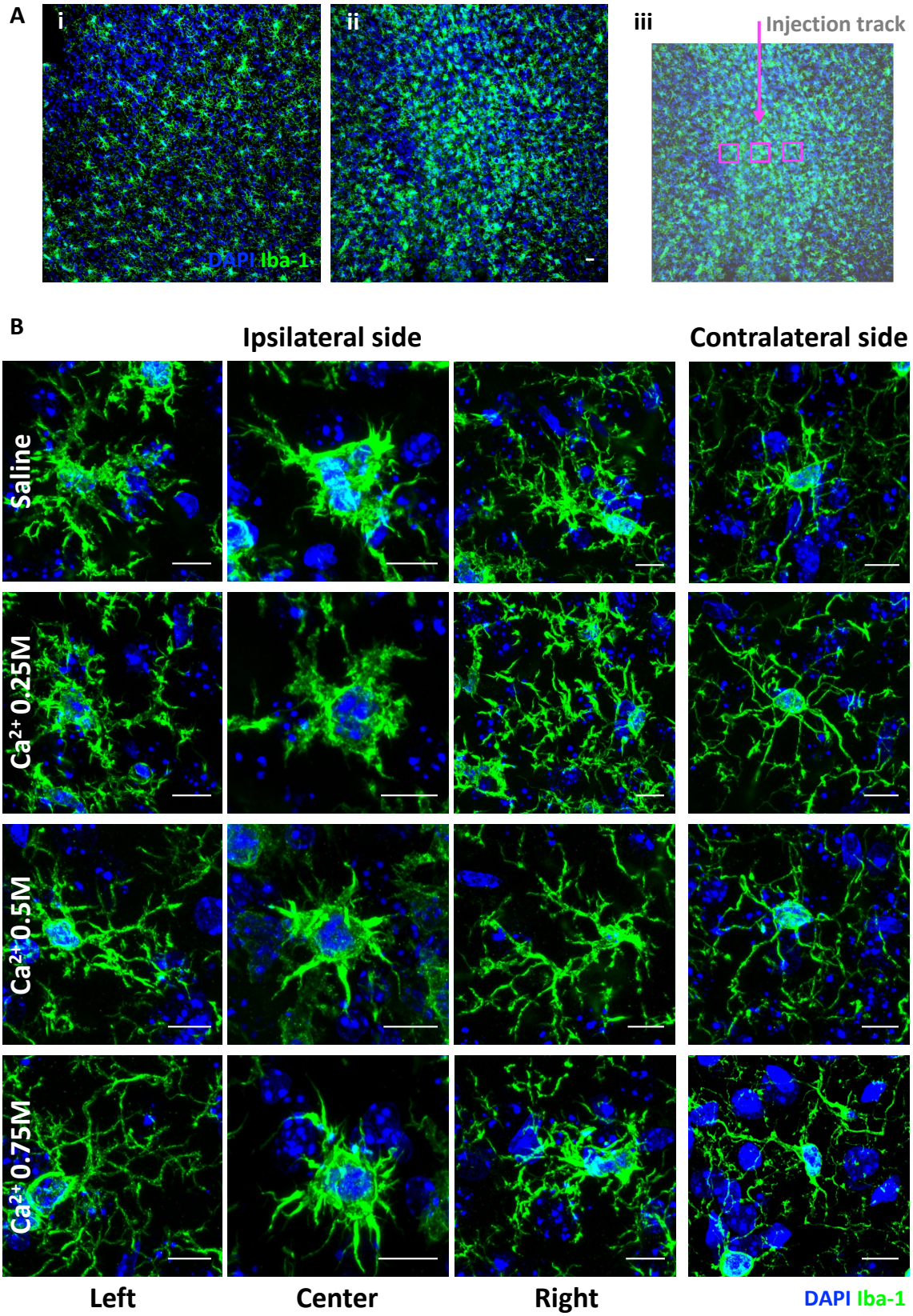


Figure 28. Microglial cells are susceptible to extracellular calcium administration *in vivo*. A. Confocal images showing the differences on the reactivity response provoked by the saline injection **(i)** and a Ca^{2+} solution **(ii)**. Iba-1^{+} microglial cells in green and DAPI counterstaining in blue (Scale bar: 20 µm). **(iii)** Diagram with a rectangle and arrow with magenta broken lines to show the location where the pictures of microglial cells in panel B were taken with respect

to the injection. **B.** Individual microglial cells (green) of each side of the injection and cells located in the site of the injection of the ipsilateral side in the different conditions analyzed. Column of pictures on the right, show individual microglia of the contralateral side to compare (Scale bar: 10 µm).

First, we analyzed the effect of the injection performed with saline and compared with the injections with Ca^{2+} at different concentrations (Figure 28A). We could observe slight differences in the expression of Iba-1 when injecting Ca^{2+} (Figure 28A). Unfortunately, the highest Ca^{2+} concentration (Ca^{2+} 1M) provoked a massive loss of tissue, resulting in a large necrotic area in the site of the injection (results not shown), we considered this concentration as extremely toxic and not viable for later analyses.

After calcium injection, microglial cells appear to show certain reactivity with an activated-like morphology, thicker branches, shorter processes, but also with bigger cell bodies when comparing with a resting state on the contralateral site. In detail, we observed not only differences in morphological characteristics but also some important changes in terms of polarization. Interestingly, the shape of microglial cells varied depending on the location with respect to the injection. Microglial cells near the site of the injection were rounded and with short processes, while microglial cells located in the surroundings of the injection frequently appear to show polarization of their branches towards the injection (Figure 28B).

Considering the apparent polarization of microglia and the absence of damage in the tissue, we considered 0.5M Ca^{2+} as the best option for future experiments. In this concentration, the phenomenon of orienting branches towards the injection site was founded in most of the pictures, while in 0.25M Ca^{2+} was less frequent (Figure 28B). In contrast, although 0.75M Ca^{2+} presented a good proportion of polarized microglia (Figure 28B), the damage created in the injection site was more than the preferable.

Because 0.5M was the optimal concentration, we continued with another set of experiments to know if the extracellular calcium administration may be the responsible factor for inducing changes in morphometric parameters of microglial cells.

Given that any intracranial injection generates some level of neuroinflammation, we planned to use several controls to rule out the morphometric changes caused by this response. Besides the use of saline as a control, we also used a combination of Ca^{2+} 0.5M and EDTA, a calcium chelating component. With this combination, we could determine the level of microglial polarization due to Ca^{2+} when comparing with the injection with 0.5M Ca^{2+} alone. Then, we also added a new

experimental condition to determine the effect of EDTA. We used a 0.25M concentration for EDTA injections.

In summary, to measure the Ca^{2+}-induced morphometric changes on microglial cells we set up four different experimental conditions, 0.5M Ca^{2+} injected alone, 0.5M Ca^{2+} + 0.25M EDTA, 0.25M EDTA injected alone, and saline. Five animals per condition were injected directly to the striatum, according to the stereotaxic coordinates mentioned above. After 3 days post-injection, animals were euthanized, and the brains were extracted and fixed for sectioning and analysis.

Serial sections were used to examine in detail the microglial cell changes in the experimental conditions. To label microglial cells, an immunohistofluorescence against Iba-1 was performed. Then, high resolution confocal pictures were taken for every condition covering enough distance from the injection site to non-affected tissue (see more details in the methods).

Considering the different morphometric characteristics of microglial cells depending on the level of activation (i.e., number and size of ramifications), we designed a detailed analysis. The quantification was planned to determine differences in morphometric parameters including the total number of branches per single cell, the total number of branching points per cell, and the arborization length (summatory of all the branches length).

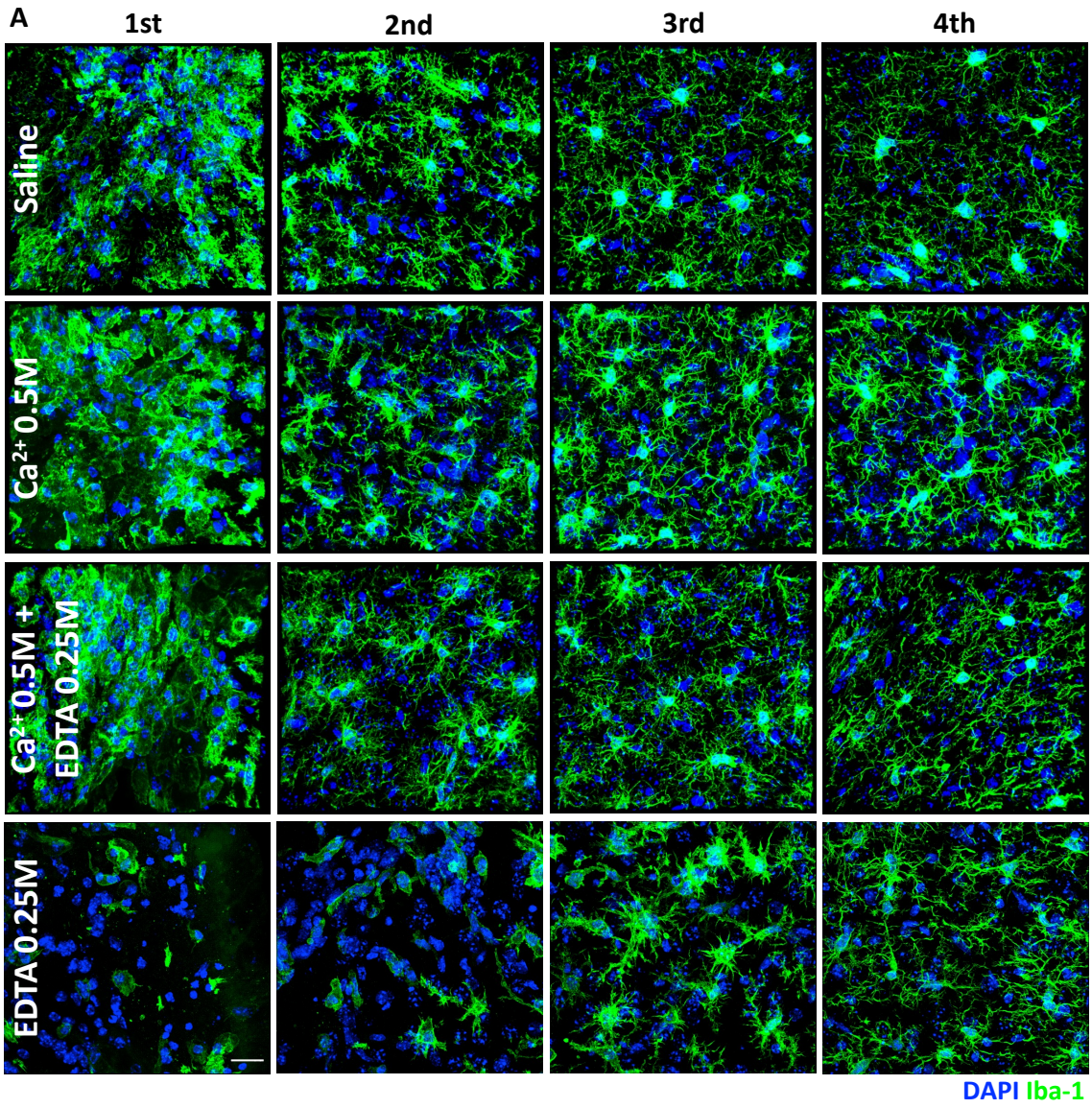

A
1st
2nd
3rd
4th
Saline
Ca2+ 0.5M
Ca2+ 0.5M + EDTA 0.25M
EDTA 0.25M
DAPI Iba-1
B
i
Nº of microglial cells
Total number
ii
Cell length (sum)
Cell length (µm)
v
0 µm
1280 µm
iii
Number branches/cell
Total number
Quadrant of injection
iv
Number branching points/cell
Total number
Quadrant of injection
Saline
Ca2+ 0.5M
Ca2+ 0.5M + EDTA 0.25M
EDTA 0.25M

Figure 28. Calcium injected intrastriatally promotes minor changes in morphometric parameters, equivalent to saline injection. A. Confocal pictures of every condition analyzed showing representative microglial cells (green). Note the differences in shape in every picture with respect to the location of the injection. The numbers indicate how closer to the injection site the picture was taken [1st quadrant (closer to the injection site) to 4th quadrant (farther to the injection site)]. **B.** Graphs showing the differences in terms of number of microglial cells **(i)**, total cell length **(ii)**, number of branches/cell **(iii)** and degree of arborization **(iv)** for every quadrant of the analysis. **(v)** Diagram to illustrate naming of the quadrants and distance from the injection (* p<0.05; ** p<0.005, *** p<0.0005, **** p<0.0001).

The injection of calcium alone induced slight changes on microglial cells, that were equivalent to the injections of saline and the combination of Ca^{2+}/EDTA. Our pictures showed different microglial cell shape depending on their location with respect to the injection site (Figure 28A). Near the injection track (Figure 28A, 1st quadrant) Iba-1^{+} cells appeared rounded, with no protrusions. Besides, in this specific region, we observed a high density of cells, which is probably due to a combination of resident microglial cells but also a good number of macrophages coming from the blood stream.

However, in the other positions, further away from the injection track (Figure 28A, 2nd, 3rd and 4th quadrant) the density of cells appears to be standard and could be considered as resident microglial cells.

Interestingly, after injecting the combination Ca^{2+}+EDTA, microglia also behave similar to saline. Comparing the graphs and statistics, we observed similar cellular density, numbers of branches, branching points, as well as arborization length than the animals injected with saline (Figure 28B). As the three experimental conditions Ca^{2+}, Ca^{2+}+EDTA and saline showed equivalent parameters, suggests that the administration of 0.5M Ca^{2+} does not induce a major inflammatory response.

Most surprisingly, the animals injected with EDTA alone presented an abnormal population of microglial cells, not only different in numbers but also in some of the parameters analyzed. In the 1st quadrant, we observed a very low number of Iba-1^{+} cells compared with the rest of the groups (Figure 28A). We also observed that they show rounded shape, with a very low number of branches, branching points and arborization length in some quadrants (2nd and 3rd) when compared with the rest of the experimental conditions (Figure 28B).

With these results, since reactive microglial cells show rounded shape and reduced number of branches, we wanted to test whether EDTA was able to produce activation of microglia.

For that, because EDTA chelates the calcium present in the brain parenchyma, we hypothesized that the absence of available calcium may hamper the migration and motility of microglial cells. The morphometry observed in this condition could be potentially due to the activation of microglia but, most probably, may be due to the depletion of calcium.

Trying to clarify whether the shape of microglia after EDTA injection corresponded to a neuroinflammatory response or not and checking if calcium promotes more activation – by using a series of sections of the same experiment – we performed an immunohistofluorescence for F4/80 – a commonly used marker to label activated microglia/macrophages – in combination with Iba-1 to verify the location of microglia. With this combination of labeling, we were able to observe the complete morphology of microglial cells – with Iba-1 – and their level of activation by the expression of F4/80.

Confocal pictures were taken starting from the injection site and going further away continuously to generate a mosaic of the complete extension of the injections in all the analyzed conditions. The intensity of F4/80 relative fluorescence was measured and represented as a plot profile of the complete mosaic.

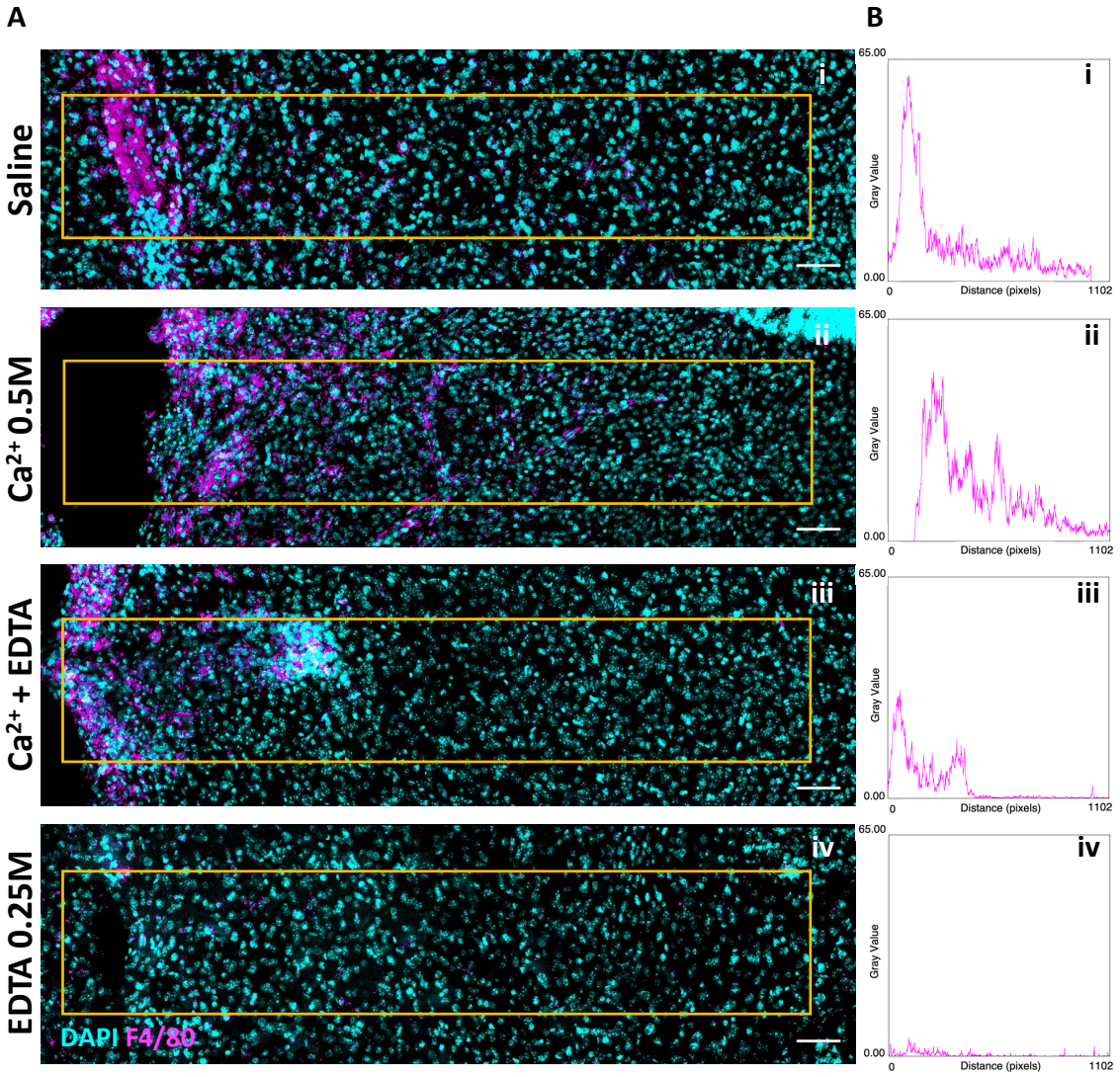


Figure 29. Activated-like morphology provoked by EDTA doesn't mean activation of microglial cells. A. Mosaic reconstruction of representative images of the experimental conditions (i-iv) for Ca^{2+} administration experiment, showing F4/80 marker (magenta) and DAPI (cyan) to observe microglial activation. (Scale bar: 60 µm). The orange box delimits the region of interest (ROI) analyzed. **B.** Relative fluoresce plot profile obtained from the ROI (orange rectangle in pictures for every condition) (i-iv) to visualize the difference of F4/80 expression in the striatum of injected animals. Graphs show distance (x axis) and grey intensity (y axis).

The confocal images show similar expression of F4/80 for the animals injected with saline (Figure 29 i) and Ca^{2+} 0.5M (Figure 29 ii), which is consistent with absence of changes in the morphological analysis. Calcium injected intrastriatally induces a similar response that saline, with some activation of microglial cells close to the injection site and becoming less apparent farther away.

In the case of the injection with EDTA (Figure 29A iv), microglial cells expressed very low levels of F4/80 (Figure 29A and B iv), indicating that is not inducing an activated state. Therefore, this

activated-like appearance, in which microglial cells are rounded and less ramified, is probably due to the lack of calcium. Thus, we could conclude that the presence of calcium may be critical for microglia to both shift to an activating state but also maintain the characteristic homeostatic shape (Figure 29).

Once demonstrated that Ca^{2+} administration *in vivo* does not induce relevant changes in the morphometric parameters of microglia, and is not generating a significant inflammatory response, we planned to analyze more detailed morphological changes related with the polarization of the cell. As we shown in previous sections *in vitro*, microglial cells are susceptible to changes of extracellular calcium, inducing increasing motility and Euclidean distance, which may be related to the displacement and migration towards the target.

Then the next scientific question was to demonstrate whether extracellular calcium *in vivo* may provoke some degree of polarization in microglia.

To answer this question, we measured the polarization of the cells in terms of number of branches oriented either towards the calcium source or to the opposite side. As we showed that the number of Iba-1 branches of microglial cells did not change between the experimental conditions, this polarization may entail the reorientation and reorganization of microglial processes.

To perform this quantification, we used the *Filament tracer* tool of the IMARIS software. The key for this quantification was to individually isolate microglial cells, captured in high resolution 3D confocal images, and – one by one – divide the cell in two parts and then quantify the total number of branches emerging and oriented to each side. Either branches going towards the injection or branches located to the opposite side. This analysis was performed double blinded, not knowing neither the condition nor the location of the injection.

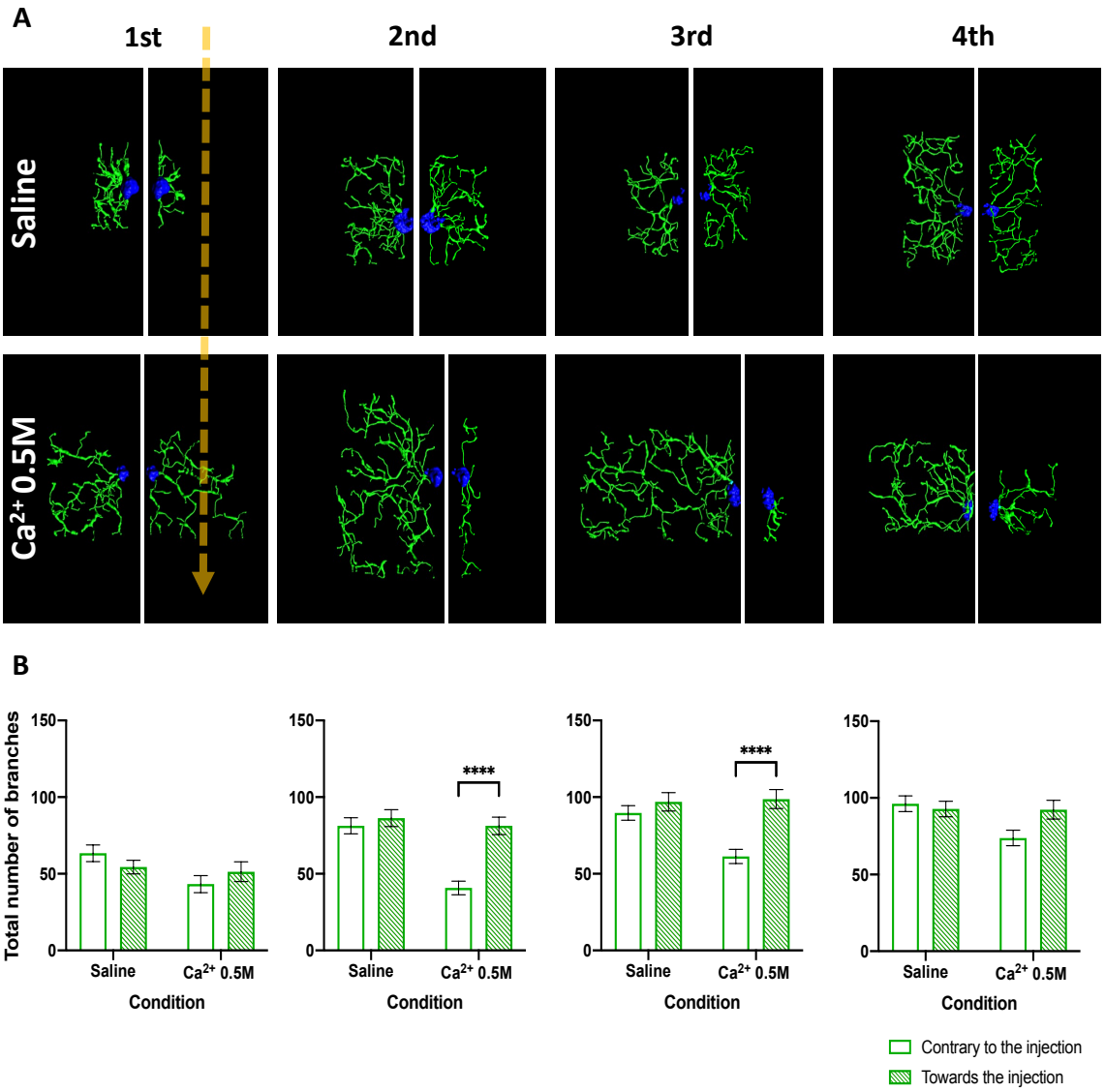


Figure 30. Microglial cells polarize most of their branches towards the extracellular calcium source. A. 3D rendering of isolated microglial cells showing the structure and number of branches in each side (injected side on the left). Images are taken and quantified in the same quadrants as in the previous experiment. Orange broken arrow indicates the track of the injection. **B.** Histograms showing the statistics of the total number of branches per cell in each side of their cell body with respect to the injection site in each of the quadrants analyzed (**** $p<0.0001$).

In the site of the injection, we could not see any sign of polarization in the two conditions analyzed (Figure 30B 1st quadrant). Cells located in this specific region were probably surrounded by the injected solution and with no gradient, showing approximately the same number of branches towards each side (Figure 30A and B 1st quadrant). However, going farther away of the injection site – 2nd and 3rd quadrant – we could see a significant difference between the number of branches polarized towards the calcium injection (Figure 30B), while no changes were seen when the injection was performed with saline (Figure 30B). The 3D reconstructions clearly show the different number of polarized branches towards the injection site that microglia display to

the calcium injection. In contrast, microglia in saline injected animals remains equal (Figure 30A). We expected, however, an increased number of branches polarized towards the Ca^{2+} injection, on the contrary and surprisingly, the difference in the number of polarized branches was due to a decrease in the branches of the opposite side (Figure 30B). That means, that microglial cells do not increase the number of branches, but rather reorganize them. Thus, combined with the fact that the total arborization length of microglia was approximately the same in both conditions (Figure 30B iii), indicates that branches from the opposite side of the injection are retracting while the branches that are polarized towards the injection are being elongated.

These results show that, even though calcium does not induce major morphological changes appears to be crucial to signal the sensitization of microglia and the subsequent polarization, reflected in the extension of their branches to the source. These results are consistent with the results obtained before in cell cultures, where calcium may be considered as a crucial component to potentiate motility and polarization of microglia for later action.

5. Iba-1 as a key molecule present in microglial cells to sense Ca^{2+} signals

As we have shown in the previous experiments, in the scenario of a DA neurodegenerative process, neurons release calcium to the external milieu inducing the motility and polarization of microglia to the source. In this context, these variations of calcium concentrations appear to be sensed by microglial cells, functioning as a "find-me" signal – and in consequence triggering microglial polarization towards the damaging neurons.

In all this process, among other candidates, Iba-1 stands out as a molecule related with cellular motility. It is present exclusively in microglial cells (in the brain), which makes possible the cellular specificity of the response. Iba-1 – also known as AIF1 – is an ionized calcium-binding protein, as explained above, but how Ca^{2+} dynamics affects Iba-1 function remains largely unexplored. The fact that, in the brain parenchyma, Iba-1 is a protein present uniquely in microglia and that they represent the primary defense in an immune response, we hypothesize that Iba-1 should play an important role during this process of sensitization to Ca^{2+} and polarized motility.

To better understand how Iba-1 is behaving in microglial cells after changes of extracellular Ca^{2+} we performed a series of experiments *in vitro* described in the following sections.

5.1. Extracellular calcium inputs induces an increase of Iba-1 expression

To assess if extracellular Ca^{2+} variations could induce Iba-1 related changes in microglial cells, we performed a set of experiments to analyze some particular cellular responses after adding this ion to the culture medium.

As previously performed experiments, BV-2 microglial cells were cultured with normal medium and increasing concentrations of calcium were added extracellularly to study the responses. We used different calcium concentrations to know if Iba-1 increase was produced in a calcium-dependent manner and if it also was concentration-dependent.

For the first experiment, we used the same range of concentrations as used before in preceding experiments, starting from 1.8 mM Ca^{2+} and up to 20 mM Ca^{2+}. To check for differences between the expression of Iba-1, two different experimental procedures were followed, cell culture and western blot (WB). In the first procedure, cells were cultured in 24-well plates for later analysis with immunocytofluorescence. Two different set-ups of experiments were carried out, as experiments with Ca^{2+} administrations manifested differences in non-previously deprived microglia compared with deprivation of calcium in terms of microglial morphology, the same

procedures were followed here. Then, ICF was carried out to observe the Iba-1 expression, and the analysis was performed by measuring the fluorescence intensity.

All the appropriate control conditions were created (DMEM calcium-free plus FBS added in different days, other culture media also used for microglia) and analyzed to check for differences, but as they did not show any changes when compared with the main control (normal DMEM) condition they are not shown in the graphs

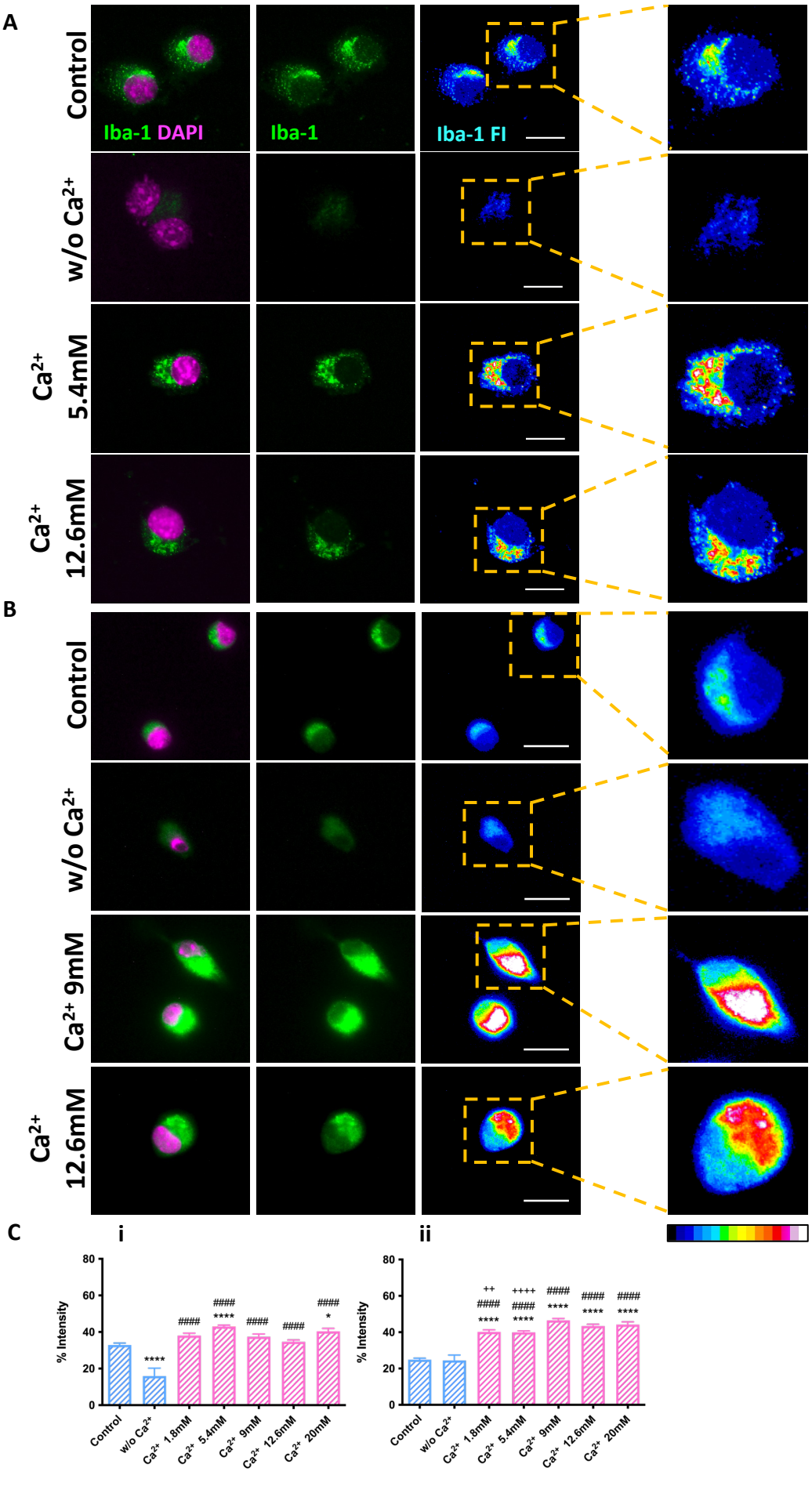

A
Control
w/o Ca2+
Ca2+ 5.4mM
Ca2+ 12.6mM
Iba-1 DAPI
Iba-1
Iba-1 FI
B
Control
w/o Ca2+
Ca2+ 9mM
Ca2+ 12.6mM
C
i
ii
% Intensity
Control
w/o Ca2+
Ca2+ 1.8mM
Ca2+ 5.4mM
Ca2+ 9mM
Ca2+ 12.6mM
Ca2+ 20mM

Figure 331. Extracellular calcium input induces higher Iba-1 expression. A. Fluorescence images for Iba-1 (green) and DAPI (magenta) to compare between four different experimental conditions in non-previously deprived microglia. To see the differences in the Iba-1 expression, the 16 colors FI scale was used (3rd column of the panel) (black, lower intensity and white, higher intensity). Representative microglial cells were magnified (indicated with the orange broken squares) and showed on the right (Scale bar: 20 µm). **B.** Fluorescence images for Iba-1 (green) and DAPI (magenta) to compare between the experimental conditions when the cells were previously deprived from calcium. To visualize the differences in Iba-1 expression, the 16 colors FI scale was also used (3rd column of the panel). Microglial cells were magnified, indicated with the orange broken lines squares and showed on the right (Scale bar: 20 µm). **C.** Graphs showing the quantification of both experiments comparing the differences in Iba-1 intensity after calcium administration. Non-previously deprived microglia **(i)** and previously deprived microglia **(ii)** (* $p<0.05$; ** $p<0.005$, *** $p<0.0005$, **** $p<0.0001$) (* compared with control, # compared with no calcium, + compared with 9mM Ca^{2+}). Control conditions are represented in blue while experimental conditions are represented in magenta.

The analysis revealed that calcium administered extracellularly provoked significant changes of Iba-1 intensity to microglial cells. When cells were treated with calcium administered extracellularly, the changes in the Iba-1 expression were notorious. Our images showed that Iba-1 expression increased when microglial cells were placed in a calcium-enriched environment, especially when surpassing the concentration from the typical of the culture medium (Figure 331A and C i). In non-previously deprived cultures, the highest intensity of Iba-1 was shown after the administration of 5.4 mM Ca^{2+}, in which we could see Iba-1 intensity reaching the maximum (white in the 16 colors scale) (Figure 331A). Surpassing 5.4 mM Ca^{2+} concentration in the media also induces increased expression of Iba-1 in microglial cells but in less proportion than with 5.4 mM Ca^{2+} (Figure 331A and C i).

Microglial cells that were previously deprived from calcium during 24h also presented clear changes in Iba-1 expression. In this case, cells tend to present more Iba-1 expression with the increasing concentrations of Ca^{2+} in contrast with non-previously deprived microglia. Specifically, microglial cells with the highest Iba-1 expression were those treated with 9 mM calcium (Figure 331B and C ii). These cells showed almost the entire cytoplasm displaying the highest Iba-1 intensity according to the 16 colors scale (Figure 331B). Higher calcium concentration administrations were also able to induce drastic increases of the Iba-1 intensity but in all cases of lesser extent than the 9 mM calcium (Figure 331C ii).

These results indicate that when microglial cells are placed in a normo-calcemic environment – with the standard 1.8 mM calcium concentration in the medium – are able to respond increasing Iba-1 expression when surpassing this concentration range. In this scenario, we saw that the increase to 5.4 mM Ca^{2+} induces relevant Iba-1 expression but going beyond, the intensity of Iba-1 reached a plateau, probably due to the achievement of a point of saturation.

However, when microglia are previously deprived from calcium, and then calcium is added to the cells the threshold of tolerance appears to be higher, responding with Iba-1 increase up to 9 mM, exceeding 5.4 mM concentration (Figure 331B and C ii). A plausible explanation is that the expression of Iba-1 may depend on the internalization of calcium, then, microglial cells may be able to accept more calcium when they are previously deprived, generating more de novo Iba-1 (Figure 331C ii).

Interestingly, in both experiments, when microglial cells were deprived from calcium, they presented lower Iba-1 intensity compared with the control (Figure 331C), which reinforced the concept that Iba-1 expression is Ca^{2+} dependent.

These results point to calcium as an important ion to trigger critical changes on microglial cells, but most importantly, changes in the expression of Iba-1, a Ca^{2+}-dependent molecule, that may be essentially involved in cellular motility. In addition, the fact that microglial cells are the only cell type in the brain expressing this molecule, emphasize the concept of cell-specificity for this response to calcium. Overall, since extracellular calcium is able to modify Iba-1 expression in microglia, suggests that there is a linear communication process in which the extracellular calcium – released by DA degenerating neurons – is sensed by microglial cells, modifying Iba-1 expression and triggering a later response.

Because the microscopy analysis of Iba-1 fluorescence intensity is not standardized to ensure the increase of Iba-1 production, we performed a backup analysis by using western blot. We performed another experiment administering extracellular calcium inputs to see the effects on microglia and quantifying the protein amount.

To assess this, BV-2 microglial cells were cultured in 6-well plates to facilitate the later scraping. Once obtained the lysates from each condition, samples were examined by western blotting to quantify the amount of Iba-1 protein. The quantification was performed by measuring the intensity of every single band and graphed comparing each condition with their control blot (β-actin).

We observed a clear Iba-1 increase in the experimental conditions in which different calcium concentration were added, compared with the calcium-free culture (Supplementary figure 3A). Similar proportions were obtained in all the Ca^{2+} concentrations, indicating that Iba-1 production is calcium-dependent, matching the results obtained in the previous experiment, with the highest Iba-1 production with 9 mM calcium, and potentially reaching a saturation point (Supplementary figure 3B).

With these results, analyzed by microscopy and backuped by western blot, we can certainly conclude that extracellular calcium – exceeding the normo-calcemic concentration – is able to induce the production of Iba-1 in microglia (Figure 331 and Supplementary figure 3), which may potentially be key for signaling essential functions in the neurodegenerative process.

5.2. After microglial activation Iba-1 is positioned in essential cytoskeletal elements for motility

Once ascertained that Iba-1 is produced by microglia when they sense extracellular calcium, knowing that calcium released by degenerating neurons may serve as a "find-me" signal, and having evaluated that microglial cells *in vivo* – stimulated with extracellular calcium – polarized their branches towards the calcium source, we wanted to explore whether Iba-1 could be involved in the arrangement of the cellular features leading to kinetic morphology, polarization and migration to the target.

To assess this, experiments with BV-2 microglial cells and primary microglia were performed. As the most common process by which microglial cells adapt a kinetic morphology is when they become active, we activated microglial cells by using pro-inflammatory stimuli.

In pro-inflammatory phenotype, microglial cells *in vitro* rapidly change their shape to a kinetic morphology (Figure 117). For this, microglial cells rearrange the cytoskeletal actin fibers to organize the formation of the leading lamella, as well as the trailing uropod, enriching these cellular structures with the expression of high levels of F-actin (Cross & Woodroofe, 1999).

We administered the canonical stimuli for inducing a pro-inflammatory phenotype in microglia – LPS – combined with IFN γ – which, indeed, is typically increased in Parkinsonian patients (Mount et al., 2007a). After 24h under the stimuli, microglial cells were fixed and used to stain the F-actin fibers in combination with Iba-1 immunolabeling to visualize the cellular component of both markers. For the analysis, microglial cells were categorized in kinetic and non-kinetic morphology to analyze the distribution of Iba-1 in relation the actin fibers in specific microanatomical sites.

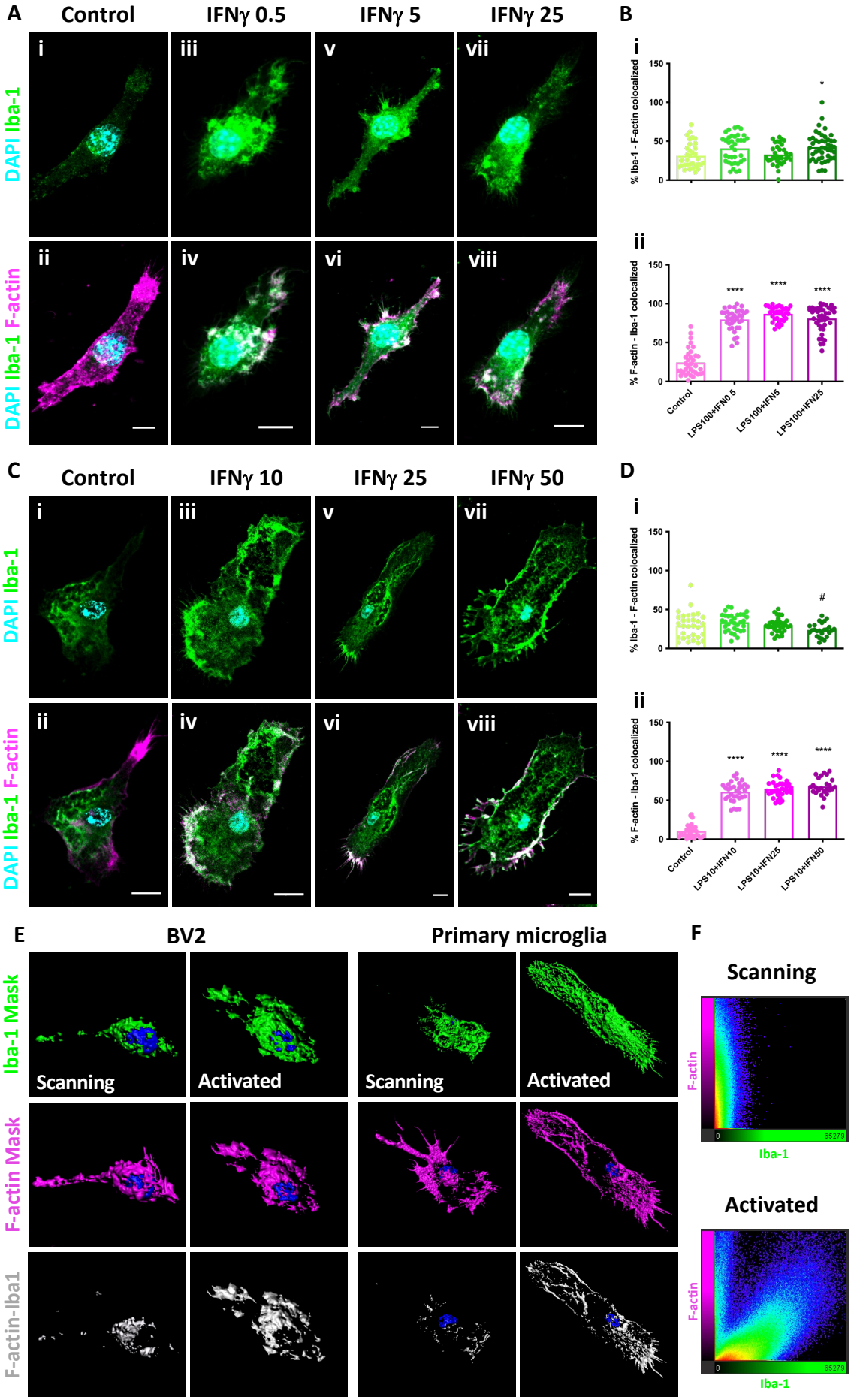

A
Control
IFNγ 0.5
IFNγ 5
IFNγ 25
DAPI Iba-1
DAPI Iba-1 F-actin
i
ii
iii
iv
v
vi
vii
viii
B
% Iba-1 - F-actin colocalized
% F-actin - Iba-1 colocalized
Control
LPS100+IFN0.5
LPS100+IFN5
LPS100+IFN25
C
Control
IFNγ 10
IFNγ 25
IFNγ 50
D
LPS10+IFN10
LPS10+IFN25
LPS10+IFN50
E
BV2
Primary microglia
Iba-1 Mask
F-actin Mask
F-actin-Iba1
Scanning
Activated
F
Scanning
Activated
F-actin
Iba-1

Figure 32. Activation of microglial cells induces higher Iba-1 expression and colonization of the F-actin rich structures. A. Fluorescence images for Iba-1 (green) (i, iii, v and vii), and the combination of Iba-1 with F-actin (magenta) (ii, iv, vi and viii) to compare between non-activated (i-ii) and activated (iii-viii) BV2 microglial cells. Activation was induced with LPS (100ng) and three different concentrations of IFN γ (0.5, 5 and 25ng) (Scale bar: 10 µm). **B.** Graphs showing the quantification of colocalization of both markers. Percentage of total Iba-1 coinciding with F-actin **(i)** and the % of the total F-actin invaded by Iba-1 **(ii)** in all the experimental conditions (* p<0.05; ** p<0.005, *** p<0.0005, **** p<0.0001). **C.** Fluorescence images for Iba-1 (green) (i, iii, v and vii) and the combination of Iba-1 with F-actin (magenta) (ii, iv, vi and viii) to compare between non-activated (i-ii) and activated (iii-viii) primary microglia. Activation was induced with LPS (10ng) and three different concentrations of IFN γ (10, 25 and 50ng) (Scale bar: 10 µm). **D.** Graphs showing the quantification of colocalization for both markers. The % of total Iba-1 coinciding with F-actin **(i)** and the % of the total F-actin colocalizing with Iba-1 **(ii)** in all the treatments (* p<0.05; ** p<0.005, *** p<0.0005, **** p<0.0001) (* compared with control, # compared with LPS10 IFNγ10). **E.** 3D rendering isosurface images (masks) for Iba-1 in green (upper panel) and F-actin in magenta (middle panel), but also the colocalizing points surface (bottom panel) between both markers. Both BV2 cells and primary microglia in the scanning and activated state are shown. **F.** Representative histograms obtained from the colocalization analysis. The distribution of the colocalizing points is shown in both conditions. Along the X and Y axis is represented the fluorescence intensity scale for both markers respectively.

In BV2 microglial cells we found that non-activated cells, in a potentially homeostatic scanning state, presented lower levels of Iba-1 expression (Figure 32A i). In this condition, we saw a scarce number of cells displaying a kinetic shape. Most of them were rounded, as they were not stimulated with the pro-inflammatory treatment. Non-activated cells with kinetic morphology were also showing lower levels of Iba-1 expression (Figure 32A i and ii). This observation indicates that the increase in Iba-1 expression and the arrangement of a kinetic shape are not concomitant (Figure 32A iii-viii).

In primary microglia we frequently found either homeostatic/scanning or activated state (Figure 32C). Cells were treated as BV2 cells but with the appropriate concentrations for reaching activation with a pro-inflammatory stimulus*. Our images show that primary microglia adapt different appearances and morphologies than BV2 cell line, displaying a more complex kinetic shape than BV2 cells. These microglial cells showed similar features to the cell line, being the non-activated scanning cells those presenting low levels of Iba-1 (Figure 32C i) and no strong correlation between the location of the F-actin rich areas and Iba-1 (Figure 32C i and ii).

However, when both types of microglial cells were stimulated to exhibit a pro-inflammatory phenotype, most of them were found with a characteristic kinetic shape (Figure 32A and C iii-viii). The pro-inflammatory stimuli induced dramatic changes in the microglial cells shape – becoming more elongated and capable for a possible later migration. Moreover, these microglial

cells presented higher Iba-1 expression with a strong colocalization with F-actin rich areas. (Figure 32A and C iii-viii).

This colocalization between the Iba-1 expression and the F-actin staining was measured with the IMARIS *Colocalization tool* in both cell types to see the differences between the activation and the control. We observed apparent differences in the colocalization between control and activated cells in both, BV2 and primary microglia. Microglial cells presented a vast colocalization between F-actin and Iba-1 after activation compared with the homeostatic cells (Figure 32B and D ii). We represented two different sets of results. First, the colocalization of F-actin inside the total Iba-1 material was at similar levels in all the conditions (around 30-40% of the total) (Figure 32B and D i), meaning that of the total amount of Iba-1 present in the cell, only the 30-40% was coinciding with F-actin-rich structures. However, the second set of results, the colocalization of Iba-1 inside the F-actin material showed clear differences. While in a scanning non-activated state, the colocalization was only about 10-20% of the total (Figure 32B and D ii), in an activated state, cells colocalized their Iba-1 material with F-actin-rich structures in a 70-90% (Figure 32B and D ii). This colocalization refers to the total amount of F-actin that was being invaded by Iba-1.

This analysis indicates that when microglial cells become activated, in contrast with a homeostatic scanning state, Iba-1 is increased and positioned in essential cytoskeletal elements related with cellular motility. Therefore, the response against a pro-inflammatory stimulus promotes the migration of Iba-1 to the F-actin-rich structures, as the leading lamellas, as we observed in the rendering of both activation states and in both cell types (Figure 32E).

These results indicate that major activating stimuli presented to microglial cells, not only induce the mere increase of Iba-1 but also the rearrangement and distribution to the F-actin cytoskeletal structures, mostly the leading lamellas, suggesting the direct implication of Iba-1 in the movement and polarization of microglial cells.

6. Ca^{2+}-mediated polarization is Iba-1-dependent

Once examined how microglial cells respond when an extracellular high calcium amount is sensed, and examined our previous results in which we saw how microglial cells change the orientation of most of their branches to the calcium source, being polarized, whereas the saline did not promote this polarization. But also combining all these previous results in which the calcium administration promoted increased Iba-1 expression; procedures using an experimental model with deficient Iba-1 expression could be of interest to better understand in which microglial functions Iba-1 is involved.

6.1. Ca^{2+} administration results in migration impairment in Aif-1 knock out mice

Iba-1 is a calcium-binding protein, as widely explained before. We know that microglial cells respond to extracellular calcium, and, as an action or as a consequence, increase the Iba-1 expression. To better understand in which process but also when the Iba-1 takes part in the activation, polarization and migration signaling cascade we used Aif-1 deficient KO mice.

We wondered if microglial cells might have their migration and polarization ability impaired due to the deficiency in Iba-1. First of all, we must test this mice strain for Iba-1 expression to be sure the lack of expression. In this case, some mice of the colony were tested by genotyping procedures for Aif-1 gene expression. Additionally, some animals used in pilot experiments were euthanized, dissected, extracted the brain and posteriorly sectioned for immunolabeling as second evidence of their Iba-1 deficiency. Immunohistofluorescence was performed for the same animals with two different stainings typical for microglia, $P2Y_{12}R$ and Iba-1, being the second, supposedly, absent. Whereas the genotyping was performed against Aif-1 gene in KO and WT mice.

The analysis performed by immunofluorescence clearly revealed that Aif-1 deficient mice do not express Iba-1 (Supplementary figure 4A ii), compared with the typical expression normally found in WT animals (Supplementary figure 4A i), whereas both mice strains revealed similar expression of the $P2Y_{12}R$ (Supplementary FigA iii-iv). Moreover, with genotypic analysis we found similar results, as WT mice express normal amounts of the Aif-1 gene while KO mice are absent (Supplementary figure 4B).

Following experiments were performed with the Aif-$1^{-/-}$ mice. The aim of this experiment was to simulate the same physiological condition already performed with WT animals injecting calcium but also using KO mice and examine calcium-dependent changes on microglia. For that, same

procedure above mentioned was used to administer the calcium intracranially. The same solution of high concentration of calcium (0.5M) already used was injected directly to the striatum to examine the polarization of microglial cells in the cerebral parenchyma. Injections of saline solution were used as control of the inoculated solution. Solutions were administered into the striatum by using a stereotaxic frame as in previous experiments. We used the C57BL/6j mice strain as WT mice and the Aif-$1^{-/-}$ mice as the Iba-1 KO mice. At third day post-injection, we euthanized the animals by intracardial perfusion and obtained the brains to be processed for immunohistofluorescence and analyzed by confocal microscopy. High resolution confocal pictures were taken for every experimental condition as in the calcium-injected WT mice experiment previously performed, covering enough distance from the injection site to non-affected tissue. Brain sections were immunostained with $P2Y_{12}R$ antibody and combined with DAPI as a counterstaining.

The key question was to ascertain in which manner Iba-1 could be involved in the Ca^{2+}-mediated polarization. To assess this question, same type of polarization analysis was performed in these animals. On isolated microglial cells, by dividing the cell in two parts emerging from the cell body, we counted the number of branches towards each side and compare between them, being one side closer to the injected solution while the opposite side don't. This analysis was performed double blinded, not knowing neither the condition nor the location of the injection.

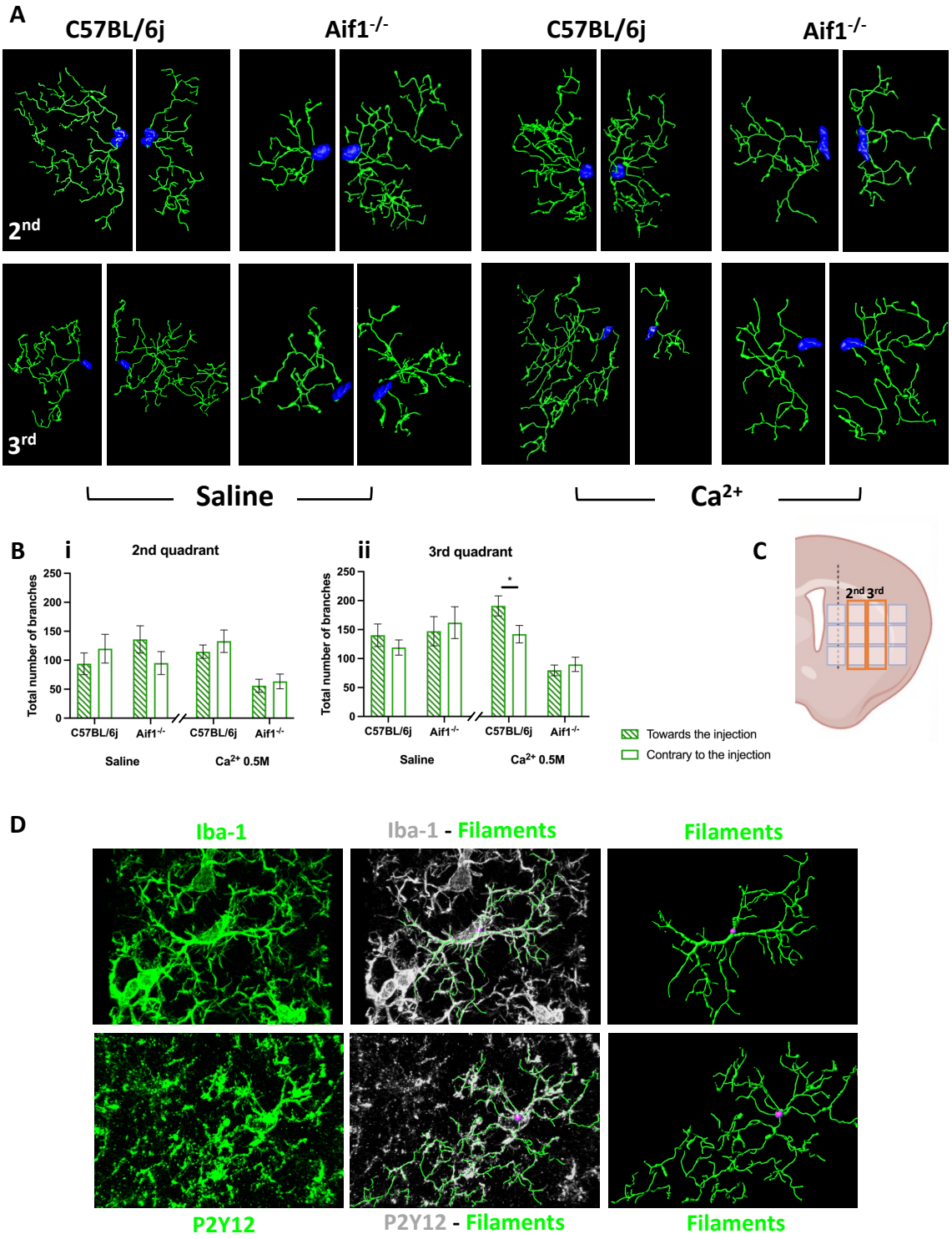


Figure 334. Analysis of the polarization in Aif1$^{-/-}$ mice show an impairment in the polarization capacity compared to C57BL/6j mice. A. Representative images of the microglial cells' filaments rendering served to quantify the number of branches. Microglia is exhibited in two parts by dividing the cell within the nucleus and its corresponding branches oriented to each side for each condition analyzed. **B.** Graphs showing the different number of branches in each side of the cells, being one side the polarized branches to the injection and the others located to the opposite side in the four conditions analyzed and the two quadrants. **C.** Diagram of how the pictures were taken in the animals and which pictures have been taken for quantification marked with orange squares. **D.** Representative images of how different

the immunolabelling of the two different markers (Iba-1 and P2Y12) are staining microglial cells, represented by the raw fluorescence image (1st panel), the fluorescence in grey superposed with the filaments created in green (2nd panel) and only the filaments to better see the branches (3rd panel).

As the last experiment showed significant differences in the 2nd and 3rd quadrant pictures taken, only these two regions were thought appropriate to be quantified, even though pictures were taken in the same four regions as in the last experiment to be aware of the regions were in concordance in both experiments.

Both sexes were used for the surgical procedure and posterior analyses. However, female mice were showing very big differences within the same conditions, but also in the previous experiment only males were used, reason for what females were excluded from the statistical analysis.

As the animals used were Aif-$1^{-/-}$ mice but also WT mice and the solutions injected were saline and Ca^{2+} 0.5M, we expected no signs of polarization between animals injected with saline, regardless of the animal genotype; but differences between KO and WT mice in the Ca^{2+}-injected animals, meaning the Iba-1 being involved during the Ca^{2+}-mediated polarization.

When analyzing the polarization in the 2nd quadrant, no significant differences were found (Figure 334A). The saline-injected animals, both WT and KO mice, presented similar levels in number of branches oriented towards the injection and to the opposite side (Figure 334A and B i), meaning no signs of polarization. When analyzed the calcium-injected animals, KO mice were not different in terms of number of branches polarized and non-polarized towards the injection (Figure 334A and B i), as expected. However, contrary to what we hypothesized and obtained in past experiments, in the WT mice the number of branches oriented towards the injection of calcium and the opposite-oriented branches were no different (Figure 334A and B i).

Interestingly, when analyzed the 3rd quadrant, significative differences were found. In this specific region, while saline injection did not provoke any changes in the total number of branches oriented to the injection compared to the opposite branches' numbers, regardless the type of mice (Figure 334A and B ii); Ca^{2+} injected intrastriatally did it. In these injections, calcium administered into the animals provoked no changes in the number of branches polarized and non-polarized towards the injection in Aif-1 deficient mice (Figure 334A and B ii), but WT mice experienced differences, being higher the number of branches polarized towards the injection than the branches oriented to the opposite side (Figure 334A and B ii).

The 3D reconstructions clearly show the different number of polarized branches towards the injection site that microglia display to the calcium injection in WT mice but not in the KO mice (Figure 334A). In contrast, microglia in saline-injected animals remains equal (Figure 334A) in both cases. Not only for that, 3D reconstructions and fluorescence images are also represented (Figure 34D) to show the different immunolabeling of $P2Y_{12}R$ compared with Iba-1, which considerably differs in how microglial cells processes are stained. This could be a reason to explain the differences obtained in the 2nd quadrant between WT animals stained with $P2Y_{12}R$ and the previous experiment in which the Iba-1 marker was used.

These results show clearly that the polarization of microglia towards the calcium is mediated by Iba-1, as deficient Aif-1 mice present an impairment in their branching polarization capacity. Altogether, knowing the process by which microglia sense specific “find-me” signals coming from the target – DA degenerating neurons in the PD scenario – the results obtained suggest that Iba-1 is crucial for sensing the Ca^{2+}-mediated “find-me” signal. Therefore, we suggest an impairment, in Aif-1 $^{-/-}$ mice, of the polarization and subsequent migration to the target.

GENERAL DISCUSSION

In the present work we aimed to understand some of the key roles of microglial cells during a neuroinflammatory process in PD. Our first analysis in PD human samples attempts to unravel how microglial cells are implicated in the progression of the disease and most importantly how are related with remaining DA neurons. As PD is characterized by the loss of DA neurons of the SNpc (Greco, 1983; GREENFIELD & BOSANQUET, 1953; McGeer & McGeer, 2004; Moore et al., 2005; Spillantini et al., 1997), and glial-mediated neuroinflammation may be involved in the progression of the disease (Hirsch et al., 2012; McGeer et al., 1988; McGeer & McGeer, 2004), we focused on the analysis of microglia in this particular area. To better understand this response, post-mortem PD samples were analyzed in terms of microglial reactivity. First of all, we characterized the dopaminergic neuronal loss in the PD samples, showing a significant decrease of TH^+-dopaminergic neurons (Figure 11). Then, the typical morphological change of reactive microglial cells (Barcia et al., 2012; Nayak et al., 2014; Nimmerjahn et al., 2005), with thick but shorter processes and with a bigger cell body (Perry et al., 2010), was measured in terms of Iba-1 expression (Hirsch & Hunot, 2009). Our results revealed an increased microglial reactivity in the SNpc of PD samples compared with controls (Figure 11), suggesting a persistent and exacerbated response of microglial cells during the neurodegenerative process. Most importantly, we intended to examine the polarization of microglial branches towards the potentially dying or degenerating neurons in the SNpc. However, the complexity of the spatial structure of the SNpc did not allow to measure this parameter. Although Iba-1 and TH staining was of good quality, it was no clear to detect the location of each microglial cell body with respect to the mesh of microglial processes, therefore the orientation of the processes towards DA neurons was not possible to define. Conversely, we found clear interactions of microglial cells with dopaminergic neurons in both conditions, PD and controls, so we decided to quantify the number of interactions instead as an indirect measurement of polarization. The interactions were measured in terms of number per square millimeter but also the total area of interaction, showing significant increases in PD (Figure 12). As a result of their constant scanning of their surroundings (Nimmerjahn et al., 2005), homeostatic stochastic interactions between microglia and neurons were defined. In these stochastic interactions, microglia interact with neurons by contacting with their branches, being the area of interaction limited to the minimum. However, when the interaction is taking place in this pathological condition, the contact created by microglial cells appears to be larger, suggesting that the interaction with DA neurons is somehow

active and specific. As it happens in the MPTP model (Barcia, 2013; Barcia et al., 2012), the first steps of the interaction, microglia would contact the neuron only by the processes, then the polarization to the neuron is promoted with the subsequent interaction cell body-cell body, which potentially end up with phagocytosis. Our results showed, not only a greater number of microglia-neuron interactions in the DA degenerating area but a higher area of interaction in samples from patients suffering PD compared to controls (Figure 12).

These results lead to conclude that in PD, microglial cells increase their contacts with DA neurons, most probably in the process of degeneration, following a "find-me" signal released by degenerating neurons to surrounding microglial cells. These interactions found in PD patients could be due to multiple signals released by dying neurons that may represent a protective role but also result in the subsequent phagocytosis.

Similar to patients, parkinsonian mice also showed microglial reactivity in the SNpc (Figure 14). In this model we were able to study the microglial polarization in terms of number of branches oriented towards the MPTP-damaged neurons located in the SNpc, especially in the ventrolateral part, which is the most affected region in PD (Goldstein et al., 1967; Poirier & Sourkes, 1965). The analysis revealed increased numbers of branches per microglial cell going towards the potentially degenerating neurons in parkinsonian mice compared with controls (Figure 14C). These results suggested that the mice model parallels the response of microglial cells found in an environment of parkinsonian neurodegeneration, indicating that MPTP induces "find-me" and "eat-me" from DA neurons analogous to the human degenerative process. In addition, three days after the MPTP mice showed dopaminergic loss (previously measured in a previous study from our laboratory) concomitant to microglial reactivity.

To better understand how the microglia-neuron contacts are generated in a homeostatic scenario or neuroinflammatory environment, our cocultures of primary neurons and microglia provided some important clues. The results indicate that, depending on the context, neurons and microglia interact differently. In any case, when primary microglia and neurons are mixed together, the effect of microglia to neurons is promoting the neuronal death, even in a supposedly "homeostatic" state, meaning with no further molecules added for stimulating microglial activation. However, this could be due to many factors, since it is an artificial scenario in which neurons and microglia are obtained from rats at early stages of development. Taking naïve conditions as basal, the results showed a clear increase in neuronal death when microglial cells are stimulated with pro-inflammatory molecules such as IFN γ and LPS (Figure 16). It is known that IFNγ is elevated in PD patients' samples, both in brain tissue (Hunot et al., 1999;

Mogi et al., 1996; Mogi, Harada, Riederer, et al., 1994) or CSF and blood plasma (Brodacki et al., 2008; Mogi et al., 1996; Mogi, Harada, Riederer, et al., 1994; Nagatsu et al., 2000), and in chronic parkinsonian non-human primates, and specifically activates microglia in experimental parkinsonism (Barcia et al., 2011). Together with LPS, a potentially harmful antigen present in the gut microbiota that may affect PD patients (Sampson et al., 2016). Interestingly, neurons intoxicated with these same pro-inflammatory stimuli did not show a significant decrease in number, meaning that the combination of LPS+IFNγ is not able, by itself, to provoke neuronal death, in contrast, the activation of microglial cells and then the cascade of reactions after that, end up promoting neuronal death. Cocultures of neurons and microglia were also stimulated with MPP^+, to induce a parkinsonian degeneration, and also with the combination of both, parkinsonian degeneration and pro-inflammatory stimuli to better understand the neuronal degeneration and interactions.

Different numbers of neurons, dopaminergic and non-dopaminergic, were found in the conditions (Figure 22). Taking the neurons cultured alone as basal, in all the conditions combined with microglia, either activated or not, the number of neurons rapidly decreased. When neurons are combined with pro-inflammatory reactive microglia are more susceptible to die, when exposed to the neurotoxin MPP^+ they seem to appear also vulnerable, being the combination of both detrimental for the neuronal survival, especially DA neurons. Moreover, some interactions and phagocytic events were also seen. The different numbers obtained between conditions for each type of neurons but also for the phagocytic events and interactions could be due to the complex variability of the experimental model performed and all the variable events which could be occurring at the same time. For example, neurons intoxicated are supposed to be signalling their death to microglia, which, in consequence will eliminate them; but non-intoxicated neurons combined with reactive pro-inflammatory microglia could being sensing some stimuli that promotes neuronal death and in consequence also die. The number of microglia in every condition is another variable to take into account, since a smaller number of microglial cells could promote less inflammation and in consequence less neuronal death induction. As an *in vitro* model trying to mimic the parkinsonian neuroinflammation in the brain parenchyma, it is very difficult to success with clear conclusions due to the high variability.

On the other hand, we clearly saw more phagocytic events in all the conditions in which microglial cells were activated with pro-inflammatory stimulus. Thus, with LPS and IFNγ, microglia were able to phagocytose increased numbers of surrounding neurons. The increase in phagocytic events was directly related with the decrease in the number of interactions. We

hypothesize a linear progression of the microglial response to activation and concomitant damage, in which first the interactions between neurons and microglia are established, and subsequently the phagocytosis is taking place. The fact that we could not see phagocytic events in other conditions or in smaller numbers, does not mean they are not occurring. A plausible explanation could be the timepoint in which we stopped the co-cultures progression. Importantly, in those experimental conditions in which we induced microglial activation or combine with MPP^+ to induce neuronal death, phagocytic contacts were more frequent, with a peak at 24h of the coculture establishment (Supplementary Figure 1).

Co-culture experiments revealed that the neurodegenerative process *in vitro*, damaged neurons where able to attract microglia with "find-me" or "eat-me" signals, replicating the interactions seen in PD and animal models.

Among the neuronal signals, we hypothesized in this thesis that Ca^{2+} ions may be a crucial and specific signal involved in the microglial sensitization and related with parkinsonian degeneration. Indeed, our results show that DA neurons, obtained from rat MSF and intoxicated with the parkinsonian neurotoxic MPP^+, release calcium to the external environment as a consequence of neuronal death (Figure 19). In fact, calcium release, measured in the external medium, is only significantly higher, compared with the control, when a significant neuronal loss is reached when exposed to MPP^+ 100 µM (Figure 19).

Interestingly, while 24h after MPP^+ we only see a decrease of dopaminergic neuronal loss, after 48h MPP^+ administration of we also observe the loss of potentially non-dopaminergic neurons. As it is known, MPP^+ is a neurotoxin primarily affecting dopaminergic neurons (Castagnoli et al., 1985; Chiba et al., 1984; Langston et al., 1984; Markey et al., 1984), because it is specifically taken up specifically by the DAT (Shen et al., 1985) provoking cell death, that *in vivo* may result in PD like symptoms. However, MPP^+, once converted from the MPTP by the astrocytes (Ransom et al., 1987b), is released to the external milieu, and stays free until internalized by DA neurons through DAT. However, other studies have pointed out that serotoninergic transporters may also uptake MPP^+ (Martí et al., 2017) inducing neuronal loss in non-DA neurons.

Looking at our results, we saw TH-negative neuronal loss ($MAP2^+/TH^-$) at 48h but not at 24h with the administration of 100 µM MPP^+ (Figure 19). We suggest three different hypotheses for these results. First, we think that the long-lasting administration of MPP^+ could also be affecting non-dopaminergic neurons, as previously reported (Henze et al., 2005), in which not only TH^+ neurons would be intoxicated, a reason that could explain why we observed a decrease in the

number of both dopaminergic neurons (TH^+) but also non-dopaminergic ($MAP2^+$) neurons. The second hypothesis is that, although MPP^+ is primarily intoxicating dopaminergic neurons, when the exposure is longer than 24h, as happens in 48h, the dramatic dopaminergic neuronal death may indirectly provoke a stressful situation to the rest of neurons, in which some of them may also end up dying. Finally, the third hypothesis is that dopaminergic neurons, as it has been described in MPTP-treated mice, may lose their capacity to express TH in a long exposure to the neurotoxic insult. Then, the decrease in the number of MAP2 neurons may reflect the degeneration of non-TH expressing dopaminergic neurons.

Considering all the latter results, we conclude that our *in vitro* model, employing the neurotoxic insult MPP^+, recapitulates the parkinsonian dopaminergic neural loss, and, as a consequence, the release of calcium to the external environment can be detected. Importantly, the significant increase of calcium only occurs when the administration of MPP^+ reaches the concentration of 100 µM, concomitant with the DA neuronal loss. In contrast, when the MPP^+ is administered at low doses, it has no effect on the neuronal loss and, consequently, it is not reflected on the increase of Ca^{2+} concentration.

Following the demonstration that Ca^{2+} is released by degenerating neurons and related with the microglial behavior during the process of activation and sensitization, the next part of the thesis was focused on the role of free calcium sensitizing microglia.

We reported here that microglial cells are responders to external calcium inputs. As the calcium is being administered extracellularly to microglial cells, they respond becoming more elongated reflecting higher motility (Figures 25 and 26). In contrast, when no calcium is available in the milieu the movement, or the kinetic shape are hampered. These results suggest that calcium is an important molecule promoting microglial movement. Interestingly, we noticed dramatic changes in microglial cells when they are previously deprived from calcium. We assume that basal calcium concentration should always be available for microglial cells to move their branches and scanning the environment. Notwithstanding, as basal Ca^{2+} is crucial for microglial function, when cells are previously deprived most probably provoked a stressed situation in which, when the external calcium is added, the transformations to a kinetic shape appeared more drastically (Figure 25). In this case, knowing the ability of microglial cells to internalize external amounts of calcium (Figure 21), and because of the lack of calcium they previously had, microglia could sense the external calcium and internalize it, faster or in higher amount, resulting in considerable changes.

As stressed neurons promote calcium release by the formation of calcium waves (D. Sieger et al., 2012) that travel along the cerebral parenchyma stimulating surrounding microglial cells, we performed experiments with microglia in microfluidic plates. Our analyses show microglial cells move more and straighter and most interestingly, coinciding with the calcium wave peaks (Figure 27).

Understanding the process of calcium internalization by microglial cells is not the object of this thesis. However, our work suggests some ideas for further investigation in this research line. For example, what ion channels are involved in the process. Some researchers pointed to ion channels ORAI1 and TRPC1, present in the microglial membrane, that could be implicated in the microglial activation, (A. Chauhan et al., 2018; Quintana et al., 2011).

Whereas in the *in vitro* experiments the differences in movement were quantifiable and clearly seen, in the *in vivo* experiments we were not able to measure the microglial movement due to the technical procedure. Since TPM is a good option to visualize microglial movement *in vivo,* planning new procedures in this experimental set up will serve to better understand microglial cells motility after calcium inputs. Our first approach was to observe microanatomical differences in microglia when calcium was injected into mice striatum. As preceding results with parkinsonian animals led us to determine differences in polarization of microglial branches as a result of calcium release by the neurotoxin, brain sections for calcium injected animals were studied in terms of number of polarized branches. Microglial cells from calcium injected mice showed similar numbers of total branches and arborization but also similar cell length when compared with controls, saline and Ca^{2+}+ EDTA injections (Figure 29). The results showed that calcium is somehow driving the microglial response but inducing small and detailed changes in contrast with a high inflammatory response. However, animals injected with EDTA, a calcium chelator, showed dramatic changes suggesting a general impairment of the microglial motility (Figure 29). As reactive microglia is characterized by shortened processes and rounded cell shape (Perry et al., 2010), the first impression of microglial morphology from EDTA-injected animals pointed microglial activation. However, when double checked with F4/80, a well-known marker for reactive microglia, EDTA-injected animals expressed low levels of activation, similar or even lower than other conditions (Figure 30). Knowing that EDTA is a calcium chelator, among other cations, in animals injected with EDTA, microglial cells appear to be unable to migrate towards the lesion, providing evidence of the importance of Ca^{2+} in this process.

Polarization analysis revealed a higher number of branches oriented towards the calcium inoculation compared with the branches on the opposite side (Figure 31). Phenomenon that was

not seen when saline was injected. Interestingly, the total number of microglial branches was not changing between the saline and calcium injected animals. In contrast, while in the saline approximately the same number of branches were positioned in each side of the cell body, in calcium injected animals the number of branches oriented towards the calcium source were approximately the same, but a considerably lower number of branches were located on the opposite side. This indicates that microglial cells, when are sensing the Ca^{2+} from a specific point, instead of creating more branches they focally extend the processes towards the target while non-oriented branches are retracted.

Summarizing we could state that extracellular calcium in the brain parenchyma induce a fine polarization of microglia towards the source. In a physiological and pathological scenario, this extracellular calcium could be released by dying neurons and, in consequence, microglia responds with a focal polarization of branches and potentially migrating towards the damaged or dying neurons and likely phagocytose them.

We suggest that calcium is a crucial ion participating in the microglial-mediated response in PD. As we have shown that dying neurons in a parkinsonian scenario, as MPP^+, release calcium to the extracellular space, it is sensed by microglial cells responding with motility features. The response appears to be dependent on the internalization of calcium. When internalized, calcium may occupy different cellular compartments, and it is something to be further explored. Importantly, calcium response may be related to regions involving the cytoskeleton reorganization. In this process, calcium could promote actin recruitment to reorganize the cells to a kinetic shape, characterized by a F-actin rich protrusion at the leading edge, and a uropod with abundant F-actin fibers (Figure 25).

Much attention has been paid to proteins present in the microglial membrane, as fractalkine ligand and receptor (CX_3CL1 and CX_3CR1), TREM2, TLRs, FcRs and purinergic receptors. However, the role of cytoplasmic proteins involved in the microglial-mediated inflammatory processes have been scarcely studied. The interest of this research work has been Iba-1, aiming to understand its involvement in Ca^{2+} mediated responses by microglial cells.

Because Iba-1 is a cytoplasmatic protein armed with two EF hands motifs that could bind calcium (Imai et al., 1996; Ito et al., 1998), and its expression in the CNS is restricted to microglial cells, Iba-1 became the principal candidate to be involved in this response.

Importantly, when analyzing microglial cell cultures, Iba-1 expression was increased with the administration of extracellular calcium, meaning a direct correlation between the calcium and

Iba-1. We assume that microglial cells could internalize free calcium that binds to Iba-1 but also inducing the increase of Iba-1 (Figure 32). This increase of Iba-1 appears to be concomitant to the capacity of adapting to a kinetic shape, up to a point of potential saturation where cells become rounded.

In our *in vitro* experiments, microglial cells showed, when activated, not only higher Iba-1 expression but also changes in Iba-1 colocalization with the F-actin cytoskeleton (Figure 33). While microglia show low levels of Iba-1 expression in a naïve state and almost restricted to the cytoplasm, when activated, the expression of Iba-1 increases but also is translocated to the edges where the cytoskeleton fibers are reorganized for motility. Iba-1 increased expression appears to be a step previous to the rearrangement of the cell to later migrate towards the microglial lamellas, becoming a key molecule driving the movement, migration and phagocytosis. Altogether, with these results we can conclude the Iba-1 as a key molecule involved in the process of sensitization of external inputs, especially calcium, and also linked with the rearrangement of the cytoskeleton in order to allow the movement of microglia if necessary. This is consistent with previous findings, where Iba-1 has been closely linked with the cytoskeleton formation, especially with rearrangement of F-actin fibers (Sasaki et al., 2001), involved in the restructuration of the cells. The actin rearrangement has been described as one of the most important processes critically involved in the formation of motility-like structures, like the kinetic morphology, and more important with the formation of the phagocytic cups (Ohsawa et al., 2000).

To understand the function of Iba-1 our first approach was to inhibit its expression with siRNA. For that, several vectors, based on adenoviruses and adeno-associated viruses, with the GFP gene expression were tested in cell lines to determine the optimal vector type (Ad5 and Ad5/40 and AAV1, AAV6, AAV9 and AAVrh10) and concentration for a later suppressing the Iba-1 expression. Both Ad and the AAV1 were able to transfect microglia *in vitro*. Because transfecting microglia with viral vectors is reported as challenging, we only attempted three different vectors (Ad5, Ad5/40 and AAV1) with three different concentrations by intracranial injection into the striatum for a later immunolabelling of the different cell types present in the brain parenchyma. However, even though in cell lines they seemed to promote a good transfection rate of microglial cells, in the mouse tissue none of the vectors where able to infect microglia (Data not shown). Vectors mostly transfected neurons and astrocytes, but no microglial cells were seen to express GFP. Recent studies, due to the technical challenge of transfecting microglia *in vivo*,

have designed and produced a new vector, AAV9, as very efficient adeno-associated virus to infect microglia (R. Lin et al., 2022), which may be a possibility to test in the near future.

Fortunately, we had the chance to use a mouse strain, lacking Iba-1, that was used for subsequent studies. As the key point was to ascertain the function of Iba-1 in Ca^{2+}-mediated motility of microglia the polarization experiment performed with C57BL/6j mice and calcium injection was performed. Since we hypothesize that Iba-1 is a key molecule for microglia to sense calcium from the extracellular space, Iba-1 deficiency may result in an impairment in the microglial capacity to polarize towards the calcium input.

The absence of Iba-1 in these animals force us to use a different marker for microglia, in this case we decided to use the $P2Y_{12}R$, also known as a common marker to stain microglial cells, which added some technical challenges to the quantification. On the one hand, microglial cells examined in the 2nd quadrant from the injection track did not show differences in terms of number of branches oriented towards the calcium or saline injection compared with the opposite side of the cell, either in WT mice or $Aif1^{-/-}$. On the other hand, analyzing the 3rd quadrant, WT mice showed a greater number of microglial branches oriented towards the calcium injection than the branches on the opposite side, but not when the injection was performed with saline. This result is consistent with the results previously performed in this thesis, analyzing the same quantification of polarization but using Iba-1 as an immunolabel. Most importantly, when analyzing $Aif1^{-/-}$ mice, the injection of calcium had no effect on microglial polarization, presenting no differences on the number of branches positioned in each side of the cell.

The use of a different immunolabeling, $P2Y_{12}R$ instead of Iba-1, could be the reason of the differences observed in the 2nd quadrant, but also the slight difference in the number of branches. Research lines have postulated that $P2Y_{12}R$ is a good option to label microglia, because always expresses a core profile gene, independently of the brain region (Morillas et al., 2021), being a very stable marker. However, in pathological conditions, such as neuroinflammation, reactive microglial cells appear to lose the capacity of expressing all the core genes (Morillas et al., 2021). Moreover, $P2Y_{12}R$ has been reported as an indispensable molecule for the continued surveillance of the brain parenchyma (Haynes et al., 2006a), but that may differ when microglia enter in a reactive state. Purinergic receptors density is modified depending on microglial activation state (Illes et al., 2020), when scanning, microglial cells express high levels of $P2Y_{12}R$ in order to sense the slightly changes of “find-me” signal ATP. However, once reactive, microglial expression of $P2Y_{12}R$ is downregulated (Paolicelli et al., 2022), and the expression of $P2Y_{12}R$ in

microglial branches is no longer needed due to their ameboid activated phenotype and morphology (Morillas et al., 2021). For those reasons, we had some technical problems while analyzing the pictures of some tissue samples, specially at the regions near the Ca^{2+} injections where $P2Y_{12}R$ expression was lacking. Besides, the expression of $P2Y_{12}R$ and Iba-1 was different along the branches, being $P2Y_{12}R$ more discontinuous than Iba-1, which added some difficulties for the definition of branches by the specialized software (Figure 34). These facts are to be considered for explaining the differences between both experiments. For us, the most plausible explanation for the lack of $P2Y_{12}R$ expression, especially in the 2^{nd} quadrant, is due to the potential activation of surrounding microglial cells close to the calcium source. Reactive microglial cells with low or absent expression of $P2Y_{12}R$ result in a more difficult quantification than cells immunolabelled with Iba-1. In addition, $P2Y_{12}R$ also appears to better label the tips of the processes, which may be another feature affecting the analysis of the number of branches compared with Iba-1.

Altogether, the results obtained in this thesis indicate that Iba-1 is a key molecule for microglial motility, sensing Ca^{2+} ions as extracellular "find me" signal. Importantly, in the context of PD degeneration, the release of Ca^{2+}, induced by degenerating DA neurons, suggest a cross talk between neurons and microglia that may be critical for the pathological process. In this communication, the internalization of Ca^{2+} by microglia, the concomitant increased expression of Iba-1, together with the reorganization of cellular Iba-1/F-actin distribution suggest a direct involvement in the cellular movement of microglia. *In vitro* studies demonstrated the Ca^{2+}-dependent motility of microglia and its response to extracellular changes. *In vivo* analysis demonstrated the polarization of microglial branches towards the Ca^{2+} source, phenomenon that is abolished in $Aif1^{-/-}$ mice, corroborating the importance of Iba-1 in this response.

The present thesis contributes to the understanding of microglial response in PD. We strongly suggest that Ca^{2+}-dependent motility of microglia, mediated by Iba-1, may be the result of the process of dopaminergic degeneration. The results, open at multiple levels, new aspects that should be further explore and points to Iba-1 and Ca^{2+} as potential targets to modulate the neuroinflammatory response related with the course of the disease.

CONCLUSIONS

The main conclusions of this thesis are:

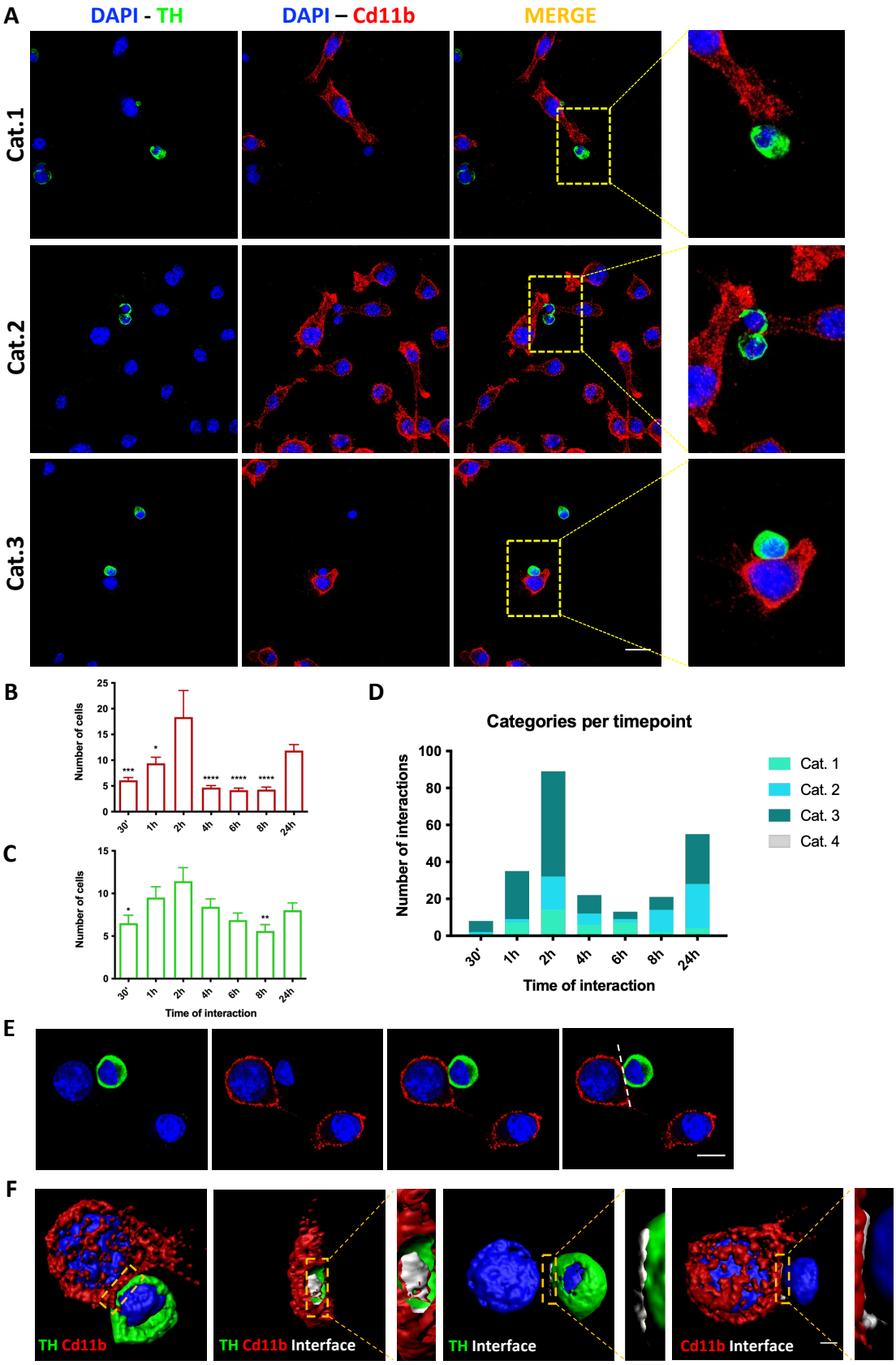
- PD human samples express high reactivity of microglial cells compared with non-PD patients, found with more activated-like morphology.
- Microglial cells in PD patients contact more and strongly with dopaminergic neurons than in healthy patients.
- Microglial reactivity in MPTP-treated mice is expressed in more polarized microglial branches towards the dying neurons than in controls.
- Neurons are not affected by the canonical pro-inflammatory stimulus (LPS and IFN γ) directly but by microglial cells previously activated with the same stimulus. Dopaminergic neurons are more susceptible to die in the same circumstances, suggesting the phagocytic potential microglia has over the neurons.
- The MTOC in microglial cells is primarily found in front of the nucleus regardless the activation state, acting as an effective tool to examine microglial orientation.
- Dopaminergic neurons are vulnerable to die when the neurotoxic insult MPP^+ is administered in high doses during the first 24h. When the exposition to the insult is prolonged (48h) not only dopaminergic neurons are susceptible but other mesencephalic neurons.
- Neuronal death in a parkinsonian scenario is closely linked with higher amounts of calcium found in the media, suggesting the implication of the release of calcium in the progression of the neuronal death as a “find-me” signal.
- Microglial cells are sensitive to differential concentrations of Ca^{2+} present in the medium, internalizing it in consequence.
- Neurons treated with MPP^+ and combined with microglia, either naïve or pro-inflammatory activated, presented a difficult calcium release pattern to understand; however, the pro-inflammatory molecules released by activated microglia are, by itself, harmful enough to provoke neuronal death and the subsequent calcium release.
- Primary mesencephalic cocultures are characterized by some phagocytic events and interactions microglia-neurons, meaning the neuroinflammatory response is occurring and even enhanced when microglial cells are classically activated.

- Extracellular calcium inputs promote microglial kinetic shape. This morphology is enhanced when microglial cells are previously deprived from the stimulus.
- Continuously Ca^{2+} stimulation, either by Ca^{2+} waves or continued renewed medium, increases microglial movement, suggesting the implication of Ca^{2+} in promoting the microglial migration to the source.
- Ca^{2+} injected intrastriatally in mice does not provoke major signs of inflammation but a clear polarized morphology of microglia compared with saline administration.
- Extracellular calcium administration to microglial cells is traduced in more Iba-1 expression than normally.
- Iba-1 expression is specially expressed in high expressed F-actin regions when microglia is classically activated, suggesting the Iba-1 involvement in the cytoskeleton rearrangement for a later migration.
- $Aif1^{-/-}$ mice experienced an impairment in the microglial branches polarization when calcium is administered intrastriatally, reinforcing the idea of the polarization to be Iba-1 dependent.

SCIENTIFIC CONTRIBUTIONS

1. **Roig-Martinez M**, Saavedra-Lopez E, Casanova PV, Cribaro GP, Barcia C. The MTOC/Golgi Complex at the T-Cell Immunological Synapse. Results Probl Cell Differ. 2019;67:223-231. doi: 10.1007/978-3-030-23173-6_9. PMID: 31435797.
2. Saavedra-López E, **Roig-Martínez M**, Cribaro GP, Casanova PV, Gallego JM, Pérez-Vallés A, Barcia C. Phagocytic glioblastoma-associated microglia and macrophages populate invading pseudopalisades. Brain Commun. 2019 Dec 4;2(1):fcz043. doi: 10.1093/braincomms/fcz043. PMID: 32954312; PMCID: PMC7491442.
3. Cribaro GP, Saavedra-López E, Romarate L, Mitxitorena I, Díaz LR, Casanova PV, **Roig-Martínez M**, Gallego JM, Perez-Vallés A, Barcia C. Three-dimensional vascular microenvironment landscape in human glioblastoma. Acta Neuropathol Commun. 2021 Feb 12;9(1):24. doi: 10.1186/s40478-020-01115-0. PMID: 33579378; PMCID: PMC7879533.
4. Heman-Bozadas P, Romero C, Martínez-Remedios P, Freitag I, Frías A, Saavedra-López E, Casanova PV, **Roig-Martínez M**, Cribaro GP, Rovirosa-Hernández MJ, Hernandez-Baltazar D, Barcia C. Lesion-associated microglia and macrophages mediate corralling and react with massive phagocytosis for debris clearance and wound healing after LPS-induced dopaminergic depletion. J Neuroimmunol. 2022 Jun 15;367:577874. doi: 10.1016/j.jneuroim.2022.577874. Epub 2022 Apr 22. PMID: 35490443.
5. Martínez-Escardó L, Alemany M, Sánchez-Osuna M, Sánchez-Chardi A, **Roig-Martínez M**, Suárez-García S, Ruiz-Molina D, Vidal N, Plans G, Majós C, Ribas J, Baltrons MA, Bayascas JR, Barcia C, Bruna J, Yuste VJ. Gossypol Treatment Restores Insufficient Apoptotic Function of DFF40/CAD in Human Glioblastoma Cells. Cancers (Basel). 2021 Nov 8;13(21):5579. doi: 10.3390/cancers13215579. PMID: 34771741; PMCID: PMC8583586.

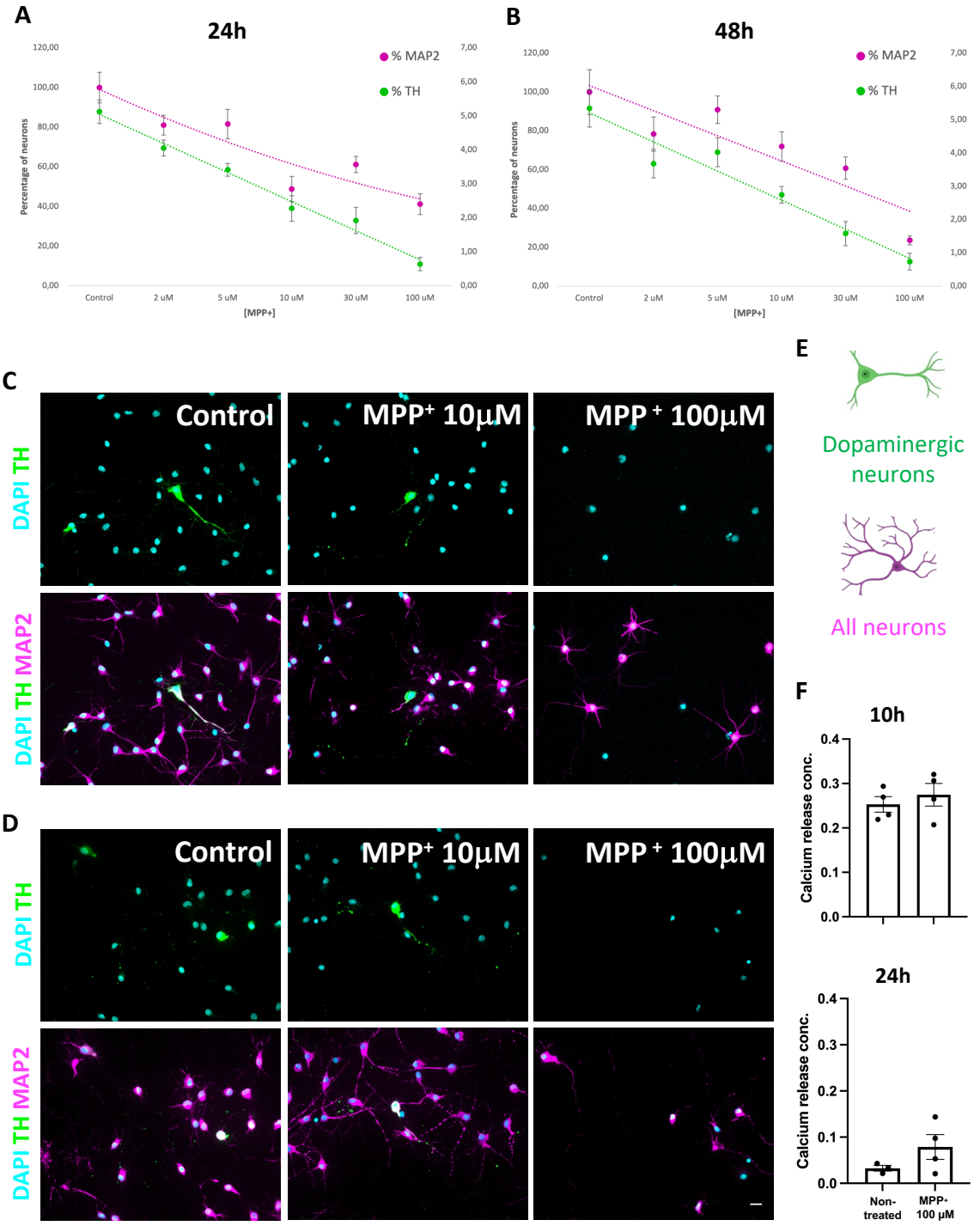
SUPPLEMENTARY MATERIAL



Supplementary Fig 1. Two hours of coculturing microglia and neurons is the best timing to find more interactions.

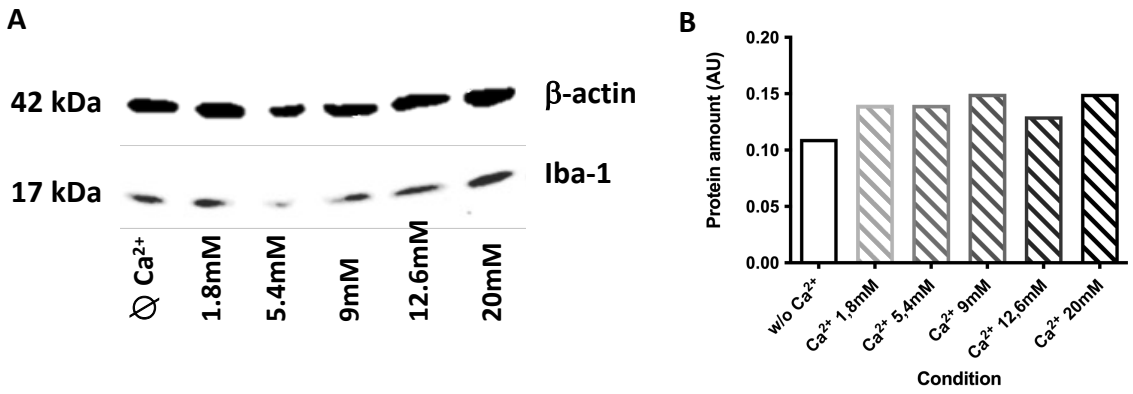
A. Representative images of the different categories proposed with the nuclei in blue, dopaminergic neurons stained

in green (TH) and microglial cells stained in red (Cd11b). (Scale bar: 20 µm). The rectangle with the yellow broken lines represents a zoom in of each category to better see the interactions. **B.** Number of BV2 cells in the co-culture compared between conditions. **C.** Number of PC12 cells compared per condition. (* $p<0.05$; ** $p<0.005$, *** $p<0.0005$, **** $p<0.0001$) **D.** Total number of interactions graphed per categories in the different timepoints. **E.** Confocal representation of a category 3 interaction in which we can observe the flat interface created when contacting the microglial cell (red) with the PC12 (green). (Scale bar: 10 µm). White broken line represents the flat interface created in the interaction. **F.** Rendering representation of a category 3 interaction with a yellow broken lines rectangle illucidating the flat interface created, and subsequently highlighted in white and cropped in each cell for better observation. (Scale bar: 5 µm).

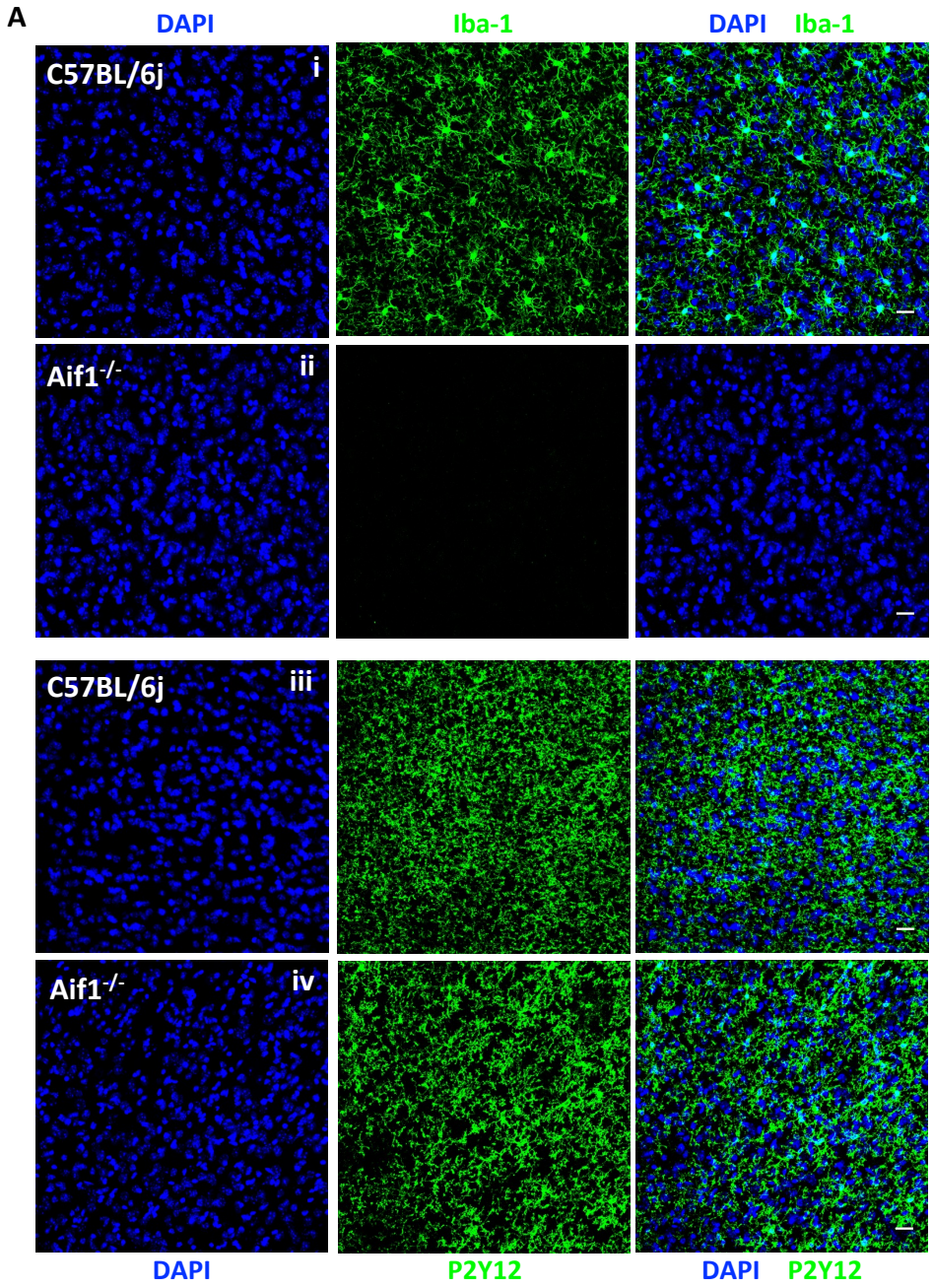


Supplementary Fig 2. Primary mesencephalic cultures recapitulate parkinsonian dopaminergic neurodegeneration after MPP⁺ treatment showing a tendency of calcium release at early timepoint range. A and **B.** Relative percentage respect to control of MAP2 (magenta) and TH (green) positive neurons counted at 24h (A) and 48h (B) in every MPP⁺ concentration administered. **C** and **D.** Representative images of TH positive dopaminergic neurons (green) and MAP2 positive neurons (magenta) in 3 of the 6 conditions performed, comparing the non-treated neurons (Control) with an intermediate condition (10 µM) and the highest MPP⁺ concentration (100 µM) at 24h and 48h respectively. (Scale bar: 20 µm). **E.** Diagrams of the representative shape of dopaminergic neurons (polarized) and other type of neurons (non-polarized) present in the culture. **F.** Graphs showing the differences in the calcium concentration released by

neurons after exposure to the neurotoxic insult MPP^+ at 100 μM, both at 10h and 24h and compared with non-treated neurons.



Supplementary Fig 3. Calcium inputs induces Iba-1 production by microglial cells. A. Western blot analysis for Iba-1 and the control protein (β-actin) comparing the experimental treatment with increasing Ca^{2+} concentration. **B.** Quantification of the western blot analysis for the experimental conditions. Histogram is graphed as changes of protein amount in arbitrary units for in each condition.



Supplementary Fig 4. Aif-1 deficient mice do not express Iba-1 compared with normal expression of WT. A. Representative images comparing WT animals and KO Aif-1 animals in the expression of Iba-1 in green **(i and ii)** and $P2Y_{12}R$ **(iii and iv)** in green and DAPI as a counterstaining in blue **(i-iv)**. (Scale bar: 20 µm).

ANNEX OF MATERIALS USED

Product references used		
Product name	**Company**	**Reference**
T-75 cm^2 culture flasks	Sarstedt	83.3911
RPMI media	ThermoFisher	11875093
DMEM media	ThermoFisher	11995065
DMEM w/o Ca^{2+} media	ThermoFisher	21068028
Calcium chloride	Merck	102382
Collagen I	Cultek	45356236
Trypsin (for cell passages)	Sigma-Aldrich	T4049
0.2 µm filters	Sarstedt	83.1826.001
BSA	Sigma-Aldrich	A7906-100UG
Trypsin (for primary cultures)	Sigma-Aldrich	T9201-500MG
DNase	Sigma-Aldrich	D5025-150KU
Trypsin inhibitor	ThermoFisher	17075-029
T-175 cm^2 culture flasks	BD/Fisher	353112
24 well plates	Sigma-Aldrich	353047
Neurobasal™ media	ThermoFisher	21103049
B27 supplement 50X	ThermoFisher	17504044
GlutaMAX™ 100X	ThermoFisher	35050061
GDNF	Sigma-Aldrich	SRP3239-10UG

PFA		
Griess reactive	Sigma-Aldrich	G4410
$NaNO_2$	Sigma-Aldrich	237213
96 well plates	Sigma-Aldrich	353072
Prolong Gold antifade reagent	Life Technologies	P36930
CellASIC™ gradient plate	EMD Millipore Corporation	M04G-02-5PK
CellASIC™ switching plate	EMD Millipore Corporation	M04S-03-5PK
CellASIC™ ONIX manifold	EMD Millipore Corporation	CAX2-MBC20
CellASIC™ ONIX microfluidic system	EMD Millipore Corporation	CAX2-S0000
CellASIC™ ONIX FG User interface software	EMD Millipore Corporation	CX2-SSW01
MPP^+ iodide	Sigma-Aldrich	D048-100MG
Scrappers	Sarstedt	83.3950
Microcentrifuge tubes	Deltalab	200400P
BCA Pierce™ assay	ThermoFisher	23225
Mini-PROTEAN® Precast gels	Bio-Rad	4561093
Amersham™ ECL™ Rainbow™ Marker	Sigma-Aldrich	GERPN800E
Amersham™Protran™ nitrocellulose membrane	Dd Biolab	10600002
Calcium colorimetric assay	Sigma-Aldrich	MAK022-1KT
35 mm Petri dishes	Sigma-Aldrich	351008
Fura-2, AM	ThermoFisher	F1221
IBIDI µ-slide chemotaxis	Ibidi	80326
Corning® Matrigel® Matrix	Corning	356234

Hamilton 5 µL 75RN syringe	Hamilton Company	87930
Sodium azide	Merck	822335
O.C.T	Fisher Scientific	23730625
Anti-freeze solution		

BIBLIOGRAPHY

Abbracchio, M. P., Burnstock, G., Boeynaems, J. M., Barnard, E. A., Boyer, J. L., Kennedy, C., Knight, G. E., Fumagalli, M., Gachet, C., Jacobson, K. A., & Weisman, G. A. (2006). International Union of Pharmacology LVIII: update on the P2Y G protein-coupled nucleotide receptors: from molecular mechanisms and pathophysiology to therapy. *Pharmacological Reviews*, *58*(3), 281–341. https://doi.org/10.1124/PR.58.3.3

Abbracchio, M. P., & Ceruti, S. (2007). P1 receptors and cytokine secretion. *Purinergic Signalling*, *3*(1–2), 13–25. https://doi.org/10.1007/S11302-006-9033-Z/FIGURES/4

Aderem, A. (2002). How to eat something bigger than your head. *Cell*, *110*(1), 5–8. https://doi.org/10.1016/S0092-8674(02)00819-X

Aktas, O., Smorodchenko, A., Brocke, S., Infante-Duarte, C., Topphoff, U. S., Vogt, J., Prozorovski, T., Meier, S., Osmanova, V., Pohl, E., Bechmann, I., Nitsch, R., & Zipp, F. (2005). Neuronal damage in autoimmune neuroinflammation mediated by the death ligand TRAIL. *Neuron*, *46*(3), 421–432. https://doi.org/10.1016/J.NEURON.2005.03.018

Allen, W. E., Jones, G. E., Pollard, J. W., & Ridley, A. J. (1997). Rho, Rac and Cdc42 regulate actin organization and cell adhesion in macrophages. *Journal of Cell Science*, *110 (Pt 6)*(6), 707–720. https://doi.org/10.1242/JCS.110.6.707

Andén, N. E., Carlsson, A., Dahlström, A., Fuxe, K., Hillarp, N. Å., & Larsson, K. (1964). Demonstration and mapping out of nigro-neostriatal dopamine neurons. *Life Sciences*, *3*(6), 523–530. https://doi.org/10.1016/0024-3205(64)90161-4

Andén, N. -E, Dahlström, A., Fuxe, K., & Larsson, K. (1965). FURTHER EVIDENCE FOR THE PRESENCE OF NIGRO-NEOSTRIATAL DOPAMINE NEURONS IN THE RAT. *The American Journal of Anatomy*, *116*(1), 329–333. https://doi.org/10.1002/AJA.1001160117

Angelova, P. R., Ludtmann, M. H. R., Horrocks, M. H., Negoda, A., Cremades, N., Klenerman, D., Dobson, C. M., Wood, N. W., Pavlov, E. v., Gandhi, S., & Abramov, A. Y. (2016). Ca2+ is a key factor in α-synuclein-induced neurotoxicity. *Journal of Cell Science*, *129*(9), 1792–1801. https://doi.org/10.1242/JCS.180737

Araujo, D. M., & Cotman, C. W. (1992). Basic FGF in astroglial, microglial, and neuronal cultures: characterization of binding sites and modulation of release by lymphokines and trophic factors. *The Journal of Neuroscience : The Official Journal of the Society for Neuroscience*, *12*(5), 1668–1678. https://doi.org/10.1523/JNEUROSCI.12-05-01668.1992

Autieri, M. V., Carbone, C., & Mu, A. (2000). Expression of allograft inflammatory factor-1 is a marker of activated human vascular smooth muscle cells and arterial injury. *Arteriosclerosis, Thrombosis, and Vascular Biology*, *20*(7), 1737–1744. https://doi.org/10.1161/01.ATV.20.7.1737

Autieri, M. V., & Chen, X. (2005). The ability of AIF-1 to activate human vascular smooth muscle cells is lost by mutations in the EF-hand calcium-binding region. *Experimental Cell Research*, *307*(1), 204–211. https://doi.org/10.1016/J.YEXCR.2005.03.002

Balicki, D., & Beutler, E. (1995). Gaucher disease. *Medicine*, *74*(6), 305–323. https://doi.org/10.1097/00005792-199511000-00002

Ballard, P. A., Tetrud, J. W., & Langston, J. W. (1985). Permanent human parkinsonism due to 1-methyl-4-phenyl-1,2,3,6-tetrahydropyridine (MPTP): seven cases. *Neurology*, *35*(7), 949–956. https://doi.org/10.1212/WNL.35.7.949

Barcia, C. (2013). Glial-mediated inflammation underlying parkinsonism. *Scientifica*, *2013*, 1–15. https://doi.org/10.1155/2013/357805

Barcia, C., Barreiro, A. F., Poza, M., & Herrero, M. T. (2003). Parkinson's disease and inflammatory changes. *Neurotoxicity Research*, *5*(6), 411–417. https://doi.org/10.1007/BF03033170

Barcia, C., Jimenez-Dalmaroni, M., Kroeger, K. M., Puntel, M., Rapaport, A. J., Larocque, D., King, G. D., Johnson, S. A., Liu, C., Xiong, W., Candolfi, M., Mondkar, S., Ng, P., Palmer, D., Castro, M. G., & Lowenstein, P. R. (2007). One-year expression from high-capacity adenoviral vectors in the brains of animals with pre-existing anti-adenoviral immunity: Clinical implications. *Molecular Therapy*, *15*(12), 2154–2163. https://doi.org/10.1038/sj.mt.6300305

Barcia, C., Ros, C. M., Annese, V., Gómez, A., Ros-Bernal, F., Aguado-Year, C., Martínez-Paǵn, M. E., De Pablos, V., Fernandez-Villalba, E., & Herrero, M. T. (2011). IFN-γ signaling, with the synergistic contribution of TNF-α, mediates cell specific microglial and astroglial activation

in experimental models of Parkinson's disease. *Cell Death & Disease*, *2*(4). https://doi.org/10.1038/CDDIS.2011.17

Barcia, C., Ros, C. M., Annese, V., Sauvage, M. A. C. De, Ros-Bernal, F., Gómez, A., Yuste, J. E., Campuzano, C. M., De Pablos, V., Fernandez-Villalba, E., & Herrero, M. T. (2012). ROCK/Cdc42-mediated microglial motility and gliapse formation lead to phagocytosis of degenerating dopaminergic neurons in vivo. *Scientific Reports*, *2*. https://doi.org/10.1038/SREP00809

Barcia, C., Ros, F., Carrillo, M. A., Aguado-Llera, D., Ros, C. M., Gómez, A., Nombela, C., De Pablos, V., Fernández-Villalba, E., & Herrero, M. T. (2009). Inflammatory response in Parkinsonism. *Journal of Neural Transmission. Supplementum*, *73*, 245–252. https://doi.org/10.1007/978-3-211-92660-4_19

Barcia, C., Sánchez Bahillo, A., Fernández-Villalba, E., Bautista, V., Poza Y Poza, M., Fernández-Barreiro, A., Hirsch, E. C., & Herrero, M. T. (2004). Evidence of active microglia in substantia nigra pars compacta of parkinsonian monkeys 1 year after MPTP exposure. *GLIA*, *46*(4), 402–409. https://doi.org/10.1002/glia.20015

Batista, F. D., & Harwood, N. E. (2009). The who, how and where of antigen presentation to B cells. *Nature Reviews Immunology 2008 9:1*, *9*(1), 15–27. https://doi.org/10.1038/nri2454

Beal, M. F. (2005). Mitochondria take center stage in aging and neurodegeneration. *Annals of Neurology*, *58*(4), 495–505. https://doi.org/10.1002/ana.20624

Beiter, T., Artelt, M. R., Trautmann, K., & Schluesener, H. J. (2005). Experimental autoimmune neuritis induces differential microglia activation in the rat spinal cord. *Journal of Neuroimmunology*, *160*(1–2), 25–31. https://doi.org/10.1016/J.JNEUROIM.2004.10.027

Beitz, J. M. (2014). Parkinson's disease: a review. *Frontiers in Bioscience (Scholar Edition)*, *6*(1), 65–74. https://doi.org/10.2741/S415

Berg, D., Postuma, R. B., Bloem, B., Chan, P., Dubois, B., Gasser, T., Goetz, C. G., Halliday, G. M., Hardy, J., Lang, A. E., Litvan, I., Marek, K., Obeso, J., Oertel, W., Olanow, C. W., Poewe, W., Stern, M., & Deuschl, G. (2014). Time to redefine PD? Introductory statement of the MDS Task Force on the definition of Parkinson's disease. *Movement Disorders : Official Journal of the Movement Disorder Society*, *29*(4), 454–462. https://doi.org/10.1002/MDS.25844

Bianchin, M. M., Capella, H. M., Chaves, D. L., Steindel, M., Grisard, E. C., Ganev, G. G., Da Silva, J. P., Neto, E. S., Poffo, M. A., Walz, R., Carlotti, C. G., & Sakamoto, A. C. (2004). Nasu-Hakola disease (polycystic lipomembranous osteodysplasia with sclerosing leukoencephalopathy--PLOSL): a dementia associated with bone cystic lesions. From clinical to genetic and molecular aspects. *Cellular and Molecular Neurobiology*, *24*(1), 1–24. https://doi.org/10.1023/B:CEMN.0000012721.08168.EE

Biber, K., Neumann, H., Inoue, K., & Boddeke, H. W. G. M. (2007). Neuronal "On" and "Off" signals control microglia. *Trends in Neurosciences*, *30*(11), 596–602. https://doi.org/10.1016/J.TINS.2007.08.007

Boche, D., Perry, V. H., & Nicoll, J. A. R. (2013). Review: activation patterns of microglia and their identification in the human brain. *Neuropathology and Applied Neurobiology*, *39*(1), 3–18. https://doi.org/10.1111/NAN.12011

Bolmont, T., Haiss, F., Eicke, D., Radde, R., Mathis, C. A., Klunk, W. E., Kohsaka, S., Jucker, M., & Calhoun, M. E. (2008). Dynamics of the microglial/amyloid interaction indicate a role in plaque maintenance. *The Journal of Neuroscience : The Official Journal of the Society for Neuroscience*, *28*(16), 4283–4292. https://doi.org/10.1523/JNEUROSCI.4814-07.2008

Booth, P. L., & Thomas, W. E. (1991). Evidence for motility and pinocytosis in ramified microglia in tissue culture. *Brain Research*, *548*(1–2), 163–171. https://doi.org/10.1016/0006-8993(91)91118-K

Borish, L. C., & Steinke, J. W. (2003). 2. Cytokines and chemokines. *Journal of Allergy and Clinical Immunology*, *111*(2 SUPPL. 2). https://doi.org/10.1067/mai.2003.108

Boss, J. M., & Jensen, P. E. (2003). Transcriptional regulation of the MHC class II antigen presentation pathway. *Current Opinion in Immunology*, *15*(1), 105–111. https://doi.org/10.1016/S0952-7915(02)00015-8

Boué-Grabot, E., & Pankratov, Y. (2017). Modulation of Central Synapses by Astrocyte-Released ATP and Postsynaptic P2X Receptors. *Neural Plasticity*, *2017*, 1–11. https://doi.org/10.1155/2017/9454275

Braak, H., Del Tredici, K., Rüb, U., De Vos, R. A. I., Jansen Steur, E. N. H., & Braak, E. (2003). Staging of brain pathology related to sporadic Parkinson's disease. *Neurobiology of Aging*, *24*(2), 197–211. https://doi.org/10.1016/S0197-4580(02)00065-9

Braak, H., Rüb, U., Gai, W. P., & Del Tredici, K. (2003). Idiopathic Parkinson's disease: possible routes by which vulnerable neuronal types may be subject to neuroinvasion by an unknown pathogen. *Journal of Neural Transmission (Vienna, Austria : 1996)*, *110*(5), 517–536. https://doi.org/10.1007/S00702-002-0808-2

Braud, V. M., Allan, D. S., & McMichael, A. J. (1999). Functions of nonclassical MHC and non-MHC-encoded class I molecules. *Current Opinion in Immunology*, *11*(1), 100–108. https://doi.org/10.1016/S0952-7915(99)80018-1

Brissaud, E. (1899). *Leçons sur les maladies nerveuses Salpêtrière, 1893-94 . Recueillies et publiées par Henry Meige. avec : Leçons sur les maladies nerveuses. Deuxième série Hôpital*. Lectures on Nervous Diseases (Second Series). JAMA: The Journal of the American Medical Association, XXXII(25). https://www.latude.net/loc/en_US/pages/books/11287/edouard-brissaud/lecons-sur-les-maladies-nerveuses-salpetriere-1893-94-recueillies-et-publiees-par-henry-meige

Brochard, V., Combadière, B., Prigent, A., Laouar, Y., Perrin, A., Beray-Berthat, V., Bonduelle, O., Alvarez-Fischer, D., Callebert, J., Launay, J. M., Duyckaerts, C., Flavell, R. A., Hirsch, E. C., & Hunot, S. (2009). Infiltration of CD4+ lymphocytes into the brain contributes to neurodegeneration in a mouse model of Parkinson disease. *The Journal of Clinical Investigation*, *119*(1), 182–192. https://doi.org/10.1172/JCI36470

Brockhaus J, Moller T, & Kettenmann H. (1996). Phagocytozing ameboid microglial cells studied in a mouse corpus callosum slice preparation - PubMed. *Glia*. https://pubmed.ncbi.nlm.nih.gov/8787776/

Brodacki, B., Staszewski, J., Toczyłowska, B., Kozłowska, E., Drela, N., Chalimoniuk, M., & Stepien, A. (2008). Serum interleukin (IL-2, IL-10, IL-6, IL-4), TNFα, and INFγ concentrations are elevated in patients with atypical and idiopathic parkinsonism. *Neuroscience Letters*, *441*(2), 158–162. https://doi.org/10.1016/J.NEULET.2008.06.040

Brown, G. C., & Neher, J. J. (2010). Inflammatory neurodegeneration and mechanisms of microglial killing of neurons. *Molecular Neurobiology*, *41*(2–3), 242–247. https://doi.org/10.1007/S12035-010-8105-9

Brown, G. C., & Neher, J. J. (2014). Microglial phagocytosis of live neurons. *Nature Reviews. Neuroscience*, *15*(4), 209–216. https://doi.org/10.1038/NRN3710

Bsibsi, M., Ravid, R., Gveric, D., & Van Noort, J. M. (2002). Broad Expression of Toll-Like Receptors in the Human Central Nervous System. *Journal of Neuropathology & Experimental Neurology*, *61*(11), 1013–1021. https://doi.org/10.1093/JNEN/61.11.1013

Burnstock, G. (2006). Historical review: ATP as a neurotransmitter. *Trends in Pharmacological Sciences*, *27*(3), 166–176. https://doi.org/10.1016/j.tips.2006.01.005

Burnstock, G. (2007). Physiology and Pathophysiology of Purinergic Neurotransmission. *Physiological Reviews*, *87*(2), 659–797. https://doi.org/10.1152/physrev.00043.2006

Burnstock, G. (2008). Purinergic signalling and disorders of the central nervous system. *Nature Reviews Drug Discovery*, *7*(7), 575–590. https://doi.org/10.1038/nrd2605

Burnstock, G. (2015). Physiopathological roles of P2X receptors in the central nervous system. *Current Medicinal Chemistry*, *22*(7), 819–844. https://doi.org/10.2174/0929867321666140706130415

Burnstock, G. (2016). An introduction to the roles of purinergic signalling in neurodegeneration, neuroprotection and neuroregeneration. *Neuropharmacology*, *104*, 4–17. https://doi.org/10.1016/J.NEUROPHARM.2015.05.031

Burnstock, G. (2017). Purinergic Signalling and Neurological Diseases: An Update. *CNS & Neurological Disorders - Drug Targets*, *16*(3), 257–265. https://doi.org/10.2174/1871527315666160922104848

Butler, C. L., Valenzuela, N. M., Thomas, K. A., & Reed, E. F. (2017). Not All Antibodies Are Created Equal: Factors That Influence Antibody Mediated Rejection. *Journal of Immunology Research*, *2017*. https://doi.org/10.1155/2017/7903471

Cardona, A. E., Pioro, E. P., Sasse, M. E., Kostenko, V., Cardona, S. M., Dijkstra, I. M., Huang, D. R., Kidd, G., Dombrowski, S., Dutta, R., Lee, J. C., Cook, D. N., Jung, S., Lira, S. A., Littman, D. R., & Ransohoff, R. M. (2006). Control of microglial neurotoxicity by the fractalkine receptor. *Nature Neuroscience*, *9*(7), 917–924. https://doi.org/10.1038/NN1715

Cardozo, D. L., & Bean, B. P. (1995). Voltage-dependent calcium channels in rat midbrain dopamine neurons: modulation by dopamine and GABAB receptors. *Journal of Neurophysiology*, *74*(3), 1137–1148. https://doi.org/10.1152/JN.1995.74.3.1137

Carey, B. S., Poulton, K. V., & Poles, A. (2019). Factors affecting HLA expression: A review. *International Journal of Immunogenetics*, *46*(5), 307–320. https://doi.org/10.1111/IJI.12443

Carlsson, A., Lindqvist, M., & Magnusson, T. (1957). 3,4-Dihydroxyphenylalanine and 5-hydroxytryptophan as reserpine antagonists. *Nature*, *180*(4596), 1200. https://doi.org/10.1038/1801200A0

Caron, E., & Hall, A. (1998). Identification of two distinct mechanisms of phagocytosis controlled by different Rho GTPases. *Science (New York, N.Y.)*, *282*(5394), 1717–1721. https://doi.org/10.1126/SCIENCE.282.5394.1717

Casimiro, I., Chinnasamy, P., & Sibinga, N. E. S. (2013). Genetic inactivation of the allograft inflammatory factor-1 locus. *Genesis (New York, N.Y. : 2000)*, *51*(10), 734–740. https://doi.org/10.1002/DVG.22424

Castagnoli, N., Chiba, K., & Trevor, A. J. (1985). V. Potential bioactivation pathways for the neurotoxin 1-methyl-4-phenyl-1,2,3,6-tetrahydropyridine (MPTP). *Life Sciences*, *36*(3), 225–230. https://doi.org/10.1016/0024-3205(85)90063-3

Chauhan, A., Sun, Y., Sukumaran, P., Quenum Zangbede, F. O., Jondle, C. N., Sharma, A., Evans, D. L., Chauhan, P., Szlabick, R. E., Aaland, M. O., Birnbaumer, L., Sharma, J., Singh, B. B., & Mishra, B. B. (2018). M1 Macrophage Polarization Is Dependent on TRPC1-Mediated Calcium Entry. *IScience*, *8*, 85–102. https://doi.org/10.1016/J.ISCI.2018.09.014

Chauhan, P., Hu, S., Sheng, W. S., Prasad, S., & Lokensgard, J. R. (2017). Modulation of Microglial Cell Fcγ Receptor Expression Following Viral Brain Infection. *Scientific Reports*, *7*. https://doi.org/10.1038/SREP41889

Chauhan, P., Sheng, W. S., Hu, S., Prasad, S., & Lokensgard, J. R. (2021). Differential Cytokine-Induced Responses of Polarized Microglia. *Brain Sciences*, *11*(11). https://doi.org/10.3390/BRAINSCI11111482

Chen, G. Y., & Nuñez, G. (2010). Sterile inflammation: sensing and reacting to damage. *Nature Reviews. Immunology*, *10*(12), 826–837. https://doi.org/10.1038/NRI2873

Chen, J., DeVivo, M., Dingus, J., Harry, A., Li, J., Sui, J., Carty, D. J., Blank, J. L., Exton, J. H., Stoffel, R. H., Inglese, J., Lefkowitz, R. J., Logothetis, D. E., Hildebrandt, J. D., & Iyengar, R. (1995).

A region of adenylyl cyclase 2 critical for regulation by G protein beta gamma subunits. *Science (New York, N.Y.)*, *268*(5214), 1166–1169. https://doi.org/10.1126/SCIENCE.7761832

Chen, K., Iribarren, P., Hu, J., Chen, J., Gong, W., Cho, E. H., Lockett, S., Dunlop, N. M., & Ji, M. W. (2006). Activation of Toll-like Receptor 2 on Microglia Promotes Cell Uptake of Alzheimer Disease-associated Amyloid β Peptide. *Journal of Biological Chemistry*, *281*(6), 3651–3659. https://doi.org/10.1074/JBC.M508125200

Chen, L., & Brosnan, C. F. (2006). Exacerbation of Experimental Autoimmune Encephalomyelitis in P2X7R−/− Mice: Evidence for Loss of Apoptotic Activity in Lymphocytes. *The Journal of Immunology*, *176*(5), 3115–3126. https://doi.org/10.4049/JIMMUNOL.176.5.3115

Chiba, K., Trevor, A., & Castagnoli, N. (1984). Metabolism of the neurotoxic tertiary amine, MPTP, by brain monoamine oxidase. *Biochemical and Biophysical Research Communications*, *120*(2), 574–578. https://doi.org/10.1016/0006-291X(84)91293-2

Colonna, M. (2003). TREMs in the immune system and beyond. *Nature Reviews. Immunology*, *3*(6), 445–453. https://doi.org/10.1038/NRI1106

Colton, C. A. (2009). Heterogeneity of microglial activation in the innate immune response in the brain. *Journal of Neuroimmune Pharmacology : The Official Journal of the Society on NeuroImmune Pharmacology*, *4*(4), 399–418. https://doi.org/10.1007/S11481-009-9164-4

Colton, C. A., & Wilcock, D. M. (2010). Assessing activation states in microglia. *CNS & Neurological Disorders Drug Targets*, *9*(2), 174–191. https://doi.org/10.2174/187152710791012053

Compston, A. (2009). Progressive lenticular degeneration: a familial nervous disease associated with cirrhosis of the liver, by S. A. Kinnier Wilson, (From the National Hospital, and the Laboratory of the National Hospital, Queen Square, London) Brain 1912: 34; 295-509. *Brain : A Journal of Neurology*, *132*(Pt 8), 1997–2001. https://doi.org/10.1093/BRAIN/AWP193

Cox, D., Chang, P., Zhang, Q., Reddy, P. G., Bokoch, G. M., & Greenberg, S. (1997). Requirements for both Rac1 and Cdc42 in membrane ruffling and phagocytosis in leukocytes. *The Journal of Experimental Medicine*, *186*(9), 1487–1494. https://doi.org/10.1084/JEM.186.9.1487

Cross, A. K., & Woodroofe, M. N. (1999). Chemokines induce migration and changes in actin polymerization in adult rat brain microglia and a human fetal microglial cell line in vitro. *Journal of Neuroscience Research*, *55*(1), 17–23. https://doi.org/10.1002/(sici)1097-4547(19990101)55:1<17::aid-jnr3>3.0.co;2-j

Cuadros, M. A., Martin, C., Coltey, P., Almendros, A., & Navascués, J. (1993). First appearance, distribution, and origin of macrophages in the early development of the avian central nervous system. *The Journal of Comparative Neurology*, *330*(1), 113–129. https://doi.org/10.1002/CNE.903300110

Dailey, M. E., & Waite, M. (1999). Confocal imaging of microglial cell dynamics in hippocampal slice cultures. *Methods (San Diego, Calif.)*, *18*(2), 222–230. https://doi.org/10.1006/METH.1999.0775

Dauer, W., & Przedborski, S. (2003). Parkinson's disease: Mechanisms and models. *Neuron*, *39*(6), 889–909. https://doi.org/10.1016/S0896-6273(03)00568-3

Davalos, D., Grutzendler, J., Yang, G., Kim, J. V., Zuo, Y., Jung, S., Littman, D. R., Dustin, M. L., & Gan, W. B. (2005). ATP mediates rapid microglial response to local brain injury in vivo. *Nature Neuroscience*, *8*(6), 752–758. https://doi.org/10.1038/NN1472

Davis, G. C., Williams, A. C., Markey, S. P., Ebert, M. H., Caine, E. D., Reichert, C. M., & Kopin, I. J. (1979). Chronic Parkinsonism secondary to intravenous injection of meperidine analogues. *Psychiatry Research*, *1*(3), 249–254. https://doi.org/10.1016/0165-1781(79)90006-4

de Vor, I. C., van der Meulen, P. M., Bekker, V., Verhard, E. M., Breuning, M. H., Harnisch, E., van Tol, M. J. D., Wieringa, J. W., van de Vosse, E., & Bredius, R. G. M. (2016). Deletion of the entire interferon-γ receptor 1 gene causing complete deficiency in three related patients. *Journal of Clinical Immunology*, *36*(3), 195–203. https://doi.org/10.1007/S10875-016-0244-Y/FIGURES/1

Deckert-Schlüter, M., Rang, A., Weiner, D., Huang, S., Wiestler, O. D., Hof, H., & Schlüter, D. (1996). Interferon-gamma receptor-deficiency renders mice highly susceptible to toxoplasmosis by decreased macrophage activation. *Laboratory Investigation; a Journal of Technical Methods and Pathology*, *75*(6), 827–841. https://europepmc.org/article/med/8973478

Deininger, M. H., Meyermann, R., & Schluesener, H. J. (2002). The allograft inflammatory factor-1 family of proteins. *FEBS Letters*, *514*(2–3), 115–121. https://doi.org/10.1016/S0014-5793(02)02430-4

Del Galdo, F., Artlett, C. M., & Jimenez, S. A. (2006). The role of allograft inflammatory factor 1 in systemic sclerosis. *Current Opinion in Rheumatology*, *18*(6), 588–593. https://doi.org/10.1097/01.BOR.0000245724.94887.C4

Di Virgilio, F., Dal Ben, D., Sarti, A. C., Giuliani, A. L., & Falzoni, S. (2017). The P2X7 Receptor in Infection and Inflammation. *Immunity*, *47*(1), 15–31. https://doi.org/10.1016/j.immuni.2017.06.020

Ding, H., Wang, G., Yu, Z., Sun, H., & Wang, L. (2022). Role of interferon-gamma (IFN-γ) and IFN-γ receptor 1/2 (IFNγR1/2) in regulation of immunity, infection, and cancer development: IFN-γ-dependent or independent pathway. *Biomedicine & Pharmacotherapy = Biomedecine & Pharmacotherapie*, *155*. https://doi.org/10.1016/J.BIOPHA.2022.113683

Doran, J. F., Jackson, P., Kynoch, P. A. M., & Thompson, R. J. (1983). Isolation of PGP 9.5, a new human neurone-specific protein detected by high-resolution two-dimensional electrophoresis. *Journal of Neurochemistry*, *40*(6), 1542–1547. https://doi.org/10.1111/J.1471-4159.1983.TB08124.X

Duchen, M. R. (2000). Mitochondria and calcium: from cell signalling to cell death. *The Journal of Physiology*, *529 Pt 1*(Pt 1), 57–68. https://doi.org/10.1111/J.1469-7793.2000.00057.X

Durante, P., Cardenas, C. G., Whittaker, J. A., Kitai, S. T., & Scroggs, R. S. (2004). Low-threshold L-type calcium channels in rat dopamine neurons. *Journal of Neurophysiology*, *91*(3), 1450–1454. https://doi.org/10.1152/JN.01015.2003

Dutta, G., Zhang, P., & Liu, B. (2008). The lipopolysaccharide Parkinson's disease animal model: mechanistic studies and drug discovery. *Fundamental & Clinical Pharmacology*, *22*(5), 453–464. https://doi.org/10.1111/J.1472-8206.2008.00616.X

Dzamko, N., Deak, M., Hentati, F., Reith, A. D., Prescott, A. R., Alessi, D. R., & Nichols, R. J. (2010). Inhibition of LRRK2 kinase activity leads to dephosphorylation of Ser(910)/Ser(935), disruption of 14-3-3 binding and altered cytoplasmic localization. *The Biochemical Journal*, *430*(3), 405–413. https://doi.org/10.1042/BJ20100784

Egaña-Gorroño, L., Chinnasamy, P., Casimiro, I., Almonte, V. M., Parikh, D., Oliveira-Paula, G. H., Jayakumar, S., Law, C., Riascos-Bernal, D. F., & Sibinga, N. E. S. (2019). Allograft inflammatory factor-1 supports macrophage survival and efferocytosis and limits necrosis in atherosclerotic plaques. *Atherosclerosis*, *289*, 184–194. https://doi.org/10.1016/J.ATHEROSCLEROSIS.2019.07.022

Eglitis, M. A., & Mezey, É. (1997). Hematopoietic cells differentiate into both microglia and macroglia in the brains of adult mice. *Proceedings of the National Academy of Sciences of the United States of America*, *94*(8), 4080–4085. https://doi.org/10.1073/PNAS.94.8.4080

Ehringer, H., & Hornykiewicz, O. (1960). [Distribution of noradrenaline and dopamine (3-hydroxytyramine) in the human brain and their behavior in diseases of the extrapyramidal system]. *Klinische Wochenschrift*, *38*(24), 1236–1239. https://doi.org/10.1007/BF01485901

Fahn, S. (2015). The medical treatment of Parkinson disease from James Parkinson to George Cotzias. *Movement Disorders : Official Journal of the Movement Disorder Society*, *30*(1), 4–18. https://doi.org/10.1002/MDS.26102

Fairless, R., Williams, S. K., & Diem, R. (2014). Dysfunction of neuronal calcium signalling in neuroinflammation and neurodegeneration. *Cell and Tissue Research*, *357*(2), 455–462. https://doi.org/10.1007/S00441-013-1758-8

Floyd, R. A. (1999). Antioxidants, oxidative stress, and degenerative neurological disorders. *Proceedings of the Society for Experimental Biology and Medicine. Society for Experimental Biology and Medicine (New York, N.Y.)*, *222*(3), 236–245. https://doi.org/10.1046/J.1525-1373.1999.D01-140.X

Forno, L. S., DeLanney, L. E., Irwin, I., Monte, D. Di, & Langston, J. W. (1992). *Chapter 36: Astrocytes and Parkinson's disease* (pp. 429–436). https://doi.org/10.1016/S0079-6123(08)61770-7

Frade, J. M., & Barde, Y. A. (1998). Microglia-derived nerve growth factor causes cell death in the developing retina. *Neuron*, *20*(1), 35–41. https://doi.org/10.1016/S0896-6273(00)80432-8

Frandsen, A., & Schousboe, A. (1991). Dantrolene prevents glutamate cytotoxicity and Ca2+ release from intracellular stores in cultured cerebral cortical neurons. *Journal of Neurochemistry*, *56*(3), 1075–1078. https://doi.org/10.1111/J.1471-4159.1991.TB02031.X

Fredholm, B. B., IJzerman, A. P., Jacobson, K. A., Linden, J., & Müller, C. E. (2011). International Union of Basic and Clinical Pharmacology. LXXXI. Nomenclature and classification of adenosine receptors--an update. *Pharmacological Reviews*, *63*(1), 1–34. https://doi.org/10.1124/PR.110.003285

Fricker, M., Neher, J. J., Zhao, J. W., Théry, C., Tolkovsky, A. M., & Brown, G. C. (2012). MFG-E8 mediates primary phagocytosis of viable neurons during neuroinflammation. *The Journal of Neuroscience : The Official Journal of the Society for Neuroscience*, *32*(8), 2657–2666. https://doi.org/10.1523/JNEUROSCI.4837-11.2012

Fridman, W. H. (1991). Fc receptors and immunoglobulin binding factors. *FASEB Journal : Official Publication of the Federation of American Societies for Experimental Biology*, *5*(12), 2684–2690. https://doi.org/10.1096/FASEBJ.5.12.1916092

Fuhrmann, M., Bittner, T., Jung, C. K. E., Burgold, S., Page, R. M., Mitteregger, G., Haass, C., Laferla, F. M., Kretzschmar, H., & Herms, J. (2010). Microglial Cx3cr1 knockout prevents neuron loss in a mouse model of Alzheimer's disease. *Nature Neuroscience*, *13*(4), 411–413. https://doi.org/10.1038/NN.2511

Galiano-Landeira, J., Torra, A., Vila, M., & Bové, J. (2020). CD8 T cell nigral infiltration precedes synucleinopathy in early stages of Parkinson's disease. *Brain : A Journal of Neurology*, *143*(12), 3717–3733. https://doi.org/10.1093/BRAIN/AWAA269

Gao, H. M., & Hong, J. S. (2008). Why neurodegenerative diseases are progressive: uncontrolled inflammation drives disease progression. *Trends in Immunology*, *29*(8), 357–365. https://doi.org/10.1016/J.IT.2008.05.002

Gao, H. M., Liu, B., Zhang, W., & Hong, J. S. (2003a). Novel anti-inflammatory therapy for Parkinson's disease. *Trends in Pharmacological Sciences*, *24*(8), 395–401. https://doi.org/10.1016/S0165-6147(03)00176-7

Gao, H. M., Liu, B., Zhang, W., & Hong, J. S. (2003b). Synergistic dopaminergic neurotoxicity of MPTP and inflammogen lipopolysaccharide: relevance to the etiology of Parkinson's

disease. *FASEB Journal : Official Publication of the Federation of American Societies for Experimental Biology*, *17*(13), 1–25. https://doi.org/10.1096/FJ.03-0203FJE

Garcia, J. A., Pino, P. A., Mizutani, M., Cardona, S. M., Charo, I. F., Ransohoff, R. M., Forsthuber, T. G., & Cardona, A. E. (2013). Regulation of adaptive immunity by the fractalkine receptor during autoimmune inflammation. *Journal of Immunology (Baltimore, Md. : 1950)*, *191*(3), 1063–1072. https://doi.org/10.4049/JIMMUNOL.1300040

Gardet, A., Benita, Y., Li, C., Sands, B. E., Ballester, I., Stevens, C., Korzenik, J. R., Rioux, J. D., Daly, M. J., Xavier, R. J., & Podolsky, D. K. (2010). LRRK2 is involved in the IFN-gamma response and host response to pathogens. *Journal of Immunology (Baltimore, Md. : 1950)*, *185*(9), 5577–5585. https://doi.org/10.4049/JIMMUNOL.1000548

Geisler, S., Holmström, K. M., Skujat, D., Fiesel, F. C., Rothfuss, O. C., Kahle, P. J., & Springer, W. (2010). PINK1/Parkin-mediated mitophagy is dependent on VDAC1 and p62/SQSTM1. *Nature Cell Biology*, *12*(2), 119–131. https://doi.org/10.1038/NCB2012

Gelders, G., Baekelandt, V., & Van der Perren, A. (2018). Linking Neuroinflammation and Neurodegeneration in Parkinson's Disease. *Journal of Immunology Research*, *2018*. https://doi.org/10.1155/2018/4784268

GIBBONS, S. J., BRORSON, J. R., BLEAKMAN, D., CHARD, P. S., & MILLER, R. J. (1993). Calcium influx and neurodegeneration. *Annals of the New York Academy of Sciences*, *679*(1), 22–33. https://doi.org/10.1111/J.1749-6632.1993.TB18286.X

Ginhoux, F., Greter, M., Leboeuf, M., Nandi, S., See, P., Gokhan, S., Mehler, M. F., Conway, S. J., Ng, L. G., Stanley, E. R., Samokhvalov, I. M., & Merad, M. (2010). Fate Mapping Analysis Reveals That Adult Microglia Derive from Primitive Macrophages. *Science*, *330*(6005), 841–845. https://doi.org/10.1126/science.1194637

Glezer, I., Simard, A. R., & Rivest, S. (2007). Neuroprotective role of the innate immune system by microglia. *Neuroscience*, *147*(4), 867–883. https://doi.org/10.1016/J.NEUROSCIENCE.2007.02.055

Goldstein, M., Anagnoste, B., Owen, W. S., & Battista, A. F. (1967). The effects of ventromedial tegmental lesions on the disposition of dopamine in the caudate nucleus of the monkey. *Brain Research*, *4*(2), 298–300. https://doi.org/10.1016/0006-8993(67)90013-3

Gomez-Nicola, D., & Perry, V. H. (2015). Microglial dynamics and role in the healthy and diseased brain: a paradigm of functional plasticity. *The Neuroscientist : A Review Journal Bringing Neurobiology, Neurology and Psychiatry*, *21*(2), 169–184. https://doi.org/10.1177/1073858414530512

Gordon, S., & Taylor, P. R. (2005). Monocyte and macrophage heterogeneity. *Nature Reviews. Immunology*, *5*(12), 953–964. https://doi.org/10.1038/NRI1733

Gorman, A. M. (2008). Neuronal cell death in neurodegenerative diseases: recurring themes around protein handling. *Journal of Cellular and Molecular Medicine*, *12*(6a), 2263–2280. https://doi.org/10.1111/j.1582-4934.2008.00402.x

Gorman, A. M., Szegezdi, E., Quigney, D. J., & Samali, A. (2005). Hsp27 inhibits 6-hydroxydopamine-induced cytochrome c release and apoptosis in PC12 cells. *Biochemical and Biophysical Research Communications*, *327*(3), 801–810. https://doi.org/10.1016/J.BBRC.2004.12.066

Greco, G. (1983). Neuromelanin and Parkinson's disease. *Journal of Neural Transmission. Supplementum*, *19*, 913–932. https://doi.org/10.1007/978-1-4614-5836-4_12

GREENFIELD, J. G., & BOSANQUET, F. D. (1953). The brain-stem lesions in Parkinsonism. *Journal of Neurology, Neurosurgery, and Psychiatry*, *16*(4), 213–226. https://doi.org/10.1136/JNNP.16.4.213

Grimm, P. C., McKenna, R., Nickerson, P., Russell, M. E., Gough, J., Gospodarek, E., Liu, B., Jeffery, J., & Rush, D. N. (1999). Clinical rejection is distinguished from subclinical rejection by increased infiltration by a population of activated macrophages. *Journal of the American Society of Nephrology : JASN*, *10*(7), 1582–1589. https://doi.org/10.1681/ASN.V1071582

Guo, Y., Dai, W., Zheng, Y., Qiao, W., Chen, W., Peng, L., Zhou, H., Zhao, T., Liu, H., Zheng, F., & Sun, P. (2022). Mechanism and Regulation of Microglia Polarization in Intracerebral Hemorrhage. *Molecules (Basel, Switzerland)*, *27*(20). https://doi.org/10.3390/MOLECULES27207080

Guzman, S. J., & Gerevich, Z. (2016). P2Y Receptors in Synaptic Transmission and Plasticity: Therapeutic Potential in Cognitive Dysfunction. *Neural Plasticity*, *2016*. https://doi.org/10.1155/2016/1207393

Hackam, D. J., Rotstein, O. D., Schreiber, A., Zhang, W. J., & Grinstein, S. (1997). Rho is required for the initiation of calcium signaling and phagocytosis by Fcgamma receptors in macrophages. *The Journal of Experimental Medicine*, *186*(6), 955–966. https://doi.org/10.1084/JEM.186.6.955

Hakola, H. P. (1972). Neuropsychiatric and genetic aspects of a new hereditary disease characterized by progressive dementia and lipomembranous polycystic osteodysplasia. *Acta Psychiatrica Scandinavica. Supplementum*, *232*, 1–173.

Hakola, H. P. A., & Puranen, M. (1993). Neuropsychiatric and brain CT findings in polycystic lipomembranous osteodysplasia with sclerosing leukoencephalopathy. *Acta Neurologica Scandinavica*, *88*(5), 370–375. https://doi.org/10.1111/J.1600-0404.1993.TB05360.X

Hall, A. (1998). Rho GTPases and the actin cytoskeleton. *Science (New York, N.Y.)*, *279*(5350), 509–514. https://doi.org/10.1126/SCIENCE.279.5350.509

Hammond, C., Bergman, H., & Brown, P. (2007). Pathological synchronization in Parkinson's disease: networks, models and treatments. *Trends in Neurosciences*, *30*(7), 357–364. https://doi.org/10.1016/j.tins.2007.05.004

Hamza, T. H., Zabetian, C. P., Tenesa, A., Laederach, A., Montimurro, J., Yearout, D., Kay, D. M., Doheny, K. F., Paschall, J., Pugh, E., Kusel, V. I., Collura, R., Roberts, J., Griffith, A., Samii, A., Scott, W. K., Nutt, J., Factor, S. A., & Payami, H. (2010). Common genetic variation in the HLA region is associated with late-onset sporadic Parkinson's disease. *Nature Genetics*, *42*(9), 781–785. https://doi.org/10.1038/ng.642

Hanisch, U. K., & Kettenmann, H. (2007). Microglia: active sensor and versatile effector cells in the normal and pathologic brain. *Nature Neuroscience*, *10*(11), 1387–1394. https://doi.org/10.1038/NN1997

Harrison, J. K., Jiang, Y., Chen, S., Xia, Y., Maciejewski, D., Mcnamara, R. K., Streit, W. J., Salafranca, M. N., Adhikari, S., Thompson, D. A., Botti, P., Bacon, K. B., & Feng, L. (1998). Role for neuronally derived fractalkine in mediating interactions between neurons and CX3CR1-expressing microglia. *Proceedings of the National Academy of Sciences of the United States of America*, *95*(18), 10896–10901. https://doi.org/10.1073/PNAS.95.18.10896

Hashioka, S., Klegeris, A., Schwab, C., & McGeer, P. L. (2009). Interferon-γ-dependent cytotoxic activation of human astrocytes and astrocytoma cells. *Neurobiology of Aging*, *30*(12), 1924–1935. https://doi.org/10.1016/J.NEUROBIOLAGING.2008.02.019

Haynes, S. E., Hollopeter, G., Yang, G., Kurpius, D., Dailey, M. E., Gan, W. B., & Julius, D. (2006a). The P2Y12 receptor regulates microglial activation by extracellular nucleotides. *Nature Neuroscience*, *9*(12), 1512–1519. https://doi.org/10.1038/NN1805

Haynes, S. E., Hollopeter, G., Yang, G., Kurpius, D., Dailey, M. E., Gan, W. B., & Julius, D. (2006b). The P2Y12 receptor regulates microglial activation by extracellular nucleotides. *Nature Neuroscience*, *9*(12), 1512–1519. https://doi.org/10.1038/NN1805

He, Y., Le, W. D., & Appel, S. H. (2002). Role of Fcγ receptors in nigral cell injury induced by Parkinson disease immunoglobulin injection into mouse substantia Nigra. *Experimental Neurology*, *176*(2), 322–327. https://doi.org/10.1006/exnr.2002.7946

Hébert, G., Arsaut, J., Dantzer, R., & Demotes-Mainard, J. (2003). Time-course of the expression of inflammatory cytokines and matrix metalloproteinases in the striatum and mesencephalon of mice injected with 1-methyl-4-phenyl-1,2,3,6-tetrahydropyridine, a dopaminergic neurotoxin. *Neuroscience Letters*, *349*(3), 191–195. https://doi.org/10.1016/S0304-3940(03)00832-2

Heman-Bozadas, P., Romero, C., Martínez-Remedios, P., Freitag, I., Frías, A., Saavedra-López, E., Casanova, P. V., Roig-Martínez, M., Cribaro, G. P., Rovirosa-Hernández, M. J., Hernandez-Baltazar, D., & Barcia, C. (2022). Lesion-associated microglia and macrophages mediate corralling and react with massive phagocytosis for debris clearance and wound healing after LPS-induced dopaminergic depletion. *Journal of Neuroimmunology*, *367*. https://doi.org/10.1016/J.JNEUROIM.2022.577874

Heneka, M. T., Kummer, M. P., & Latz, E. (2014). Innate immune activation in neurodegenerative disease. *Nature Reviews. Immunology*, *14*(7), 463–477. https://doi.org/10.1038/NRI3705

Henkel, J. S., Beers, D. R., Zhao, W., & Appel, S. H. (2009). Microglia in ALS: the good, the bad, and the resting. *Journal of Neuroimmune Pharmacology : The Official Journal of the Society on NeuroImmune Pharmacology*, *4*(4), 389–398. https://doi.org/10.1007/S11481-009-9171-5

Henze, C., Hartmann, A., Lescot, T., Hirsch, E. C., & Michel, P. P. (2005). Proliferation of microglial cells induced by 1-methyl-4-phenylpyridinium in mesencephalic cultures results from an astrocyte-dependent mechanism: Role of granulocyte macrophage colony-stimulating factor. *Journal of Neurochemistry*, *95*(4), 1069–1077. https://doi.org/10.1111/j.1471-4159.2005.03416.x

Heppner FL, Skutella T, Hailer NP, Haas D, & Nitsch R. (1998). Activated microglial cells migrate towards sites of excitotoxic neuronal injury inside organotypic hippocampal slice cultures. *The European Journal of Neuroscience*, *10*(10), 3284–3290. https://doi.org/10.1046/J.1460-9568.1998.00379.X

Herrera, A. J., Castaño, A., Venero, J. L., Cano, J., & Machado, A. (2000). The single intranigral injection of LPS as a new model for studying the selective effects of inflammatory reactions on dopaminergic system. *Neurobiology of Disease*, *7*(4), 429–447. https://doi.org/10.1006/NBDI.2000.0289

Hickey, W. F., & Kimura, H. (1988). Perivascular microglial cells of the CNS are bone marrow-derived and present antigen in vivo. *Science (New York, N.Y.)*, *239*(4837), 290–292. https://doi.org/10.1126/SCIENCE.3276004

Hide, I., Shiraki, H., Masuda, A., Maeda, T., Kumagai, M., Kunishige, N., Yanase, Y., Harada, K., Tanaka, S., & Sakai, N. (2023). P2Y2 receptor mediates dying cell removal via inflammatory activated microglia. *Journal of Pharmacological Sciences*, *153*(1), 55–67. https://doi.org/10.1016/J.JPHS.2023.06.004

Hirayama, K., Matsushita, S., Kikuchi, I., Iuchi, M., Ohta, N., & Sasazuki, T. (1987). HLA-DQ is epistatic to HLA-DR in controlling the immune response to schistosomal antigen in humans. *Nature*, *327*(6121), 426–430. https://doi.org/10.1038/327426a0

Hirayama, K., Nishimura, Y., Tsukamoto, K., & Sasazuki, T. (1986). Functional and molecular analysis of three distinct HLA-DR4 beta-chains responsible for the MLR between HLA-Dw4, Dw15, and DKT2. *Journal of Immunology (Baltimore, Md. : 1950)*, *137*(3), 924–933.

Hirsch, E. C., & Hunot, S. (2009). Neuroinflammation in Parkinson's disease: a target for neuroprotection? *The Lancet. Neurology*, *8*(4), 382–397. https://doi.org/10.1016/S1474-4422(09)70062-6

Hirsch, E. C., Vyas, S., & Hunot, S. (2012). Neuroinflammation in Parkinson's disease. *Parkinsonism & Related Disorders*, *18 Suppl 1*(SUPPL. 1). https://doi.org/10.1016/S1353-8020(11)70065-7

Honda, S., Sasaki, Y., Ohsawa, K., Imai, Y., Nakamura, Y., Inoue, K., & Kohsaka, S. (2001). Extracellular ATP or ADP induce chemotaxis of cultured microglia through Gi/o-coupled P2Y receptors. *The Journal of Neuroscience : The Official Journal of the Society for Neuroscience*, *21*(6), 1975–1982. https://doi.org/10.1523/JNEUROSCI.21-06-01975.2001

Hristova, M., Cuthill, D., Zbarsky, V., Acosta-Saltos, A., Wallace, A., Blight, K., Buckley, S. M. K., Peebles, D., Heuer, H., Waddington, S. N., & Raivich, G. (2010). Activation and deactivation of periventricular white matter phagocytes during postnatal mouse development. *Glia*, *58*(1), 11–28. https://doi.org/10.1002/GLIA.20896

Hsieh, J., Aimone, J. B., Kaspar, B. K., Kuwabara, T., Nakashima, K., & Gage, F. H. (2004). IGF-I instructs multipotent adult neural progenitor cells to become oligodendrocytes. *The Journal of Cell Biology*, *164*(1), 111–122. https://doi.org/10.1083/JCB.200308101

Hung, A. Y., & Sheng, M. (2002). PDZ domains: structural modules for protein complex assembly. *The Journal of Biological Chemistry*, *277*(8), 5699–5702. https://doi.org/10.1074/JBC.R100065200

Hunot, S., Boissière, F., Faucheux, B., Brugg, B., Mouatt-Prigent, A., Agid, Y., & Hirsch, E. C. (1996). Nitric oxide synthase and neuronal vulnerability in Parkinson's disease. *Neuroscience*, *72*(2), 355–363. https://doi.org/10.1016/0306-4522(95)00578-1

Hunot, S., Dugas, N., Faucheux, B., Hartmann, A., Tardieu, M., Debré, P., Agid, Y., Dugas, B., & Hirsch, E. C. (1999). FcepsilonRII/CD23 is expressed in Parkinson's disease and induces, in vitro, production of nitric oxide and tumor necrosis factor-alpha in glial cells. *The Journal of Neuroscience : The Official Journal of the Society for Neuroscience*, *19*(9), 3440–3447. https://doi.org/10.1523/JNEUROSCI.19-09-03440.1999

Hurwitz, B. (2017). The Status of "Nonmotor" Features of the Malady in an Essay on the Shaking Palsy (1817). *International Review of Neurobiology*, *133*, 3–12. https://doi.org/10.1016/BS.IRN.2017.04.008

Iida, H., Doiguchi, M., Yamashita, H., Sugimachi, S., Ichinose, J., Mori, T., & Shibata, Y. (2001). Spermatid-specific expression of Iba1, an ionized calcium binding adapter molecule-1, in

rat testis. *Biology of Reproduction*, *64*(4), 1138–1146. https://doi.org/10.1095/BIOLREPROD64.4.1138

Illes, P., Rubini, P., Ulrich, H., Zhao, Y., & Tang, Y. (2020). Regulation of Microglial Functions by Purinergic Mechanisms in the Healthy and Diseased CNS. *Cells 2020, Vol. 9, Page 1108*, *9*(5), 1108. https://doi.org/10.3390/CELLS9051108

Imai, Y., Ibata, I., Ito, D., Ohsawa, K., & Kohsaka, S. (1996). A novel gene iba1 in the major histocompatibility complex class III region encoding an EF hand protein expressed in a monocytic lineage. *Biochemical and Biophysical Research Communications*, *224*(3), 855–862. https://doi.org/10.1006/BBRC.1996.1112

Imamura, K., Hishikawa, N., Ono, K., Suzuki, H., Sawada, M., Nagatsu, T., Yoshida, M., & Hashizume, Y. (2005). Cytokine production of activated microglia and decrease in neurotrophic factors of neurons in the hippocampus of Lewy body disease brains. *Acta Neuropathologica*, *109*(2), 141–150. https://doi.org/10.1007/S00401-004-0919-Y

Inoue, K. (2007). UDP Facilitates Microglial Phagocytosis Through P2Y6 Receptors. *Cell Adhesion & Migration*, *1*(3), 131–132. https://doi.org/10.4161/cam.1.3.4937

Inoue, K. (2008). Purinergic systems in microglia. *Cellular and Molecular Life Sciences*, *65*(19), 3074–3080. https://doi.org/10.1007/s00018-008-8210-3

Ito, D., Imai, Y., Ohsawa, K., Nakajima, K., Fukuuchi, Y., & Kohsaka, S. (1998). Microglia-specific localisation of a novel calcium binding protein, Iba1. *Molecular Brain Research*, *57*(1), 1–9. https://doi.org/10.1016/S0169-328X(98)00040-0

James Surmeier, D., Obeso, J. A., & Halliday, G. M. (2017). Parkinson's Disease Is Not Simply a Prion Disorder. *The Journal of Neuroscience : The Official Journal of the Society for Neuroscience*, *37*(41), 9799–9807. https://doi.org/10.1523/JNEUROSCI.1787-16.2017

Jana, M., Palencia, C. A., & Pahan, K. (2008). Fibrillar Amyloid-β Peptides Activate Microglia via TLR2: Implications for Alzheimer's Disease. *The Journal of Immunology*, *181*(10), 7254–7262. https://doi.org/10.4049/JIMMUNOL.181.10.7254

Janda, E., Boi, L., & Carta, A. R. (2018). Microglial Phagocytosis and Its Regulation: A Therapeutic Target in Parkinson's Disease? *Frontiers in Molecular Neuroscience*, *11*. https://doi.org/10.3389/FNMOL.2018.00144

Jenner, P., & Olanow, C. W. (1996). Oxidative stress and the pathogenesis of Parkinson's disease. *Neurology*, *47*(6 Suppl 3). https://doi.org/10.1212/WNL.47.6_SUPPL_3.161S

Jeong, S. Y., Jeon, R., Choi, Y. K., Jung, J. E., Liang, A., Xing, C., Wang, X., Lo, E. H., & Song, Y. S. (2016). Activation of microglial Toll-like receptor 3 promotes neuronal survival against cerebral ischemia. *Journal of Neurochemistry*, *136*(4), 851–858. https://doi.org/10.1111/JNC.13441

Jiang, Q., Wei, D., He, X., Gan, C., Long, X., & Zhang, H. (2021). Phillyrin Prevents Neuroinflammation-Induced Blood-Brain Barrier Damage Following Traumatic Brain Injury via Altering Microglial Polarization. *Frontiers in Pharmacology*, *12*. https://doi.org/10.3389/FPHAR.2021.719823

Jimenez-Ferrer, I., & Swanberg, M. (2018a). Immunogenetics of Parkinson's Disease. *Parkinson's Disease: Pathogenesis and Clinical Aspects*, 27–44. https://doi.org/10.15586/CODONPUBLICATIONS.PARKINSONSDISEASE.2018.CH2

Jimenez-Ferrer, I., & Swanberg, M. (2018b). Immunogenetics of Parkinson's Disease. *Parkinson's Disease: Pathogenesis and Clinical Aspects*, 27–44. https://doi.org/10.15586/CODONPUBLICATIONS.PARKINSONSDISEASE.2018.CH2

Junttila, I. S. (2018). Tuning the Cytokine Responses: An Update on Interleukin (IL)-4 and IL-13 Receptor Complexes. *Frontiers in Immunology*, *9*(JUN). https://doi.org/10.3389/FIMMU.2018.00888

Kalia, L. V., Brotchie, J. M., & Fox, S. H. (2013). Novel nondopaminergic targets for motor features of Parkinson's disease: review of recent trials. *Movement Disorders : Official Journal of the Movement Disorder Society*, *28*(2), 131–144. https://doi.org/10.1002/MDS.25273

Kalia, L. V., & Lang, A. E. (2015). Parkinson's disease. *Lancet (London, England)*, *386*(9996), 896–912. https://doi.org/10.1016/S0140-6736(14)61393-3

Karpenko, M. N., Vasilishina, A. A., Gromova, E. A., Muruzheva, Z. M., & Bernadotte, A. (2018). Interleukin-1β, interleukin-1 receptor antagonist, interleukin-6, interleukin-10, and tumor necrosis factor-α levels in CSF and serum in relation to the clinical diversity of Parkinson's disease. *Cellular Immunology*, *327*, 77–82. https://doi.org/10.1016/J.CELLIMM.2018.02.011

Kawahara, M., & Kuroda, Y. (2000). Molecular mechanism of neurodegeneration induced by Alzheimer's beta-amyloid protein: channel formation and disruption of calcium homeostasis. *Brain Research Bulletin*, *53*(4), 389–397. https://doi.org/10.1016/S0361-9230(00)00370-1

Keller, J. N., Kindy, M. S., Holtsberg, F. W., St. Clair, D. K., Yen, H. C., Germeyer, A., Steiner, S. M., Bruce-Keller, A. J., Hutchins, J. B., & Mattson, M. P. (1998). Mitochondrial manganese superoxide dismutase prevents neural apoptosis and reduces ischemic brain injury: suppression of peroxynitrite production, lipid peroxidation, and mitochondrial dysfunction. *The Journal of Neuroscience : The Official Journal of the Society for Neuroscience*, *18*(2), 687–697. https://doi.org/10.1523/JNEUROSCI.18-02-00687.1998

Kerr, J. F. R., Wyllie, A. H., & Currie, A. R. (1972). Apoptosis: a basic biological phenomenon with wide-ranging implications in tissue kinetics. *British Journal of Cancer*, *26*(4), 239–257. https://doi.org/10.1038/BJC.1972.33

Kett, L. R., & Dauer, W. T. (2012). Leucine-rich repeat kinase 2 for beginners: six key questions. *Cold Spring Harbor Perspectives in Medicine*, *2*(3). https://doi.org/10.1101/CSHPERSPECT.A009407

Kettenmann, H., Kirchhoff, F., & Verkhratsky, A. (2013). Microglia: new roles for the synaptic stripper. *Neuron*, *77*(1), 10–18. https://doi.org/10.1016/J.NEURON.2012.12.023

Khakh, B. S., & North, R. A. (2012). Neuromodulation by extracellular ATP and P2X receptors in the CNS. *Neuron*, *76*(1), 51–69. https://doi.org/10.1016/J.NEURON.2012.09.024

Kikuchi, I., Ozawa, T., Hirayama, K., & Sasazuki, T. (1986). An HLA-linked gene controls susceptibility to lepromatous leprosy through T cell regulation. *Leprosy Review*, *57 Suppl 2*(SUPPL. 2), 139–142. https://doi.org/10.5935/0305-7518.19860064

Kim, H. J., Ajit, D., Peterson, T. S., Wang, Y., Camden, J. M., Wood, W. G., Sun, G. Y., Erb, L., Petris, M., & Weisman, G. A. (2012). Nucleotides released from Aβ 1-42-treated microglial cells increase cell migration and Aβ 1-42 uptake through P2Y 2 receptor activation. *Journal of Neurochemistry*, *121*(2), 228–238. https://doi.org/10.1111/J.1471-4159.2012.07700.X

Kim, H., Park, J. H., & Kim, K. (2012). Lipid-like components released from degenerating dopaminergic neurons trigger the dynamic migration of microglia. *Biochemical and*

Biophysical Research Communications, *426*(1), 18–25. https://doi.org/10.1016/J.BBRC.2012.07.167

Kim, W. G., Mohney, R. P., Wilson, B., Jeohn, G. H., Liu, B., & Hong, J. S. (2000). Regional Difference in Susceptibility to Lipopolysaccharide-Induced Neurotoxicity in the Rat Brain: Role of Microglia. *Journal of Neuroscience*, *20*(16), 6309–6316. https://doi.org/10.1523/JNEUROSCI.20-16-06309.2000

Kim, Y. S., & Joh, T. H. (2006). Microglia, major player in the brain inflammation: their roles in the pathogenesis of Parkinson's disease. *Experimental & Molecular Medicine*, *38*(4), 333–347. https://doi.org/10.1038/EMM.2006.40

Kimura, M., Kawahito, Y., Obayashi, H., Ohta, M., Hara, H., Adachi, T., Tokunaga, D., Hojo, T., Hamaguchi, M., Omoto, A., Ishino, H., Wada, M., Kohno, M., Tsubouchi, Y., & Yoshikawa, T. (2007). A critical role for allograft inflammatory factor-1 in the pathogenesis of rheumatoid arthritis. *Journal of Immunology (Baltimore, Md. : 1950)*, *178*(5), 3316–3322. https://doi.org/10.4049/JIMMUNOL.178.5.3316

Koizumi, S., Shigemoto-Mogami, Y., Nasu-Tada, K., Shinozaki, Y., Ohsawa, K., Tsuda, M., Joshi, B. V., Jacobson, K. A., Kohsaka, S., & Inoue, K. (2007a). UDP acting at P2Y6 receptors is a mediator of microglial phagocytosis. *Nature*, *446*(7139), 1091–1095. https://doi.org/10.1038/NATURE05704

Koizumi, S., Shigemoto-Mogami, Y., Nasu-Tada, K., Shinozaki, Y., Ohsawa, K., Tsuda, M., Joshi, B. V., Jacobson, K. A., Kohsaka, S., & Inoue, K. (2007b). UDP acting at P2Y6 receptors is a mediator of microglial phagocytosis. *Nature*, *446*(7139), 1091–1095. https://doi.org/10.1038/NATURE05704

Kozma, R., Ahmed, S., Best, A., & Lim, L. (1995). The Ras-related protein Cdc42Hs and bradykinin promote formation of peripheral actin microspikes and filopodia in Swiss 3T3 fibroblasts. *Molecular and Cellular Biology*, *15*(4), 1942–1952. https://doi.org/10.1128/MCB.15.4.1942

Kristián, T., & Siesjö, B. K. (1998). Calcium in ischemic cell death. *Stroke*, *29*(3), 705–718. https://doi.org/10.1161/01.STR.29.3.705

Krüger, R., Kuhn, W., Müller, T., Woitalla, D., Graeber, M., Kösel, S., Przuntek, H., Epplen, J. T., Schöls, L., & Riess, O. (1998). Ala30Pro mutation in the gene encoding alpha-synuclein in

Parkinson's disease. *Nature Genetics*, *18*(2), 106–108. https://doi.org/10.1038/NG0298-106

Kurkowska-Jastrzebska, I., Wrońska, A., Kohutnicka, M. S., Czlonkowski, A., & Czlonkowska, A. (1999). The inflammatory reaction following 1-methyl-4-phenyl-1,2,3, 6-tetrahydropyridine intoxication in mouse. *Experimental Neurology*, *156*(1), 50–61. https://doi.org/10.1006/EXNR.1998.6993

Landreth, G. E., & Reed-Geaghan, E. G. (2009). Toll-like receptors in Alzheimer's disease. *Current Topics in Microbiology and Immunology*, *336*(1), 137–153. https://doi.org/10.1007/978-3-642-00549-7_8/COVER

Langston, J. W. (2017). The MPTP Story. *Journal of Parkinson's Disease*, *7*(s1), S11–S19. https://doi.org/10.3233/JPD-179006

Langston, J. W., Forno, L. S., Tetrud, J., Reeves, A. G., Kaplan, J. A., & Karluk, D. (1999). *Evidence of active nerve cell degeneration in the substantia nigra of humans years after 1-methyl-4-phenyl-1,2,3,6-tetrahydropyridine exposure - PubMed*. https://pubmed.ncbi.nlm.nih.gov/10514096/

Langston, J. W., Irwin, I., Langston, E. B., & Forno, L. S. (1984). 1-Methyl-4-phenylpyridinium ion (MPP+): identification of a metabolite of MPTP, a toxin selective to the substantia nigra. *Neuroscience Letters*, *48*(1), 87–92. https://doi.org/10.1016/0304-3940(84)90293-3

Lashuel, H. A., Overk, C. R., Oueslati, A., & Masliah, E. (2013). The many faces of α-synuclein: from structure and toxicity to therapeutic target. *Nature Reviews. Neuroscience*, *14*(1), 38–48. https://doi.org/10.1038/NRN3406

Lauro, C., Catalano, M., Trettel, F., & Limatola, C. (2015). Fractalkine in the nervous system: neuroprotective or neurotoxic molecule? *Annals of the New York Academy of Sciences*, *1351*(1), 141–148. https://doi.org/10.1111/NYAS.12805

Lee, E. Y., Schultz, K. L. W., & Griffin, D. E. (2013). Mice Deficient in Interferon-Gamma or Interferon-Gamma Receptor 1 Have Distinct Inflammatory Responses to Acute Viral Encephalomyelitis. *PLOS ONE*, *8*(10), e76412. https://doi.org/10.1371/JOURNAL.PONE.0076412

Lee, J.-K., Tran, T., & Tansey, M. G. (2009). Neuroinflammation in Parkinson's Disease. *Journal of Neuroimmune Pharmacology*, *4*(4), 419–429. https://doi.org/10.1007/s11481-009-9176-0

Lees, A. J., Hardy, J., & Revesz, T. (2009). Parkinson's disease. *The Lancet*, *373*(9680), 2055–2066. https://doi.org/10.1016/S0140-6736(09)60492-X

Lesage, S., Anheim, M., Letournel, F., Bousset, L., Honoré, A., Rozas, N., Pieri, L., Madiona, K., Dürr, A., Melki, R., Verny, C., & Brice, A. (2013). G51D α-synuclein mutation causes a novel parkinsonian-pyramidal syndrome. *Annals of Neurology*, *73*(4), 459–471. https://doi.org/10.1002/ANA.23894

Lewy, F. (1913). Zur pathologischen Anatomie der Paralysis agitans. *Archiv Für Psychiatrie Und Nervenkrankheit*, *44*(2), 789–814. https://doi.org/10.1007/BF01821569/METRICS

Li, Q., & Barres, B. A. (2018). Microglia and macrophages in brain homeostasis and disease. *Nature Reviews. Immunology*, *18*(4), 225–242. https://doi.org/10.1038/NRI.2017.125

Liddelow, S. A., & Barres, B. A. (2017). Reactive Astrocytes: Production, Function, and Therapeutic Potential. *Immunity*, *46*(6), 957–967. https://doi.org/10.1016/J.IMMUNI.2017.06.006

Lim, D., Semyanov, A., Genazzani, A., & Verkhratsky, A. (2021). Calcium signaling in neuroglia. *International Review of Cell and Molecular Biology*, *362*, 1–53. https://doi.org/10.1016/BS.IRCMB.2021.01.003

Lim, S. Y., & Lang, A. E. (2010). The nonmotor symptoms of Parkinson's disease--an overview. *Movement Disorders : Official Journal of the Movement Disorder Society*, *25 Suppl 1*(SUPPL. 1). https://doi.org/10.1002/MDS.22786

Lin, M. T., & Beal, M. F. (2006). Mitochondrial dysfunction and oxidative stress in neurodegenerative diseases. *Nature*, *443*(7113), 787–795. https://doi.org/10.1038/NATURE05292

Lin, R., Zhou, Y., Yan, T., Wang, R., Li, H., Wu, Z., Zhang, X., Zhou, X., Zhao, F., Zhang, L., Li, Y., & Luo, M. (2022). Directed evolution of adeno-associated virus for efficient gene delivery to microglia. *Nature Methods 2022 19:8*, *19*(8), 976–985. https://doi.org/10.1038/s41592-022-01547-7

Lindqvist, D., Kaufman, E., Brundin, L., Hall, S., Surova, Y., & Hansson, O. (2012). Non-Motor Symptoms in Patients with Parkinson's Disease - Correlations with Inflammatory Cytokines in Serum. *PLoS ONE*, *7*(10). https://doi.org/10.1371/journal.pone.0047387

Lituma, P. J., Woo, E., O'Hara, B. F., Castillo, P. E., Sibinga, N. E. S., & Nandi, S. (2021). Altered synaptic connectivity and brain function in mice lacking microglial adapter protein Iba1. *Proceedings of the National Academy of Sciences of the United States of America*, *118*(46). https://doi.org/10.1073/PNAS.2115539118/-/DCSUPPLEMENTAL

Liu, B., & Hong, J. S. (2003). Role of microglia in inflammation-mediated neurodegenerative diseases: mechanisms and strategies for therapeutic intervention. *The Journal of Pharmacology and Experimental Therapeutics*, *304*(1), 1–7. https://doi.org/10.1124/JPET.102.035048

Liu, S., Tan, W. Y., Chen, Q. R., Chen, X. P., Fu, K., Zhao, Y. Y., & Chen, Z. W. (2008). Daintain/AIF-1 promotes breast cancer proliferation via activation of the NF-kappaB/cyclin D1 pathway and facilitates tumor growth. *Cancer Science*, *99*(5), 952–957. https://doi.org/10.1111/J.1349-7006.2008.00787.X

Liu, T., Sun, L., Xiong, Y., Shang, S., Guo, N., Teng, S., Wang, Y., Liu, B., Wang, C., Wang, L., Zheng, L., Zhang, C. X., Han, W., & Zhou, Z. (2011). Calcium triggers exocytosis from two types of organelles in a single astrocyte. *The Journal of Neuroscience : The Official Journal of the Society for Neuroscience*, *31*(29), 10593–10601. https://doi.org/10.1523/JNEUROSCI.6401-10.2011

Luchtman, D. W., Shao, D., & Song, C. (2009). Behavior, neurotransmitters and inflammation in three regimens of the MPTP mouse model of Parkinson's disease. *Physiology & Behavior*, *98*(1–2), 130–138. https://doi.org/10.1016/J.PHYSBEH.2009.04.021

Lwin, A., Orvisky, E., Goker-Alpan, O., LaMarca, M. E., & Sidransky, E. (2004). Glucocerebrosidase mutations in subjects with parkinsonism. *Molecular Genetics and Metabolism*, *81*(1), 70–73. https://doi.org/10.1016/j.ymgme.2003.11.004

Lyons, A., Lynch, A. M., Downer, E. J., Hanley, R., O'Sullivan, J. B., Smith, A., & Lynch, M. A. (2009). Fractalkine-induced activation of the phosphatidylinositol-3 kinase pathway attentuates microglial activation in vivo and in vitro. *Journal of Neurochemistry*, *110*(5), 1547–1556. https://doi.org/10.1111/J.1471-4159.2009.06253.X

Maciejewski-Lenoir, D., Chen, S., Feng, L., Maki, R., & Bacon, K. B. (1999). Characterization of fractalkine in rat brain cells: migratory and activation signals for CX3CR-1-expressing microglia. *Journal of Immunology (Baltimore, Md. : 1950)*, *163*(3), 1628–1635.

Marín-Teva, J. L., Dusart, I., Colin, C., Gervais, A., Van Rooijen, N., & Mallat, M. (2004). Microglia Promote the Death of Developing Purkinje Cells. *Neuron*, *41*(4), 535–547. https://doi.org/10.1016/S0896-6273(04)00069-8

Markey, S. P., Johannessen, J. N., Chiueh, C. C., Burns, R. S., & Herkenham, M. A. (1984). Intraneuronal generation of a pyridinium metabolite may cause drug-induced parkinsonism. *Nature*, *311*(5985), 464–467. https://doi.org/10.1038/311464A0

Martí, Y., Matthaeus, F., Lau, T., & Schloss, P. (2017). Methyl-4-phenylpyridinium (MPP+) differentially affects monoamine release and re-uptake in murine embryonic stem cell-derived dopaminergic and serotonergic neurons. *Molecular and Cellular Neurosciences*, *83*, 37–45. https://doi.org/10.1016/J.MCN.2017.06.009

Martinez, F. O., & Gordon, S. (2014). The M1 and M2 paradigm of macrophage activation: time for reassessment. *F1000prime Reports*, *6*. https://doi.org/10.12703/P6-13

Martinez, F. O., Helming, L., & Gordon, S. (2009). Alternative activation of macrophages: an immunologic functional perspective. *Annual Review of Immunology*, *27*, 451–483. https://doi.org/10.1146/ANNUREV.IMMUNOL.021908.132532

Massol, P., Montcourrier, P., Guillemot, J. C., & Chavrier, P. (1998). Fc receptor-mediated phagocytosis requires CDC42 and Rac1. *The EMBO Journal*, *17*(21), 6219–6229. https://doi.org/10.1093/EMBOJ/17.21.6219

Mattison, H. A., Nie, H., Gao, H., Zhou, H., Hong, J. S., & Zhang, J. (2013). Suppressed pro-inflammatory response of microglia in CX3CR1 knockout mice. *Journal of Neuroimmunology*, *257*(1–2), 110–115. https://doi.org/10.1016/J.JNEUROIM.2013.02.008

Mattson, M. P. (2007). Calcium and neurodegeneration. *Aging Cell*, *6*(3), 337–350. https://doi.org/10.1111/j.1474-9726.2007.00275.x

Mattson, M. P., Zhu, H., Yu, J., & Kindy, M. S. (2000). Presenilin-1 mutation increases neuronal vulnerability to focal ischemia in vivo and to hypoxia and glucose deprivation in cell culture: involvement of perturbed calcium homeostasis. *The Journal of Neuroscience : The Official*

Journal of the Society for Neuroscience, *20*(4), 1358–1364. https://doi.org/10.1523/JNEUROSCI.20-04-01358.2000

McCoy, M. K., Martinez, T. N., Ruhn, K. A., Szymkowski, D. E., Smith, C. G., Botterman, B. R., Tansey, K. E., & Tansey, M. G. (2006). Blocking soluble tumor necrosis factor signaling with dominant-negative tumor necrosis factor inhibitor attenuates loss of dopaminergic neurons in models of Parkinson's disease. *The Journal of Neuroscience : The Official Journal of the Society for Neuroscience*, *26*(37), 9365–9375. https://doi.org/10.1523/JNEUROSCI.1504-06.2006

McGeer, P. L., Itagaki, S., Boyes, B. E., & McGeer, E. G. (1988). Reactive microglia are positive for HLA-DR in the substantia nigra of Parkinson's and Alzheimer's disease brains. *Neurology*, *38*(8), 1285–1291. https://doi.org/10.1212/WNL.38.8.1285

McGeer, P. L., Itagaki, S., Tago, H., & McGeer, E. G. (1987). Reactive microglia in patients with senile dementia of the Alzheimer type are positive for the histocompatibility glycoprotein HLA-DR. *Neuroscience Letters*, *79*(1–2), 195–200. https://doi.org/10.1016/0304-3940(87)90696-3

McGeer, P. L., & McGeer, E. G. (2004). Inflammation and neurodegeneration in Parkinson's disease. *Parkinsonism and Related Disorders*, *10*(SUPPL. 1), S3. https://doi.org/10.1016/j.parkreldis.2004.01.005

McGeer, P. L., & McGeer, E. G. (2008). Glial reactions in Parkinson's disease. *Movement Disorders*, *23*(4), 474–483. https://doi.org/10.1002/mds.21751

McGeer, P. L., Schwab, C., Parent, A., & Doudet, D. (2003). Presence of reactive microglia in monkey substantia nigra years after 1-methyl-4-phenyl-1,2,3,6-tetrahydropyridine administration. *Annals of Neurology*, *54*(5), 599–604. https://doi.org/10.1002/ANA.10728

McPherson, C. A., Merrick, B. A., & Harry, G. J. (2014). In vivo molecular markers for pro-inflammatory cytokine M1 stage and resident microglia in trimethyltin-induced hippocampal injury. *Neurotoxicity Research*, *25*(1), 45–56. https://doi.org/10.1007/S12640-013-9422-3

Mecca, C., Giambanco, I., Donato, R., & Arcuri, C. (2018). Microglia and Aging: The Role of the TREM2-DAP12 and CX3CL1-CX3CR1 Axes. *International Journal of Molecular Sciences*, *19*(1). https://doi.org/10.3390/IJMS19010318

Mehra, S., Sahay, S., & Maji, S. K. (2019). α-Synuclein misfolding and aggregation: Implications in Parkinson's disease pathogenesis. *Biochimica et Biophysica Acta. Proteins and Proteomics*, *1867*(10), 890–908. https://doi.org/10.1016/J.BBAPAP.2019.03.001

Menza, M., Dobkin, R. D. F., Marin, H., Mark, M. H., Gara, M., Bienfait, K., Dicke, A., & Kusnekov, A. (2010). The role of inflammatory cytokines in cognition and other non-motor symptoms of Parkinson's disease. *Psychosomatics*, *51*(6), 474–479. https://doi.org/10.1176/APPI.PSY.51.6.474

Meyer-Luehmann, M., Spires-Jones, T. L., Prada, C., Garcia-Alloza, M., De Calignon, A., Rozkalne, A., Koenigsknecht-Talboo, J., Holtzman, D. M., Bacskai, B. J., & Hyman, B. T. (2008). Rapid appearance and local toxicity of amyloid-beta plaques in a mouse model of Alzheimer's disease. *Nature*, *451*(7179), 720–724. https://doi.org/10.1038/NATURE06616

Michel, P. P., Hirsch, E. C., & Hunot, S. (2016). Understanding Dopaminergic Cell Death Pathways in Parkinson Disease. *Neuron*, *90*(4), 675–691. https://doi.org/10.1016/j.neuron.2016.03.038

Mizuno, T., Kawanokuchi, J., Numata, K., & Suzumura, A. (2003). Production and neuroprotective functions of fractalkine in the central nervous system. *Brain Research*, *979*(1–2), 65–70. https://doi.org/10.1016/S0006-8993(03)02867-1

Mizuno, Y., Hattori, N., Mori, H., Suzuki, T., & Tanaka, K. (2001). Parkin and Parkinson's disease. *Current Opinion in Neurology*, *14*(4), 477–482. https://doi.org/10.1097/00019052-200108000-00008

Mochizuki, H., Nakamura, N., Nishi, K., & Mizuno, Y. (1994). Apoptosis is induced by 1-methyl-4-phenylpyridinium ion (MPP+) in ventral mesencephalic-striatal co-culture in rat. *Neuroscience Letters*, *170*(1), 191–194. https://doi.org/10.1016/0304-3940(94)90271-2

Mogi, M., Harada, M., Kondo, T., Riederer, P., Inagaki, H., Minami, M., & Nagatsu, T. (1994a). Interleukin-1 beta, interleukin-6, epidermal growth factor and transforming growth factor-alpha are elevated in the brain from parkinsonian patients. *Neuroscience Letters*, *180*(2), 147–150. https://doi.org/10.1016/0304-3940(94)90508-8

Mogi, M., Harada, M., Kondo, T., Riederer, P., Inagaki, H., Minami, M., & Nagatsu, T. (1994b). Interleukin-1 beta, interleukin-6, epidermal growth factor and transforming growth factor-

alpha are elevated in the brain from parkinsonian patients. *Neuroscience Letters*, *180*(2), 147–150. https://doi.org/10.1016/0304-3940(94)90508-8

Mogi, M., Harada, M., Narabayashi, H., Inagaki, H., Minami, M., & Nagatsu, T. (1996). Interleukin (IL)-1β, IL-2, IL-4, IL-6 and transforming growth factor-α levels are elevated in ventricular cerebrospinal fluid in juvenile parkinsonism and Parkinson's disease. *Neuroscience Letters*, *211*(1), 13–16. https://doi.org/10.1016/0304-3940(96)12706-3

Mogi, M., Harada, M., Riederer, P., Narabayashi, H., Fujita, K., & Nagatsu, T. (1994). Tumor necrosis factor-α (TNF-α) increases both in the brain and in the cerebrospinal fluid from parkinsonian patients. *Neuroscience Letters*, *165*(1–2), 208–210. https://doi.org/10.1016/0304-3940(94)90746-3

Moore, D. J., West, A. B., Dawson, V. L., & Dawson, T. M. (2005). MOLECULAR PATHOPHYSIOLOGY OF PARKINSON'S DISEASE. *Annual Review of Neuroscience*, *28*(1), 57–87. https://doi.org/10.1146/annurev.neuro.28.061604.135718

Morillas, A. G., Besson, V. C., & Lerouet, D. (2021). Microglia and Neuroinflammation: What Place for P2RY12? *International Journal of Molecular Sciences*, *22*(4), 1–16. https://doi.org/10.3390/IJMS22041636

Morohashi, T., Iwabuchi, K., Watano, K., Dashtsoodol, N., Mishima, T., Nakai, Y., Shimada, S., Nishida, R., Fujii, S., & Onoté, K. (2003). Allograft inflammatory factor-1 regulates trinitrobenzene sulphonic acid-induced colitis. *Immunology*, *110*(1), 112–119. https://doi.org/10.1046/J.1365-2567.2003.01714.X

Moujalled, D., Strasser, A., & Liddell, J. R. (2021). Molecular mechanisms of cell death in neurological diseases. *Cell Death and Differentiation*, *28*(7), 2029–2044. https://doi.org/10.1038/S41418-021-00814-Y

Mount, M. P., Lira, A., Grimes, D., Smith, P. D., Faucher, S., Slack, R., Anisman, H., Hayley, S., & Park, D. S. (2007a). Involvement of Interferon- in Microglial-Mediated Loss of Dopaminergic Neurons. *Journal of Neuroscience*, *27*(12), 3328–3337. https://doi.org/10.1523/JNEUROSCI.5321-06.2007

Mount, M. P., Lira, A., Grimes, D., Smith, P. D., Faucher, S., Slack, R., Anisman, H., Hayley, S., & Park, D. S. (2007b). Involvement of interferon-gamma in microglial-mediated loss of

dopaminergic neurons. *The Journal of Neuroscience : The Official Journal of the Society for Neuroscience*, *27*(12), 3328–3337. https://doi.org/10.1523/JNEUROSCI.5321-06.2007

Muñoz, E., Oliva, R., Obach, V., Martí, M. J., Pastor, P., Ballesta, F., & Tolosa, E. (1997). Identification of Spanish familial Parkinson's disease and screening for the Ala53Thr mutation of the alpha-synuclein gene in early onset patients. *Neuroscience Letters*, *235*(1–2), 57–60. https://doi.org/10.1016/S0304-3940(97)00710-6

Murray, F. E., Landsberg, J. P., Williams, R. J., Esiri, M. M., & Watt, F. (1992). Elemental analysis of neurofibrillary tangles in Alzheimer's disease using proton-induced X-ray analysis. *Ciba Foundation Symposium*, *169*. https://doi.org/10.1002/9780470514306.CH12

Nagakawa, Y., Nomoto, S., Kato, Y., Montgomery, R. A., Williams, G. M., Klein, A. S., & Sun, Z. (2004). Over-expression of AIF-1 in liver allografts and peripheral blood correlates with acute rejection after transplantation in rats. *American Journal of Transplantation : Official Journal of the American Society of Transplantation and the American Society of Transplant Surgeons*, *4*(12), 1949–1957. https://doi.org/10.1111/J.1600-6143.2004.00621.X

Nagatsu, T., Mogi, M., Ichinose, H., & Togari, A. (2000). Changes in cytokines and neurotrophins in Parkinson's disease. *Journal of Neural Transmission. Supplementum*, *60*, 277–290. https://doi.org/10.1007/978-3-7091-6301-6_19

Nakajima, K., Honda, S., Tohyama, Y., Imai, Y., Kohsaka, S., & Kurihara, T. (2001). Neurotrophin secretion from cultured microglia. *Journal of Neuroscience Research*, *65*(4), 322–331. https://doi.org/10.1002/JNR.1157

Narendra, D. P., Jin, S. M., Tanaka, A., Suen, D. F., Gautier, C. A., Shen, J., Cookson, M. R., & Youle, R. J. (2010). PINK1 is selectively stabilized on impaired mitochondria to activate Parkin. *PLoS Biology*, *8*(1). https://doi.org/10.1371/JOURNAL.PBIO.1000298

Nasu, T., Tsukahara, Y., & Terayama, K. (1973). A lipid metabolic disease-"membranous lipodystrophy"-an autopsy case demonstrating numerous peculiar membrane-structures composed of compound lipid in bone and bone marrow and various adipose tissues. *Acta Pathologica Japonica*, *23*(3), 539–558. https://doi.org/10.1111/J.1440-1827.1973.TB01223.X

Nayak, D., Johnson, K. R., Heydari, S., Roth, T. L., Zinselmeyer, B. H., & McGavern, D. B. (2013). Type I interferon programs innate myeloid dynamics and gene expression in the virally

infected nervous system. *PLoS Pathogens*, *9*(5). https://doi.org/10.1371/JOURNAL.PPAT.1003395

Nayak, D., Roth, T. L., & McGavern, D. B. (2014). Microglia Development and Function. *Annual Review of Immunology*, *32*(1), 367–402. https://doi.org/10.1146/annurev-immunol-032713-120240

Nayak, D., Zinselmeyer, B. H., Corps, K. N., & McGavern, D. B. (2012). In vivo dynamics of innate immune sentinels in the CNS. *Intravital*, *1*(2), 95–106. https://doi.org/10.4161/INTV.22823

Neal, M., & Richardson, J. R. (2018). Epigenetic regulation of astrocyte function in neuroinflammation and neurodegeneration. *Biochimica et Biophysica Acta. Molecular Basis of Disease*, *1864*(2), 432–443. https://doi.org/10.1016/J.BBADIS.2017.11.004

Nedergaard, S., Flatman, J. A., & Engberg, I. (1993). Nifedipine- and omega-conotoxin-sensitive Ca2+ conductances in guinea-pig substantia nigra pars compacta neurones. *The Journal of Physiology*, *466*, 727–747.

Neher, J. J., Neniskyte, U., Zhao, J.-W., Bal-Price, A., Tolkovsky, A. M., & Brown, G. C. (2011a). Inhibition of Microglial Phagocytosis Is Sufficient To Prevent Inflammatory Neuronal Death. *The Journal of Immunology*, *186*(8), 4973–4983. https://doi.org/10.4049/JIMMUNOL.1003600

Neher, J. J., Neniskyte, U., Zhao, J.-W., Bal-Price, A., Tolkovsky, A. M., & Brown, G. C. (2011b). Inhibition of microglial phagocytosis is sufficient to prevent inflammatory neuronal death. *Journal of Immunology (Baltimore, Md. : 1950)*, *186*(8), 4973–4983. https://doi.org/10.4049/JIMMUNOL.1003600

Nellgård, B., & Wieloch, T. (1992). Cerebral protection by AMPA- and NMDA-receptor antagonists administered after severe insulin-induced hypoglycemia. *Experimental Brain Research*, *92*(2), 259–266. https://doi.org/10.1007/BF00227969

Ness, J. K., & Wood, T. L. (2002). Insulin-like growth factor I, but not neurotrophin-3, sustains Akt activation and provides long-term protection of immature oligodendrocytes from glutamate-mediated apoptosis. *Molecular and Cellular Neuroscience*, *20*(3), 476–488. https://doi.org/10.1006/mcne.2002.1149

Neumann, H., Kotter, M. R., & Franklin, R. J. M. (2009). Debris clearance by microglia: an essential link between degeneration and regeneration. *Brain*, *132*(2), 288–295. https://doi.org/10.1093/BRAIN/AWN109

Neumann, H., & Takahashi, K. (2007). Essential role of the microglial triggering receptor expressed on myeloid cells-2 (TREM2) for central nervous tissue immune homeostasis. *Journal of Neuroimmunology*, *184*(1–2), 92–99. https://doi.org/10.1016/J.JNEUROIM.2006.11.032

Neve, B. P., Fruchart, J. C., & Staels, B. (2000). Role of the peroxisome proliferator-activated receptors (PPAR) in atherosclerosis. *Biochemical Pharmacology*, *60*(8), 1245–1250. https://doi.org/10.1016/S0006-2952(00)00430-5

Nichols, R. J., Dzamko, N., Morrice, N. A., Campbell, D. G., Deak, M., Ordureau, A., Macartney, T., Tong, Y., Shen, J., Prescott, A. R., & Alessi, D. R. (2010). 14-3-3 Binding to LRRK2 is disrupted by multiple Parkinson's disease-associated mutations and regulates cytoplasmic localization. *Biochemical Journal*, *430*(3), 393–404. https://doi.org/10.1042/BJ20100483

Nimmerjahn, A., Kirchhoff, F., & Helmchen, F. (2005). Resting microglial cells are highly dynamic surveillants of brain parenchyma in vivo. *Science (New York, N.Y.)*, *308*(5726), 1314–1318. https://doi.org/10.1126/SCIENCE.1110647

Nishimura, Y., & Sasazuki, T. (1983). Suppressor T cells control the HLA-linked low responsiveness to streptococcal antigen in man. *Nature*, *302*(5903), 67–69. https://doi.org/10.1038/302067A0

Nixon, R. A. (2003). The calpains in aging and aging-related diseases. *Ageing Research Reviews*, *2*(4), 407–418. https://doi.org/10.1016/S1568-1637(03)00029-1

Nobes, C. D., & Hall, A. (1995). Rho, rac, and cdc42 GTPases regulate the assembly of multimolecular focal complexes associated with actin stress fibers, lamellipodia, and filopodia. *Cell*, *81*(1), 53–62. https://doi.org/10.1016/0092-8674(95)90370-4

North, R. A. (2016). P2X receptors. *Philosophical Transactions of the Royal Society of London. Series B, Biological Sciences*, *371*(1700). https://doi.org/10.1098/RSTB.2015.0427

Odegaard, J. I., & Chawla, A. (2011). Alternative macrophage activation and metabolism. *Annual Review of Pathology*, *6*, 275–297. https://doi.org/10.1146/ANNUREV-PATHOL-011110-130138

Ohsawa, K., Imai, Y., Kanazawa, H., Sasaki, Y., & Kohsaka, S. (2000). Involvement of Iba1 in membrane ruffling and phagocytosis of macrophages/microglia. *Journal of Cell Science*, *113 (Pt 17)*(17), 3073–3084. https://doi.org/10.1242/JCS.113.17.3073

Ohsawa, K., Irino, Y., Nakamura, Y., Akazawa, C., Inoue, K., & Kohsaka, S. (2007). Involvement of P2X4 and P2Y12 receptors in ATP-induced microglial chemotaxis. *GLIA*, *55*(6), 604–616. https://doi.org/10.1002/glia.20489

Ohsawa, K., Irino, Y., Sanagi, T., Nakamura, Y., Suzuki, E., Inoue, K., & Kohsaka, S. (2010). P2Y12 receptor-mediated integrin-beta1 activation regulates microglial process extension induced by ATP. *Glia*, *58*(7), 790–801. https://doi.org/10.1002/GLIA.20963

Olanow, C. W., Obeso, J. A., & Stocchi, F. (2006). Drug insight: Continuous dopaminergic stimulation in the treatment of Parkinson's disease. *Nature Clinical Practice. Neurology*, *2*(7), 382–392. https://doi.org/10.1038/NCPNEURO0222

Olson, J. K., & Miller, S. D. (2004). Microglia Initiate Central Nervous System Innate and Adaptive Immune Responses through Multiple TLRs. *The Journal of Immunology*, *173*(6), 3916–3924. https://doi.org/10.4049/JIMMUNOL.173.6.3916

Orellana, J. A., Shoji, K. F., Abudara, V., Ezan, P., Amigou, E., Sáez, P. J., Jiang, J. X., Naus, C. C., Sáez, J. C., & Giaume, C. (2011). Amyloid β-induced death in neurons involves glial and neuronal hemichannels. *The Journal of Neuroscience : The Official Journal of the Society for Neuroscience*, *31*(13), 4962–4977. https://doi.org/10.1523/JNEUROSCI.6417-10.2011

Orr, C. F., Rowe, D. B., Mizuno, Y., Mori, H., & Halliday, G. M. (2005). A possible role for humoral immunity in the pathogenesis of Parkinson's disease. *Brain : A Journal of Neurology*, *128*(Pt 11), 2665–2674. https://doi.org/10.1093/BRAIN/AWH625

Owen, A. D., Schapira, A. H. V., Jenner, P., & Marsden, C. D. (1996). Oxidative stress and Parkinson's disease. *Annals of the New York Academy of Sciences*, *786*, 217–223. https://doi.org/10.1111/J.1749-6632.1996.TB39064.X

Paisán-Ruíz, C., Jain, S., Evans, E. W., Gilks, W. P., Simón, J., Van Der Brug, M., De Munain, A. L., Aparicio, S., Gil, A. M., Khan, N., Johnson, J., Martinez, J. R., Nicholl, D., Carrera, I. M., Peňa, A. S., De Silva, R., Lees, A., Martí-Massó, J. F., Pérez-Tur, J., … Singleton, A. B. (2004). Cloning of the gene containing mutations that cause PARK8-linked Parkinson's disease. *Neuron*, *44*(4), 595–600. https://doi.org/10.1016/j.neuron.2004.10.023

Paloneva, J., Autti, T., Raininko, R., Partanen, J., Salonen, O., Puranen, M., Hakola, P., & Haltia, M. (2001). CNS manifestations of Nasu-Hakola disease: a frontal dementia with bone cysts. *Neurology*, *56*(11), 1552–1558. https://doi.org/10.1212/WNL.56.11.1552

Pangršič, T., Potokar, M., Stenovec, M., Kreft, M., Fabbretti, E., Nistri, A., Pryazhnikov, E., Khiroug, L., Giniatullin, R., & Zorec, R. (2007). Exocytotic release of ATP from cultured astrocytes. *The Journal of Biological Chemistry*, *282*(39), 28749–28758. https://doi.org/10.1074/JBC.M700290200

Paolicelli, R. C., Bolasco, G., Pagani, F., Maggi, L., Scianni, M., Panzanelli, P., Giustetto, M., Ferreira, T. A., Guiducci, E., Dumas, L., Ragozzino, D., & Gross, C. T. (2011). Synaptic pruning by microglia is necessary for normal brain development. *Science (New York, N.Y.)*, *333*(6048), 1456–1458. https://doi.org/10.1126/SCIENCE.1202529

Paolicelli, R. C., Sierra, A., Stevens, B., Tremblay, M. E., Aguzzi, A., Ajami, B., Amit, I., Audinat, E., Bechmann, I., Bennett, M., Bennett, F., Bessis, A., Biber, K., Bilbo, S., Blurton-Jones, M., Boddeke, E., Brites, D., Brône, B., Brown, G. C., … Wyss-Coray, T. (2022). Microglia states and nomenclature: A field at its crossroads. *Neuron*, *110*(21), 3458–3483. https://doi.org/10.1016/J.NEURON.2022.10.020

Park, J.-Y., Kim, B.-W., Lee, H. U., Choi, D.-K., & Yoon, S.-H. (2017). Synthesis of Clovamide Analogues That Inhibit NO Production in Activated BV-2 Microglial Cells. *Biological & Pharmaceutical Bulletin*, *40*(9), 1475–1482. https://doi.org/10.1248/bpb.b17-00303

Parkinson, J. (1817). An essay on the shaking palsy. 1817. In *The Journal of neuropsychiatry and clinical neurosciences* (Vol. 14, Issue 2). J Neuropsychiatry Clin Neurosci. https://doi.org/10.1176/JNP.14.2.223

Pérez-Cerdá, F., Sánchez-Gómez, M. V., & Matute, C. (2015). Pío del Río Hortega and the discovery of the oligodendrocytes. *Frontiers in Neuroanatomy*, *9*(July). https://doi.org/10.3389/FNANA.2015.00092

Perry, V. H., Cunningham, C., & Holmes, C. (2007). Systemic infections and inflammation affect chronic neurodegeneration. *Nature Reviews. Immunology*, *7*(2), 161–167. https://doi.org/10.1038/NRI2015

Perry, V. H., Nicoll, J. A. R., & Holmes, C. (2010). Microglia in neurodegenerative disease. *Nature Reviews. Neurology*, *6*(4), 193–201. https://doi.org/10.1038/NRNEUROL.2010.17

Pinna, A. (2014). Adenosine A2A receptor antagonists in Parkinson's disease: Progress in clinical trials from the newly approved istradefylline to drugs in early development and those already discontinued. *CNS Drugs*, *28*(5), 455–474. https://doi.org/10.1007/S40263-014-0161-7

Poewe, W., Seppi, K., Tanner, C. M., Halliday, G. M., Brundin, P., Volkmann, J., Schrag, A. E., & Lang, A. E. (2017). Parkinson disease. *Nature Reviews. Disease Primers*, *3*, 1–21. https://doi.org/10.1038/NRDP.2017.13

Poirier, L. J., & Sourkes, T. L. (1965). INFLUENCE OF THE SUBSTANTIA NIGRA ON THE CATECHOLAMINE CONTENT OF THE STRIATUM. *Brain : A Journal of Neurology*, *88*(1), 181–192. https://doi.org/10.1093/BRAIN/88.1.181

Polymeropoulos, M. H., Lavedan, C., Leroy, E., Ide, S. E., Dehejia, A., Dutra, A., Pike, B., Root, H., Rubenstein, J., Boyer, R., Stenroos, E. S., Chandrasekharappa, S., Athanassiadou, A., Papapetropoulos, T., Johnson, W. G., Lazzarini, A. M., Duvoisin, R. C., Di Iorio, G., Golbe, L. I., & Nussbaum, R. L. (1997). Mutation in the alpha-synuclein gene identified in families with Parkinson's disease. *Science (New York, N.Y.)*, *276*(5321), 2045–2047. https://doi.org/10.1126/SCIENCE.276.5321.2045

Poniatowski, Ł. A., Wojdasiewicz, P., Krawczyk, M., Szukiewicz, D., Gasik, R., Kubaszewski, Ł., & Kurkowska-Jastrzębska, I. (2017). Analysis of the Role of CX3CL1 (Fractalkine) and Its Receptor CX3CR1 in Traumatic Brain and Spinal Cord Injury: Insight into Recent Advances in Actions of Neurochemokine Agents. *Molecular Neurobiology*, *54*(3), 2167–2188. https://doi.org/10.1007/S12035-016-9787-4

Proukakis, C., Dudzik, C. G., Brier, T., MacKay, D. S., Cooper, J. M., Millhauser, G. L., Houlden, H., & Schapira, A. H. (2013). A novel α-synuclein missense mutation in Parkinson disease. *Neurology*, *80*(11), 1062–1064. https://doi.org/10.1212/WNL.0B013E31828727BA

Przedborski, S. (2017). The two-century journey of Parkinson disease research. *Nature Reviews. Neuroscience*, *18*(4), 251–259. https://doi.org/10.1038/NRN.2017.25

Purisai, M. G., McCormack, A. L., Cumine, S., Li, J., Isla, M. Z., & Di Monte, D. A. (2007). Microglial activation as a priming event leading to paraquat-induced dopaminergic cell degeneration. *Neurobiology of Disease*, *25*(2), 392–400. https://doi.org/10.1016/J.NBD.2006.10.008

Quintana, A., Pasche, M., Junker, C., Al-Ansary, D., Rieger, H., Kummerow, C., Nuñez, L., Villalobos, C., Meraner, P., Becherer, U., Rettig, J., Niemeyer, B. A., & Hoth, M. (2011). Calcium microdomains at the immunological synapse: how ORAI channels, mitochondria and calcium pumps generate local calcium signals for efficient T-cell activation. *The EMBO Journal*, *30*(19), 3895. https://doi.org/10.1038/EMBOJ.2011.289

Ramsay, R. R., Dadgar, J., Trevor, A., & Singer, T. P. (1986). Energy-driven uptake of N-methyl-4-phenylpyridine by brain mitochondria mediates the neurotoxicity of MPTP. *Life Sciences*, *39*(7), 581–588. https://doi.org/10.1016/0024-3205(86)90037-8

Ransohoff, R. M. (2016). A polarizing question: do M1 and M2 microglia exist? *Nature Neuroscience*, *19*(8), 987–991. https://doi.org/10.1038/NN.4338

Ransohoff, R. M., & Perry, V. H. (2009). Microglial physiology: unique stimuli, specialized responses. *Annual Review of Immunology*, *27*, 119–145. https://doi.org/10.1146/ANNUREV.IMMUNOL.021908.132528

Ransom, B. R., Kunis, D. M., Irwin, I., & Langston, J. W. (1987a). Astrocytes convert the parkinsonism inducing neurotoxin, MPTP, to its active metabolite, MPP+. *Neuroscience Letters*, *75*(3), 323–328. https://doi.org/10.1016/0304-3940(87)90543-X

Ransom, B. R., Kunis, D. M., Irwin, I., & Langston, J. W. (1987b). Astrocytes convert the parkinsonism inducing neurotoxin, MPTP, to its active metabolite, MPP+. *Neuroscience Letters*, *75*(3), 323–328. https://doi.org/10.1016/0304-3940(87)90543-X

Reed-Geaghan, E. G., Savage, J. C., Hise, A. G., & Landreth, G. E. (2009). CD14 and toll-like receptors 2 and 4 are required for fibrillar Aβ-stimulated microglial activation. *Journal of Neuroscience*, *29*(38), 11982–11992. https://doi.org/10.1523/JNEUROSCI.3158-09.2009

Reich, S. G., & Savitt, J. M. (2019). Parkinson's Disease. *The Medical Clinics of North America*, *103*(2), 337–350. https://doi.org/10.1016/J.MCNA.2018.10.014

Ren, J., Lin, Y., Tang, J., Yue, H., & Zhao, Y. (2018). Allograft Inflammatory Factor-1 Mediates Macrophage-Induced Impairment of Insulin Signaling in Adipocytes. *Cellular Physiology and Biochemistry*, *47*(1), 403–413. https://doi.org/10.1159/000489952

Richard, K. L., Filali, M., Préfontaine, P., & Rivest, S. (2008). Toll-like receptor 2 acts as a natural innate immune receptor to clear amyloid β1-42 and delay the cognitive decline in a mouse model of Alzheimer's disease. *Journal of Neuroscience*, *28*(22), 5784–5793. https://doi.org/10.1523/JNEUROSCI.1146-08.2008

Ridley, A. J., Paterson, H. F., Johnston, C. L., Diekmann, D., & Hall, A. (1992). The small GTP-binding protein rac regulates growth factor-induced membrane ruffling. *Cell*, *70*(3), 401–410. https://doi.org/10.1016/0092-8674(92)90164-8

Río-Hortega Pío. (1919). El tercer elemento de los centros nerviosos. III. *Bol. Soc. Esp. Biol 9*.

Riteau, N., Gasse, P., Fauconnier, L., Gombault, A., Couegnat, M., Fick, L., Kanellopoulos, J., Quesniaux, V. F. J., Marchand-Adam, S., Crestani, B., Ryffel, B., & Couillin, I. (2010). Extracellular ATP is a danger signal activating P2X7 receptor in lung inflammation and fibrosis. *American Journal of Respiratory and Critical Care Medicine*, *182*(6), 774–783. https://doi.org/10.1164/RCCM.201003-0359OC

Rock, K. L., Reits, E., & Neefjes, J. (2016). Present Yourself! By MHC Class I and MHC Class II Molecules. *Trends in Immunology*, *37*(11), 724–737. https://doi.org/10.1016/J.IT.2016.08.010

Roig-Martinez, M., Saavedra-Lopez, E., Casanova, P. V., Cribaro, G. P., & Barcia, C. (2019). The MTOC/Golgi Complex at the T-Cell Immunological Synapse. In *Results and Problems in Cell Differentiation* (Vol. 67, pp. 223–231). https://doi.org/10.1007/978-3-030-23173-6_9

Rostène, W., Kitabgi, P., & Parsadaniantz, S. M. (2007). Chemokines: a new class of neuromodulator? *Nature Reviews. Neuroscience*, *8*(11), 895–904. https://doi.org/10.1038/NRN2255

Roszek, K., & Czarnecka, J. (2015). Is Ecto-nucleoside Triphosphate Diphosphohydrolase (NTPDase)-based Therapy of Central Nervous System Disorders Possible? *Mini-Reviews in Medicinal Chemistry*, *15*(1), 5–20. https://doi.org/10.2174/1389557515666150219114416

Rottenberg, M. E., Gigliotti Rothfuchs, A. C., Gigliotti, D., Svanholm, C., Bandholtz, L., & Wigzell, H. (1999). Role of Innate and Adaptive Immunity in the Outcome of Primary Infection with Chlamydia pneumoniae, as Analyzed in Genetically Modified Mice. *The Journal of Immunology*, *162*(5), 2829–2836. https://doi.org/10.4049/JIMMUNOL.162.5.2829

Roumier, A., Béchade, C., Poncer, J. C., Smalla, K. H., Tomasello, E., Vivier, E., Gundelfinger, E. D., Triller, A., & Bessis, A. (2004). Impaired synaptic function in the microglial KARAP/DAP12-deficient mouse. *The Journal of Neuroscience : The Official Journal of the Society for Neuroscience*, *24*(50), 11421–11428. https://doi.org/10.1523/JNEUROSCI.2251-04.2004

Russo, I., Bubacco, L., & Greggio, E. (2014). LRRK2 and neuroinflammation: partners in crime in Parkinson's disease? *Journal of Neuroinflammation*, *11*(1), 52. https://doi.org/10.1186/1742-2094-11-52

Saavedra-López, E., Casanova, P. V., Cribaro, G. P., & Barcia, C. (2016). Neuroinflammation in Movement Disorders. *Handbook of Behavioral Neuroscience*, *24*, 771–782. https://doi.org/10.1016/B978-0-12-802206-1.00038-6

Saijo, K., & Glass, C. K. (2011a). Microglial cell origin and phenotypes in health and disease. *Nature Reviews Immunology*, *11*(11), 775–787. https://doi.org/10.1038/nri3086

Saijo, K., & Glass, C. K. (2011b). Microglial cell origin and phenotypes in health and disease. *Nature Reviews Immunology*, *11*(11), 775–787. https://doi.org/10.1038/nri3086

Samii, A., Nutt, J. G., & Ransom, B. R. (2004). Parkinson's disease. *Lancet (London, England)*, *363*(9423), 1783–1793. https://doi.org/10.1016/S0140-6736(04)16305-8

Sampson, T. R., Debelius, J. W., Thron, T., Janssen, S., Shastri, G. G., Ilhan, Z. E., Challis, C., Schretter, C. E., Rocha, S., Gradinaru, V., Chesselet, M. F., Keshavarzian, A., Shannon, K. M., Krajmalnik-Brown, R., Wittung-Stafshede, P., Knight, R., & Mazmanian, S. K. (2016). Gut Microbiota Regulate Motor Deficits and Neuroinflammation in a Model of Parkinson's Disease. *Cell*, *167*(6), 1469-1480.e12. https://doi.org/10.1016/J.CELL.2016.11.018

Sano, Y., & Murase, Y. (1968). [Biochemistry of the extrapyramidal system--from anatomical viewpoint]. *Shinkei Kenkyu No Shimpo. Advances in Neurological Sciences*, *12*(4), 859–868.

Sasaki, Y., Ohsawa, K., Kanazawa, H., Kohsaka, S., & Imai, Y. (2001). Iba1 is an actin-cross-linking protein in macrophages/microglia. *Biochemical and Biophysical Research Communications*, *286*(2), 292–297. https://doi.org/10.1006/BBRC.2001.5388

Schipke, C. G., Boucsein, C., Ohlemeyer, C., Kirchhoff, F., & Kettenmann, H. (2002). Astrocyte Ca2+ waves trigger responses in microglial cells in brain slices. *FASEB Journal : Official Publication of the Federation of American Societies for Experimental Biology*, *16*(2), 255–257. https://doi.org/10.1096/FJ.01-0514FJE

Schluesener, H. J., Seid, K., Kretzschmar, J., & Meyermann, R. (1998). Allograft-inflammatory factor-1 in rat experimental autoimmune encephalomyelitis, neuritis, and uveitis: expression by activated macrophages and microglial cells. *Glia*, *24*(2), 244–251. https://doi.org/10.1002/(sici)1098-1136(199810)24:2<244::aid-glia9>3.0.co;2-3

Schmid, C. D., Sautkulis, L. N., Danielson, P. E., Cooper, J., Hasel, K. W., Hilbush, B. S., Sutcliffe, J. G., & Carson, M. J. (2002). Heterogeneous expression of the triggering receptor expressed on myeloid cells-2 on adult murine microglia. *Journal of Neurochemistry*, *83*(6), 1309–1320. https://doi.org/10.1046/J.1471-4159.2002.01243.X

Schmid, B. V., Kesmir, C., & de Boer, R. J. (2010). Quantifying how MHC polymorphism prevents pathogens from adapting to the antigen presentation pathway. *Epidemics*, *2*(3), 99–108. https://doi.org/10.1016/J.EPIDEM.2010.05.003

Schulte, C., & Gasser, T. (2011). Genetic basis of Parkinson's disease: inheritance, penetrance, and expression. *The Application of Clinical Genetics*, *4*, 67–80. https://doi.org/10.2147/TACG.S11639

Schulz, C., Perdiguero, E. G., Chorro, L., Szabo-Rogers, H., Cagnard, N., Kierdorf, K., Prinz, M., Wu, B., Jacobsen, S. E. W., Pollard, J. W., Frampton, J., Liu, K. J., & Geissmann, F. (2012). A lineage of myeloid cells independent of Myb and hematopoietic stem cells. *Science (New York, N.Y.)*, *336*(6077), 86–90. https://doi.org/10.1126/SCIENCE.1219179

Schwartz, M., & Kipnis, J. (2004). A common vaccine for fighting neurodegenerative disorders: recharging immunity for homeostasis. *Trends in Pharmacological Sciences*, *25*(8), 407–412. https://doi.org/10.1016/J.TIPS.2004.06.010

Schwartz, M., & Ziv, Y. (2008). Immunity to self and self-maintenance: a unified theory of brain pathologies. *Trends in Immunology*, *29*(5), 211–219. https://doi.org/10.1016/J.IT.2008.01.003

Shechter, R., & Schwartz, M. (2013). CNS sterile injury: just another wound healing? *Trends in Molecular Medicine*, *19*(3), 135–143. https://doi.org/10.1016/J.MOLMED.2012.11.007

Shen, R. S., Abell, C. W., Gessner, W., & Brossi, A. (1985). Serotonergic conversion of MPTP and dopaminergic accumulation of MPP+. *FEBS Letters*, *189*(2), 225–230. https://doi.org/10.1016/0014-5793(85)81028-0

Shimoji, M., Pagan, F., Healton, E. B., & Mocchetti, I. (2009). CXCR4 and CXCL12 expression is increased in the nigro-striatal system of Parkinson's disease. *Neurotoxicity Research*, *16*(3), 318–328. https://doi.org/10.1007/S12640-009-9076-3

Sica, A., Larghi, P., Mancino, A., Rubino, L., Porta, C., Totaro, M. G., Rimoldi, M., Biswas, S. K., Allavena, P., & Mantovani, A. (2008). Macrophage polarization in tumour progression. *Seminars in Cancer Biology*, *18*(5), 349–355. https://doi.org/10.1016/J.SEMCANCER.2008.03.004

Sieger, D., Moritz, C., Ziegenhals, T., Prykhozhij, S., & Peri, F. (2012). Long-range Ca2+ waves transmit brain-damage signals to microglia. *Developmental Cell*, *22*(6), 1138–1148. https://doi.org/10.1016/J.DEVCEL.2012.04.012

Sieger, T., Bonnet, C., Serranová, T., Wild, J., Novák, D., Růžička, F., Urgošík, D., Růžička, E., Gaymard, B., & Jech, R. (2013). Basal ganglia neuronal activity during scanning eye movements in Parkinson's disease. *PloS One*, *8*(11). https://doi.org/10.1371/JOURNAL.PONE.0078581

Simard, A. R., & Rivest, S. (2004). Bone marrow stem cells have the ability to populate the entire central nervous system into fully differentiated parenchymal microglia. *FASEB Journal : Official Publication of the Federation of American Societies for Experimental Biology*, *18*(9), 998–1000. https://doi.org/10.1096/FJ.04-1517FJE

Simard, A. R., Soulet, D., Gowing, G., Julien, J. P., & Rivest, S. (2006). Bone marrow-derived microglia play a critical role in restricting senile plaque formation in Alzheimer's disease. *Neuron*, *49*(4), 489–502. https://doi.org/10.1016/J.NEURON.2006.01.022

Smaili, S., Hirata, H., Ureshino, R., Monteforte, P. T., Morales, A. P., Muler, M. L., Terashima, J., Oseki, K., Rosenstock, T. R., Lopes, G. S., & Bincoletto, C. (2009). Calcium and cell death signaling in neurodegeneration and aging. *Anais Da Academia Brasileira de Ciencias*, *81*(3), 467–475. https://doi.org/10.1590/S0001-37652009000300011

Smith, Y., Wichmann, T., Factor, S. A., & Delong, M. R. (2012). Parkinson's disease therapeutics: new developments and challenges since the introduction of levodopa. *Neuropsychopharmacology : Official Publication of the American College of Neuropsychopharmacology*, *37*(1), 213–246. https://doi.org/10.1038/NPP.2011.212

Sommerville, L. J., Kelemen, S. E., Ellison, S. P., England, R. N., & Autieri, M. V. (2012). Increased atherosclerosis and vascular smooth muscle cell activation in AIF-1 transgenic mice fed a high-fat diet. *Atherosclerosis*, *220*(1), 45–52. https://doi.org/10.1016/J.ATHEROSCLEROSIS.2011.07.095

Sone, T., Tsukamoto, K., Hirayama, K., Nishimura, Y., Takenouchi, T., Aizawa, M., & Sasazuki, T. (1985). Two distinct class II molecules encoded by the genes within HLA-DR subregion of HLA-Dw2 and Dw12 can act as stimulating and restriction molecules. *Journal of Immunology (Baltimore, Md. : 1950)*, *135*(2), 1288–1298.

Song, M., Jin, J. J., Lim, J. E., Kou, J., Pattanayak, A., Rehman, J. A., Kim, H. D., Tahara, K., Lalonde, R., & Fukuchi, K. I. (2011). TLR4 mutation reduces microglial activation, increases Aβ deposits and exacerbates cognitive deficits in a mouse model of Alzheimer's disease. *Journal of Neuroinflammation*, *8*. https://doi.org/10.1186/1742-2094-8-92

Spillantini, M. G., Schmidt, M. L., Lee, V. M. Y., Trojanowski, J. Q., Jakes, R., & Goedert, M. (1997). Alpha-synuclein in Lewy bodies. *Nature*, *388*(6645), 839–840. https://doi.org/10.1038/42166

Stence, N., Waite, M., & Dailey, M. E. (2001). Dynamics of microglial activation: A confocal time-lapse analysis in hippocampal slices. *GLIA*, *33*(3), 256–266. https://doi.org/10.1002/1098-1136(200103)33:3<256::AID-GLIA1024>3.0.CO;2-J

Stern, Y., Tetrud, J. W., Martin, W. R. W., Kutner, S. J., & Langston, J. W. (1990). Cognitive change following MPTP exposure. *Neurology*, *40*(2), 261–264. https://doi.org/10.1212/WNL.40.2.261

Stewart, P. A., & Wiley, M. J. (1981). Developing nervous tissue induces formation of blood-brain barrier characteristics in invading endothelial cells: A study using quail-chick transplantation chimeras. *Developmental Biology*, *84*(1), 183–192. https://doi.org/10.1016/0012-1606(81)90382-1

Striedinger, K., Meda, P., & Scemes, E. (2007). Exocytosis of ATP from astrocyte progenitors modulates spontaneous Ca2+ oscillations and cell migration. *Glia*, *55*(6), 652–662. https://doi.org/10.1002/GLIA.20494

Sulzer, D. (2007). Multiple hit hypotheses for dopamine neuron loss in Parkinson's disease. *Trends in Neurosciences*, *30*(5), 244–250. https://doi.org/10.1016/J.TINS.2007.03.009

Sunnemark, D., Eltayeb, S., Nilsson, M., Wallström, E., Lassmann, H., Olsson, T., Berg, A. L., & Ericsson-Dahlstrand, A. (2005). CX3CL1 (fractalkine) and CX3CR1 expression in myelin oligodendrocyte glycoprotein-induced experimental autoimmune encephalomyelitis: kinetics and cellular origin. *Journal of Neuroinflammation*, *2*. https://doi.org/10.1186/1742-2094-2-17

Surmeier, D. J. (2007). Calcium, ageing, and neuronal vulnerability in Parkinson's disease. *The Lancet. Neurology*, *6*(10), 933–938. https://doi.org/10.1016/S1474-4422(07)70246-6

Taetzsch, T., Levesque, S., Mcgraw, C., Brookins, S., Luqa, R., Bonini, M. G., Mason, R. P., Oh, U., & Block, M. L. (2015). Redox regulation of NF-κB p50 and M1 polarization in microglia. *Glia*, *63*(3), 423–440. https://doi.org/10.1002/GLIA.22762

Tahara, K., Kim, H. D., Jin, J. J., Maxwell, J. A., Li, L., & Fukuchi, K. I. (2006). Role of toll-like receptor signalling in Aβ uptake and clearance. *Brain*, *129*(11), 3006–3019. https://doi.org/10.1093/BRAIN/AWL249

Takahashi, K., Rochford, C. D. P., & Neumann, H. (2005a). Clearance of apoptotic neurons without inflammation by microglial triggering receptor expressed on myeloid cells-2. *The Journal of Experimental Medicine*, *201*(4), 647–657. https://doi.org/10.1084/JEM.20041611

Takahashi, K., Rochford, C. D. P., & Neumann, H. (2005b). Clearance of apoptotic neurons without inflammation by microglial triggering receptor expressed on myeloid cells-2. *The Journal of Experimental Medicine*, *201*(4), 647–657. https://doi.org/10.1084/JEM.20041611

Tamashiro, T. T., Dalgard, C. L., & Byrnes, K. R. (2012). Primary microglia isolation from mixed glial cell cultures of neonatal rat brain tissue. *Journal of Visualized Experiments : JoVE*, *66*, e3814. https://doi.org/10.3791/3814

Tansey, M. G., & Goldberg, M. S. (2010). Neuroinflammation in Parkinson's disease: its role in neuronal death and implications for therapeutic intervention. *Neurobiology of Disease*, *37*(3), 510–518. https://doi.org/10.1016/J.NBD.2009.11.004

Thomas, W. E. (1990). Characterization of the dynamic nature of microglial cells. *Brain Research Bulletin*, *25*(2), 351–354. https://doi.org/10.1016/0361-9230(90)90083-C

Tian, Y., Kelemen, S. E., & Autieri, M. V. (2006). Inhibition of AIF-1 expression by constitutive siRNA expression reduces macrophage migration, proliferation, and signal transduction initiated by atherogenic stimuli. *American Journal of Physiology. Cell Physiology*, *290*(4). https://doi.org/10.1152/AJPCELL.00381.2005

Trang, T., Beggs, S., & Salter, M. W. (2011). Brain-derived neurotrophic factor from microglia: a molecular substrate for neuropathic pain. *Neuron Glia Biology*, *7*(1), 99–108. https://doi.org/10.1017/S1740925X12000087

Trautmann, A. (2009). Extracellular ATP in the immune system: More than just a "danger signal." *Science Signaling*, *2*(56). https://doi.org/10.1126/SCISIGNAL.256PE6

Tsuda, M., Shigemoto-Mogami, Y., Koizumi, S., Mizokoshi, A., Kohsaka, S., Salter, M. W., & Inoue, K. (2003). P2X4 receptors induced in spinal microglia gate tactile allodynia after nerve injury. *Nature*, *424*(6950), 778–783. https://doi.org/10.1038/NATURE01786

Ueno, M., Fujita, Y., Tanaka, T., Nakamura, Y., Kikuta, J., Ishii, M., & Yamashita, T. (2013). Layer V cortical neurons require microglial support for survival during postnatal development. *Nature Neuroscience*, *16*(5), 543–551. https://doi.org/10.1038/NN.3358

Ulmann, L., Hatcher, J. P., Hughes, J. P., Chaumont, S., Green, P. J., Conquet, F., Buell, G. N., Reeve, A. J., Chessell, I. P., & Rassendren, F. (2008). Up-Regulation of P2X $_4$ Receptors in Spinal Microglia after Peripheral Nerve Injury Mediates BDNF Release and Neuropathic Pain. *The Journal of Neuroscience*, *28*(44), 11263–11268. https://doi.org/10.1523/JNEUROSCI.2308-08.2008

Uribe-Querol, E., & Rosales, C. (2020). Phagocytosis: Our Current Understanding of a Universal Biological Process. *Frontiers in Immunology*, *11*. https://doi.org/10.3389/FIMMU.2020.01066

Utans, U., Arceci, R. J., Yamashita, Y., & Russell, M. E. (1995). Cloning and characterization of allograft inflammatory factor-1: a novel macrophage factor identified in rat cardiac allografts with chronic rejection. *The Journal of Clinical Investigation*, *95*(6), 2954–2962. https://doi.org/10.1172/JCI118003

Valente, E. M., Abou-Sleiman, P. M., Caputo, V., Muqit, M. M. K., Harvey, K., Gispert, S., Ali, Z., Del Turco, D., Bentivoglio, A. R., Healy, D. G., Albanese, A., Nussbaum, R., González-Maldonado, R., Deller, T., Salvi, S., Cortelli, P., Gilks, W. P., Latchman, D. S., Harvey, R. J., … Wood, N. W. (2004). Hereditary early-onset Parkinson's disease caused by mutations in PINK1. *Science (New York, N.Y.)*, *304*(5674), 1158–1160. https://doi.org/10.1126/SCIENCE.1096284

van den Elsen, P. J. (2011). Expression regulation of major histocompatibility complex class I and class II encoding genes. *Frontiers in Immunology*, *2*(OCT), 15473. https://doi.org/10.3389/FIMMU.2011.00048/BIBTEX

Van Den Elsen, P. J., Holling, T. M., Kuipers, H. F., & Van Der Stoep, N. (2004). Transcriptional regulation of antigen presentation. *Current Opinion in Immunology*, *16*(1), 67–75. https://doi.org/10.1016/J.COI.2003.11.015

Varnum, M. M., & Ikezu, T. (2012). The classification of microglial activation phenotypes on neurodegeneration and regeneration in Alzheimer's disease brain. *Archivum Immunologiae et Therapiae Experimentalis*, *60*(4), 251–266. https://doi.org/10.1007/S00005-012-0181-2

Vázquez-Villoldo, N., Domercq, M., Martín, A., Llop, J., Gómez-Vallejo, V., & Matute, C. (2014). P2X4 receptors control the fate and survival of activated microglia. *Glia*, *62*(2), 171–184. https://doi.org/10.1002/glia.22596

Vilalta, A., & Brown, G. C. (2018). Neurophagy, the phagocytosis of live neurons and synapses by glia, contributes to brain development and disease. *The FEBS Journal*, *285*(19), 3566–3575. https://doi.org/10.1111/FEBS.14323

Villalta, S. A., Nguyen, H. X., Deng, B., Gotoh, T., & Tidbal, J. G. (2009). Shifts in macrophage phenotypes and macrophage competition for arginine metabolism affect the severity of muscle pathology in muscular dystrophy. *Human Molecular Genetics*, *18*(3), 482–496. https://doi.org/10.1093/HMG/DDN376

Virdi, G. S., Choi, M. L., Evans, J. R., Yao, Z., Athauda, D., Strohbuecker, S., Nirujogi, R. S., Wernick, A. I., Pelegrina-Hidalgo, N., Leighton, C., Saleeb, R. S., Kopach, O., Alrashidi, H., Melandri, D., Perez-Lloret, J., Angelova, P. R., Sylantyev, S., Eaton, S., Heales, S., … Gandhi, S. (2022). Protein aggregation and calcium dysregulation are hallmarks of familial Parkinson's disease in midbrain dopaminergic neurons. *NPJ Parkinson's Disease*, *8*(1), 162. https://doi.org/10.1038/S41531-022-00423-7

Vives-Bauza, C., Zhou, C., Huang, Y., Cui, M., De Vries, R. L. A., Kim, J., May, J., Tocilescu, M. A., Liu, W., Ko, H. S., Magrané, J., Moore, D. J., Dawson, V. L., Grailhe, R., Dawson, T. M., Li, C., Tieu, K., & Przedborski, S. (2010). PINK1-dependent recruitment of Parkin to mitochondria in mitophagy. *Proceedings of the National Academy of Sciences of the United States of America*, *107*(1), 378–383. https://doi.org/10.1073/PNAS.0911187107

Wake, H., Moorhouse, A. J., Jinno, S., Kohsaka, S., & Nabekura, J. (2009). Resting microglia directly monitor the functional state of synapses in vivo and determine the fate of ischemic terminals. *The Journal of Neuroscience : The Official Journal of the Society for Neuroscience*, *29*(13), 3974–3980. https://doi.org/10.1523/JNEUROSCI.4363-08.2009

Wakselman, S., Béchade, C., Roumier, A., Bernard, D., Triller, A., & Bessis, A. (2008). Developmental neuronal death in hippocampus requires the microglial CD11b integrin and DAP12 immunoreceptor. *The Journal of Neuroscience : The Official Journal of the Society for Neuroscience*, *28*(32), 8138–8143. https://doi.org/10.1523/JNEUROSCI.1006-08.2008

Walter, S., Letiembre, M., Liu, Y., Heine, H., Penke, B., Hao, W., Bode, B., Manietta, N., Walter, J., Schulz-Schüffer, W., & Faßbender, K. (2007). Role of the Toll-Like Receptor 4 in Neuroinflammation in Alzheimer's Disease. *Cellular Physiology and Biochemistry*, *20*(6), 947–956. https://doi.org/10.1159/000110455

Watano, K., Iwabuchi, K., Fujii, S., Ishimori, N., Mitsuhashi, S., Ato, M., Kitabatake, A., & Onoé, K. (2001). Allograft inflammatory factor-1 augments production of interleukin-6, -10 and -12 by a mouse macrophage line. *Immunology*, *104*(3), 307–316. https://doi.org/10.1046/J.1365-2567.2001.01301.X

Westerink, R. H. S., & Ewing, A. G. (2008). The PC12 cell as model for neurosecretion. *Acta Physiologica (Oxford, England)*, *192*(2), 273–285. https://doi.org/10.1111/j.1748-1716.2007.01805.x

Wilkinson, K. D., Lee, K., Deshpande, S., Duerksen-Hughes, P., Boss, J. M., & Pohl, J. (1989). The neuron-specific protein PGP 9.5 is a ubiquitin carboxyl-terminal hydrolase. *Science (New York, N.Y.)*, *246*(4930), 670–673. https://doi.org/10.1126/SCIENCE.2530630

William Langston, J., Ballard, P., Tetrud, J. W., & Irwin, I. (1983). Chronic Parkinsonism in humans due to a product of meperidine-analog synthesis. *Science (New York, N.Y.)*, *219*(4587), 979–980. https://doi.org/10.1126/SCIENCE.6823561

Wilson, C. J., & Callaway, J. C. (2000). Coupled oscillator model of the dopaminergic neuron of the substantia nigra. *Journal of Neurophysiology*, *83*(5), 3084–3100. https://doi.org/10.1152/JN.2000.83.5.3084

Wojda, U., Salinska, E., & Kuznicki, J. (2008). Calcium ions in neuronal degeneration. *IUBMB Life*, *60*(9), 575–590. https://doi.org/10.1002/iub.91

Wolfart, J., & Roeper, J. (2002). Selective coupling of T-type calcium channels to SK potassium channels prevents intrinsic bursting in dopaminergic midbrain neurons. *The Journal of Neuroscience : The Official Journal of the Society for Neuroscience*, *22*(9), 3404–3413. https://doi.org/10.1523/JNEUROSCI.22-09-03404.2002

Wong, K., Sidransky, E., Verma, A., Mixon, T., Sandberg, G. D., Wakefield, L. K., Morrison, A., Lwin, A., Colegial, C., Allman, J. M., & Schiffmann, R. (2004). Neuropathology provides clues to the pathophysiology of Gaucher disease. *Molecular Genetics and Metabolism*, *82*(3), 192–207. https://doi.org/10.1016/j.ymgme.2004.04.011

Woods, L. T., Ajit, D., Camden, J. M., Erb, L., & Weisman, G. A. (2016). Purinergic receptors as potential therapeutic targets in Alzheimer's disease. *Neuropharmacology*, *104*, 169–179. https://doi.org/10.1016/J.NEUROPHARM.2015.10.031

Wu, D. C., Teismann, P., Tieu, K., Vila, M., Jackson-Lewis, V., Ischiropoulos, H., & Przedborski, S. (2003). NADPH oxidase mediates oxidative stress in the 1-methyl-4-phenyl-1,2,3,6-tetrahydropyridine model of Parkinson's disease. *Proceedings of the National Academy of Sciences of the United States of America*, *100*(10), 6145–6150. https://doi.org/10.1073/PNAS.0937239100

Wu, J., & Akhmanova, A. (2017). Microtubule-Organizing Centers. *Annual Review of Cell and Developmental Biology*, *33*, 51–75. https://doi.org/10.1146/ANNUREV-CELLBIO-100616-060615

Wyss-Coray, T., & Mucke, L. (2002). Inflammation in neurodegenerative disease - A double-edged sword. *Neuron*, *35*(3), 419–432. https://doi.org/10.1016/S0896-6273(02)00794-8

Yamagata, T., Muroya, K., Mukasa, T., Igarashi, H., Momoi, M., Tsukahara, T., Arahata, K., Kumagai, H., & Momoi, T. (1995). Hepatocyte growth factor specifically expressed in microglia activated Ras in the neurons, similar to the action of neurotrophic factors. *Biochemical and Biophysical Research Communications*, *210*(1), 231–237. https://doi.org/10.1006/BBRC.1995.1651

Yao, Y., & Tsirka, S. E. (2012). Chemokines and their receptors in intracerebral hemorrhage. *Translational Stroke Research*, *3*(Suppl 1), 70–79. https://doi.org/10.1007/S12975-012-0155-Z

Yegutkin, G. G. (2008). Nucleotide- and nucleoside-converting ectoenzymes: Important modulators of purinergic signalling cascade. *Biochimica et Biophysica Acta (BBA) - Molecular Cell Research*, *1783*(5), 673–694. https://doi.org/10.1016/j.bbamcr.2008.01.024

Yoshida, H., Imaizumi, T., Fujimoto, K., Matsuo, N., Kimura, K., Cui, X. F., Matsumiya, T., Tanji, K., Shibata, T., Tamo, W., Kumagai, M., & Satoh, K. (2001). Synergistic stimulation, by tumor necrosis factor-α and interferon-γ, of fractalkine expression in human astrocytes. *Neuroscience Letters*, *303*(2), 132–136. https://doi.org/10.1016/S0304-3940(01)01699-8

Yoshimura, A., Naka, T., & Kubo, M. (2007). SOCS proteins, cytokine signalling and immune regulation. *Nature Reviews. Immunology*, *7*(6), 454–465. https://doi.org/10.1038/NRI2093

Zahoor, I., Shafi, A., & Haq, • Ehtishamul. (2018). Pharmacological Treatment of Parkinson's Disease. *Exon Publications*, 129–144. https://doi.org/10.15586/CODONPUBLICATIONS.PARKINSONSDISEASE.2018.CH7

Zarranz, J. J., Alegre, J., Gómez-Esteban, J. C., Lezcano, E., Ros, R., Ampuero, I., Vidal, L., Hoenicka, J., Rodriguez, O., Atarés, B., Llorens, V., Gomez Tortosa, E., Del Ser, T., Muñoz, D. G., & De Yebenes, J. G. (2004). The new mutation, E46K, of alpha-synuclein causes Parkinson and

Lewy body dementia. *Annals of Neurology*, *55*(2), 164–173. https://doi.org/10.1002/ANA.10795

Zarrinmayeh, H., & Territo, P. R. (2020). Purinergic Receptors of the Central Nervous System: Biology, PET Ligands, and Their Applications. *Molecular Imaging*, *19*. https://doi.org/10.1177/1536012120927609

Zhang, W., Wang, T., Pei, Z., Miller, D. S., Wu, X., Block, M. L., Wilson, B., Zhang, W., Zhou, Y., Hong, J.-S., & Zhang, J. (2005). Aggregated alpha-synuclein activates microglia: a process leading to disease progression in Parkinson's disease. *FASEB Journal : Official Publication of the Federation of American Societies for Experimental Biology*, *19*(6), 533–542. https://doi.org/10.1096/FJ.04-2751COM

Zhang, Z. L., Liu, Y. G., Huang, Q. B., Wang, H. W., Song, Y., Xu, Z. K., & Li, F. (2015). Nuclear factor-κB activation in perihematomal brain tissue correlates with outcome in patients with intracerebral hemorrhage. *Journal of Neuroinflammation*, *12*(1). https://doi.org/10.1186/S12974-015-0277-9

Zhao, H., Garton, T., Keep, R. F., Hua, Y., & Xi, G. (2015). Microglia/Macrophage Polarization After Experimental Intracerebral Hemorrhage. *Translational Stroke Research*, *6*(6), 407–409. https://doi.org/10.1007/S12975-015-0428-4

Zhao, X., Sun, G., Zhang, J., Strong, R., Song, W., Gonzales, N., Grotta, J. C., & Aronowski, J. (2007). Hematoma resolution as a target for intracerebral hemorrhage treatment: role for peroxisome proliferator-activated receptor gamma in microglia/macrophages. *Annals of Neurology*, *61*(4), 352–362. https://doi.org/10.1002/ANA.21097

Zhao, X., Zhang, Y., Strong, R., Grotta, J. C., & Aronowski, J. (2006). 15d-Prostaglandin J2 activates peroxisome proliferator-activated receptor-gamma, promotes expression of catalase, and reduces inflammation, behavioral dysfunction, and neuronal loss after intracerebral hemorrhage in rats. *Journal of Cerebral Blood Flow and Metabolism : Official Journal of the International Society of Cerebral Blood Flow and Metabolism*, *26*(6), 811–820. https://doi.org/10.1038/SJ.JCBFM.9600233

Zhao, Y., Gan, L., Ren, L., Lin, Y., Ma, C., & Lin, X. (2022). Factors influencing the blood-brain barrier permeability. *Brain Research*, *1788*, 147937. https://doi.org/10.1016/J.BRAINRES.2022.147937

Zheng, Z. V., Chen, J., Lyu, H., Lam, S. Y. E., Lu, G., Chan, W. Y., & Wong, G. K. C. (2022). Novel role of STAT3 in microglia-dependent neuroinflammation after experimental subarachnoid haemorrhage. *Stroke and Vascular Neurology*, *7*(1), 62–70. https://doi.org/10.1136/SVN-2021-001028

Zimmermann, H. (2000). Extracellular metabolism of ATP and other nucleotides. *Naunyn-Schmiedeberg's Archives of Pharmacology*, *362*(4–5), 299–309. https://doi.org/10.1007/S002100000309

Zimprich, A., Biskup, S., Leitner, P., Lichtner, P., Farrer, M., Lincoln, S., Kachergus, J., Hulihan, M., Uitti, R. J., Calne, D. B., Stoessl, A. J., Pfeiffer, R. F., Patenge, N., Carbajal, I. C., Vieregge, P., Asmus, F., Müller-Myhsok, B., Dickson, D. W., Meitinger, T., … Gasser, T. (2004). Mutations in LRRK2 cause autosomal-dominant parkinsonism with pleomorphic pathology. *Neuron*, *44*(4), 601–607. https://doi.org/10.1016/j.neuron.2004.11.005

Zinger, A., Barcia, C., Herrero, M. T., & Guillemin, G. J. (2011). The involvement of neuroinflammation and kynurenine pathway in Parkinson's disease. *Parkinson's Disease*, *2011*. https://doi.org/10.4061/2011/716859